



university of
 groningen



Parasporal proteins as an approach to control diseases

Genetic modifications, and characterization

PhD thesis

to obtain the degree of PhD at the University of Groningen on the authority of the Rector Magnificus Prof. C. Wijmenga and in accordance with the decision by the College of Deans.

to obtain the degree of PhD at the Universidad de Antioquia on the authority of the Rector Magnificus Prof. J.J Arboleda Cespedes and in accordance with the decision by the College of Deans.

Double PhD degree

by

Miguel Orlando Suarez Barrera

born on 3 October 1986
in Bucaramanga, Colombia

Supervisors

Prof. J.H.M. van den Berg

Prof. J. Orozco

Co-supervisor

Prof. A. Visser

Prof. E. Moreno

Assessment Committee

Prof. A.J. Moshage

Prof. J.M. van Dijk

Prof. M.A. Bravo De La Parra

Contents

	Page.
1. Introduction and Scope of the thesis	17
1.1 Bacillus thuringiensis (Bt) overview	17
1.2 Cry proteins	19
1.3 Mechanisms of action of Bt Cry toxins	21
1.4 The use of Cry proteins in controlling mosquitoes	24
1.5 Cry11 proteins	24
1.6 Parasporal proteins modifications	26
1.6.1 Truncated toxins.....	26
1.6.2 Modification of cleavage sites	27
1.6.3 Non-rational studies based on directed evolution in cry genes	28
1.6.4 Phage display library	28
1.7 Parasporins	30
1.7.1 Parasporins with anti-cancer properties	30
1.7.2 3D structure of the PS2Aa1 protein.....	34
1.7.3 Mechanism of action of PS2Aa1	35
1.7.4 Parasporin 2: a β -type pore-forming protein.....	36
1.8 Research problem	37
1.9 Research question	40
1.10 Aims	40
1.11 Global Methodology of this Work.....	41
1.11.1 Chapter 3: Computational study, synthesis and evaluation of active peptides derived from Parasporin-2 and spike protein from Alphacoronavirus against colorectal cancer cells.	41
1.11.2 Chapter 4: Site-Directed Mutants of Parasporin PS2Aa1 with Enhanced Cytotoxic Activity in Colorectal Cancer Cell Lines.	42
1.11.3 Chapter 5: Toxic Determination of Cry11 Mutated Proteins Obtained Using Rational Design and Its Computational Analysis.....	44

1.12 Scope of the thesis	45
1.13 References	45
2. Review Genetic Modification Approaches for Parasporins <i>Bacillus thuringiensis</i>	
Proteins with Anticancer Activity	58
2.1 Abstract	59
2.2 Background - introduction.....	59
2.3 Overview of the Classification and Structure of Parasporins Found in Bacillus....	60
2.3.1 β -Type-Like Pore-Forming Parasporins	64
2.4 Effects of Parasporins on Cancer Cells	66
2.5 Perspectives on the Improvement of Bt Parasporins as an Innovative Strategy for Controlling Cancer Cells.....	68
2.6 Conclusions.....	73
2.7 References	73
3. Computational study, synthesis and evaluation of active peptides derived from Parasporin-2 and spike protein from Alphacoronavirus against colorectal cancer cells	81
3.1 Abstract	82
3.2 Introduction.....	83
3.3 Materials and Methods	86
3.3.1 Materials and reagents.....	86
3.3.2 Peptide synthesis and characterization	86
3.3.3 Hemolytic activity assay	86
3.3.4 Cell and culture conditions	87
3.3.5 Cytotoxicity assay	87
3.3.6 In vitro binding assay	88
3.3.7 Fluorescence microscopy	89
3.3.8 Annexin V-Cy3 staining.....	89
3.3.9 Caspase 3-7 assay	90
3.3.10 LDH assay.....	90
3.3.11 Molecular docking of peptides and APN receptor	91
3.3.12 Statistical analysis.....	91
3.4 Results	92

3.4.1 Design and characterization of the peptides	92
3.4.2 Anticancer and hemolytic activities	94
3.4.3 In vitro binding assay	95
3.4.4 Fluorescence morphological evaluation	98
3.4.5 Annexin V-CY3 staining	99
3.4.6 Caspase and LDH mechanism.....	102
3.4.7 Molecular docking of peptides and h-APN receptor	103
3.5 Discussion	104
3.6 References	111
3.7 Supporting information	117
4. Site-Directed Mutants of Parasporin PS2Aa1 with Enhanced Cytotoxic Activity in Colorectal Cancer Cell Lines	122
4.1 Abstract	123
4.2 Introduction.....	124
4.3 Results	125
4.3.1 Cloning and Obtention of PS2Aa1 Mutants.....	125
4.3.2 Description of Parasporins Obtained from PS2Aa1 Using Site-Directed Mutagenesis.....	127
4.3.3 Cytocidal Activities of PS2Aa1 Variants in Human Colorectal Cancer Cells.....	127
4.3.4 Variants of PS2Aa1 Induce Apoptosis in Human Colorectal Cancer Cells.....	129
4.3.5 Cytotoxic Activity of PS2Aa1 Variants Is Affected by APN Receptor Inhibition.....	130
4.3.6 Molecular Docking and Molecular Dynamics Analysis Highlight Residues 256 and 257 of Domain I of PS2Aa1	131
4.4 Discussion	134
4.5 Materials and Methods	138
4.5.1 Bacterial Strains and Culture Conditions.....	138
4.5.2 Parasporin Site-Directed Mutagenesis.....	138
4.5.3 Library Verification	139

4.5.4 Preparation of Activated Parasporin Proteins	139
4.5.5 Colon Cancer Cell Lines	140
4.5.6 Cytotoxicity Assays of PS2Aa1 Mutants in Colon Cancer Cells	140
4.5.7 APN Detection and Blocking Assay	140
4.5.8 Molecular Docking and Molecular Dynamics Analysis	141
4.5.9 Statistical Analysis	142
4.6 References	142
4.7 Supplementary information.....	145
5. Toxic Determination of Cry11 Mutated Proteins Obtained Using Rational Design and Its Computational Analysis	147
5.1 Abstract	148
5.2 Introduction.....	149
5.3 Results	151
5.3.1 Variants Were Successfully Obtained from Variant 8 and Cry11Aa.....	151
5.3.2 Cry 11 Proteins and Variants Are Produced in Bt BMB171	151
5.3.3 The Residues Phenylalanine (553) and Tryptophan (556) Are Relevant to the Insecticidal Activity of the Variant 8 Protein	152
5.3.4 Cry Proteins Have an Antiproliferative Effect on the SW480 Cell Line.....	152
5.3.5 Modeled Structures by De Novo Methodology.....	153
5.4 Discussion	157
5.5 Materials and Methods	161
5.5.1 Culture Media, Strains, and DNA Extraction	161
5.5.2 Synthesis and Design of Cry11Bb and Variant 8 Mutants.....	161
5.5.2.1 Cry11Bb Mutant Library	161
5.5.2.2 Variant 8 Mutant Library.....	162
5.5.3 Obtaining Final Complete Culture (FCC) of Bt	162
5.5.4 Protein Electrophoresis on Sodium Dodecyl Sulfate-Polyacrylamide Gel Electrophoresis (SDS-PAGE)	163
5.5.5 Protein Preparation and Half-Lethal Concentration (LC ₅₀)	163
5.5.6 Variants of Cry in the Control of the Human Colorectal Cancer Cells	164
5.5.7 Structural Modeling of Cry11 Variants.....	164

5.5.8 Generation of Additional Variants and Sampling of the Models	165
5.6 References	165
6. Summary, Conclusions, and Future Perspectives	171
6.1 Summary and Conclusions	171
6.2 Discussion and future perspectives	176
6.2.1 Parasporal proteins: anticancer biomolecules	179
6.2.1.1 New studies of the interaction of PS2Aa1 (Mpp46Aa1) with the cell- membrane receptor GPI-Ap	179
6.2.1.2 Colorectal cancer (CRC) as a target of Parasporin strategies	179
6.2.1.3 Personalized medicine using parasporins, and other molecules in the control of CRC	181
6.2.1.4 Variant 8 peptide-based nanoconjugates as a new resource	181
6.3 References	182
7. Appendices	186
7.1 Author affiliations	186
7.2 Acknowledgements	187
7.3 About Me: Miguel Orlando Suárez Barrera (MOSB)	190
7.4 Funding	191
7.5 List of publications	191
7.6 Other publications derived from the work.	192
7.7 Paper: Toxic Activity, Molecular Modeling and Docking Simulations of <i>Bacillus thuringiensis</i> Cry11 Toxin Variants Obtained via DNA Shuffling	193
7.7.1 Abstract	193
7.7.2 Introduction	194
7.7.3 Materials and methods	198
7.7.3.1 Microbial Strains, Clone Selection and Gene Constructs	198
7.7.3.2 Isolation of cry11 Genes via PCR	199
7.7.3.3 cry11 Gene Cloning, Insert Validation, and Sequencing	200
7.7.3.4 Test Primers for Reassembly via PCR	200
7.7.3.5 DNA Shuffling	201
7.7.3.6 Cloning, DNA Sequencing and Homology Analysis	202

7.7.3.7 Transformation of <i>Bacillus thuringiensis</i>	202
7.7.3.8 Cultures, Solubilization, Cry Protein Quantification, and SDS–PAGE.....	203
7.7.3.9 SEM	204
7.7.3.10 Half Lethal Concentration (LC ₅₀) in <i>A. aegypti</i> and <i>C. quinquefasciatus</i> Larvae.....	204
7.7.3.11 3D Structure Prediction and Validation and Secondary Structure Analysis of Non-conserved Regions	204
7.7.3.12 Molecular Docking of Cry11 Domains with ALP1	205
7.7.4 Results	206
7.7.4.1 Parental cry11 Genes	206
7.7.4.2 Assembly of Full-Length cry11 Genes	207
7.7.4.3 Characteristics and Sequence Homology of cry11 Variants	208
7.7.4.4 Protein Expression and Crystal Formation.....	209
7.7.4.5 The Interactions of Cry11Aa With ALP1 Are Conserved in Variants 8 and 23.....	210
7.7.5 Discussion.....	214
7.7.6 References.....	220
7.7.7 Supplementary Material	226

List of Figures

	Page.
Figure 1. Bt potential in biotechnology and medical fields. Cry (Crystal proteins) and PS (Parasporins). Inspired by Jouzani G.S et 2017 [12]. Credits: author (s).....	18
Figure 2. The 3D-Cry proteins (partially) were taken and adjusted from [19]......	20
Figure 3. Three-strand structure of three-domain Cry proteins. A) Domain I of the Cry11Aa toxin. B) Domain II of the Cry11Aa toxin, the enlarged circle allows visualizing the Greek key formation of Domain II. C) Domain III of the Cry11Aa toxin. This scheme represents the formation of its β -folded sheets (β -sandwich). The structures were obtained using the YASARA engine.	21
Figure 4. The three-domain Cry toxin pore formation model in the insect midgut membrane. A) Insect midgut proteases solubilize cry11 protein. B) Cry11 binds to GPI-anchored APN and ALP receptors on lipid rafts. This union promotes the localization and concentration of activated toxins. C) Binding to the cadherin receptor facilitates proteolytic cleavage of the α -1 helix at the N-terminus. D-E) N-terminal cleavage induces pre-pore oligomer formation and increases the binding affinity of the oligomer to APN and ALP receptors. F) The oligomer is introduced into the membrane, which generates the formation of pores and cell death, inspired by: (Chengchen, Bi-Cheng, Ziniu, & Ming, 2014 [40]. Image modified by the author.	23
Figure 5. Mechanism of action of the Cry toxin, according to the signaling pathway mode: The Cry protein binds to cadherin receptors in the plasma membrane to produce the formation of pores that will subsequently trigger cell apoptosis (Fernández-Chapa et al., 2019) [36]. Image modified by the author (s).	24
Figure 6. Three-dimensional modeled structure of the Cry11Aa protein through the YASARA engine. The amino acid sequence was taken from UniProt for modeling. (https://www.uniprot.org/uniprotkb/P21256/entry).....	25
Figure 7. Multiple alignments of Cry11Aa, Cry11Ba, and Cry11Bb protein sequences. The outlined areas expose the regions of the highest identity.	26

- Figure 8.** Dendrogram of parasporins, showing percentages of identity among sequences. Taken from [95]. 33
- Figure 9.** Visualization of models from YASARA, using Geno3D to obtain the PDB files. A. Structural model of higher molecular mass parasporins (PS3Aa1) with its three Domains. B. Structural model of PS2Aa1. Source Author 34
- Figure 10.** Structure (A) and mechanism of action of PS2Aa1 (B). Inspired by Xu et al. 2014 [103]. Adapted by author(s). 36
- Figure 11.** Structural comparison of parasporins(A) Structural model of higher-molecular-weight PS3Aa1 with its three domains. (B) Low-molecular-weight PS2Aa1 structural model. (C–E) Structural comparison between parasporin-2, the 26-kDa nontoxic protein, and aerolysin-like α -PFT. Membrane-binding-related domain I is colored yellow. The membrane insertion and pore-formation regions are colored blue (domain II) and red (Domain III). It is suggested that the purple amphipathic α -hairpin is necessary for pore formation (C–E). Parasporin 4 (PS4) was modeled using the 26-kDa nontoxic protein as an adapted template from Xu et al. [9], modified by the authors..... 61
- Figure 12.** Action mode of aerolysin-like parasporins (PS2Aa). Figure adapted from [9]. According to this model, the mechanism of action could be as follows: 1. The solubilized protein binds to the GPI-anchored receptors at the N-terminus. 2. After C-terminal proteolytic digestion, the activated protein monomers assemble (oligomerization). 3. Through reorganization, a transmembrane α -barrel is formed..... 65
- Figure 13.** Secondary structure of peptides. A) theoretical in silico secondary structure of P264-G274, Loop1-PS2Aa, Loop2-PS2Aa, and Loop1-HCoV-229E. B) circular dichroism spectra of the peptides in TFE (30% p/V). CD was recorded after four accumulations at 20 °C, using a 1mm path length quartz cell, between 190 and 250 nm at 100 nm min⁻¹, with a bandwidth of 0.5 nm. Peptide concentration: 1 mg/mL. 93
- Figure 14.** Effect of peptides (P264-G274, Loop1-PS2Aa, Loop2-PS2Aa, Loop1-HCoV-229E, and A4W-GGN5) and the chemotherapeutic drug (5-FU), on the viability of - cancerous and non-cancerous cells measured by the SRB assay. A4W-GGN5 and 5-FU were used as a positive control. (A-C) SW480, SW620, and CHO-K1 cells were incubated with peptides in the concentration range of 0-150 μ M for 48 h. Dosages that caused a statically significant decrease in cell growth compared to the untreated control

- at each time point were indicated by asterisks (* $p < 0.05$; one-way ANOVA followed by Tukey's test). 97
- Figure 15.** Hemolytic activity of peptides (P264-G274, Loop1-PS2Aa, Loop2-PS2Aa, Loop1-HCoV-229E, and A4W-GGN5). Hemolytic activity of peptides against human red blood cells at different peptide concentrations (4-100 μM), in Hank's glucose at 37°C for 4h of exposure. Experiments were performed in three independent replicates. Dosages that caused a statically significant decrease in cell growth compared to the untreated control at each time point were indicated by asterisks (* $p < 0.05$; one-way ANOVA followed by Tukey's test). 98
- Figure 16.** In vitro cell binding of the most active peptides (A) Cell binding of Loop1-PS2Aa peptide on the cancerous cell line SW480. (B) Cell binding of P264-G274 peptide on the cancerous cell line SW620. Experiments were performed in three independent replicates..... 100
- Figure 17.** SW480 and SW620 colon cancer cells were stained by Hoechst and observed under fluorescence microscopy (20X). Cell morphology was observed under fluorescence microscopy, the bar represent 100 μm 101
- Figure 18.** Photomicrographs of control and Annexin V-Cy3/6-CFDA stained SW480 and SW620 colon cancer cells treated with the peptides Loop1-PS2Aa and P264-G274, respectively for 24 h and 48 h. 5-FU was taken as a positive control, the bar represent 100 μm 103
- Figure 19.** Caspase and LDH assay. A) intrinsic apoptosis of Loop1-PS2Aa peptide on the cancerous cell line SW480 after 4 hours of exposure. B) intrinsic apoptosis of P264-G274 peptide on the cancerous cell line SW620 after 4 hours of exposure. C) No detection of LDH enzyme in the extracellular medium after 4 hours of exposure with the peptides Loop1-PS2Aa peptide on the cancerous cell line SW480 and P264-G274 peptide on the cancerous cell line SW620. Experiments were performed in three independent replicates..... 105
- Figure 20.** APN residues involved in hydrogen bonds with P264-G274 peptide. This figure shows the top 10 of the APN residues involved in hydrogen bonds with peptide P264-G274, in 500 models obtained in global simulations (left) and 100 models obtained in the refinement round (right). 106

- Figure 21.** Interactions in the resulting complex between P264-G274 peptide and the APN. a) Complex between the P264-G274 peptide and APN, b) Hydrogen bonds and hydrophobic interactions found in the complex..... 107
- Figure 22.** APN residues involved in hydrogen bonds with Loop1-PS2Aa peptide. This figure shows the top 10 of APN residues involved in hydrogen bonds with peptide P264-G274, in 500 models obtained in global simulations (left) and 100 models obtained in the refinement round (right). 108
- Figure 23.** Interactions in the resulting complex between Loop1-PS2Aa peptide and the APN. a) Complex between the Loop1-PS2Aa peptide and APN, b) Hydrogen bonds and hydrophobic interactions found in the complex..... 110
- Figure 24.** Agarose gel showing the construct pET-30a/ps2Aa1 treated with the restriction enzymes KpnI and HindIII; Lane 1: construct pET-30a/ps2Aa1; Lane 2: construct pET-30a/ps2Aa1 treated with the restriction enzymes KpnI and HindIII; Lane M: molecular weight marker..... 126
- Figure 25.** Tukey's multiple comparison test for **(A)** SW480 and **(B)** CaCo-2. The results for the percentage of cell growth inhibition correspond to $5 \mu\text{g}\cdot\text{mL}^{-1}$ for each parasporin. PS2Aa1 was used as a control. ** $p \leq 0.01$, and *** $p \leq 0.001$, ns (non-significant)..... 128
- Figure 26.** Cytotoxic effects of parasporins to CaCo-2 and SW480. Detection of annexin V/PI **(A)**, statistical analysis of induction of apoptosis by parasporins **(B)**. Western blot of PARP, caspase-3 (Casp3), and γH2AX in SW480 and CaCO-2 after treatment with the indicated parasporins **(C)**. GAPDH was used as a loading control. The amount of toxins used for each treatment was $5 \mu\text{g}/\text{mL}$ over 48 h. * $p \leq 0.05$, ** $p \leq 0.01$, ns (non-significant) 130
- Figure 27.** **(A)** Detection of APN receptor in different cell lines HL60, MCF-7, U2932, CaCo-2, and SW480. Metabolic activity of **(B)** SW480 and **(C)** CaCO-2 without parasporin (NP), parasporin 0015, 3-35, and the recombinant of PS2Aa1 (PS2Aa1.r) at $5 \mu\text{g}\cdot\text{mL}^{-1}$ in the presence or absence of the APN inhibitor..... 131
- Figure 28.** Relevant residues for PS2Aa1–APN interaction. Relevant residues for interacting with the APN receptor are displayed. GLY256, ARG76, ARG266, and SER273. PS2Aa1 and APN are colored blue and teal, respectively..... 132

- Figure 29.** Residues relevant for the interaction with APN at distances less than 6 Å between the center of mass of the relevant PS2Aa1 residues and the nearest APN residue. Above, PS2Aa1 and APN are colored blue and teal, respectively. 133
- Figure 30.** PS2Aa1–APN interaction. Relevant residues for interaction with APN are analyzed in Figure 6. Distances were computed between the center of mass of the relevant residues of PS2Aa1 and the closest residue from APN. 137
- Figure 31.** Cytotoxicity activity of the Cry proteins on the colorectal cancer cell line SW480 at 48 h (A). and 72 h (B). The measurements were determined with Alamar Blue staining. The IC₅₀ was calculated with different concentrations of Cry proteins (0.5–10 µg·mL⁻¹) at 48 and 72 h (C). No IC₅₀ was calculated for BMB171..... 153
- Figure 32.** Structural model of variant 8 (A). Representations of the variants 8F553L (B), 8W556L (C), and the combination of 8F553L and 8W556L (D) after running MD simulations of the mutated complexes..... 154
- Figure 33.** Structural model of Cry11Bb (A). Representations of the variants A92D (B) and C157R (C) after running MD simulations of the mutated complexes. 155
- Figure 34.** RMSD of simulated (A): red color (variant 8) and blue color (Cry11). The radius of gyration of the simulated (B): red color (variant 8) and blue color (Cry11)..... 156
- Figure 35.** The activity of PS2Aa1 and the mutant N65 against SW480 in the presence (10nM) or absence of Tosedostat..... 174
- Figure 36.** Structure of the Cry toxins, domains, and their mode of action. (A) Ribbon diagram of Cry deduced 3D structure. Three domains are colored in red blue and green, respectively. (B) Sequential binding mechanism. 1. The toxin binds to GPI-anchored APN and ALP receptors in the lipid rafts; 2. Binding to cadherin receptor 3. Proteolytic cleavage of the helix α1 at N-terminal end; 4. N-terminal cleavage induces the formation of pre-pore oligomer 5. Increasing of the oligomer binding affinity to GPI-anchored APN and ALP receptors; 6. Oligomer inserts into the membrane, leading to pore-formation and cell lysis; and 7. Cellular death. 197
- Figure 37.** Molecular characteristics of Cry11 variants obtained via DNA shuffling. 210
- Figure 38.** Half lethal concentrations of Cry11 variants obtained via DNA shuffling in *Aedes aegypti* and *Culex quinquefasciatus* larvae. The values are expressed as ng/ml of spore-crystal mixtures, 95% confidence limit (CL)..... 211

Figure 39. Prediction of the 3D Structures of Cry11Aa and Variants 8, 23, and 79. (A) Conserved region of variant 8 in light blue and Cry11Aa in beige, RMSD: 1,084 with 247 aa. (B) Non-conserved region of variant 8 in light blue and Cry11Aa in beige. (C) Conserved region of variant 23 in light blue and Cry11Aa in beige, RMSD: 1,132 with 488 aa. (D) Non-conserved region of variant 23 in light blue and Cry11Aa in beige. (E) Conserved region of variant 79 in light blue and Cry11Aa in beige, RMSD: 1,084 with 247 aa. (F) Non-conserved region of variant 79 in light blue and Cry11Aa in beige. (G) Ribbon representation of the non-conserved region of variant 79 generated using the Robetta server.213

Figure 40. Molecular docking of the interactions of domain II of Cry11Aa and its variants with ALP1. (A,B) Interactions formed by 11-amino acid peptides within domain II of Cry11Aa. (A) Variant 8 (B) Cry11Aa. (C–F) Interactions formed by 5-amino acid peptides within domain II of Cry11Aa (C) variant 8 (D) Cry11Aa (E) Variant 23 (F) Variant 79...215

Figure 41. Interactions visualized in LigPlot of ALP1 against peptides of Cry11Aa and its variants 8 and 23. (A) Cry11Aa, (B) Variant 23, and (C) Variant 8.217

List of Tables

	Page.
Table 1. Some studies of mutagenesis were carried out on Cry toxins.	29
Table 2. Families of Parasporins, strains, molecular weight, target cells, and references.	31
Table 3. New nomenclature of Parasporins taken from Crickmore . N., et al.. 2021 [94]. Adapted by the author.	34
Table 4. Selectivity of PS2Aa1 for some carcinogenic cell lines taken from Xu., et al.. 2014 [98]. Adapted by the author.	37
Table 5. Parasporin families, family-containing strains, molecular weights, target cells, cytotoxic activity and references.	61
Table 6. Modifications made to Bt toxins to improve their efficacy.	70
Table 7. Peptides sequence, molecular characterization and physicochemical properties (net positive charge) (https://www.bachem.com/service-support/peptide-calculator/), H (hydrophobicity), μ H (hydrophobic moment).	92
Table 8. EC ₅₀ and HC ₅₀ values of the anticancer and hemolytic activity of the peptides.	94
Table 9. Top 10 of the APN residues that were found to interact with peptide P264-G274 through hydrogen bonds.	101
Table 10. Top 10 of the APN residues that were found to interact with peptide Loop1-PS2Aa through hydrogen bonds.	105
Table 11. Summary of APN and peptides residues involved in molecular interactions in the best complexes.	106
Table 12. Description of parasporins obtained from PS2Aa1 using site-directed mutagenesis.	127
Table 13. Cytocidal activities of PS2Aa1 variants in human colorectal cancer cells. ...	128
Table 14. Top 10 models according to the number of hydrogen bonds in the interface.	132
Table 15. Residues in contact with APN receptors.	132

Table 16. Prevalence of PS2Aa1 residues among MD replicates.	133
Table 17. Distances of the residues of PS2Aa1 relevant to interacting with APN.	134
Table 18. Primers designed for site-directed mutagenesis of PS2Aa1.....	138
Table 19. LC ₅₀ for each of the variants obtained in this study.	152
Table 20. The difference in RMSF is the difference in Å of the spatial position of the same amino acid in the two systems, wild-type (Cry11), and mutant (Variant 8).....	157

1. Introduction and Scope of the thesis

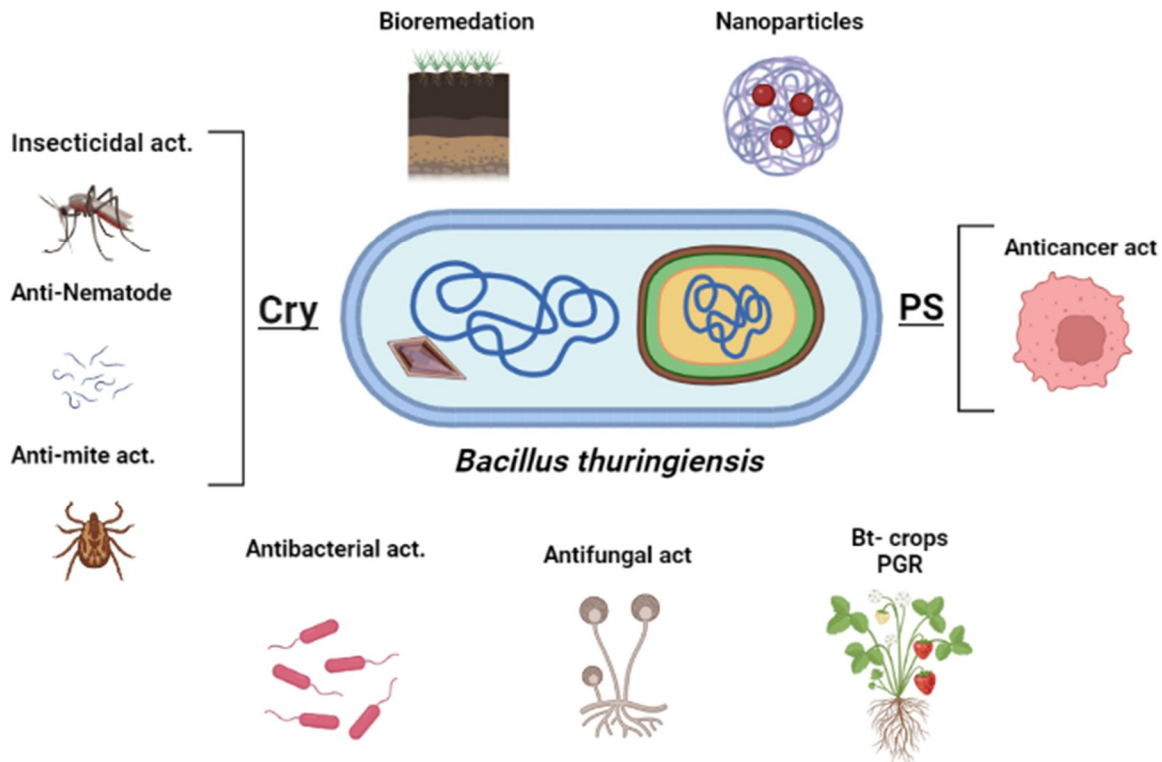
Miguel Orlando Suárez Barrera

1.1 *Bacillus thuringiensis* (Bt) overview

Bt is a ubiquitous rod-shaped soil bacterium. It is a Gram-positive, aerobic bacterium with various biological characteristics, such as the capacity to resist high temperatures and desiccation. These features are related to its ability to form endospores, which are between 1 to 1.2 micrometers wide and 3 to 5 micrometers long [1]. The genome of Bt strains contains 2.4 to 5.7 million base pairs, most of which are made up of extrachromosomal circular and linear elements. Additionally, it is known that Bt can produce crystalline inclusions in its sporulation cycle that contain insecticide-type proteins called δ -endotoxins [2].

Although the potential of Bt-derived proteins such as Cry toxins has been exploited for a long time, research on Bt remains incomplete. Exploiting Cry toxins includes producing genetically modified plants to control pests and vector-borne diseases (VBD) in humans. Knowledge about Bt is expanding, which is the basis for designing new products with applications in industry, human health, and agriculture [3]. Bt-derived factors have increased over the years, making it the most used bioinsecticide nowadays [4]. These factors have been efficiently used in plant genetic engineering, for example, as a source of cry genes to make transgenic plants resistant to various pests [3], [5], [6], and as a nematicide to control plant pathogenic nematodes [7]. More recent studies have indicated new potentials of various Bt strains. These new properties include the promotion of plant growth, bioremediation of heavy metals and other chemicals [3], [8], [9], anticancer activity (Parasporins) [3], polymer production [10], and antagonistic effects against plant and animal pathogenic microorganisms [11], [12] (Figure 1).

Figure 1. Bt potential in biotechnology and medical fields. Cry (Crystal proteins) and PS (Parasporins). Inspired by Jouzani G.S et 2017 [12]. Credits: author (s).



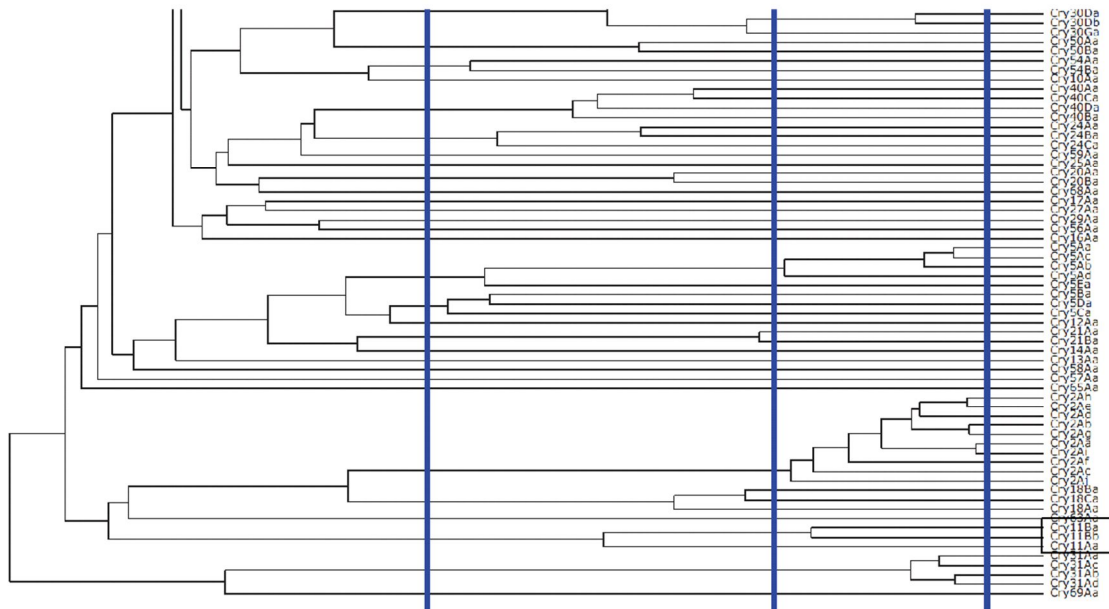
Bt has a life cycle comprising various phases, where its first phase is vegetative growth, followed by a transition to sporulation (phases two and three), and finally, the maturation of the spore and cell lysis of the microorganism [13]. The insecticide-like proteins or crystals are synthesized in the second phase of sporulation and accumulate in the cell, representing up to 30% of the total dry weight of the sporulated cells [14]. The structural presentation of these crystals can be classified according to their pyramidal, bipyramidal, flat rhomboid, spherical, cubic, and rectangular shapes. The bipyramidal crystal is the most frequently occurring form, and these might include more than one δ -endotoxin [15]. The crystals that contain these proteins (Cry proteins) produced by Bt have toxic activity against different orders of insects, including Lepidoptera, Coleoptera, Hemiptera, Diptera, and Hymenoptera in their different larval stages, generating a rupture in the tissue of the midgut, which triggers septicemia and later the death of the insect [16].

1.2 Cry proteins

The name Cry is derived from the parasporal body (Crystal). The most studied group of Cry are the three-domain (3D-Cry) Cry proteins, mostly found in Bt strains. Besides the Bt-derived Cry proteins, Cry proteins with insecticidal activity produced by *Bacillus sphaericus*, such as the BIN toxins. BIN toxins use GPI-anchored α -glucosidase as a receptor to control *Culex pipens*, a vector-borne disease that includes West Nile virus (WNV) [17]. In addition, mtx-type insecticidal crystal proteins (ICPs) are Cry-related toxins. The Mtx Cry protein Cry51Aa2 is used to control the cotton pest *Lygus hesperus*, among others. This group of Mtx-Cry proteins includes toxins such as Cry64Ba and Cry64Ca, which are being studied to combat liver cancer. Cry45Aa and Cry64Aa are also called parasporin4A1 and parasporin5A1 due to their toxicity against human cancer cells [17].

The 3D-Cry name is based on the Cry prefix and four hierarchical rows of numbers used to classify them in the phylogenetic tree described by Crickmore and collaborators [18], [19]. Based on the newest nomenclature, there are 775 Cry genes categorized into 74 groups [18], [20] (Figure 2) [20], including new groups of toxins that have activity against insects of the orders Hymenoptera, Orthoptera, Hemiptera, Isoptera, Mallophaga, Thysanoptera, etc., and some others such as nematodes and mites ([18], [20]). These toxins are the most used and studied for controlling pest insects and, in turn, have been expressed in genetically modified plants [21], [22]. In addition, IN and Mtx type Cry proteins are named for sharing similarities with binary toxins and specific mosquitocides for Diptera produced by *Lysinibacillus sphaericus*, which, when found in their active form, are toxic against some Coleoptera and Hemiptera larvae [21], [22]. Finally, the family of Cry toxins described in other groups is characterized by maintaining a similarity with the *Clostridium perfringens* epsilon toxin and these have shown toxic activity against nematodes, Diptera, Coleoptera, and Cancer cell lines [21], [23].

Figure 2. The 3D-Cry proteins (partially) were taken and adjusted from [19].



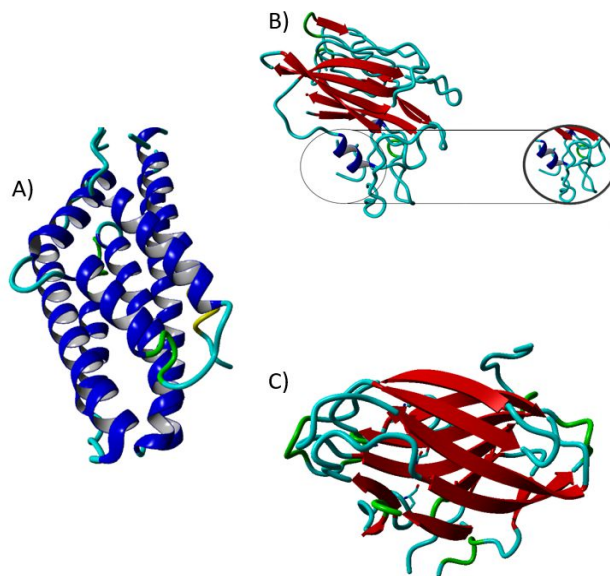
Domain I of 3D-Cry proteins is made up of 7 hydrophobic and amphipathic anti-parallel α -helices with polar residues located at the N-terminus (Figure 3A). The pore formation process is mediated by this domain, in which a hydrophobic helical hairpin formed by the α 4- α 5 helix is wrapped by the amphipathic helices, giving rise to the polar groups located in the interhelical space forming bonds, hydrogen, and salt bridges [24]. It has also been theorized that the hydrophobic α -5 and α -6 helices' union forms a loop ("Pen knife") at the end of the structure. The loop opens through the midgut lipid membrane while the rest of the protein remains anchored to the membrane [25].

Domain II is arranged in a Greek key-type topology as a β -prism, formed by three parallel β -anti sheets packed around a hydrophobic nucleus (Figure 3B) [25]. This domain was reported to be responsible for recognizing the midgut receptor of insects. These binding junctions are a model like the antibody-antigen binding sites due to the loops on the three β -sheets surfaces exposed at the apices of this structure [26], [27].

Domain III has a structure like carbohydrate-binding proteins and very similar to β -galactosidase, and xylanase, among others [28]. Studies carried out on the Cry1Ac protein indicated that domain III of this toxin exhibits a structure like lecithin, presenting a specific

binding to N-acetylgalactosamine located in the N-aminopeptidase (APN) receptor [29], [30]. This domain is described as a β sandwich composed of two anti-parallel β sheets with less structure variability than domain II (Figure 3C) [29]. The function of this domain is very versatile, with its main functions ranging from providing stability to maintaining the structural integrity of the protein during the proteolysis process in the midgut of the target insect and participating in the formation of ion channels that produce osmotic imbalance, as well as the formation of pores in the membranes [25], [31].

Figure 3. Three-strand structure of three-domain Cry proteins. A) Domain I of the Cry11Aa toxin. B) Domain II of the Cry11Aa toxin, the enlarged circle allows visualizing the Greek key formation of Domain II. C) Domain III of the Cry11Aa toxin. This scheme represents the formation of its β -folded sheets (β -sandwich). The structures were obtained using the YASARA engine.

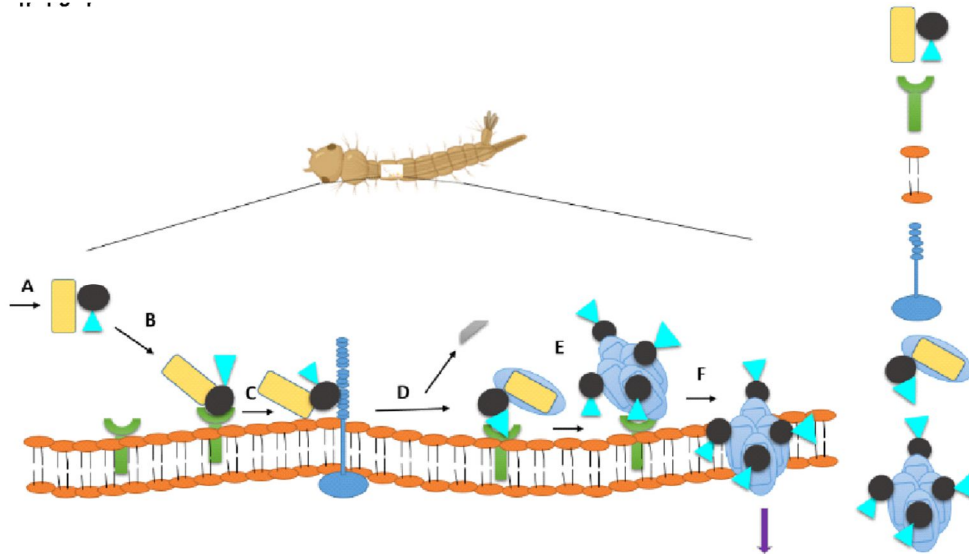


1.3 Mechanisms of action of Bt Cry toxins

The mechanism of action of the best-studied Cry proteins corresponds to the so-called 3D Cry. Two main models of action have been proposed. The first model includes sequential binding, in which the δ -endotoxin is ingested and activated by the digestive protease of the target insect. The active Cry toxin then forms oligomers with N-aminopeptidase (APN), alkaline phosphatase (ALP), and cadherin (CDN) receptors,

which eventually leads to the formation of pores and triggers an osmotic imbalance that causes cell death [32], [33]. Signaling is induced through the formation of ion channels generated by Mg^{+2} , which activates an adenylyl cyclase that promotes the intracellular production of cyclic adenosine monophosphate (cAMP). The increase in cAMP activates protein kinase A, leading to cell death [34], [35]. This sequential binding model (Figure 4) postulates that the toxic properties come from the protein's active form since the crystals and their subunits are inert and not biologically active [36]. Initially, insects ingest δ -endotoxins to be solubilized in the midgut by the alkaline pH of the gastric juices. The proteases present in the intestine activate these proteins, resulting in active toxins with an approximate weight between 30 and 70 kDa (depending on the Cry protein) (Figure 4A), which will encounter CDN, APN, and/or ALP on the membrane surface of midgut cells (Figure 4B) [37]. The affinity between the receptors and the activated toxins induces structural changes in the protein, leading to oligomers that have functionality as a pre-pore [38]. Helix α -4 and helix α -5 that present hydrophobic hairpins penetrate the membrane to start the lytic pore formation, while domain I remain on the membrane in a globular state [37], [38]. Once the formation of this pore occurs, it has been suggested, based on biochemical and electrophysiological evidence, that an osmotic imbalance is generated that leads to lysis and cell death, where the intestine is paralyzed and subsequently causes the insect to stop feeding; total paralysis occurs, and finally the death of the target insect [36], [39].

Figure 4. The three-domain Cry toxin pore formation model in the insect midgut membrane. A) Insect midgut proteases solubilize cry11 protein. B) Cry11 binds to GPI-anchored APN and ALP receptors on lipid rafts. This union promotes the localization and concentration of activated toxins. C) Binding to the cadherin receptor facilitates proteolytic cleavage of the α -1 helix at the N-terminus. D-E) N-terminal cleavage induces pre-pore oligomer formation and increases the binding affinity of the oligomer to APN and ALP receptors. F) The oligomer is introduced into the membrane, which generates the formation of pores and cell death, inspired by: (Chengchen, Bi-Cheng, Ziniu, & Ming, 2014 [40]). Image modified by the author.

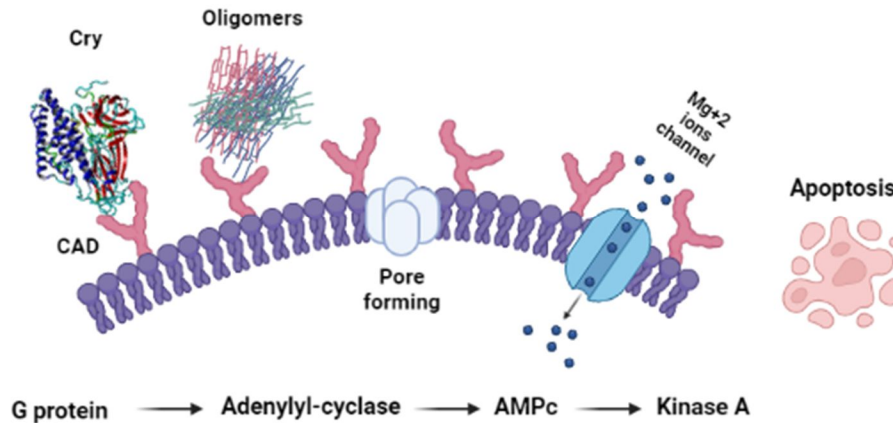


The second model postulated for the action of Cry proteins (Figure 5) has similar characteristics to the previously mentioned model, but with the difference that cell death is attributed to different factors [3]. In this model, the interactions of the Cry toxins with the CDN receptor led to the activation of a magnesium-dependent signaling pathway, in which the adenylyl cyclase pathway and protein kinase A are involved [36]. Initially, the binding between the receptor and the toxin stimulates increased production of cAMP, adenylyl cyclase, and heterotrimeric G-protein. Then, the overproduction of cAMP results in the activation of protein kinase A, which stimulates apoptosis with the activation of magnesium channels in the plasma membrane; these channels generate an abnormal movement of ions in the cytosol [41].

The two mechanisms described above can act simultaneously, but the pore formation model is the most studied. Furthermore, the main cytotoxic effects of the proteins are attributed to the midgut of insects. Therefore, the biochemical and

physiological characteristics of the intestine of each insect will define the action model [38].

Figure 5. Mechanism of action of the Cry toxin, according to the signaling pathway mode: The Cry protein binds to cadherin receptors in the plasma membrane to produce the formation of pores that will subsequently trigger cell apoptosis (Fernández-Chapa et al., 2019) [36]. Image modified by the author (s).



1.4 The use of Cry proteins in controlling mosquitoes

Various approaches have been proposed worldwide to control *A. aegypti*, ranging from chemicals to biological measures. The latter, without recalcitrant and harmful effects on the environment. Recent measures include the release of Wolbachia-bearing mosquitoes, bacteria that prevent virus transmission [43], creating transgenic mosquitoes [42]. However, the production of insecticidal toxins, including Cry toxins, which are specific and have been used to control Dipterans, [43] [44], [45]. These toxins include the Cry11 family, which has been shown to have toxic activity against mosquitoes [46]–[49], making this group of 3D-Cry proteins attractive candidates for protein engineering.

1.5 Cry11 proteins

Cry11 proteins are a family of toxins consisting of three active domains against the dipteran order vector-borne diseases insects [52]. The best-characterized family member is Cry11Aa, a protein of approximately 70 kDa produced by Bti (Figure 6), in which around

28 amino acids are removed from the N-terminus through its proteolytic activation. The resulting protein is cleaved into 32 and 34 kDa fragments, respectively. These fragments remain associated and have an insecticidal activity mainly against *A. aegypti* [50], [51]. Cry11Ba, produced by *Bt subsp Jegathesan* (Btjeg), is more toxic than Cry11b or Cry11 proteins derived from *Aedes*, *Anopheles*, and *Culex* larvae. Its molecular weight is around 80 kDa, and a proteinase K cleavage step generates its active fragments of 30 and 35 kDa [29], [51]. Cry11Bb has the peculiarity of having toxic effects on mosquito genera such as *Culex* and *Anopheles*. This toxin weighs 94 kDa and its toxic effect occurs through solubilization and proteolytic processing into a fragment of 30 and a fragment of 35 kDa in the midgut of insects [52]. The toxin is produced by *Bt subsp Medellín* (Btmed) during its sporulation phase [51]. The amino acid sequence of the three Cry11 holotype proteins shows a high percentage of identity. The Cry11Bb toxin is 69% identical to Cry11Aa and 83% identical to Cry11Ba (Figure 7). The nucleotide sequence of the cry11Bb gene is 60.9% and 83% identical to the cry11Aa and cry11Ba genes, respectively [53], [54].

Figure 6. Three-dimensional modeled structure of the Cry11Aa protein through the YASARA engine. The amino acid sequence was taken from UniProt for modeling. (<https://www.uniprot.org/uniprotkb/P21256/entry>)

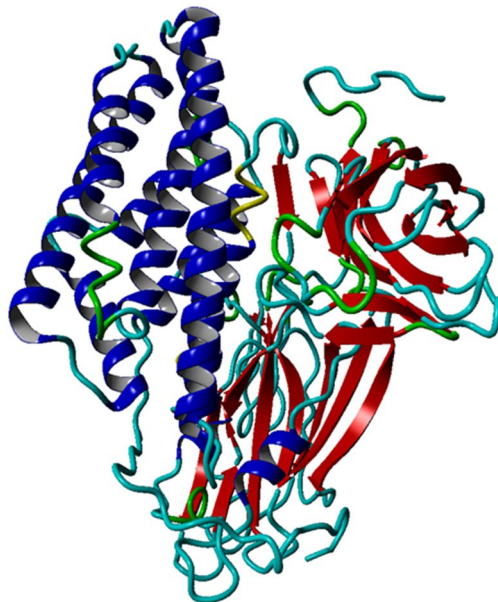
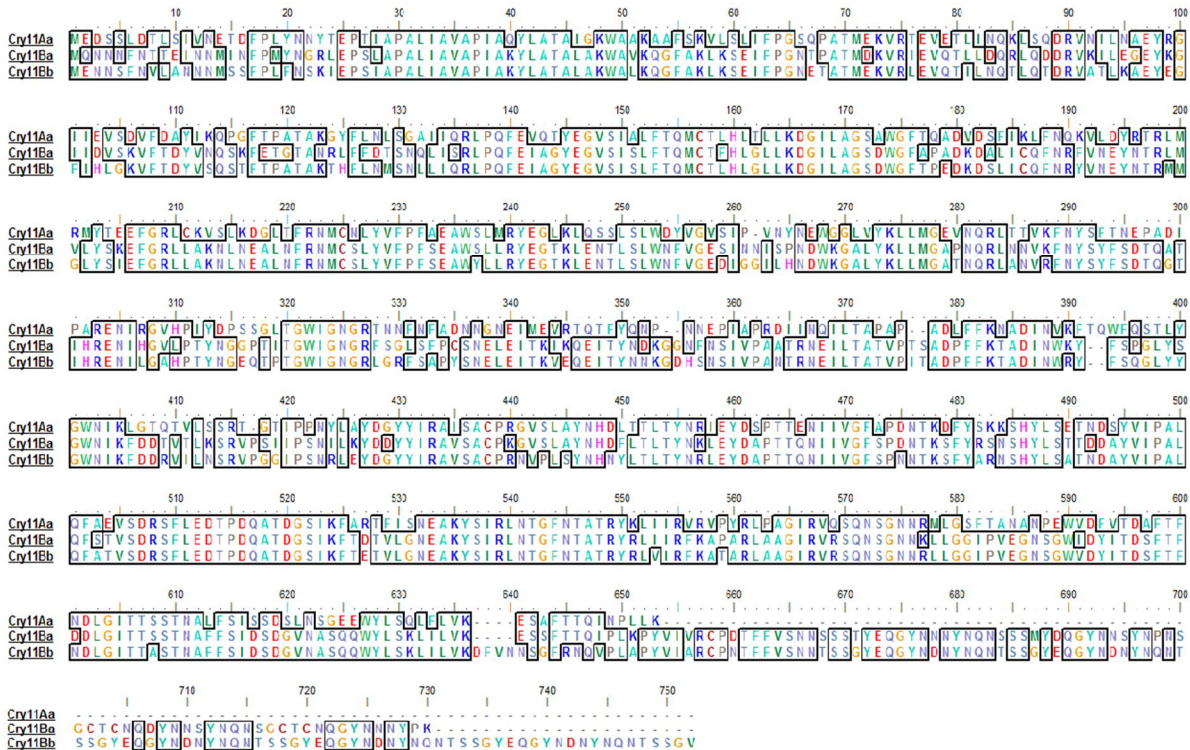


Figure 7. Multiple alignments of Cry11Aa, Cry11Ba, and Cry11Bb protein sequences. The outlined areas expose the regions of the highest identity.



1.6 Parasporal proteins modifications

Cry toxins have been subject to modifications to obtain information regarding the functionality of specific structures and to elucidate their mechanism of action. In addition, these modifications have generated Cry variants with different toxicities compared to their native proteins, optimizing and diversifying their potential for biotechnological applications (**Table 1. Some mutagenesis studies were carried out on Cry toxins. Table 1**) [45].

1.6.1 Truncated toxins

The Bt toxin truncation technique has been used to determine the implications of amino and carboxyl-terminal for protein toxicity by deletion analysis. Some 3' and 5' end deletion mutants have been generated to identify the regions that encode the toxic peptide. This approach revealed that the amino-terminal halves of Bt *kurstaki* Cry1Ab and Cry1Ac were sufficient to kill insects [55]. On the other hand, a study carried out by Pang

et al. in 1992 showed that the expression of an amino-terminal truncated from Cry11A protein was not toxic for first-stage larvae of *Aedes aegypti* [56].

Enhanced expression of truncated toxins was achieved by Hayawaka et al. in 2008, who adapted the nucleotide sequence of the Cry4Aa gene in such a way that it contains a high GC content and codon usage by the preference by *Escherichia coli*. This process resulted in a high expression and a toxic activity like the native toxin against *Culex pipiens* [57]. In 2010, Craveiro et al. obtained variants from Cry11a (lacking a carboxyl-terminal) through DNA shuffling and a phage library (see below for explanation). The new proteins had the binding capacity to the brush-shaped membranes of *T. licus licus* and, at the same time, had a 3-fold increased toxicity compared to the truncated and native parent [58].

1.6.2 Modification of cleavage sites

The processing of Cry protoxins is an important event in the passage to toxins. This mechanism is reviewed by [47] and focuses on the removal of amino and carboxy-terminal regions, producing large (Cry3) or intermediate (Cry1, Cry4, Cry11) proteins, and poor proteolytic cleavage alters or abolishes toxicity. Therefore, it has been proposed that knowing these cleavage sites may be necessary for designing and constructing modified toxins [45].

Proteolytic activation of toxins can also increase solubility. In this case, proteins with limited solubility precipitate and restrict the interaction with receptors in the insect gut [59]. The solubility of Cry toxins is pH dependent, which also restricts the target insects since the pH of the intestines varies per order. Lepidoptera and Diptera's pH is alkaline, while Coleoptera and Hemiptera's pH ranges between neutral and acid [60]. On the other hand, the solubility of Cry also changes after proteolytic cleavage. Treatment of the Cry3A toxin with chymotrypsin makes it soluble at neutral pH [59]. The type of proteases of the insects determines the target specificity of Cry toxins. Resistance to Cry toxins can be achieved by slight modifications in the proteases required for cleavage and activation of the toxin, rendering the protein harmless [45], [61]. By altering the cleavage sites on Cry3A, a non-toxic protein is generated against to *Diabrotica virgifera virgifera* LeConte,

making this insect resistant to Cry3A and Cry1Ab [62]. This approach has generated active toxins against non-susceptible insects, suggesting broader applications [45].

1.6.3 Non-rational studies based on directed evolution in cry genes

Unlike rational approaches, non-rational approaches such as directed evolution employ molecular techniques that cause random mutations in DNA. DNA shuffling is a technique where variants of a gene or a group of homologous genes are fragmented and recombined to obtain genes with different base compositions [63]. Several studies applied DNA shuffling or error-prone polymerase chain reaction (PCR) (EP-PCR) to generate genetically improved Cry proteins [58]. Shu et al. identified two variants of the Cry8Ca2 toxin using EP-PCR technology with an average of 3.9-fold increased activity against *Anomala corpulenta* larvae [64]. Carvalho et al. reported constructing a combinatorial library of *cry11a* genes truncated and fused to phages, of which four toxin variants were active against *T. licus* ([65].

The targeted evolution of Cry1Ac revealed a T524N variant, which showed increased insecticidal activity against *S. exigua*, and *H. armigera* larvae. This study demonstrated that a single mutation could be critical for insecticidal activity and provides biological evidence for the structural role of domain III [66]. In the same way and to control the lepidopteran *T. licus licus* in sugarcane crops, a D233N mutant of the Cry11a12 variant (Cry11a without the C-terminal end) was generated, which resulted in a mortality rate of 75.43%, while the parental protein showed no toxic activity [58].

1.6.4 Phage display library

Phage display libraries, first introduced in 1985, are a strategy to express peptides on the surface of bacteriophages [67]. The technique is based on the reaction between the peptides produced on the capsid surface, and purified receptors immobilized on a substrate [68]. Protein display on the surface of a phage is a reliable strategy for selecting protein fragments with high binding activity. Non-binding phages are removed by washing, while phages with good binding affinities are retained and can be amplified in *E. coli* and

subjected to subsequent selection rounds. This way, phages with high binding affinity are obtained and can be sequenced to characterize the nucleotide sequence encoding for the peptides of interest [45]. This tool is helpful for the genetic improvement of Cry proteins and, in a later phase, to carry out binding assays to target receptors. The first study on Cry toxins was based on the expression of peptides associated with the domain II in loop 2 of the Cry1Aa protein in phage M13. Although the peptide was expressed, *E. coli* failed to produce the toxin, which opened a new pathway for producing Cry toxins with different activities against insects of public health interest [69].

Table 1. Some studies of mutagenesis were carried out on Cry toxins.

Type of modification	Bt toxin	Target	Reference
Truncation and selection of mutant toxins from a phage library based on binding affinity	Cry11	<i>Telchin licks licus</i>	[58], [70]
Truncation of Helix α -1 of domain I	Cry1A	<i>Pectinophora gossypiella</i>	[71]
Truncation of Helix α -1 of domain I	Cry1A	<i>Plutella xylostella</i> ; <i>Ostrinia nubilalis</i>	[72]
Truncation of the C- and N- terminus	Cry1 HD-1 Dipel	<i>Manduca sexta</i>	[73]
C-Terminal Truncation	Cry1 HD-1	<i>Manduca sexta</i>	[74]
Substitution in loops 1,2 and 3 of domain II	Cry4Ba	<i>Culex pipiens</i> ; <i>C. quinquefasciatus</i>	[75]
Substitution in loops 1 and 2 of domain II	Cry19Aa	<i>Aedes aegypti</i>	[76]
Substitutions and deletions in domain II	Cry1Ab	<i>Lymantria dispar</i>	[68], [77]
Selection of mutant toxins from phage libraries based on binding affinity	Cry1Aa	<i>Bombyx mori</i>	[68]
Selection of mutant toxins from phage libraries based on binding affinity	Cry8Ka	<i>Anthonomus grandis</i>	[78]
Exchange of domain III for that of Cry1Ca	Cry1Ab; Cry1Ac; Cry1Ba; Cry1Ea; Cry1Fa	<i>Spodoptera exigua</i>	[79]
Exchange of domain III for that of Cry1Ac	Cry1Ca; Cry1Fb; Cry1Ba; Cry1Da; Cry1Ea	<i>Heliothis virescens</i>	[69], [79]
Selection of mutant toxins from phage libraries based on binding affinity	Cry8Ka	<i>Anthonomus grandis</i>	[69]
Selection of mutant toxins from phage libraries based on binding affinity	Cry1Aa	<i>Bombyx mori</i>	[80]

1.7 Parasporins

Bt parasporal toxins, such as the Cry and Cyt proteins, are described as crystal-shaped proteins, which have been shown to have toxic effects on disease and pest vector organisms. In addition, these crystals also contain proteins with relevant cytotoxic activity for human cancer cell lines; these are called Parasporins (PS). The interest in parasporins has increased in biotechnological and medical fields, welcoming Bt as one of the most important microorganisms. PS is currently used as a bio-controller and producer of non-insecticidal proteins [81].

The first study on PS was published by Mizuki et al. in 2000 [82]. The authors identified and analyzed isolates of 42 Bt strains without hemolytic or insecticidal activity. Cytotoxic activity was first determined in human lymphoblastic leukemia cell lines in 2006. Six families of parasporins (PS1-PS6) comprising at least 19 proteins produced by about 11 different Bt strain isolates have been identified, mainly in Japan, Vietnam, India, and Canada [83]. No effects were found for any of the 19 proteins against normal cell lines [84].

1.7.1 Parasporins with anti-cancer properties

The interest in parasporins has led to the isolation of Bt strains worldwide. In the Caribbean Islands of Trinidad, 160 isolates of strain 64-1-94 were shown to have cytotoxic activity against several human cancer cell lines. Prasad and Seki, together with their team members, described in the 1970s the existence of a 13 kDa parasporal toxin of a Bt strain that was toxic to *Bombyx mori* and, at the same time, had antitumor activities [85], [86] In 1999, Mizuki et al. carried out a bioprospection study using around 1700 Bt isolates, of which a group of 42 were selected; based on the absence of hemolytic activity, these were all shown to have cytotoxic activity against T cell leukemia [87].

Mizuki and colleagues demonstrated that a non-insecticidal protein containing five conserved building blocks also found in Bt had a very low homology (< 25%) to widely studied Bt proteins such as Cry and Cyt. This protein demonstrated cytotoxic activity against T-cell leukemia and human cervical cancer but no toxic effect against normal cells

[82]. Subsequently, in 2004, Akio et al. used cloning tools to study PS of Bt strain A1547, which belongs to Serovar Dakota. The gene is 1.014 bp and encodes for the PS2Aa1 protein of 338 amino acids with a predicted molecular mass of approximately 37 kDa. Purified PS2Aa1 had potent cytotoxic activity against colon, liver, and leukemia cancer cells, whereas no or negligible activity was found against normal cells [88]. This Bt-derived protein could be potentially used as a novel treatment option with limited side effects, having more potent effects than currently applied treatment approaches such as surgery, radiotherapy, and chemotherapy [88], [89]

In 2005, studies were conducted on parasporal inclusions of Bt strain A1470, which like strain A1547, exhibited a very high toxic effect on leukemia T cells (15). This PS had a high affinity for membrane receptors, which was not described previously. The strict specificity of PS with membrane receptors and lipid molecules was formerly described for other parasporal proteins [88]. At the same time, the authors observed cytotoxic effects such as swelling and fragmentation of cancer cells suggesting that this type of PS alters the ionic permeability of the cell membrane. These data were the starting point for a more focused scientific interest aiming to solve the puzzle of this pronounced specificity and, at the same time, provide insight into the specific receptor(s) PS proteins use to exert their activity [88].

Due to the increase in the number of identified PS proteins, a Committee on the Classification and Nomenclature of Parasporins was formed, and the term "parasporin" was defined as "parasporal proteins from Bt and related bacteria that are not hemolytic but can preferentially kill cancer cells" [90]–[92]. To date, six families of parasporins (PS1-PS6) have been described in only four countries worldwide, such as Japan, Vietnam, India, and Canada [91], [92]. In Table 2, there is a description more extended about the PS family, showing parameters as targets and characteristics, among others.

Table 2. *Families of Parasporins, strains, molecular weight, target cells, and references.*

PS family	Bt strain	Molecular weight kDa	Cytotoxicity shown in Cell line	References
PS1	Bt A1190	81	MOLT-4, HL-60, HepG2, HeLa	(12, 16, 19-21)
PS2	Bt A1547	37	MOLT-4, JURKAT, HL-60, HepG2, Sawano, CACO-2, HCT116.	(16, 21, 22) (6)

PS family	Bt strain	Molecular weight kDa	Cytotoxicity shown in Cell line	References
PS3	Bt A1462	93	HL-60, HepG2	(16, 21, 23)
PS4	Bt A1470	34	MOLT-4, HL-60, HepG2, Sawano, TCS, CACO-2	(16, 21, 24)
PS5	Bt A1100	31	MOLT-4, CACO-2, HepG2, TCS, HeLa, Sawano,	(21, 25)
PS6	Bt M109/CP84	73	HepG2, HeLa, CaCo-2	(19, 21)

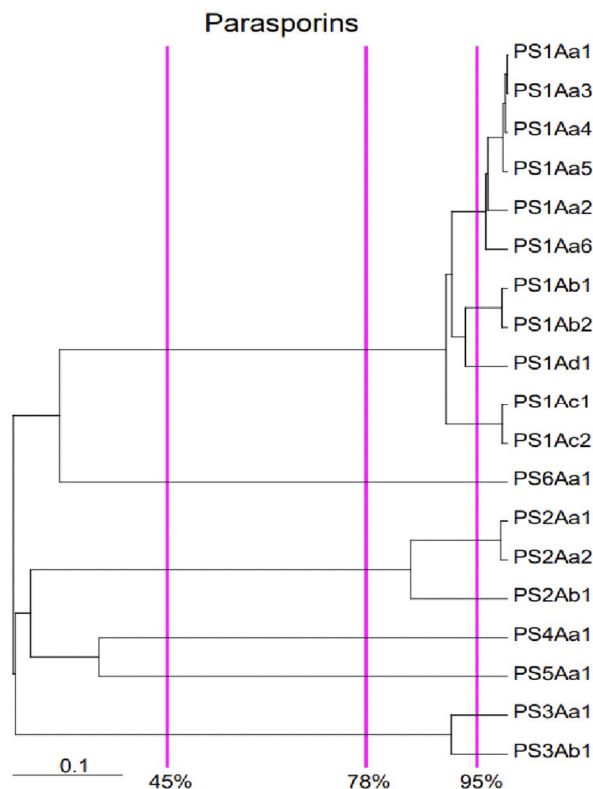
Yasutake, K et al. reported a new gene called *ps1Ac* that was discovered in strains isolated from Vietnamese soils and, like its counterparts, exhibited toxic activity specifically against human cancer cells. One of the goals of this study was to generate the complete sequences of the genes to allow further bioprospecting studies on new PS genes [93]. In 2008, a study conducted by Okumura et al. cloned parasporin 4 (PS4), a protein produced by Bt strain A1470 [94]. Cloning was performed in *E. coli*, and inclusion bodies were solubilized using acidic conditions and purified using an anion-exchange chromatography approach. After purification, PS4 was activated by pepsin and showed cytotoxic activity against CaCO-2 cells equivalent to the protein produced by the conventional method (at alkaline pH) from a Bt strain. There are no other reports of Bt inclusion bodies being dissolved in an acidic solution before purification; this new method allowed isolating PS proteins at a concentration up to 27-fold higher than achieved by the standard method. This contribution is helpful for other studies in which PS4 or other members of the parasporin family are used to treat cell lines or apply it in animal models [94].

This Bt strain has one gene encoding *ps6* and two for *ps1*, which is quite unusual [92]. The two *ps1* genes are approximately 6 kb apart and show a similar spatial arrangement. In addition, these genes have high sequence homology with two *ps1* genes (*ps1Aa6* and *ps1Ad1*) obtained from a Japanese isolate. Moreover, these genes also show homology with a strain from a Canadian isolate. In addition, all three strains shared the presence of a gene encoding the parasporin *ps6*, which is thought to be located on a separate plasmid. The DNA sequences of the genes of the three geographically dispersed strains had a high degree of homology, suggesting that these *ps1* genes have recently become globally distributed. The high homology suggests that the parasporins found in this study share a common role in nature, and it is also logical to assume that these

parasporins (PS1 and PS6) have conserved regions that are required to kill cancer cells [92].

So far, 19 parasporins have been identified, produced by at least 11 Bt strains. Within this group, 11 belong to the PS1 family, 3 to PS2, 2 to PS3, 3 to PS4, PS5, and PS6 (Figure 8).

Figure 8. Dendrogram of parasporins, showing percentages of identity among sequences. Taken from [95].

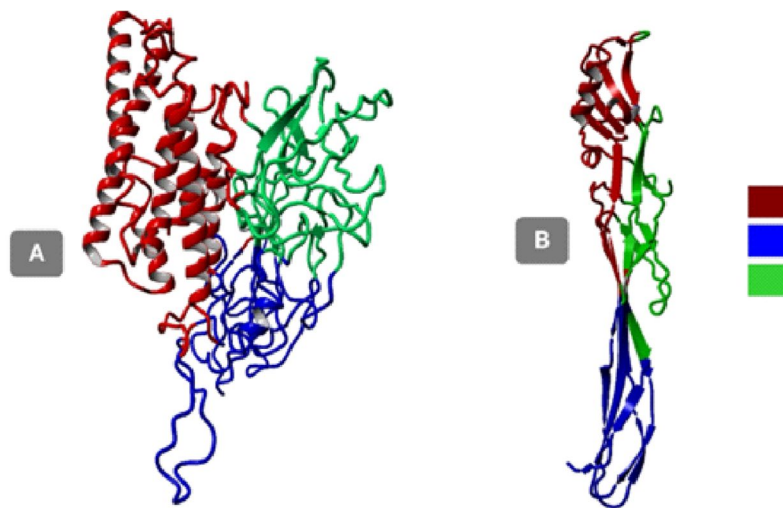


The PS can be divided into two types according to their molecular mass. The group with higher molecular mass includes PS1, PS3, and PS6; the group with lower molecular mass includes PS2 and PS4, and PS5. PSs of the more significant type are expressed as precursor proteins with a molecular mass of about 80 kDa and are processed into active forms of 60 kDa. In contrast, small-type PSs are 30-kDa activated proteins proteolytically processed from precursor proteins with a molecular mass of 33-37 kDa and have a non-conserved three-domain structure (Figure 9). More recently, by 2021, a new nomenclature of these proteins was released [94] (Table 3).

Table 3. *New nomenclature of Parasporins taken from Crickmore . N., et al.. 2021 [94]. Adapted by the author.*

Name	Old name	Other name	Accession number
Mpp45Ba1	Cry45Ba1	Parasporin 4	WP_029440439
Mpp46Aa1	Cry46Aa1	Parasporin 2	BAC79010
Mpp64Aa1	Cry64Aa1	Parasporin 5	BAJ05397
Cry31Aa1	Cry31Aa1	Parasporin 1	BAB11757
Cry41Aa1	Cry41Aa1	Parasporin 3	BAD35157
Cry63Aa1	Cry63Aa1	Parasporin 6	BAI44028

Figure 9. Visualization of models from YASARA, using Geno3D to obtain the PDB files. A. Structural model of higher molecular mass parasporins (PS3Aa1) with its three Domains. B. Structural model of PS2Aa1. Source Author



1.7.2 3D structure of the PS2Aa1 protein

Domain I of PS2Aa1 is a sandwiched structure consisting of a β -hairpin (S6 and S7 for the nontoxic protein; S8 and S9 for PS2Aa) and a lamina. Curved antiparallel five-stranded β -hairpin (S3, S9, S12, S5, and S8 for the nontoxic protein; S5, S6, S7, S10, S11, and S13 in PS2Aa) (Figure 10A) [96], [97]. In parasporin 2, the β -hairpin forms a hydrophobic core with the inner surface of the β -sheet; this surface is covered with hydrophilic residues surrounding the core and stabilized by hydrogen bonds. The organization of the hydrophobic and hydrophilic residues is a critical factor in protein folding [97], [98]. In addition, three of the five β -sheet strands rearrange with the S1 strand

to form a four-stranded β -sheet near domain I, a boundary that associates with the domain I helices through hydrophobic interactions [97].

In *Clostridium septicum* α -toxins, which belong to the aerolysin-type toxin family, domain II is involved in pore formation and may also be responsible for membrane crossing. In one study, site-directed mutagenesis was performed on the amphipathic β -strand of an epsilon toxin, which altered the properties of the channel formed in the lipid bilayer of the cell. The study suggests that domain II may be involved in the insertion and formation of lytic pores [98].

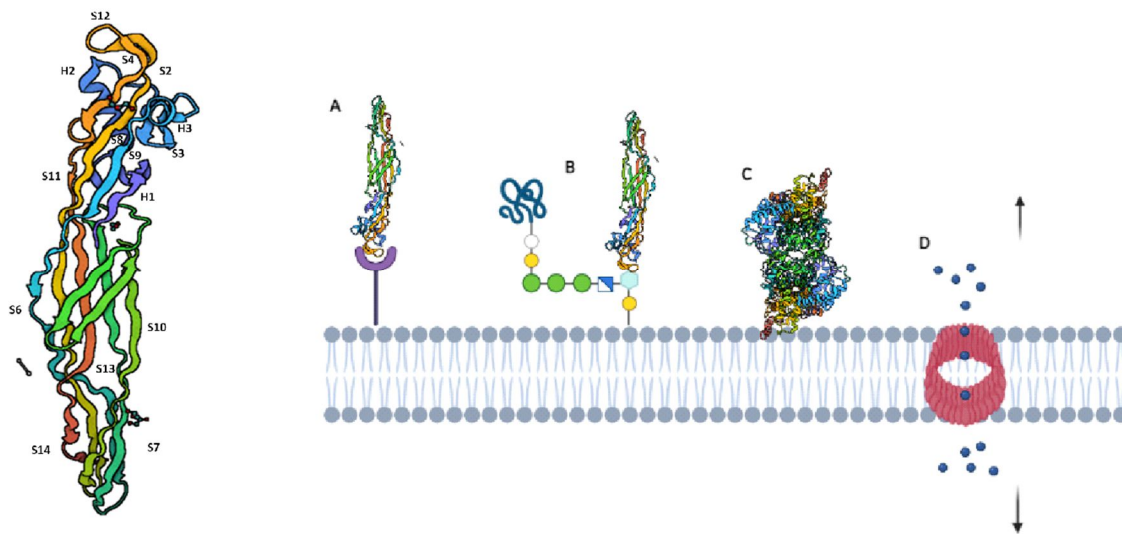
Domain III plays an essential role in the interaction between monomers in the oligomer. In parasporin 2Aa1, the five-stranded β -sheet is rearranged into a three-stranded β -sheet and two antiparallel strands (S6, S11, S13/S14; S7 and S10) (Figure 10A); these two β -sheets form a β -sandwich in this domain, as in domain II [97]. This structure is similar to that of the nontoxic protein of Bt A1470, which terminates in two β -sheets, one with three strands and the other with two strands (S4, S9, and S12; S5 and S8) (Figure 10A) [96]. In PS2Aa, some hydrophobic residues are exposed within the β -sandwich on both sides of the domain, forming small hydrophobic surface patches along the β -strands. A pair of antiparallel β -strands (S4-S8 and S9-S11) (Figure 10A) rotates toward the distal end of the domain, describing two loops [97]. The C-terminal residue is adjacent to this pair of loops and indicates the outer terminus. This residue is removed during proteolytic digestion, exposing part of the hydrophobic core within the β -sandwich to the solvent and creating a hydrophobic zone in the β -strand; thus, the C-terminal residue is essential for oligomerization [98]. Domain III is also involved in pore formation because it has a loop that crosses the membrane [99]

1.7.3 Mechanism of action of PS2Aa1

Parasporins PS2Aa1, PS3Aa1, and PS4Aa1 induce cytotoxicity in cancer cells within 1 hour [88], in contrast to parasporin PS1Aa1, which induces cytotoxicity after 8-10 hours [82]. The mechanisms of action of PS1Aa1 include changes in intracellular Ca^{2+} fluxes that promote the apoptotic cascade associated with caspase activation. PS2Aa1, in turn, causes an increase in the permeability of the plasma membrane of tumor cells

[100]. Therefore, the first step is binding PS2Aa1 to a specific membrane receptor located in lipid rafts of membranes of susceptible cells. This is followed by interaction with the GPI-anchored protein and the glucan region required for binding and assembly in the membrane and the formation of PS2Aa1 oligomers (Figure 10A-C), which leads to pore formation and cell death (Figure 10B-D) [101]. Periyasamy et al. [101] found that one of the possible PS receptors in colon cancer cells is aminopeptidase N (APN) [101]. They showed that the cytotoxic activity of PS2Aa1 decreased when cells were treated with an APN inhibitor, suggesting that the presence of this receptor is essential for its cytotoxic activity. However, the identity of other potential membrane receptors remains unknown.

Figure 10. Structure (A) and mechanism of action of PS2Aa1 (B). Inspired by Xu et al. 2014 [103]. Adapted by author(s).









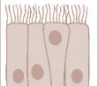
1.7.4 Parasporin 2: a β -type pore-forming protein.

The cytotoxic activity of PS2Aa1 is particularly pronounced for Caco-2, HCT-116, and MOLT-4 (Table 2) [97], [102], [103] PS2Aa1 has been used as a template for various genetic modification strategies [104], [105], including *in silico* and *in vitro* mutagenesis technologies. These studies aimed to obtain a series of biomolecules with anti-cancer activities and to gather information to understand the mode of action of parasporins. The cytotoxicity of PS2Aa1 was determined in Sawano cell lines (0.0017 $\mu\text{g}/\text{mL}$), CaCo-2

(0.013 $\mu\text{g/mL}$), Jurkat (0.018 $\mu\text{g/mL}$), HL60 and HepG2 (0.019 $\mu\text{g/mL}$), and Molt4 (0.022 $\mu\text{g/mL}$) (Xu et al., 2014). Finally, it was shown that cytotoxicity occurs through apoptosis, as determined by the activation of caspases 3/7 [103].

Cancer cells exposed to PS2Aa1 induce apoptosis by activating caspases [103] and triggering increased permeability [106]. The cytotoxic activity of PS2Aa1 is closely linked to its activation by proteinase K, as cleavage by this enzyme exposes specific regions that can subsequently bind to the receptor [103]. The cytotoxic characterization of PS2Aa1 has provided insight into the range of PS2Aa1 required to induce a cytotoxic effect in different cancer cell lines (Table 4). These anti-cancer properties make them candidates for alternatives to current cancer treatment and highlight the need to explore further their properties, mechanisms of action, safety, and availability.

Table 4. Selectivity of PS2Aa1 for some carcinogenic cell lines taken from Xu., et al. 2014 [98]. Adapted by the author.

Cell line	Cancer type		Activity IC ₅₀ $\mu\text{g/mL}$
MOLT-4	T-lymphoblast		0.022
Jurkat	T-lymphocyte		0.018
HL-60	Leukemia		0.019
HepG2	Liver		0.019
HeLa	Cervical		>10
Sawano	Endometrium		0.0017
CaCo-2	Colo-rectal		0.013

1.8 Research problem

Bacillus thuringiensis Bt is a gram-positive, aerobic, spore-forming bacterium recognized worldwide as a source of bioinsecticides. During its sporulation stage, it

produces a crystalline inclusion of proteins called δ -endotoxins (Akiba & Okumura, 2017). They are classified into two families, the crystal (Cry) and cytolytic (Cyt) proteins (Brasseur, et al., (Brasseur, et al., 2015). Cry proteins are characterized by specific insecticidal activity against Lepidoptera, Diptera and Coleoptera (Brasseur, et al., 2015), which has led to a detailed study of the different Bt isolates, considered one of the most representative sources of bioinsecticides on the market (González, et al., 2011). In 1999, some strains that do not have insecticidal activity were found to produce proteins with activity against human cancer cells (Mizuki, et al., 1999); these were termed parasporins (Mizuki, et al., 2000). The definition of parasporins is attributed to bacterial parasporin proteins from Bt or related bacteria that are not hemolytic but can preferentially kill cancer cells (Katayama et al., 2007).

The Molecular Biology and Biotechnology Research Group from the University of Santander, UDES, has excelled and gained extensive experience with Cry proteins of Bt, especially Cry11 in controlling Diptera. At the same time, computational biology and genetic improvement have been used to obtain different populations of proteins with improved activity. As a result of previous work, the laboratory has Cry muteins that share structural features with parasporin 4 and, being the product of a cross of the cry11Aa, Bb, and Ba genes, provide a means of understanding the activity of these proteins. In addition, there is experience with genetic improvement of Cry proteins by random and targeted strategies, which provides an advantage in studying these proteins to control colon cancer proliferation. The interest in improving and testing these proteins arises from the problem posed by the development of this disease in Colombia and its high incidence and mortality worldwide.

Cancer is currently one of the leading causes of death worldwide. According to the World Health Organization, in 2020, there were nearly 10 million deaths worldwide due to various types of cancer, and it is estimated that one in six deaths is due to a type of cancer, making cancer the second leading cause of death (WHO, 2020). The most common cancers worldwide include colorectal cancer and leukemia, which added approximately 2.5 million new cases in 2020 (WHO, 2020). Of these, 474.519 new cases and 311.594 deaths were reported for leukemia, ranking 13th in new cancer cases and 10th in deaths caused by a cancer type (Organization, 2020). On the other hand, 1.930.000 new cases

and 916.000 deaths were reported for colorectal cancer worldwide for the same year, ranking third in new cancer cases and second in cancer-related deaths (Favoriti et al., 2016; WHO, 2020). In Colombia, the outlook is quite discouraging, as some 113.221 Colombians were diagnosed with cancer in 2020, and 54.987 died from it, according to data from WHO. Of these newly reported cases, colorectal cancer accounted for 10,300 (9.1% of total cases) and leukemia for 3.367 (3% of total cases), resulting in 5,313 and 2,192 deaths, respectively (WHO, 2020).

Therefore, it is necessary to explore strategies and molecules for treating various cancers without producing side effects; one of these alternatives is parasporins, proteins produced by Bt (Abe et al., 2008; Chubicka et al., 2018). Currently, several parasporins have been identified by the Parasporin Classification and Nomenclature Committee, divided into six groups (Okumura, S., Ohba, M., Mizuki, E., Crickmore, N., Côté, J.-C., Nagamatsu, Y., Kitada, S., Sakai, H., Harata, K., and Shin, 2010). Among these, PS2Aa1 is characterized by potent cytotoxic activity against leukemia, colon cancer, and lung cancer cell lines, among others, whereas it has little or no detectable effects in non-cancer cells (Abe et al., 2008; Brasseur et al., 2015; Ohba et al., 2009).

Considering this scenario, it is crucial to integrate the experience of the research group in the study of Bt parasporin proteins and genetic improvement to generate relevant knowledge about the structure-function relationship of the parasporin PS2Aa1, leading to the development of alternatives for the control of colon cancer proliferation and contributing to the creation of new treatments that can promote the well-being of the patient. This proposal is in line with the policy of the Ministry of Health outlined in the Ten-Year Plan for Cancer Control in Colombia 2012-2021 regarding knowledge management and technology for cancer control through research on bacterial products with anticancer potentials, such as PS2A1a parasporin.

This project is the first attempt to create a library of new parasporins using the Ps2Aa1 as a mold and different strategies, including *in silico* and *in vitro* site-directed mutagenesis technologies to shed light on the understanding of the mode of action of parasporin and obtain a bank of biomolecules with anticancer activities. This project is in the frame of the NanoBiocancer program, which aims to consolidate a strategic alliance in the field of Nanobioengineering, by articulating and strengthening the research

capacities of HEIs (Higher Education Institutions), the productive sector and research centers in Colombia, linked with several international partners. This program has a translational research approach oriented towards the prevention and “theranostics” (therapy and diagnosis) of cancer, one of the worst health problems in Colombia. Therefore, the results will significantly contribute to improving the country's competitiveness and productivity in the medium term.

1.9 Research question

Based on the research problem arises de following research question: What information can be derived from studying the mutated parasporal of Bt with characterized cytotoxic activity provide relevant scientific information to understand the structure-function relationship of the protein as a promising therapeutic agent for the treatment of colon cancer, among other diseases?

1.10 Aims

This project aims to study parasporin 2Aa1 (PS2Aa1/Mpp46Aa1), focusing on Cry11 and PS2Aa1 as a target for genetic improvement to better understand its mode of action and to create a library of PS2Aa1 variants.

The following specific objectives will lead to accomplishing the main aim:

- To design engineering strategies for Parasporin PS2Aa1, combining directed evolution methodologies, site-specific mutagenesis, structural bioinformatics tools, and the structural and functional knowledge described in the literature to obtain proteins with different potentials to control cancer cell lines growing.
- To analyze the PS2Aa1-APN receptor interactions using computational strategies involving molecular docking and dynamics to explore the possible potential of this membrane receptor to bind to the domain I of this parasporin.
- To produce novel parasporal proteins with enhanced activity against colon cancer cell lines and determine the cytotoxic activity of selected mutant proteins of *Bacillus*

thuringiensis based on their binding affinity to membrane receptors by computational approaches.

This dissertation explores alternatives for a new way to control colorectal cancer cell lines. In this work, an anti-cancer protein parasporin 2Aa1, more recently also called Mpp46Aa1, was used as input for mutagenesis. Various alternatives have been used to obtain mutant biomolecules from PS2Aa1, including peptides from loops 1 and 2 of the domain I. It provided insight into obtaining proteins with substitutions in domain I by a strategy of direct mutagenesis combined with a non-rational technique. In parallel, the anti-cancer activity of the mutant Cry11 pesticide proteins in controlling colon cancer cell lines was demonstrated for the first time.

1.11 Global Methodology of this Work

1.11.1 Chapter 3: Computational study, synthesis and evaluation of active peptides derived from Parasporin-2 and spike protein from Alphacoronavirus against colorectal cancer cells.

The 5-fluorouracil (5- FU), fetal bovine serum (FBS), and sulforhodamine B (SFB) used were obtained from Sigma (Sigma Aldrich, U.S.A.). Dulbecco's modified Eagle's medium (DMEM), L-glutamine, and penicillin/streptomycin were purchased from Lonza (Walkersville, MD, U.S.A.). Trypsin-EDTA was purchased from Invitrogen/Gibco for all experiments related to the detection of the cytotoxic activity of the peptides. Subsequently, the peptides of PS2Aa1 and HCV-229E were synthesized natively using F-moc solid-phase peptide synthesis (SPPS) and the tea bag method described by Houghten. The SW480, SW620, and CHO-K1 cell lines were cultured in 75 cm² flasks containing 10ml of Dulbecco's Modified Eagle Medium (DMEM) containing 10% fetal bovine serum (FBS), 2mM glutamine, 1% MEM non-essential amino acids, 10.000U/ml penicillin, 10.000 g/ml streptomycin, and 25 g/ml amphotericin B. Cells were grown at 37°C in a 5% CO₂ environment.

Evaluation of the cytotoxicity of the tested peptides (P264-G274, Loop1-PS2Aa, Loop2-PS2Aa, and Loop1-HCoV-229E) and 5 FU in noncancerous (CHO -K1) cell lines and human colon cancer cells, SW480 and SW620, were performed using the SFB assay. In addition, SW480 and SW620 cells were seeded at a density of 2×10^5 cells/well in 24-well plates. After 24 hours of incubation, the assay was performed with six replicates for each peptide in SW620 and SW480 cells from the same number of runs. The adherent fraction of the peptide was measured by interpolation with a calibration curve for each peptide. Assay results were expressed as percent binding. The presence of phosphatidylserine at the cell surface was detected with the phosphatidylserine-binding protein annexin V conjugated to Cy3 using the commercially available annexin V-Cy3 apoptosis detection kit (APOAC, Apoptosis Detection Kit, Sigma)

To measure the specific activity of caspase 3 and 7, an assay kit called CellEvent™ Caspase-3/7 Green Detection Reagent (Invitrogen™) was used. Lactate dehydrogenase (LDH) is a cytosolic enzyme found in many different cell types and is released into the cell culture medium when the plasma membrane is damaged. The CyQUANT LDH Cytotoxicity Assay was used to accurately and quantitatively measure this extracellular LDH. The 3D structure of the peptides was predicted using the software PEP-FOLD 3.5, and the 3D structure of the APN receptor was taken from the Protein Data Bank [46] (PDB ID: 6ATK). The highest number of hydrogen bonds and the peptide located near the most abundant residues were selected for refinement using the Rosetta FlexPepDock protocol, all experiments were repeated at least three times. Results were expressed as mean values± standard error (mean± SE). Significant differences between the treatments and their respective controls were determined based on one-way ANOVA followed by Tukey's test. A level of $P < 0.05$ was considered to be significant.

1.11.2 Chapter 4: Site-Directed Mutants of Parasporin PS2Aa1 with Enhanced Cytotoxic Activity in Colorectal Cancer Cell Lines.

Bacillus thuringiensis (Bt) BMB171 and *E. coli* strain DE3BL21 containing the construct pET30a + PS2Aa1 were grown in Luria Bertani (LB) broth for 24 hours at 37 °C with continual agitation. Following that, mutagenesis experiments were performed using

the Gene-Art Site-Directed Mutagenesis Plus kit and four sets of designed primers according to the manufacturer's instructions, and a library verification was performed. The positive clones were grown in LB plates containing kanamycin (25 g/mL). A single colony was chosen and cultivated in 5 mL of LB broth overnight at 37 °C with agitation at 200 rpm. The Wizard Plus SV Minipreps DNA purification technique (Promega®) was used to isolate the plasmid pET-30PS2-Variant. Activated Parasporin Protein from Bt BMB171 variants were grown in LB broth during 5 days at 30 °C to perform the cytotoxic experiments. The cells were then harvested by centrifugation at 10.000 rpm for 10 min. The proteins were digested using proteinase K (final concentration of 185 µg/mL) for 1 h at 37 °C.

Colorectal cancer cell lines obtained from the American Type Culture Collection (ATCC) were used. SW480 and CaCo-2 were grown in Dulbecco's Modified Eagle's Medium (DMEM) supplemented with 10% fetal bovine serum (FBS), 10,000 g/mL penicillin and streptomycin, and 1% nonessential amino acids; SW620 and NCM460 were grown in RPMI supplemented with 10% FBS. Cultures were incubated at 37 °C in a humidified incubator with a 5% CO₂ environment. Activated protein concentrations ranging from 0.25 to 5 g/mL were prepared to assess the antiproliferative effect of the PS2Aa1 and variant toxins. Alamar Blue (BioRad) was used for 5 hours at 37°C in a 5% CO₂ environment. In addition, APN was detected and blocked using the antibody CD13/APN (Cell Signaling Technology®) and GAPDH as a loading control in a Western blot.

After that, a molecular dynamics analysis and molecular docking were done to investigate potential interactions between PS2Aa1 and the APN receptor. The 3D structures of PS2Aa1 and APN were retrieved from the Protein Data Bank using PDB IDs 2ZTB and 6ATK, respectively. The chosen model was used to execute molecular dynamics (MD) simulations in triplicate for PS2Aa1-APN complexes. Statistical Analysis Type 1 ANOVA and Tukey's test were performed using GraphPad Prism 8. * p 0.05, ** p 0.01, and *** p 0.001 were used to indicate statistical significance with a 95% confidence interval.

1.11.3 Chapter 5: Toxic Determination of Cry11 Mutated Proteins Obtained Using Rational Design and Its Computational Analysis.

In this work, the strain *Escherichia coli* DE3BL21 and chloramphenicol 10 µg/mL were used for the transformants of the non-crystal forming strain Bt BMB171. Plasmid DNA was then extracted using the Wizard Minipreps Kit (Promega®, Madison, WI, USA). Then, strategic rational design and synthesis of variant 8 mutants and Cry11Bb library variants were performed. The latter were designed based on toxin-receptor interaction. In addition, a final complete culture (FCC) of Bt mutants L553F, L556W, L553F-L556W, A92D, and C157R, as well as recombinants expressing Cry11Aa and Cry11Bb toxins, were grown together with the non-crystallizing strain Bt BMB171 in 10 mL LB broth containing 10 µg*mL⁻¹ chloramphenicol.

To verify the presence of the Cry proteins, Protein electrophoresis using Sodium Dodecyl Sulfate-Polyacrylamide Gel Electrophoresis (SDS-PAGE) was performed to confirm the presence of Cry proteins. A 10% acrylamide gel was used to run the samples. The gel and electrophoretic run were prepared according to the procedure book's directions by Sambrook Protein Preparation and Half-Lethal Concentration (LC₅₀). Following that, the cultures of each mutant dissolved in PBS 1 were treated to heat stress as follows: 100 L of each culture was incubated at 72 °C for 20 minutes, followed by 10 minutes at 4 °C. For the first time, assays were performed to detect the potential of Cry Variants in the control of human colorectal cancer cells. Briefly, 10 L of Alamar blue was added to each well and incubated for 4-6 h to measure the fluorescence (Ex 560 nm and Em 590 nm) and thus determine the IC₅₀.

Cry11 variation structure modeling was also obtained. To build Cry11 mutants, a de novo modeling technique was devised to analyze two Cry11 variant structures (variation 8 and Cry11Bb). To fit the model, it used a de novo prediction method called the rosetta generation of additional variants, and model sampling. By executing single-point mutations on the variation 8 and Cry11Bb structures, a new set of variants was predicted based on the initial models.

1.12 Scope of the thesis

This thesis is related to parasporal proteins of Bt, focusing on PS2Aa1 proteins as starting points for genetic improvement to increase our understanding of its mode of action. It may lead to the generation of alternative therapeutic tools based on bacterial bioproducts that could be used to treat cancer or other diseases.

Chapter 1 provides a summary of the general characteristics of Bt, an exploration of the uses of the Parasporal proteins, details of the structure and mechanism of action of PS2Aa1 (Mpp46Aa1), and Cry 11, which is known as a biocontrol agent for vector-borne diseases but whose cytotoxic effect on colorectal cancer cell lines has only now been reported. **Chapter 2** presents a compendium of academic information on parasporins PS, describing their structures and mechanisms of action. This knowledge indicates the possibility of using site-directed mutagenesis techniques to improve the effectiveness of PS. In **Chapter 3**, It presents the first study to define the PS2Aa2-derived peptides that interact with the cell membrane of colorectal cancer cell lines. The data obtained suggest that native peptide fragments of PS2Aa1 can be optimized as new potential cancer therapeutics. In **Chapter 4**, we set out to generate a library of PS2Aa1 variants using a site-directed mutagenesis strategy. These variants were characterized by *in vitro* and *silico* methods. The data suggest that some PS2Aa1 residues are relevant for interacting with PS2Aa1 and the APN membrane receptor. **Chapter 5**, about summary, discussion, and future perspectives, contains relevant findings of each chapter and some indications of why we have reached the conclusions. Forward, we propose the incorporation of new strategies such as nanoparticles, nanobioconjugates, and personalized medicine to make Bt-derived proteins more stable and robust so that they can be used to combat cancer cell lines.

1.13 References

1. H. Loutfi *et al.*, "Morphological Study of Bacillus thuringiensis Crystals and Spores," *Applied Sciences* 2021, Vol. 11, Page 155, vol. 11, no. 1, p. 155, Dec. 2020, doi: 10.3390/APP11010155.

2. D. Fernández-Chapa, J. Ramírez-Villalobos, and L. Galán-Wong, "Toxic Potential of *Bacillus thuringiensis*: An Overview," *Protecting Rice Grains in the Post-Genomic Era*, Jun. 2019, doi: 10.5772/INTECHOPEN.85756.\
3. L. D. A. Melo, V. T. Soccol, and C. R. Soccol, "Bacillus thuringiensis: mechanism of action, resistance, and new applications: a review," *Crit Rev Biotechnol*, vol. 36, no. 2, pp. 317–326, Mar. 2016, doi: 10.3109/07388551.2014.960793.
4. L. A. Lacey, D. Grzywacz, D. I. Shapiro-Ilan, R. Frutos, M. Brownbridge, and M. S. Goettel, "Insect pathogens as biological control agents: Back to the future," *J Invertebr Pathol*, vol. 132, pp. 1–41, 2015, doi: 10.1016/j.jip.2015.07.009.
5. D. Jain, V. Saharan, and S. Pareek, "Current status of Bacillus thuringiensis: Insecticidal crystal proteins and transgenic crops," *Advances in Plant Breeding Strategies: Agronomic, Abiotic and Biotic Stress Traits*, vol. 2, pp. 657–698, Jan. 2016, doi: 10.1007/978-3-319-22518-0_18.
6. R. Radhakrishnan, A. Hashem, and E. F. Abd Allah, "Bacillus: A Biological Tool for Crop Improvement through Bio-Molecular Changes in Adverse Environments," *Front Physiol*, vol. 8, no. SEP, p. 667, Sep. 2017, doi: 10.3389/FPHYS.2017.00667.
7. Iatsenko, A. Nikolov, and R. J. Sommer, "Identification of Distinct Bacillus thuringiensis 4A4 Nematicidal Factors Using the Model Nematodes *Pristionchus pacificus* and *Caenorhabditis elegans*," *Toxins (Basel)*, vol. 6, no. 7, p. 2050, 2014, doi: 10.3390/TOXINS6072050.
8. Periyasamy *et al.*, "Screening and characterization of a non-insecticidal Bacillus thuringiensis strain producing parasporal protein with selective toxicity against human colon cancer cell lines," *Ann Microbiol*, vol. 66, no. 3, pp. 1167–1178, Sep. 2016, doi: 10.1007/S13213-016-1204-8/FIGURES/6.
9. E. Aceves-Diez, K. J. Estrada-Castañeda, and L. M. Castañeda-Sandoval, "Use of bacillus thuringiensis supernatant from a fermentation process to improve bioremediation of chlorpyrifos in contaminated soils," *J Environ Manage*, vol. 157, pp. 213–219, Jul. 2015, doi: 10.1016/J.JENVMAN.2015.04.026.
10. D. Singh and D. Kumar Yadav, "Potential of Bacillus amyloliquefaciens for Biocontrol of Bacterial Wilt of Tomato Incited by *Ralstonia solanacearum*," *J Plant Pathol Microbiol*, vol. 07, no. 01, 2016, doi: 10.4172/2157-7471.1000327.
11. Roy, D. Mahata, D. Paul, S. Korpole, O. L. Franco, and S. M. Mandal, "Purification, biochemical characterization and self-assembled structure of a fengycin-like antifungal peptide from Bacillus thuringiensis strain SM1," *Front Microbiol*, vol. 4, no. NOV, 2013, doi: 10.3389/FMICB.2013.00332.
12. G. S. Jouzani, E. Valijanian, and R. Sharafi, "Bacillus thuringiensis: a successful insecticide with new environmental features and tidings," *Applied Microbiology and*

- Biotechnology* 2017 101:7, vol. 101, no. 7, pp. 2691–2711, Feb. 2017, doi: 10.1007/S00253-017-8175-Y.
13. W. Jallouli, F. Driss, L. Fillaudeau, and S. Rouis, “Review on biopesticide production by *Bacillus thuringiensis* subsp. *kurstaki* since 1990: Focus on bioprocess parameters,” *Process Biochemistry*, vol. 98, pp. 224–232, Nov. 2020, doi: 10.1016/J.PROCBIO.2020.07.023.
 14. M. C. Gonzalez-Vazquez, R. A. Vela-Sanchez, N. E. Rojas-Ruiz, and A. Carabarin-Lima, “Importance of Cry Proteins in Biotechnology: Initially a Bioinsecticide, Now a Vaccine Adjuvant,” *Life* 2021, Vol. 11, Page 999, vol. 11, no. 10, p. 999, Sep. 2021, doi: 10.3390/LIFE11100999.
 15. Mukhija and V. Khanna, “Cry Protein Profiling of *Bacillus thuringiensis* Isolated from Different Agro-Climate Soils of Punjab,” *Int J Curr Microbiol Appl Sci*, vol. 7, no. 03, pp. 2866–2870, Mar. 2018, doi: 10.20546/IJCMAS.2018.703.330.
 16. Bravo, S. Likitvivatanavong, S. S. Gill, and M. Soberón, “*Bacillus thuringiensis*: A story of a successful bioinsecticide,” *Insect Biochem Mol Biol*, vol. 41, no. 7, pp. 423–431, Jul. 2011, doi: 10.1016/J.IBMB.2011.02.006.
 17. Y. Liu *et al.*, “Cry64Ba and Cry64Ca, two ETX/MTX2-type *Bacillus thuringiensis* insecticidal proteins active against hemipteran pests,” *Appl Environ Microbiol*, vol. 84, no. 3, 2018, doi: 10.1128/AEM.01996-17.
 18. N. Crickmore *et al.*, “Revision of the Nomenclature for the *Bacillus thuringiensis* Pesticidal Crystal Proteins,” *Microbiology and Molecular Biology Reviews*, vol. 62, no. 3, p. 807, Sep. 1998, doi: 10.1128/MMBR.62.3.807-813.1998.
 19. “Revision of the Nomenclature for the *Bacillus thuringiensis* Pesticidal Crystal Proteins - PMC.” <https://www.ncbi.nlm.nih.gov/pmc/articles/PMC98935/> (accessed Aug. 22, 2022).
 20. N. Crickmore, C. Berry, S. Panneerselvam, R. Mishra, T. R. Connor, and B. C. Bonning, “A structure-based nomenclature for *Bacillus thuringiensis* and other bacteria-derived pesticidal proteins,” *J Invertebr Pathol*, vol. 186, Nov. 2021, doi: 10.1016/J.JIP.2020.107438.
 21. Bravo *et al.*, “Mechanism of action of *Bacillus thuringiensis* insecticidal toxins and their use in the control of insect pests,” *The Comprehensive Sourcebook of Bacterial Protein Toxins*, pp. 858–873, Jun. 2015, doi: 10.1016/B978-0-12-800188-2.00030-6.
 22. K. Srisucharitpanit, M. Yao, B. Promdonkoy, S. Chimnaronk, I. Tanaka, and P. Boonserm, “Crystal structure of BinB: a receptor binding component of the binary toxin from *Lysinibacillus sphaericus*,” *Proteins*, vol. 82, no. 10, pp. 2703–2712, Oct. 2014, doi: 10.1002/PROT.24636.

23. T. Akiba *et al.*, “Crystal structure of the parasporin-2 *Bacillus thuringiensis* toxin that recognizes cancer cells,” *J Mol Biol*, vol. 386, no. 1, pp. 121–133, Feb. 2009, doi: 10.1016/J.JMB.2008.12.002.
24. O. Alzate, C. Osorio, A. M. Florez, and D. H. Dean, “Participation of valine 171 in alpha-Helix 5 of *Bacillus thuringiensis* Cry1Ab delta-endotoxin in translocation of toxin into *Lymantria dispar* midgut membranes,” *Appl Environ Microbiol*, vol. 76, no. 23, pp. 7878–7880, Dec. 2010, doi: 10.1128/AEM.01428-10.
25. R. Adalat, F. Saleem, N. Crickmore, S. Naz, and A. R. Shakoori, “In Vivo Crystallization of Three-Domain Cry Toxins,” *Toxins (Basel)*, vol. 9, no. 3, Mar. 2017, doi: 10.3390/TOXINS9030080.
26. L. E. Fernandez *et al.*, “Cloning and Epitope Mapping of Cry11Aa-Binding Sites in the Cry11Aa-Receptor Alkaline Phosphatase from *Aedes aegypti*,” *Biochemistry*, vol. 48, no. 37, p. 8899, Sep. 2009, doi: 10.1021/BI900979B.
27. E. Schnepf *et al.*, “*Bacillus thuringiensis* and its pesticidal crystal proteins,” *Microbiol Mol Biol Rev*, vol. 62, no. 3, pp. 775–806, Sep. 1998, doi: 10.1128/MMBR.62.3.775-806.1998.
28. Bravo, S. S. Gill, and M. Soberón, “Mode of action of *Bacillus thuringiensis* Cry and Cyt toxins and their potential for insect control,” *Toxicon*, vol. 49, no. 4, pp. 423–435, Mar. 2007, doi: 10.1016/J.TOXICON.2006.11.022.
29. Q. Zhang, G. Hua, and M. J. Adang, “Effects and mechanisms of *Bacillus thuringiensis* crystal toxins for mosquito larvae,” *Insect Sci*, vol. 24, no. 5, pp. 714–729, Oct. 2017, doi: 10.1111/1744-7917.12401.
30. J. Derbyshire, D. J. Ellar, and J. Li, “Crystallization of the *Bacillus thuringiensis* toxin Cry1Ac and its complex with the receptor ligand N-acetyl-D-galactosamine,” *Acta Crystallogr D Biol Crystallogr*, vol. 57, no. Pt 12, pp. 1938–1944, 2001, doi: 10.1107/S090744490101040X.
31. R. A. de Maagd *et al.*, “Domain III substitution in *Bacillus thuringiensis* delta-endotoxin CryIA(b) results in superior toxicity for *Spodoptera exigua* and altered membrane protein recognition,” *Appl Environ Microbiol*, vol. 62, no. 5, pp. 1537–1543, 1996, doi: 10.1128/AEM.62.5.1537-1543.1996.
32. L. Melo, V. T. Soccol, and C. R. Soccol, “*Bacillus thuringiensis*: mechanism of action, resistance, and new applications: a review,” *Crit Rev Biotechnol*, pp. 1–10, 2015, doi: 10.3109/07388551.2014.960793.
33. M. L. Marcos and J. Echave, “Too packed to change: Side-chain packing and site-specific substitution rates in protein evolution,” *PeerJ*, vol. 2015, no. 3, 2015, doi: 10.7717/PEERJ.911/SUPP-1.

34. M. Soberon, S. S. Gill, and A. Bravo, "Signaling versus punching hole: How do *Bacillus thuringiensis* toxins kill insect midgut cells?," *Cell Mol Life Sci*, vol. 66, no. 8, pp. 1337–1349, 2009, [Online]. Available: http://www.ncbi.nlm.nih.gov/entrez/query.fcgi?cmd=Retrieve&db=PubMed&dopt=Citation&list_uids=19132293
35. X. Zhang, M. Candas, N. B. Griko, R. Taussig, and L. A. Bulla Jr., "A mechanism of cell death involving an adenylyl cyclase/PKA signaling pathway is induced by the Cry1Ab toxin of *Bacillus thuringiensis*," *Proc Natl Acad Sci U S A*, vol. 103, no. 26, pp. 9897–9902, 2006, [Online]. Available: http://www.ncbi.nlm.nih.gov/entrez/query.fcgi?cmd=Retrieve&db=PubMed&dopt=Citation&list_uids=16788061
36. Fernández-Chapa, J. Ramírez-Villalobos, and L. Galán-Wong, "Toxic Potential of *Bacillus thuringiensis*: An Overview," *Protecting Rice Grains in the Post-Genomic Era*, Jun. 2019, doi: 10.5772/INTECHOPEN.85756.
37. S. Pacheco *et al.*, "Helix α -3 inter-molecular salt bridges and conformational changes are essential for toxicity of *Bacillus thuringiensis* 3D-Cry toxin family," *Scientific Reports 2018 8:1*, vol. 8, no. 1, pp. 1–11, Jul. 2018, doi: 10.1038/s41598-018-28753-8.
38. H. Endo, "Molecular and Kinetic Models for Pore Formation of *Bacillus thuringiensis* Cry Toxin," *Toxins 2022, Vol. 14, Page 433*, vol. 14, no. 7, p. 433, Jun. 2022, doi: 10.3390/TOXINS14070433.
39. M. Land and M. Miljand, "Biological control of mosquitoes using *Bacillus thuringiensis israelensis*: a pilot study of effects on target organisms , non-target organisms and humans A Pilot Study," 2014.
40. C. Xu, B. C. Wang, Z. Yu, and M. Sun, "Structural insights into *Bacillus thuringiensis* Cry, Cyt and parasporin toxins," *Toxins (Basel)*, vol. 6, no. 9, pp. 2732–2770, Sep. 2014, doi: 10.3390/TOXINS6092732.
41. C. R. Pigott and D. J. Ellar, "Role of receptors in *Bacillus thuringiensis* crystal toxin activity," *Microbiol Mol Biol Rev*, vol. 71, no. 2, pp. 255–281, Jun. 2007, doi: 10.1128/MMBR.00034-06.
42. O. Carvalho, A. L. Costa-da-Silva, R. S. Lees, and M. L. Capurro, "Two step male release strategy using transgenic mosquito lines to control transmission of vector-borne diseases," *Acta Trop*, vol. 132 Suppl, pp. S170–7, 2014, doi: 10.1016/j.actatropica.2013.09.023.
43. U. Fillinger and S. W. Lindsay, "Suppression of exposure to malaria vectors by an order of magnitude using microbial larvicides in rural Kenya," *Trop Med Int Health*, vol. 11, no. 11, pp. 1629–1642, 2006, doi: 10.1111/j.1365-3156.2006.01733.

44. H. W. Park *et al.*, "Cyt1Aa from *Bacillus thuringiensis* subsp. *israelensis* enhances mosquitocidal activity of *B. thuringiensis* subsp. *kurstaki* HD-1 against *Aedes aegypti* but not *Culex quinquefasciatus*," *J Microbiol Biotechnol*, vol. 23, no. 1, pp. 88–91, 2013, [Online]. Available: <http://www.ncbi.nlm.nih.gov/pubmed/23314373>
45. B. R. Deist, M. A. Rausch, M. T.eresa Fernandez-Luna, M. J. Adang, and B. C. Bonning, "Bt toxin modification for enhanced efficacy," *Toxins (Basel)*, vol. 6, no. 10, pp. 3005–3027, 2014, doi: 10.3390/toxins6103005.
46. P. Servant, M. L. Rosso, S. Hamon, S. Poncet, A. del cluse, and G. Rapoport, "Production of Cry11A and Cry11Ba toxins in *Bacillus sphaericus* confers toxicity towards *Aedes aegypti* and resistant *Culex* populations," *Appl Environ Microbiol*, vol. 65, no. 7, pp. 3021–3026, 1999, [Online]. Available: <http://www.ncbi.nlm.nih.gov/pubmed/10388698>
47. H. W. Park, A. Delecluse, and B. A. Federici, "Construction and characterization of a recombinant *Bacillus thuringiensis* subsp. *israelensis* strain that produces Cry11B," *J Invertebr Pathol*, vol. 78, no. 1, pp. 37–44, 2001, doi: 10.1006/jipa.2001.5038.
48. H. Pinzón-Reyes, D. A. Sierra-Bueno, M. O. Suarez-Barrera, N. J. Rueda-Forero, S. Abaunza-Villamizar, and P. Rondón-Villareal, "Generation of Cry11 Variants of *Bacillus thuringiensis* by Heuristic Computational Modeling," *Evol Bioinform Online*, vol. 16, 2020, doi: 10.1177/1176934320924681.
49. M. Florez *et al.*, "Toxic Activity, Molecular Modeling and Docking Simulations of *Bacillus thuringiensis* Cry11 Toxin Variants Obtained via DNA Shuffling," *Front Microbiol*, vol. 9, no. 2461, 2018, doi: 10.3389/fmicb.2018.02461.
50. L. E. Fernández *et al.*, "Cry11Aa toxin from *Bacillus thuringiensis* binds its receptor in *Aedes aegypti* mosquito larvae through loop alpha-8 of domain II," *FEBS Lett*, vol. 579, no. 17, pp. 3508–3514, Jul. 2005, doi: 10.1016/J.FEBSLET.2005.05.032.
51. D. H. Sauka, R. H. Monella, and G. B. Benintende, "Detection of the mosquitocidal toxin genes encoding Cry11 proteins from *Bacillus thuringiensis* using a novel PCR-RFLP method," *Rev Argent Microbiol*, vol. 42, no. 1, pp. 23–26, Jan. 2010, doi: 10.1590/S0325-75412010000100005.
52. M. Arias, S. Orduz, and V. v Lemeshko, "Potential-dependent permeabilization of plasma membrane by the peptide BTM-P1 derived from the Cry11Bb1 protoxin," *Biochim Biophys Acta Biomembr*, vol. 1788, no. 2, pp. 532–537, Feb. 2009, doi: 10.1016/j.bbamem.2008.12.009.
53. M. Florez *et al.*, "Toxic Activity, Molecular Modeling and Docking Simulations of *Bacillus thuringiensis* Cry11 Toxin Variants Obtained via DNA Shuffling," *Front Microbiol*, vol. 9, no. OCT, Oct. 2018, doi: 10.3389/FMICB.2018.02461.

54. S. Orduz, M. Realpe, R. Arango, L. A. Murillo, and A. Delécluse, "Sequence of the cry11Bb1 gene from *Bacillus thuringiensis* subsp. medellin and toxicity analysis of its encoded protein," *Biochimica et Biophysica Acta (BBA) - Protein Structure and Molecular Enzymology*, vol. 1388, no. 1, pp. 267–272, Oct. 1998, doi: 10.1016/S0167-4838(98)00168-X.
55. B. R. Deist, M. A. Rausch, M. T. Fernandez-Luna, M. J. Adang, and B. C. Bonning, "Bt toxin modification for enhanced efficacy," *Toxins (Basel)*, vol. 6, no. 10, pp. 3005–3027, 2014, [Online]. Available: http://www.ncbi.nlm.nih.gov/entrez/query.fcgi?cmd=Retrieve&db=PubMed&dopt=Citation&list_uids=25340556
56. Y. Pang, R. Frutos, and B. A. Federici, "Synthesis and toxicity of full-length and truncated bacterial CryIVD mosquitocidal proteins expressed in lepidopteran cells using a baculovirus vector," *J Gen Virol*, vol. 73 (Pt 1), pp. 89–101, 1992, [Online]. Available: http://www.ncbi.nlm.nih.gov/entrez/query.fcgi?cmd=Retrieve&db=PubMed&dopt=Citation&list_uids=1730944
57. T. Hayakawa, M. T. Howlader, M. Yamagiwa, and H. Sakai, "Design and construction of a synthetic *Bacillus thuringiensis* Cry4Aa gene: hyperexpression in *Escherichia coli*," *Appl Microbiol Biotechnol*, vol. 80, no. 6, pp. 1033–1037, 2008, [Online]. Available: http://www.ncbi.nlm.nih.gov/entrez/query.fcgi?cmd=Retrieve&db=PubMed&dopt=Citation&list_uids=18751699
58. K. I. Craveiro *et al.*, "Variant Cry1Ia toxins generated by DNA shuffling are active against sugarcane giant borer," *J Biotechnol*, vol. 145, no. 3, pp. 215–221, 2010, [Online]. Available: http://www.ncbi.nlm.nih.gov/entrez/query.fcgi?cmd=Retrieve&db=PubMed&dopt=Citation&list_uids=19931577
59. J. Carroll, D. Convents, J. van Damme, A. Boets, J. van Rie, and D. J. Ellar, "Intramolecular proteolytic cleavage of *Bacillus thuringiensis* Cry3A delta-endotoxin may facilitate its coleopteran toxicity," *J Invertebr Pathol*, vol. 70, no. 1, pp. 41–49, 1997, doi: 10.1006/jjpa.1997.4656.
60. R. A. de Maagd, A. Bravo, C. Berry, N. Crickmore, and H. E. Schnepf, "Structure, diversity, and evolution of protein toxins from spore-forming entomopathogenic bacteria," *Annu Rev Genet*, vol. 37, pp. 409–433, 2003, [Online]. Available: http://www.ncbi.nlm.nih.gov/entrez/query.fcgi?cmd=Retrieve&db=PubMed&dopt=Citation&list_uids=14616068
61. L. Zhang *et al.*, "Susceptibility of Cry1Ab maize-resistant and -susceptible strains of sugarcane borer (*Lepidoptera*: Crambidae) to four individual Cry proteins," *J Invertebr Pathol*, vol. 112, no. 3, pp. 267–272, 2013, doi: 10.1016/j.jip.2012.12.007

- A. S. Walters, C. M. DeFontes, H. Hart, G. W. Warren, and J. S. Chen, "Lepidopteran-active variable-region sequence imparts coleopteran activity in eCry3.1Ab, an engineered *Bacillus thuringiensis* hybrid insecticidal protein," *Appl Environ Microbiol*, vol. 76, no. 10, pp. 3082–3088, 2010, [Online]. Available: http://www.ncbi.nlm.nih.gov/entrez/query.fcgi?cmd=Retrieve&db=PubMed&dopt=Citation&list_uids=20305020
62. W. P. Stemmer, "Rapid evolution of a protein in vitro by DNA shuffling," *Nature*, vol. 370, no. 6488, pp. 389–391, 1994, [Online]. Available: http://www.ncbi.nlm.nih.gov/entrez/query.fcgi?cmd=Retrieve&db=PubMed&dopt=Citation&list_uids=8047147
63. C. Shu *et al.*, "Improving toxicity of *Bacillus thuringiensis* strain contains the cry8Ca gene specific to *Anomala corpulenta* larvae," *Curr Microbiol*, vol. 55, no. 6, pp. 492–496, 2007, [Online]. Available: http://www.ncbi.nlm.nih.gov/entrez/query.fcgi?cmd=Retrieve&db=PubMed&dopt=Citation&list_uids=17805927
64. V. F. Carvalho, A. M. Vacari, A. F. Pomari, C. P. de Bortoli, D. G. Ramalho, and S. A. de Bortoli, "Interaction between the predator *Podisus nigrispinus* (Hemiptera: Pentatomidae) and the entomopathogenic bacteria *Bacillus thuringiensis*," *Environ Entomol*, vol. 41, no. 6, pp. 1454–1461, 2012, [Online]. Available: http://www.ncbi.nlm.nih.gov/entrez/query.fcgi?cmd=Retrieve&db=PubMed&dopt=Citation&list_uids=23321092
65. S. Shan *et al.*, "A Cry1Ac toxin variant generated by directed evolution has enhanced toxicity against Lepidopteran insects," *Curr Microbiol*, vol. 62, no. 2, pp. 358–365, 2011, [Online]. Available: http://www.ncbi.nlm.nih.gov/entrez/query.fcgi?cmd=Retrieve&db=PubMed&dopt=Citation&list_uids=20669019
66. Rami, M. Behdani, N. Yardehnavi, M. Habibi-Anbouhi, and F. Kazemi-Lomedasht, "An overview on application of phage display technique in immunological studies," *Asian Pac J Trop Biomed*, vol. 7, no. 7, pp. 599–602, Jul. 2017, doi: 10.1016/J.APJTb.2017.06.001.
67. Y. Fujii, S. Tanaka, M. Otsuki, Y. Hoshino, H. Endo, and R. Sato, "Affinity maturation of Cry1Aa toxin to the *Bombyx mori* cadherin-like receptor by directed evolution," *Mol Biotechnol*, vol. 54, no. 3, pp. 888–899, 2013, [Online]. Available:
68. R. Oliveira *et al.*, "Improving Cry8Ka toxin activity towards the cotton boll weevil (*Anthonomus grandis*)," *BMC Biotechnol*, vol. 11, p. 85, 2011, [Online]. Available: http://www.ncbi.nlm.nih.gov/entrez/query.fcgi?cmd=Retrieve&db=PubMed&dopt=Citation&list_uids=21906288
69. M. Soberon, L. Pardo-Lopez, I. Lopez, I. Gomez, B. E. Tabashnik, and A. Bravo, "Engineering modified Bt toxins to counter insect resistance," *Science (1979)*, vol. 318, no. 5856, pp. 1640–1642, 2007, doi: 10.1126/science.1146453.

70. M. Soberón, L. Pardo-López, I. López, I. Gómez, B. E. Tabashnik, and A. Bravo, "Engineering modified Bt toxins to counter insect resistance," *Science* (1979), vol. 318, no. 5856, pp. 1640–1642, Dec. 2007, doi: 10.1126/science.1146453.
71. B. E. Tabashnik *et al.*, "Efficacy of genetically modified Bt toxins against insects with different genetic mechanisms of resistance," *Nat Biotechnol*, vol. 29, no. 12, pp. 1128–1131, 2011, doi: 10.1038/nbt.1988.
72. E. Schnepf and H. R. Whiteley, "Delineation of a toxin-encoding segment of a *Bacillus thuringiensis* crystal protein gene," *J Biol Chem*, vol. 260, no. 10, pp. 6273–6280, 1985, [Online]. Available: <http://www.ncbi.nlm.nih.gov/pubmed/3888979>
73. C. Angelucci *et al.*, "Diversity of aminopeptidases, derived from four lepidopteran gene duplications, and polycalins expressed in the midgut of *Helicoverpa armigera*: identification of proteins binding the delta-endotoxin, Cry1Ac of *Bacillus thuringiensis*," *Insect Biochem Mol Biol*, vol. 38, no. 7, pp. 685–696, 2008, [Online]. Available: http://www.ncbi.nlm.nih.gov/entrez/query.fcgi?cmd=Retrieve&db=PubMed&dopt=Citation&list_uids=18549954
74. M. A. Abdullah, O. Alzate, M. Mohammad, R. J. McNall, M. J. Adang, and D. H. Dean, "Introduction of *Culex* toxicity into *Bacillus thuringiensis* Cry4Ba by protein engineering," *Appl Environ Microbiol*, vol. 69, no. 9, pp. 5343–5353, 2003, [Online]. Available: http://www.ncbi.nlm.nih.gov/entrez/query.fcgi?cmd=Retrieve&db=PubMed&dopt=Citation&list_uids=12957922
75. [M. A. Abdullah and D. H. Dean, "Enhancement of Cry19Aa mosquitocidal activity against *Aedes aegypti* by mutations in the putative loop regions of domain II," *Appl Environ Microbiol*, vol. 70, no. 6, pp. 3769–3771, 2004, [Online]. Available: http://www.ncbi.nlm.nih.gov/entrez/query.fcgi?cmd=Retrieve&db=PubMed&dopt=Citation&list_uids=15184189
76. F. Rajamohan, O. Alzate, J. A. Cotrill, A. Curtiss, and D. H. Dean, "Protein engineering of *Bacillus thuringiensis* δ -endotoxin: Mutations at domain II of CryIAb enhance receptor affinity and toxicity toward gypsy moth larvae," *Proc Natl Acad Sci U S A*, vol. 93, no. 25, pp. 14338–14343, 1996, doi: 10.1073/pnas.93.25.14338.
77. R. A. de Maagd, M. Weemen-Hendriks, W. Stiekema, and D. Bosch, "*Bacillus thuringiensis* delta-endotoxin Cry1C domain III can function as a specificity determinant for *Spodoptera exigua* in different, but not all, Cry1-Cry1C hybrids," *Appl Environ Microbiol*, vol. 66, no. 4, pp. 1559–1563, 2000, [Online]. Available: <http://www.ncbi.nlm.nih.gov/pubmed/10742242>
78. R. Karlova, M. Weemen-Hendriks, S. Naimov, J. Ceron, S. Dukiandjiev, and R. A. de Maagd, "*Bacillus thuringiensis* delta-endotoxin Cry1Ac domain III enhances activity against *Heliothis virescens* in some, but not all Cry1-Cry1Ac hybrids," *J Invertebr Pathol*, vol. 88, no. 2, pp. 169–172, 2005, [Online]. Available:

- http://www.ncbi.nlm.nih.gov/entrez/query.fcgi?cmd=Retrieve&db=PubMed&dopt=Citation&list_uids=15766934
79. H. Ishikawa *et al.*, "A system for the directed evolution of the insecticidal protein from *Bacillus thuringiensis*," *Mol Biotechnol*, vol. 36, no. 2, pp. 90–101, 2007, [Online]. Available: http://www.ncbi.nlm.nih.gov/entrez/query.fcgi?cmd=Retrieve&db=PubMed&dopt=Citation&list_uids=17914188
 80. D. R. Ammons *et al.*, "Anti-cancer Parasporin Toxins are Associated with Different Environments: Discovery of Two Novel Parasporin 5-like Genes," *Curr Microbiol*, vol. 72, no. 2, pp. 184–189, 2016, doi: 10.1007/s00284-015-0934-3.
 81. E. Mizuki *et al.*, "Parasporin, a human leukemic cell-recognizing parasporal protein of *Bacillus thuringiensis*," *Clin Diagn Lab Immunol*, vol. 7, no. 4, pp. 625–634, 2000, [Online]. Available: <http://www.ncbi.nlm.nih.gov/pubmed/10882663>
 82. E. Gonzalez, J. C. Granados, J. D. Short, D. R. Ammons, and J. Rampersad, "Parasporins from a Caribbean Island: evidence for a globally dispersed *Bacillus thuringiensis* strain," *Curr Microbiol*, vol. 62, no. 5, pp. 1643–1648, 2011, doi: 10.1007/s00284-011-9905-5.
 83. Brasseur, P. Auger, E. Asselin, S. Parent, J. C. Cote, and M. Sirois, "Parasporin-2 from a New *Bacillus thuringiensis* 4R2 Strain Induces Caspases Activation and Apoptosis in Human Cancer Cells," *PLoS One*, vol. 10, no. 8, p. e0135106, [Online]. Available: http://www.ncbi.nlm.nih.gov/entrez/query.fcgi?cmd=Retrieve&db=PubMed&dopt=Citation&list_uids=26263002
 84. S. S. Prasad and Y. I. Shethna, "Purification, crystallization and partial characterization of the antitumour and insecticidal protein subunit from the delta-endotoxin of *Bacillus thuringiensis* var. *thuringiensis*," *Biochim Biophys Acta*, vol. 362, no. 3, pp. 558–566, 1974, [Online]. Available: <http://www.ncbi.nlm.nih.gov/pubmed/4415403>
 85. Aldeewan, Y. Zhang, and L. Su, "*Bacillus thuringiensis* Parasporins Functions on Cancer Cells," *Int J Pure Appl Biosci*, vol. 2, no. 4, pp. 67–74, 2014.
 86. E. Mizuki, M. Ohba, T. Akao, S. Yamashita, H. Saitoh, and Y. S. Park, "Unique activity associated with non-insecticidal *Bacillus thuringiensis* parasporal inclusions: in vitro cell-killing action on human cancer cells," *J Appl Microbiol*, vol. 86, no. 3, pp. 477–486, 1999, [Online]. Available: <http://www.ncbi.nlm.nih.gov/pubmed/10196753>
 87. Ito *et al.*, "A *Bacillus thuringiensis* crystal protein with selective cytotoxic action to human cells," *J Biol Chem*, vol. 279, no. 20, pp. 21282–21286, 2004, doi: 10.1074/jbc.M401881200.

88. S. Patyar, R. Joshi, D. S. Byrav, A. Prakash, B. Medhi, and B. K. Das, "Bacteria in cancer therapy: a novel experimental strategy," *J Biomed Sci*, vol. 17, no. 1, p. 21, 2010, doi: 10.1186/1423-0127-17-21.
89. C. Xu, B. C. Wang, Z. Yu, and M. Sun, "Structural insights into *Bacillus thuringiensis* Cry, Cyt and parasporin toxins," *Toxins*, vol. 6, no. 9, pp. 2732–2770, Sep. 2014. doi: 10.3390/toxins6092732.
90. S. Kitada *et al.*, "Cytocidal actions of parasporin-2, an anti-tumor crystal toxin from *Bacillus thuringiensis*," *J Biol Chem*, vol. 281, no. 36, pp. 26350–26360, 2006, [Online]. Available: http://www.ncbi.nlm.nih.gov/entrez/query.fcgi?cmd=Retrieve&db=PubMed&dopt=Citation&list_uids=16809341
91. E. Gonzalez, J. C. Granados, J. D. Short, D. R. Ammons, and J. Rampersad, "Parasporins from a Caribbean Island: evidence for a globally dispersed *Bacillus thuringiensis* strain," *Curr Microbiol*, vol. 62, no. 5, pp. 1643–1648, [Online]. Available: http://www.ncbi.nlm.nih.gov/entrez/query.fcgi?cmd=Retrieve&db=PubMed&dopt=Citation&list_uids=21380719
92. Yasutake, A. Uemori, N. D. Binh, E. Mizuki, and M. Ohba, "Identification of parasporin genes in Vietnamese isolates of *Bacillus thuringiensis*," *Z Naturforsch C*, vol. 63, no. 1–2, pp. 139–143, 2008, [Online]. Available: http://www.ncbi.nlm.nih.gov/entrez/query.fcgi?cmd=Retrieve&db=PubMed&dopt=Citation&list_uids=18386503
93. S. Okumura, H. Saitoh, T. Ishikawa, E. Mizuki, and K. Inouye, "Identification and characterization of a novel cytotoxic protein, parasporin-4, produced by *Bacillus thuringiensis* A1470 strain," *Biotechnology Annual Review*, vol. 14, pp. 225–252, 2008. doi: 10.1016/S1387-2656(08)00009-4.
94. N. Crickmore, "Parasporin Classification," vol. 2018, no. October 10-2018. Sussex University, 2018. [Online]. Available: <http://parasporin.fitc.pref.fukuoka.jp/latestPSs.pdf>
95. T. Akiba *et al.*, "Nontoxic crystal protein from *Bacillus thuringiensis* demonstrates a remarkable structural similarity to β -pore-forming toxins," *Proteins: Structure, Function and Genetics*, vol. 63, no. 1, pp. 243–248, Apr. 2006, doi: 10.1002/prot.20843.
96. T. Akiba *et al.*, "Crystal structure of the parasporin-2 *Bacillus thuringiensis* toxin that recognizes cancer cells," *J Mol Biol*, vol. 386, no. 1, pp. 121–133, 2009, [Online]. Available: http://www.ncbi.nlm.nih.gov/entrez/query.fcgi?cmd=Retrieve&db=PubMed&dopt=Citation&list_uids=19094993

97. C. Xu, B. C. Wang, Z. Yu, and M. Sun, "Structural insights into *Bacillus thuringiensis* Cry, Cyt and parasporin toxins," *Toxins (Basel)*, vol. 6, no. 9, pp. 2732–2770, 2014, [Online]. Available: http://www.ncbi.nlm.nih.gov/entrez/query.fcgi?cmd=Retrieve&db=PubMed&dopt=Citation&list_uids=25229189
98. Iacovache *et al.*, "Dual chaperone role of the C-terminal propeptide in folding and oligomerization of the pore-forming toxin aerolysin," *PLoS Pathog*, vol. 7, no. 7, p. e1002135, 2011, doi: 10.1371/journal.ppat.1002135.
99. Ohba, E. Mizuki, and A. Uemori, "Parasporin, a new anticancer protein group from *Bacillus thuringiensis*," *Anticancer Res*, vol. 29, no. 1, pp. 427–433, 2009, [Online]. Available: http://www.ncbi.nlm.nih.gov/entrez/query.fcgi?cmd=Retrieve&db=PubMed&dopt=Citation&list_uids=19331182
100. Periyasamy *et al.*, "Screening and characterization of a non-insecticidal *Bacillus thuringiensis* strain producing parasporal protein with selective toxicity against human colon cancer cell lines," *Ann Microbiol*, vol. 66, no. 3, pp. 1167–1178, Sep. 2016, doi: 10.1007/S13213-016-1204-8/FIGURES/6.
101. S. Kitada, Y. Abe, T. Maeda, and H. Shimada, "Parasporin-2 requires GPI-anchored proteins for the efficient cytotoxic action to human hepatoma cells," *Toxicology*, vol. 264, no. 1–2, pp. 80–88, 2009, doi: 10.1016/j.tox.2009.07.016.
102. K. Brasseur, P. Auger, E. Asselin, S. Parent, J. C. Cote, and M. Sirois, "Parasporin-2 from a New *Bacillus thuringiensis* 4R2 Strain Induces Caspases Activation and Apoptosis in Human Cancer Cells," *PLoS One*, vol. 10, no. 8, p. e0135106, 2015, doi: 10.1371/journal.pone.0135106.
103. J. Cruz *et al.*, "Computational study, synthesis and evaluation of active peptides derived from Parasporin-2 and spike protein from Alphacoronavirus against colorectal cancer cells," *Biosci Rep*, vol. 41, no. 12, Dec. 2021, doi: 10.1042/BSR20211964.
104. [M. O. Suárez-Barrera *et al.*, "Genetic Modification Approaches for Parasporins *Bacillus thuringiensis* Proteins with Anticancer Activity," *Molecules* 2021, Vol. 26, Page 7476, vol. 26, no. 24, p. 7476, Dec. 2021, doi: 10.3390/MOLECULES26247476.
105. K. Ekino *et al.*, "Cloning and characterization of a unique cytotoxic protein parasporin-5 produced by *Bacillus thuringiensis* a1100 strain," *Toxins (Basel)*, vol. 6, no. 6, pp. 1882–1895, 2014, doi: 10.3390/toxins6061882.

2. Review Genetic Modification Approaches for Parasporins *Bacillus thuringiensis* Proteins with Anticancer Activity

Miguel O. Suárez-Barrera

Lydia Visser

Paola Rondón-Villarreal

Diego F. Herrera-Pineda

Juan S. Alarcón-Aldana

Anke Van den Berg

Jahir Orozco

Efraín H. Pinzón-Reyes

Ernesto Moreno

Nohora J. Rueda-Forero

Molecules

2021, 26, 7476. <https://doi.org/10.3390/molecules2624747>

Author Contributions: Conceptualization, M.O.S.-B. and N.J.R.-F.; writing—original draft preparation, M.O.S.-B., D.F.H.-P., J.S.A.-A. and N.J.R.-F.; writing—review and editing L.V., P.R.-V., E.H.P.-R., A.V.d.B., J.O., E.M. and M.O.S.-B.; supervision M.O.S.-B. and N.J.R.-F. All authors have read and agreed to the published version of the manuscript.

Funding: The work has been funded by MINCIENCIAS, MINEDUCACIÓN, MINCIT and ICETEX, through the Program Ecosistema Científico Cod. FP44842-211-2018, Project number 58668.

2.1 Abstract

Bacillus thuringiensis (Bt) is a bacterium capable of producing Cry toxins, which are recognized for their bio-controlling actions against insects. However, a few Bt strains encode proteins lacking insecticidal activity but showing cytotoxic activity against different cancer cell lines and low or no cytotoxicity toward normal human cells. A subset of Cry anticancer proteins, termed parasporins (PSs), has recently arisen as a potential alternative for cancer treatment. However, the molecular receptors that allow the binding of PSs to cells and their cytotoxic mechanisms of action have not been well established. Nonetheless, their selective cytotoxic activity against different types of cancer cell lines places PSs as a promising alternative treatment modality. In this review, we provide an overview of the classification, structures, mechanisms of action, and insights obtained from genetic modification approaches for PS proteins.

Keywords: parasporins; Cry toxins; cancer cells; genetic improvement.

2.2 Background - introduction

Bacillus thuringiensis (Bt) is an endospore-forming aerobic bacterium with a high capacity to resist elevated temperatures and desiccation conditions, characterized by producing parasporal toxins [1]. Bt was first identified in 1901 by Shigetane Ishiwata, who reported that this microorganism had an infective capacity toward *Bombyx mori*. This plague caused severe damage to the silk industry in Japan [2]. At that time, the author termed the bacteria *Bacillus sotto*. A decade later, Berliner isolated a Gram-positive bacterium in *Ephesitia kuehniella* larvae in the state of Thuringia (Germany). Ignoring the identification given by Ishiwata, Berliner designated the bacterium as *Bacillus thuringiensis*, and this nomenclature has remained ever since [3].

Bt toxins, such as the Cry and Cytolytic (Cyt) proteins, are present in crystal form, with toxic effects in several pest vectors. A subset of the Cry proteins present in the crystals are parasporins (PSs), proteins with cytotoxic activity in human cancer cell lines [4]. The wide spectrum of the potential applications of PSs in biotechnological and biological medicine research has made Bt one of the most essential microorganisms used

as a bio-controller and, more recently, as a producer of non-insecticidal parasporal proteins [5].

Previous studies on proteins produced by Bt have predominantly focused on quantifying their insecticidal potential, disregarding their possible uses in other fields of biotechnology and health. However, in recent years, new properties, such as cytotoxic activity against cancer cells, antiprotozoal activity, and lectin function, have been described for crystals extracted from various Bt strains [1,6,7]. Among these functionalities, the anticancer activity is of particular relevance, being the focus of this review.

2.3 Overview of the Classification and Structure of Parasporins Found in Bacillus

In the search for new therapeutic agents to treat cancer, bacterial proteins have become a focus of attention in the last two decades. In 1999, Mizuki et al. conducted a bioprospecting study using around 1700 Bt isolates by selecting 42 candidates with no hemolytic and cytotoxic activity to test their activity against MOLT-4 cells (human lymphoblastic leukemia) [6,7]. Prasad, Seki, and their teams described the existence of a 13-kDa parasporal toxin from a Bt strain with dual activity, i.e., insecticidal action against *Bombyx mori* and antitumor activity in colon and blood cancer cell lines [1,8]. This new promising protein, termed a parasporin, is among the Bt proteins with biological activities that potentially allow for medical applications.

The Parasporin Classification and Nomenclature Committee defined the term “parasporins” in 2006 as “Parasporal proteins of Bt and related bacteria that are non-hemolytic but are preferentially able to kill cancer cells” [9]. To date, six parasporin families (PS1–PS6) including 19 PSs produced by at least 11 Bt strains have been identified mainly in four countries (Japan, Vietnam, India, and Canada) (Table 1) [10,11]. PSs are divided into those of higher molecular mass (PS1, PS3, and PS6), approximately 80 kDa, which are processed into active 60 kDa molecules, and those with lower molecular mass (PS2, PS4, and PS5), originated from precursors of 33 to 37 kDa, which are processed by proteolytic cleavage to 30 kDa molecules. When a proteolytic cleavage is made by a serine protease, such as Proteinase K, at the C- terminal and N- terminal residues of the

precursor, the toxin of 60 kDa and 30 kDa is active with cytotoxic activity [9,10,12]. All the PS family members are characterized by a conserved structure consisting of three domains (Figure 1A, B).

Figure 11. Structural comparison of parasporins(A) Structural model of higher-molecular-weight PS3Aa1 with its three domains. (B) Low-molecular-weight PS2Aa1 structural model. (C–E) Structural comparison between parasporin-2, the 26-kDa nontoxic protein, and aerolysin-like α -PFT. Membrane-binding-related domain I is colored yellow. The membrane insertion and pore-formation regions are colored blue (domain II) and red (Domain III). It is suggested that the purple amphipathic α -hairpin is necessary for pore formation (C–E). Parasporin 4 (PS4) was modeled using the 26-kDa nontoxic protein as an adapted template from Xu et al. [9], modified by the authors.

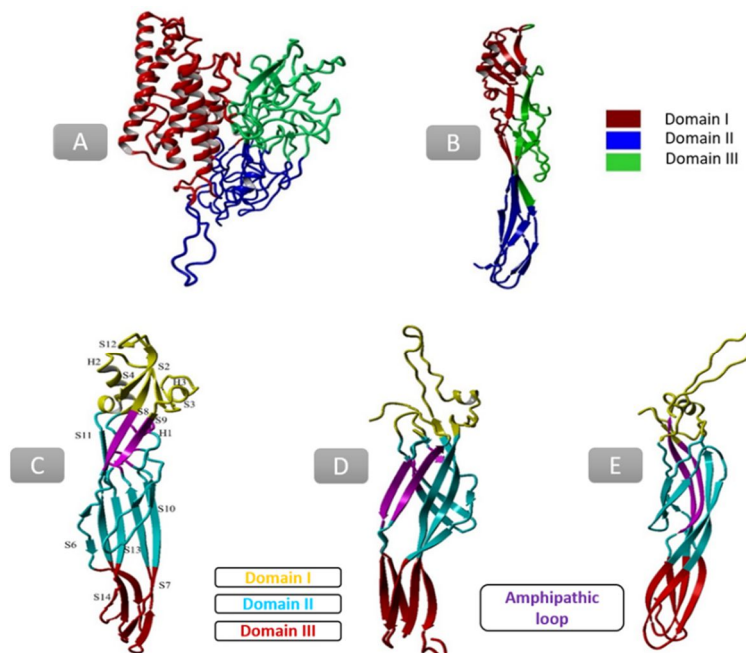


Table 5. Parasporin families, family-containing strains, molecular weights, target cells, cytotoxic activity and references.

Parasporin	Strain (Bt)	Molecular mass (kDa)	Target cell line	Cytotoxic activity IC ₅₀ (μ g/mL)	Ref.
PS1Aa1	A1190	81	MOLT-4	2.2	[9,12,13]
			HL-60	0.32	
			HepG2	3.0	
			HeLa	0.12	
			Jurkat	>10	
			Sawano	>10	
			Caco-2	>10	
A549	>10				

Parasporin	Strain (Bt)	Molecular mass (kDa)	Target cell line	Cytotoxic activity IC ₅₀ (µg/mL)	Ref.
PS2Aa1	A1547	37	MOLT-4	0.022	[8,9,13,14]
			Jurkat	0.018	
			HL-60	0.019	
			HepG2	0.019	
			Sawano	0.0017	
			Caco-2	0.013	
			HCT116	10	
			CCRF-CEM	27	
PS3Aa1	A1462	93	MOLT-4	>10	[9,13,15]
			Jurkat	>10	
			HL-60	1.32	
			HepG2	2.8	
			HeLa	>10	
			Sawano	>10	
PS4Aa1	A1470	34	MOLT-4	0.472	[9,13,16]
			HL-60	0.725	
			HepG2	1.90	
			Sawano	0.245	
			TCS	0.719	
			Caco-2	0.124	
PS5Aa1	A1100	31	MOLT-4	0.075	[13,17]
			Caco-2	0.30	
			HepG2	0.049	
			TCS	0.046	
			HeLa	0.08	
			Sawano.	0.065	
PS6Aa1	M109/CP84	73	HepG2	2.3	[13,18]
			HeLa	7.2	
			Caco-2	>10	

There are six families of parasporins described so far, from PS1 to PS6. Table 1 summarizes the families and its representative protein. Further information can be found at <http://parasporin.fitc.pref.fukuoka.jp/list.html> (last accessed on 5 December 2021) [20]. PS1Aa1, also known as Cry31Aa1, contains 723 amino acid residues yielding a molecular weight of 81 kDa. The crystal structure of the activated PS1Aa1 form was determined at a 1.76-Å resolution [5], revealing the typical three-domain structure established for Cry toxins. Domains I, II, and III have chain folds that make each unique, i.e., showing a set of seven α -helices, a β prism, and a lectin-like β sandwich, respectively. Cleavage of PSAa1 in the exposed loop connecting the third and fourth α -helices of domain I results in two polypeptides of 15 kDa and 56 kDa [5]. PS1 exerts strong cytotoxic effects against cell lines such as HeLa [21], HL-60 [10], and MOLT-4 [22], and a moderate effect toward

Sawano, Caco-2, and Jurkat [9] cells. The IC₅₀ values for each of the tested cell lines are summarized in Table 1.

According to Ito et al., PS2Aa1 (Cry46Aa1) and PS2Aa2 (Cry46Aa2) are 338-amino acid polypeptides with a deduced molecular weight of 37 kDa [21]. Unlike PS1Aa1, PS2Aa1 lacks the conserved blocks found in Cry proteins. The structure of PS2 shows homology with the aerolysin of *A. hydrophila* and the alpha-toxin of *C. perfringens* [13,23], which, similarly to the PS1 and Cry insecticides, has three domains. The processing of PS2Aa1 from a 37-kDa precursor protein results in an active 30-kDa toxin [21]. In its active form, which is formed after treatment with proteinase K [24], PS2 is toxic to HepG2, Caco-2, MOLT-4, Jurkat, and HL-60 cell lines (Table 1) [14,18] but does not present any toxicity to normal cells [25].

PS3Aa1 (Cry41Aa1) consists of 825 amino-acid residues with a deduced molecular weight of 93.68 kDa and low sequence similarity with insecticidal Cry proteins. However, it contains three domains with five conserved repetitive blocks, a typical structure for PS proteins [14]. PS3Aa1 requires proteolytic digestion at its N- and C-termini for activation, thus converting the 81-kDa precursor protein into an active 64-kDa protein, with cytotoxic effects on various cancer cell lines, such as HL-60 and HepG2 (Table 1) [14].

PS4Aa1 (Cry45Aa1) is a β -pore-forming aerolysin-type protein comprising 275 amino acids, with a predicted molecular weight of 30.07 kDa [14]. No repetitive sequence blocks, as observed in PS1Aa1 and PS3Aa1, have been reported in this protein. PS4Aa1 has three domains, whose structures do not resemble those of Cry proteins [14]. The 31-kDa protoxin is activated by cleavage in its C-terminal domain by pepsins in acidic conditions, resulting in a fully active 27-kDa toxin [26]. The active protein exhibits cytotoxic activity against human cancer cell lines, e.g., Caco-2, Sawano, MOLT-4, TCS (human cervical cancer), and HL60 cells (Table 1) [9,14,17].

PS5 and PS6 are the most scarcely studied parasporins. PS5 has been isolated from Bt strain A1100. Sequence analysis has revealed that PS5Aa1 (Cry64Aa) is an epsilon protein that acts synergistically with the drug methotrexate [18]. Its gene sequence is 918 bp in length, encoding a 305-amino-acid polypeptide with an expected molecular weight of 38 kDa. Its C-terminus is cleaved by proteinase K, producing an active 30-kDa protein [18]. PS6Aa1 (Cry63Aa) has been isolated from the Bt M109 and CP84 strains

[19]. Sequence analysis suggests a protein of three domains, closely related to Cry insecticides, with homology with and similarity to Cry2 of 21.9 and 56.4, respectively [19]. As for cytotoxic activity, PS5 has been shown to be active against MOLT-4, Caco-2, HepG2, TCS, HeLa, and Sawano cells, while PS6 shows weak cytotoxicity toward HepG2 cells (Table 1).

Like Cry proteins, Parasporins share structural and functional features with poreforming toxins (PFTs), considering that its cytotoxic activity is due to the pore formation in the cell membrane [9]. There are two larger groups of PFTs, Alpha-PFTs (α -PFTs) and Beta-PFTs (β -PFTs), based on how the secondary structure of their membrane-spanning elements are composed of α -helices and β -Barrels, respectively. Within the β -PFTs, the aerolysin family includes several parasporins [27].

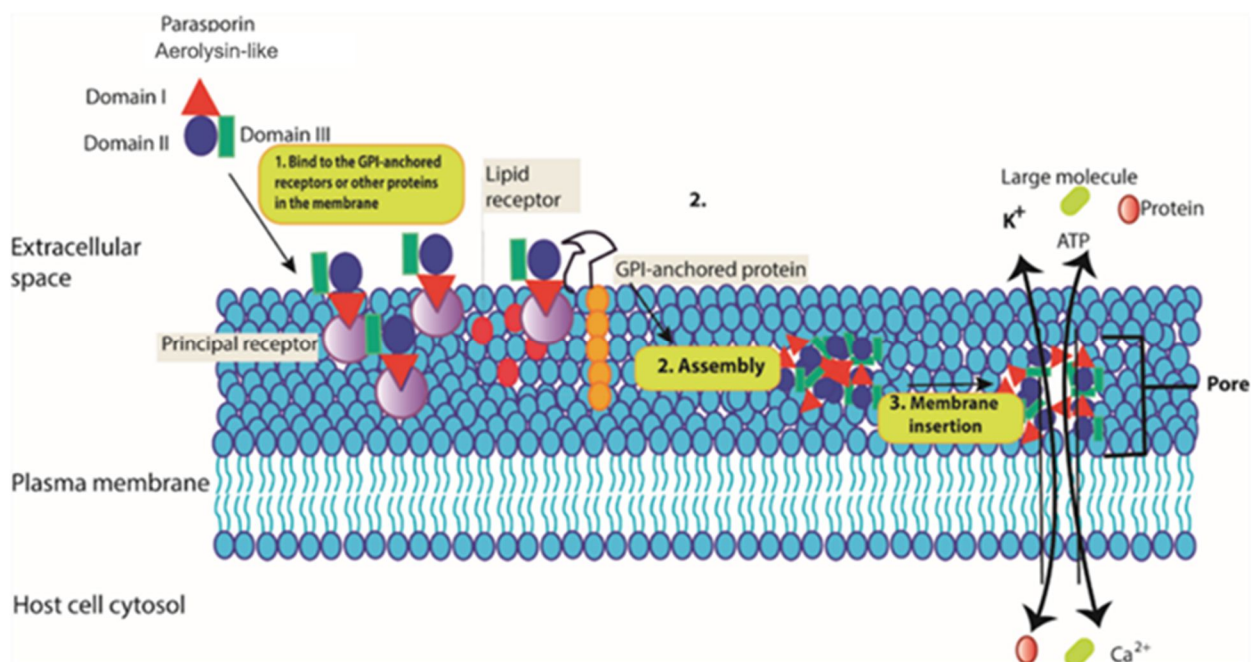
2.3.1 β -Type-Like Pore-Forming Parasporins

The nontoxic protein of the A1470 Bt strain and the toxic PS2Aa1 have similar structures, especially in domain II. Both molecules form a sandwich that comprises a β -hairpin (S6 and S7 for the nontoxic protein; S8 and S9 for PS2Aa) and an anti-parallel five-stranded β -sheet (S3, S9, S12, S5, and S8 for the nontoxic protein; S5, S6, S7, S10, S11, and S13 in PS2Aa) (Figure 1C–E) [28,29]. In PS2 family members, the β -hairpin forms a hydrophobic core with the inner surface of the β -sheet. This surface is covered with hydrophilic residues that surround the nucleus and are stabilized by hydrogen bonds. The arrangement of hydrophobic and hydrophilic residues is a critical factor involved in folding the protein [9]. In addition, three of the five strands of the β -sheet rearrange with the S1 strand to form an four-stranded β -sheet near the border of domain I, associated with the helices of domain I through hydrophobic interactions [28]. Site-directed mutagenesis was performed in the amphipathic β -strand of an epsilon toxin [9]. These mutations altered the characteristics of the channel formed in the lipid bilayer, suggesting that domain II is involved in the insertion and formation of lytic pores [9].

Domain III is also involved in pore formation and has a loop that crosses the membrane [30]. It plays a vital role in the interaction between the individual monomers in the oligomer. In PS2, the five-stranded β -sheet is rearranged into a three-stranded β -sheet

and two anti-parallel strands (S6, S11, S13/S14, S7, and S10) (Figure 1). These two β -sheets form a β -sandwich, similar to the β -sandwich in domain II [28]. The β -sheet structure is quite similar to the structure of the Bt A1470 nontoxic protein, which ends in two β -sheets: one with three strands and the other one with two (S4, S9, and S12; S5 and S8) (Figure 1) [29]. In PS2Aa1, some hydrophobic residues within the β -sandwich are exposed on both sides of the domain, forming small hydrophobic surface patches along the β -strands. A pair of anti-parallel β -strands (S4–S8 and S9–S11) (Figure 2) returns to the distal end of the domain, forming two loops [28]. The C-terminal residue is next to that pair of loops, pointing to its outer terminus. This residue is removed during proteolytic digestion, being a part of the hydrophobic nucleus inside the β -sandwich exposed to the solvent, creating a hydrophobic zone in the β strand. These findings demonstrate the critical role of the C-terminal residue in oligomerization [9].

Figure 12. Action mode of aerolysin-like parasporins (PS2Aa). Figure adapted from [9]. According to this model, the mechanism of action could be as follows: 1. The solubilized protein binds to the GPI-anchored receptors at the N-terminus. 2. After C-terminal proteolytic digestion, the activated protein monomers assemble (oligomerization). 3. Through reorganization, a transmembrane β -barrel is formed.



Sequence analysis using position-specific iterative (PSI)-BLAST indicated that the sequences of PS2, PS4, and PS5 are homologous to those of the α -PFT family [23,25,31], but they show different cytotoxic effects on normal cells [18]. Whereas PS4 did not show cytotoxic activity for any of the normal cell lines investigated [32], PS5 showed moderate cytotoxicity against the normal cell lines MRC-5 and UtSMC [18]. The high-molecular-weight PSs (Figure 1A) are more closely related to the insecticidal Cry proteins than the lower-molecular-weight PSs (Figure 1B). The bulk of the experimental data published to date related to high-molecular-weight PSs, and data from the determination of Bt have been a powerful tool for elucidating its role as a bio-controller of insect pests and disease vectors [33]. Therefore, it is imperative to consolidate the current information to characterize the great importance of the lower-molecular-weight PSs of the aerolysin type in medicine and biotechnology.

2.4 Effects of Parasporins on Cancer Cells

The mechanism of action of pore-forming proteins (PFPs) is dynamic, with three main steps: (1) the formation of water solubility, (2) self-assembly, and (3) insertion into the membrane, which leads to a pore suspected to be highly destructive for membrane integrity [34]. The points at which these proteins anchor to the membrane probably occur at specific receptors located in the microdomains rich in cholesterol and sphingolipids (lipid rafts), since these are requirements for GPI-anchored proteins, and the glucan region may be required for the binding and assembly in the membrane (Figure 2, part 1) [9]. Similarly, it was reported that the cell membrane receptor Beclin-1 could be important in the binding of three-domain parasporins (Parts 2 and 3, Figure 2) and that the Beclin-1 receptor is present in the mammary epithelium and epithelial carcinoma cells (Figure 2) [9,34,35]. The rearrangement of the domains typical for the classic protein model of three poreforming domains does not occur for PS1 [36]. Therefore, its activity is not oriented to forming pores in the membrane [21,36]. PS1 was proposed to function as an activator of the apoptotic signaling pathway [14,19,37]. Selective cytotoxicity has been reported for the HeLa, Sawano, HepG2, HL-60, and MOLT-4 cell lines after PS1's proteolytic activation

by trypsin (Table 1) [6,38]. The activity of PS1 mainly involves modulating the influx of Ca^{2+} levels [6,21,39].

The PS2 mechanism of action likely starts with recognizing and binding to a receptor located in the cancer cells' membranes [24], identifying lipid rafts, and anchoring the protein monomers in the periphery. The oligomers, resistant to sodium dodecyl sulfate (SDS), are embedded in the membrane, leading to its permeabilization [18,24]. Although PS2 is considered a selective pore-forming toxin, its primary receptors have not been fully elucidated [18]. Cells exposed to PS2 show morphological changes, including inflammation, blisters and lysis, microtubule disassembly, actin filament coiling, and fragmentation of the mitochondria and endoplasmic reticulum. PS2 resides in the plasma membrane and has been shown to activate apoptosis through caspases [14], triggering increased permeability [14,18,31]. These effects are induced by the accumulation of PS2 by large oligomers in the membrane's lipid rafts [8,18,24,39]. In turn, association of PS2 with GPI is required for cytolytic action. By contrast, membrane cholesterol slightly affects the efficiency of oligomerization [1]. The activation of PS2 induced by proteinase K [25] leads to the exposure of specific regions that bind to the receptor [18,25]. PS3 acts as a pore former in cancer cells, thereby increasing cellular permeability [12,40]. Although PS3 is structurally like the Cry proteins, containing the five conserved blocks that characterize Cry [7,40], the PS3 and Cry proteins are fundamentally different due to a castor domain [7,40,41], which is present in many unrelated proteins and is presumed to enhance/induce carbohydrate-binding capacity [40]. Similar to the above-described PS, the mechanisms of action of PS3 remain largely unknown. Krishnan et al. suggested that PS3 is most likely pore forming [16], which leads to an imbalance in ATP, increased cell size, and membrane damage [40,41]. Its cytotoxic activity was evident in the HL-60 and HepG2 cell lines [7,40,41], but it did not affect HeLa cells [41]. Studies on PS3, PS4, PS5, and PS6 are limited compared to those on PS1 and PS2, and many action modes remain undetermined. PS4 shows homology with both Cry and pore-forming β -type aerolysin. It has been reported to be cytotoxic to the Caco-2, Sawano, and MOLT cell lines [5,41]. Its structure mainly comprises β -sheet domains, and its pore forming activity is not dependent on cholesterol [21,41]. Cells treated with this protein show an increase in size due to an increase in the cytoplasmic compartment and shrinkage of the nucleus, leading to the

rupture of the cytoplasmic membrane and cell death [42]. PS5 and PS6 are the most recently discovered PS proteins. They have three domains, similar to PS1 and PS2, and presumably have pore-forming activity. They have been reported to show cytotoxic activity in liver and cervical cancer cell lines. However, there is no further information on their mechanisms of action [14].

2.5 Perspectives on the Improvement of Bt Parasporins as an Innovative Strategy for Controlling Cancer Cells

By deciphering structure–function relationships, proteins with improved properties, e.g., desired thermal activity, selectivity, specificity, or folding, can be designed [43]. For example, engineered proteins with various substitutions of amino acids are used in receptor and channel-protein-binding studies [44]. Protein engineering is called the synthesis of proteins with enhanced functionality *in vitro* and *in vivo* due to altered physical, chemical, or biological properties through genomic and post-genomic strategies. Genetic improvement is closely linked to complementary computational methods, which aim to optimize the generation of mutant libraries by simulating the experimental conditions of directed mutagenesis techniques [45–48]. In addition, other computational methods are oriented toward predicting protein structures and designing models that allow the prediction of molecular interactions and pinpoint amino-acid residues or regions at crucial positions in natural and mutant proteins [43,49].

The computational technique most widely used for studying the possible interactions of Bt Cry toxins with insect receptors is molecular docking, followed by molecular dynamics, which has proven to help predict the stability of the interactions and analyze the molecular mechanisms of action. Florez et al. [50] obtained five Cry11 variants by DNA shuffling and showed the toxic activity against *Aedes aegypti* and *Culex quinquefasciatus* for three of them. Molecular docking simulations were performed for these three variants, and the amino acids with possible interactions were identified. BenFarhat-Touzri et al. [51] cloned and sequenced the Cry1D-133 toxin and determined its toxicity against *S. littoralis* larvae. Molecular docking simulations were performed to explain the enhanced toxicity of this toxin and showed that the number of toxin–receptor

interactions was higher than that of the interactions exhibited by the Cry1D toxin. The use of computational techniques based on molecular dynamics has enabled researchers to study the mechanisms of action of Cry toxins. The study of molecular dynamics has provided novel insights into the oligomerization of Cry toxins at a molecular level. Sriwimol et al. simulated the Cry4Ba structure with a three-dimensional reconstructed map for trimeric protein states. For the first time, they showed the need for membrane-induced conformational changes in Cry4Ba toxin monomers to allow the molecular assembly of a pre-pore trimer, which can be inserted into the target membranes to generate a lytic pore [52].

Other molecular dynamic studies have been applied to investigate the residue interactions relevant to the toxicity of the Bt Cry toxin family. Pacheco et al. discovered the importance of salt-bridge formation between α -helix residues from adjacent monomers for the toxicity and oligomerization of the Cry1Ab and Cry5Ba toxins by molecular dynamics' simulations [53]. They showed a critical role for the salt bridge between the E101 and R99 residues of Cry1Ab [54]. Site-directed mutagenesis experiments confirmed decreased oligomerization and toxicity potential for Cry1Ab-E101K and Cry1Ab-R99E mutants.

Interestingly, the R99–E101 salt bridge is not fully conserved in Cry proteins, with both or one of the residues being different in Cry5Ba. However, Pacheco et al. showed that additional salt bridges with similar structural functions could also be formed in these Cry proteins. In conclusion, the computational analysis highlighted the importance of salt bridge formation between the α -3 helices of adjacent monomers for inducing/facilitating a conformational change crucial for Cry toxicity [53].

Genetic Improvement of Cry Protein as a Model to Be Followed for Parasporins Bt is an excellent candidate for producing both natural and genetically enhanced PS proteins [55]. Studies on Bt have been in progress for over 100 years since the discovery of Bt in Japan [56]. During this time, several studies have established associations between the crystal morphology, protein sequences, and molecular weight, and the specific effects against its insecticidal targets [57]. Bt continues to be of great scientific interest, and it is one of the most studied biotechnological alternatives of biological origin on Earth. By contrast, PS remains a scarcely explored option, as few researchers have awakened their

curiosity in PS and anticancer pore-forming proteins. Various approaches have been taken to modify Bt toxins' binding specificity and affinity, with the ultimate goal of producing genetically modified toxins that target new pest species and counteract the resistance developed in the field. The alteration of the binding affinity and specificity of the Bt toxin can come from domain exchanges, site directed mutagenesis, truncation, and the generation and subsequent visualization of parasporal proteins in phage libraries containing mutant toxins [55]. Although there are no reports on the genetic improvement of PS-like parasporal proteins, here we review the technology applied to other types of Bt crystal proteins, which can serve as a methodological and scientific basis for obtaining PS proteins with improved cytotoxic activity against cancer cells. Table 2 presents several examples of the directed evolution techniques that have been successful for Bt proteins and might also be used shortly for PS modification and studies.

Table 6. Modifications made to Bt toxins to improve their efficacy.

Type of modification	Bt toxin	Target insect	Increase or decrease in toxicity	References
Domain exchanges				
Domain III Exchange For Domain III of Cry1Ab.	mCry3Aa	<i>Diabrotica virgifera</i>	The toxicity increased $\geq 19\%$.	[61]
Domain III, II, I Exchange For Domains of Cry1Ac.	Cry9Aa	<i>Helicoverpa armigera</i>	The toxicity increased between 4.9 and 5.1 times, concerning parentals.	[62]
Domain III Exchange For Domain III of Cry1Ca.	Cry1Ab; Cry1Ac; Cry1Ba; Cry1Ea; Cry1Fa	<i>Spodoptera exigua</i>	Increased up to 5.5 times for Cry1Fa.	[63]
Domain III Exchange For Domain III of Cry1CAc	Cry1Ca; Cry1Fb; Cry1Ba; Cry1Da; Cry1Ea	<i>Heliothis virescens</i>	The toxicity increased 172 and 69.6 times more for Cry1Ca and Cry1Fb, respectively.	[64]
Domain exchanges of Domains II and III, between Cry1Ia and Cry1Ba.	Cry1Ia; Cry1Ba	<i>Leptinotarsa decemlineata</i>	The toxicity increased up to 1127 and 4.2 times, compared to Cry1Ba and Cry1Ia; corresponding.	[65]

Type of modification	Bt toxin	Target insect	Increase or decrease in toxicity	References
Site-directed mutagenesis				
Loop 1, 2 and 3, domain II substitution.	Cry4Ba	<i>Culex pipiens</i> ; <i>Culex quinquefasciatus</i>	The toxicity increased up to 700 times.	[66]
Loop 1 and 2 domain II substitution	Cry19Aa	<i>Aedes aegypti</i>	The toxicity increased up to 42.000 times, concerning the parental.	[67]
Substitution in the domain II	Cry2Ab	<i>Anopheles gambiae</i>	The toxicity increased up to 6.75 times.	[68]
Loop 1 and 2 domain II substitution and deletions.	Cry1Aa	<i>Culex pipiens</i>	Change in insect target.	[69]
Substitution in the domain III	Cry1Ab	<i>Spodoptera frugiperda</i>	The toxicity increased up to 44 times, correspondingly to the parental.	[70]
Truncated toxins				
Truncation and selection of mutants, derived from a phage library	Cry1Ia	<i>Telchin licus</i>	The toxicity increased, showing mortality of 50% for approach.	[71]
Helix α -1 domain I truncation.	Cry1A	<i>Pectinophora gossypiella</i>	The toxicity increased up to 100 and 150 times for Cry1Ab and CryAc, respectively.	[72]
Helix α -1 domain I truncation.	Cry1A	<i>Plutella xylostella</i> ; <i>Ostrinia nubilalis</i>	The toxicity increased \geq 350 times, against resistant insects.	[73]
C-terminal truncation	Cry1C	<i>Spodoptera exigua</i>	The toxicity increased up to 4 times.	[74]
Phage-display library				
Selection of mutant toxins from a phage-display library based on their potential of binding.	Cry1Aa	<i>Bombyx mori</i>	Increased the receptor affinity potential, up to 16, and 50 times more, contrasting the parentals.	[75]
Selection of mutant toxins from a phage-display library	Cry8Ka	<i>Anthonomus grandis</i>	Increased the toxicity up to 3.2 times, contrasting the parental.	[76]

Type of modification	Bt toxin	Target insect	Increase or decrease in toxicity	References
based on their potential of binding.				
Selection of mutant toxins from a phage-display library based on their potential of binding in the domain II.	Cry1Aa	<i>Nilaparvata lugens</i>	The toxicity increased between 1.4 and 8.9 times, concerning parentals.	[77]

Domain exchanges between related proteins might have an increased toxicity towards the target cells. For Cry proteins, several examples are presented in Table 2. Site-directed mutagenesis at specific Domains or Loops is an efficient technique for obtaining potent toxins with enhanced toxicity. An example is Cry19A, for which, by substitutions in Domain II loops 1 and 2, the toxicity increased up to 42,000 times, concerning the parental [64].

Other techniques, such as truncated toxins or filtering of promising candidates with increased receptor affinity through Phage-display libraries, are presented in Table 2. Genetic improvement of 3D-Cry toxins is reviewed extensively by Susana Vilchez [75]. PSs require extensive structural and functional studies, which will help to unravel their complex but elegant mechanism of action leading to the cytotoxic effects upon cancer cell lines. Studies addressing this knowledge gap will help to elucidate the toxic action of PSs and define the structure–function relationship. Acknowledging its potential as anticancer molecules, PSs' site-directed evolution studies might focus as well on analyzing the cellular permeability and the potency of its toxicity to cells as well as the selectivity.

In the long term, the generation of PS variants might allow new alternatives to address the threat of cancer to the well-being of humans and the burden on the health system. The current knowledge highlights the potential role that bacterial proteins might play in generating novel anticancer molecules [9].

2.6 Conclusions

The low-molecular-weight PS proteins, such as the pore-forming toxin PS-2Aa1, induce apoptosis in target cells and have cytotoxic activity against several human cancer cell lines. Remarkably, low-molecular-weight PS proteins do not show detectable cytotoxic activity against normal cells in most cases [12]. Therefore, PS proteins have emerged as a viable, efficient, and natural alternative for combating cancer, one of the types of diseases with the highest mortality rate in humans. However, limited knowledge on these toxins at the molecular level, including the mechanism of action and the receptors targeted on cancer cells, is available. PS2 is a single protein with a proposed action mode based on its structure. Therefore, there is an urgent need to establish the structural properties and mechanism of action to scale in in vivo studies and take the next step toward developing valuable products for human health [75].

In addition, there is a need to identify and evaluate new Bt native strains with improved cytotoxic activity toward cancer cells and select candidates for further genetic improvement to obtain toxins with enhanced activity. PS proteins are in the process of being consolidated as a viable alternative for cancer treatment. Compared to other current approaches, they hold the potential to produce fewer side effects, improving both the treatment outcomes and quality of life of cancer patients.

2.7 References

1. Portela-Dussán, D.D.; Chaparro-Giraldo, A.; López-Pazos, S.A. *Bacillus thuringiensis* biotechnology in agriculture. *Nova* 2013, 11, 87–96.
2. Melo, A.L.D.A.; Soccol, V.T.; Soccol, C.R. *Bacillus thuringiensis*: Mechanism of action, resistance, and new applications: A review. *Crit. Rev. Biotechnol.* 2016, 36, 317–326.
3. Akao, T.; Mizuki, E.; Yamashita, S.; Kim, H.S.; Lee, D.W.; Ohba, M. Specificity of lectin activity of *Bacillus thuringiensis* parasporal inclusion proteins. *J. Basic Microbiol.* 2001, 41, 3–6.
4. Akiba, T.; Okumura, S. Parasporins 1 and 2: Their structure and activity. *J. Invertebr. Pathol.* 2017, 142, 44–49.

5. Mizuki, E.; Ohba, M.; Akao, T.; Yamashita, S.; Saitoh, H.; Park, Y.S. Unique activity associated with non-insecticidal *Bacillus thuringiensis* parasporal inclusions: In vitro cell-killing action on human cancer cells. *J. Appl. Microbiol.* 1999, 86, 477–486. *Molecules* 2021, 26, 7476 11 of 13
6. Ammons, D.R.; Short, J.D.; Bailey, J.; Hinojosa, G.; Tavarez, L.; Salazar, M.; Rampersad, J.N. Anti-cancer Parasporin toxins are associated with different environments: Discovery of two novel Parasporin 5-like genes. *Curr. Microbiol.* 2016, 72, 184–189.
7. Moazamian, E.; Bahador, N.; Azarpira, N.; Rasouli, M. Anti-cancer Parasporin toxins of new *Bacillus thuringiensis* against human colon (HCT-116) and blood (CCRF-CEM) cancer cell lines. *Curr. Microbiol.* 2018, 75, 1090–1098.
8. Xu, C.; Wang, B.C.; Yu, Z.; Sun, M. Structural insights into *Bacillus thuringiensis* Cry, Cyt and parasporin toxins. *Toxins* 2014, 6, 2732–2770.
9. Kitada, S.; Abe, Y.; Shimada, H.; Kusaka, Y.; Matsuo, Y.; Katayama, H.; Okumura, S.; Akao, T.; Mizuki, E.; Kuge, O.; et al. Cytocidal actions of parasporin-2, an anti-tumor crystal toxin from *Bacillus thuringiensis*. *J. Biol. Chem.* 2006, 281, 26350–26360.
10. Gonzalez, E.; Granados, J.C.; Short, J.D.; Ammons, D.R.; Rampersad, J. Parasporins from a Caribbean Island: Evidence for a globally dispersed *Bacillus thuringiensis* strain. *Curr. Microbiol.* 2011, 62, 1643–1648.
11. Brasseur, K.; Auger, P.; Asselin, E.; Parent, S.; Cote, J.C.; Sirois, M. Parasporin-2 from a new *Bacillus thuringiensis* 4R2 strain induces caspases activation and apoptosis in human cancer cells. *PLoS ONE* 2015, 10, e0135106.
12. Mizuki, E.; Park, Y.S.; Saitoh, H.; Yamashita, S.; Akao, T.; Higuchi, K.; Ohba, M. Parasporin, a human leukemic cell-recognizing parasporal protein of *Bacillus thuringiensis*. *Clin. Diagn. Lab. Immunol.* 2000, 7, 625–634.
13. Okassov, A.; Nersesyan, A.; Kitada, S.; Ilin, A. Parasporins as new natural anticancer agents: A review. *J. BUON* 2015, 20, 5–16.
14. Hayakawa, T.; Kanagawa, R.; Kotani, Y.; Kimura, M.; Yamagiwa, M.; Yamane, Y.; Takebe, S.; Sakai, H. Parasporin-2Ab, a newly isolated cytotoxic crystal protein from *Bacillus thuringiensis*. *Curr. Microbiol.* 2007, 55, 278–283.
15. Krishnan, V.; Domanska, B.; Elhigazi, A.; Afolabi, F.; West, M.J.; Crickmore, N. The human cancer cell active toxin Cry41Aa from *Bacillus thuringiensis* acts like its insecticidal counterparts. *Biochem. J.* 2017, 474, 1591–1602.
16. Ohba, M.; Mizuki, E.; Uemori, A. Parasporin, a new anticancer protein group from *Bacillus thuringiensis*. *Anticancer Res.* 2009, 29, 427–433.

17. Ekino, K.; Okumura, S.; Ishikawa, T.; Kitada, S.; Saitoh, H.; Akao, T.; Oka, T.; Nomura, Y.; Ohba, M.; Shin, T.; et al. Cloning and characterization of a unique cytotoxic protein parasporin-5 produced by *Bacillus thuringiensis* A1100 strain. *Toxins* 2014, 6, 1882–1895.
18. Nagamatsu, Y.; Okamura, S.; Saitou, H.; Akao, T.; Mizuki, E. Three cry toxins in two types from *Bacillus thuringiensis* strain M019 preferentially kill human hepatocyte cancer and uterus cervix cancer cells. *Biosci. Biotechnol. Biochem.* 2010, 74, 494–498.
19. Okumura, S.; Ohba, M.; Mizuki, E.; Crickmore, N.; Côté, J.-C.; Nagamatsu, Y.; Kitada, S.; Sakai, H.; Harata, K.; Shin, T. List of Parasporins. Available online: <http://parasporin.fitc.pref.fukuoka.jp/list.html> (accessed on 29 November 2021).
20. Ito, A.; Sasaguri, Y.; Kitada, S.; Kusaka, Y.; Kuwano, K.; Masutomi, K.; Mizuki, E.; Akao, T.; Ohba, M. A *Bacillus thuringiensis* crystal protein with selective cytotoxic action to human cells. *J. Biol. Chem.* 2004, 279, 21282–21286.
21. Katayama, H.; Kusaka, Y.; Yokota, H.; Akao, T.; Kojima, M.; Nakamura, O.; Mekada, E.; Mizuki, E. Parasporin-1, a novel cytotoxic protein from *Bacillus thuringiensis*, induces Ca^{2+} influx and a sustained elevation of the cytoplasmic Ca^{2+} concentration in toxin-sensitive cells. *J. Biol. Chem.* 2007, 282, 7742–7752.
22. Moniatte, M.; Van Der Goot, F.G.; Buckley, J.T.; Pattus, F.; Van Dorsselaer, A. Characterisation of the heptameric pore-forming complex of the *Aeromonas* toxin aerolysin using MALDI-TOF mass spectrometry. *FEBS Lett.* 1996, 384, 269–272.
23. Kuroda, S.; Begum, A.; Saga, M.; Hirao, A.; Mizuki, E.; Sakai, H.; Hayakawa, T. Parasporin 1Ac2, a novel cytotoxic crystal protein isolated from *Bacillus thuringiensis* B0462 strain. *Curr. Microbiol.* 2013, 66, 475–480.
24. Nagahama, M.; Hara, H.; Fernandez-Miyakawa, M.; Itohayashi, Y.; Sakurai, J. Oligomerization of *Clostridium perfringens* α -toxin is dependent upon membrane fluidity in liposomes. *Biochemistry* 2006, 45, 296–302.
25. Okumura, S.; Koga, H.; Inouye, K.; Mizuki, E. Toxicity of Parasporin-4 and health effects of pro-parasporin-4 diet in mice. *Toxins* 2014, 6, 2115–2126.
26. Peraro, M.D.; Van Der Goot, F.G. Pore-forming toxins: Ancient, but never really out of fashion. *Nat. Rev. Microbiol.* 2016, 14, 77–92.
27. Akiba, T.; Abe, Y.; Kitada, S.; Kusaka, Y.; Ito, A.; Ichimatsu, T.; Katayama, H.; Akao, T.; Higuchi, K.; Mizuki, E.; et al. Crystal structure of the Parasporin-2 *Bacillus thuringiensis* toxin that recognizes cancer cells. *J. Mol. Biol.* 2009, 386, 121–133.
28. Akiba, T.; Higuchi, K.; Mizuki, E.; Ekino, K.; Shin, T.; Ohba, M.; Kanai, R.; Harata, K. Nontoxic crystal protein from *Bacillus thuringiensis* demonstrates a remarkable structural similarity to beta-pore-forming toxins. *Proteins* 2006, 63, 243–248.

29. Iacovache, I.; Degiacomi, M.T.; Pernot, L.; Ho, S.; Schiltz, M.; Dal Peraro, M.; van der Goot, F.G. Dual chaperone role of the C-terminal propeptide in folding and oligomerization of the pore-forming toxin aerolysin. *PLoS Pathog.* 2011, 7, e1002135.
30. Okumura, S.; Saitoh, H.; Wasano, N.; Katayama, H.; Higuchi, K.; Mizuki, E.; Inouye, K. Efficient solubilization, activation, and purification of recombinant Cry45Aa of *Bacillus thuringiensis* expressed as inclusion bodies in *Escherichia coli*. *Protein Expr. Purif.* 2006, 47, 144–151.
31. Okumura, S.; Saitoh, H.; Ishikawa, T.; Wasano, N.; Yamashita, S.; Kusumoto, K.; Akao, T.; Mizuki, E.; Ohba, M.; Inouye, K. Identification of a novel cytotoxic protein, Cry45Aa, from *Bacillus thuringiensis* A1470 and its selective cytotoxic activity against various mammalian cell lines. *J. Agric. Food. Chem.* 2005, 53, 6313–6318.
32. Pandian, G.N.; Ishikawa, T.; Togashi, M.; Shitomi, Y.; Haginoya, K.; Yamamoto, S.; Nishiumi, T.; Hori, H. *Bombyx mori* midgut membrane protein P252, which binds to *Bacillus thuringiensis* Cry1A, is a chlorophyllide-binding protein, and the resulting complex has antimicrobial activity. *Appl. Environ. Microbiol.* 2008, 74, 1324–1331.
33. Aldeewan, A.; Zhang, Y.; Su, L. *Bacillus thuringiensis* Parasporins functions on cancer cells. *Int. J. Pure Appl. Biosci.* 2014, 4, 67–74.
34. Prasad, S.S.; Shethna, Y.I. Purification, crystallization and partial characterization of the antitumour and insecticidal protein subunit from the delta-endotoxin of *Bacillus thuringiensis* var. *thuringiensis*. *Biochim. Biophys. Acta* 1974, 362, 558–566.
35. Patyar, S.; Joshi, R.; Byrav, D.P.; Prakash, A.; Medhi, B.; Das, B. Bacteria in cancer therapy: A novel experimental strategy. *J. Biomed. Sci.* 2010, 17, 21.
36. Katayama, H.; Yokota, H.; Akao, T.; Nakamura, O.; Ohba, M.; Mekada, E.; Mizuki, E. Parasporin-1, a novel cytotoxic protein to human cells from non-insecticidal parasporal inclusions of *Bacillus thuringiensis*. *J. Biochem.* 2005, 137, 17–25.
37. Sanahuja, G.; Banakar, R.; Twyman, R.M.; Capell, T.; Christou, P. *Bacillus thuringiensis*: A century of research, development and commercial applications. *Plant Biotechnol. J.* 2011, 9, 283–300.
38. Okumura, S.; Saitoh, H.; Ishikawa, T.; Mizuki, E.; Inouye, K. Identification and characterization of a novel cytotoxic protein, parasporin-4, produced by *Bacillus thuringiensis* A1470 strain. *Biotechnol. Annu. Rev.* 2008, 14, 225–252.
39. Chubicka, T.; Girija, D.; Deepa, K.; Salini, S.; Meera, N.; Raghavamenon, A.C.; Divya, M.K.; Babu, T.D. A parasporin from *Bacillus thuringiensis* native to Peninsular India induces apoptosis in cancer cells through intrinsic pathway. *J. Biosci.* 2018, 43, 407–416.

40. Nelson, K.L.; Brodsky, R.A.; Buckley, J.T. Channels formed by subnanomolar concentrations of the toxin aerolysin trigger apoptosis of T lymphomas. *Cell. Microbiol.* 1999, 1, 69–74.
41. Maagd, R.A.; Bravo, A.; Berry, C.; Crickmore, N.; Schnepf, H.E. Structure, diversity, and evolution of protein toxins from spore-forming entomopathogenic bacteria. *Annu. Rev. Genet.* 2003, 37, 409–433.
42. Balabanova, L.; Golotin, V.; Podvolotskaya, A.; Rasskazov, V. Genetically modified proteins: Functional improvement and chimeragenesis. *Bioengineered* 2015, 6, 262–274.
43. Kim, S.B.; Izumi, H. Functional artificial luciferases as an optical readout for bioassays. *Biochem. Biophys. Res. Commun.* 2014, 448, 418–423.
44. He, L.; Friedman, A.M.; Bailey-Kellogg, C. Algorithms for optimizing cross-overs in DNA shuffling. *BMC Bioinform.* 2012, 13, S3.
45. Wedge, D.C.; Rowe, W.; Kell, D.B.; Knowles, J. In silico modelling of directed evolution: Implications for experimental design and stepwise evolution. *J. Theor. Biol.* 2009, 257, 131–141.
46. Pinzon, E.H.; Sierra, D.A.; Suarez, M.O.; Orduz, S.; Florez, A.M. DNA secondary structure formation by DNA shuffling of the conserved domains of the Cry protein of *Bacillus thuringiensis*. *BMC Biophys.* 2017, 10, 1–10.
47. Stimple, S.D.; Smith, M.D.; Tessier, P.M. Directed evolution methods for overcoming trade-offs between protein activity and stability. *AIChE J.* 2020, 66, e16814.
48. Basit, N.; Wechsler, H. Prediction of enzyme mutant activity using computational mutagenesis and incremental transduction. *Adv. Bioinform.* 2011, 2011, 1–9.
49. Florez, A.M.; Suarez-Barrera, M.O.; Morales, G.M.; Rivera, K.V.; Orduz, S.; Ochoa, R.; Guerra, D.; Muskus, C. Toxic activity, molecular modeling and docking simulations of *Bacillus thuringiensis* Cry11 toxin variants obtained via DNA shuffling. *Front. Microbiol.* 2018, 9, 2461.
50. BenFarhat-Touzri, D.; Driss, F.; Jemli, S.; Tounsi, S. Molecular characterization of Cry1D-133 toxin from *Bacillus thuringiensis* strain HD133 and its toxicity against *Spodoptera littoralis*. *Int. J. Biol. Macromol.* 2018, 112, 1–6.
51. Sriwimol, W.; Aroonkesorn, A.; Sakdee, S.; Kanchanawarin, C.; Uchihashi, T.; Ando, T.; Angsuthanasombat, C. Potential prepore trimer formation by the *Bacillus thuringiensis* mosquito-specific toxin: Molecular insights into a critical prerequisite of membrane-bound monomers. *J. Biol. Chem.* 2015, 290, 20793–20803.
52. Pacheco, S.; Gómez, I.; Sánchez, J.; García-Gómez, B.I.; Czajkowsky, D.M.; Zhang, J.; Soberón, M.; Bravo, A. Helix α -3 intermolecular salt bridges and conformational

- changes are essential for toxicity of *Bacillus thuringiensis* 3D-Cry toxin family. *Sci. Rep.* 2018, 8, 10331.
53. Phillips, J.C.; Braun, R.; Wang, W.; Gumbart, J.; Tajkhorshid, E.; Villa, E.; Chipot, C.; Skeel, R.D.; Kalé, L.; Schulten, K. Scalable molecular dynamics with NAMD. *J. Comput. Chem.* 2005, 26, 1781–1802.
 54. Deist, B.R.; Rausch, M.A.; Fernandez-Luna, M.T.; Adang, M.J.; Bonning, B.C. Bt toxin modification for enhanced efficacy. *Toxins* 2014, 6, 3005–3027.
 55. Sansinenea, E. Discovery and Description of *Bacillus thuringiensis*. In *Bacillus Thuringiensis Biotechnology*; Springer: Dordrecht, The Netherlands, 2012; pp. 3–18. ISBN 978940073021
 56. López-Meza, J.E.; Ibarra, J.E. Characterization of a novel strain of *Bacillus thuringiensis*. *Appl. Environ. Microbiol.* 1996, 62, 1306–1310. *Molecules* 2021, 26, 7476 13 of 13
 57. Walters, F.S.; deFontes, C.M.; Hart, H.; Warren, G.W.; Chen, J.S. Lepidopteran-active variable-region sequence imparts coleopteran activity in eCry3.1Ab, an engineered *Bacillus thuringiensis* hybrid insecticidal protein. *Appl. Environ. Microbiol.* 2010, 76, 3082–3088.
 58. Shah, J.V.; Yadav, R.; Ingle, S.S. Engineered Cry1Ac-Cry9Aa hybrid *Bacillus thuringiensis* delta-endotoxin with improved insecticidal activity against *Helicoverpa armigera*. *Arch. Microbiol.* 2017, 199, 1069–1075.
 59. de Maagd, R.A.; Weemen-Hendriks, M.; Stiekema, W.; Bosch, D. *Bacillus thuringiensis* delta-endotoxin Cry1C domain III can function as a specificity determinant for *Spodoptera exigua* in different, but not all, Cry1-Cry1C hybrids. *Appl. Environ. Microbiol.* 2000, 66, 1559–1563.
 60. Karlova, R.; Weemen-Hendriks, M.; Naimov, S.; Ceron, J.; Dukiandjiev, S.; de Maagd, R.A. *Bacillus thuringiensis* delta-endotoxin Cry1Ac domain III enhances activity against *Heliothis virescens* in some, but not all Cry1-Cry1Ac hybrids. *J. Invertebr. Pathol.* 2005, 88, 169–172.
 61. Naimov, S.; Weemen-Hendriks, M.; Dukiandjiev, S.; De Maagd, R.A. *Bacillus thuringiensis* delta-endotoxin Cry1 hybrid proteins with increased activity against the Colorado Potato Beetle. *Appl. Environ. Microbiol.* 2001, 67, 5328–5330.
 62. Abdullah, M.A.F.; Alzate, O.; Mohammad, M.; McNall, R.J.; Adang, M.J.; Dean, D.H. Introduction of *Culex* toxicity into *Bacillus thuringiensis* Cry4Ba by protein engineering. *Appl. Environ. Microbiol.* 2003, 69, 5343–5353.
 63. Abdullah, M.A.F.; Dean, D.H. Enhancement of Cry19Aa mosquitocidal activity against *Aedes aegypti* by mutations in the putative loop regions of domain II. *Appl. Environ. Microbiol.* 2004, 70, 3769–3771.

64. McNeil, B.C.; Dean, D.H. *Bacillus thuringiensis* Cry2Ab is active on *Anopheles* mosquitoes: Single D block exchanges reveal critical residues involved in activity. *FEMS Microbiol. Lett.* 2011, 325, 16–21.
65. Liu, X.S.; Dean, D.H. Redesigning *Bacillus thuringiensis* Cry1Aa toxin into a mosquito toxin. *Protein Eng. Des. Sel.* 2006, 19, 107–111.
66. Gómez, I.; Ocelotl, J.; Sánchez, J.; Lima, C.; Martins, E.; Rosales-Juárez, A.; Aguilar-Medel, S.; Abad, A.; Dong, H.; Monnerat, R.; et al. Enhancement of *Bacillus thuringiensis* Cry1Ab and Cry1Fa toxicity to *Spodoptera frugiperda* by domain III mutations indicates there are two limiting steps in toxicity as defined by receptor binding and protein stability. *Appl. Environ. Microbiol.* 2018, 84, e01393-18.
67. Craveiro, K.I.C.; Júnior, J.E.G.; Silva, M.C.M.; Macedo, L.L.P.; Lucena, W.A.; Silva, M.S.; Júnior, J.D.A.d.S.; Oliveira, G.R.; Magalhães, M.T.Q.d.; Santiago, A.D.; et al. Variant Cry1a toxins generated by DNA shuffling are active against sugarcane giant borer. *J. Biotechnol.* 2010, 145, 215–221.
68. Soberon, M.; Pardo-Lopez, L.; Lopez, I.; Gomez, I.; Tabashnik, B.E.; Bravo, A. Engineering modified Bt toxins to counter insect resistance. *Science* 2007, 318, 1640–1642.
69. Tabashnik, B.E.; Huang, F.; Ghimire, M.N.; Leonard, B.R.; Siegfried, B.D.; Rangasamy, M.; Yang, Y.; Wu, Y.; Gahan, L.J.; Heckel, D.G.; et al. Efficacy of genetically modified Bt toxins against insects with different genetic mechanisms of resistance. *Nat. Biotechnol.* 2011, 29, 1128–1131.
70. Park, H.W.; Bideshi, D.K.; Federici, B.A. Molecular genetic manipulation of truncated Cry1C protein synthesis in *Bacillus thuringiensis* to improve stability and yield. *Appl. Environ. Microbiol.* 2000, 66, 4449–4455.
71. Fujii, Y.; Tanaka, S.; Otsuki, M.; Hoshino, Y.; Endo, H.; Sato, R. Affinity maturation of Cry1Aa toxin to the *Bombyx mori* cadherin-like receptor by directed evolution. *Mol. Biotechnol.* 2013, 54, 888–899.
72. Oliveira, G.R.; Silva, M.C.; Lucena, W.A.; Nakasu, E.Y.; Firmino, A.A.; Beneventi, M.A.; Souza, D.S.; Gomes, J.E., Jr.; de Souza, J.D., Jr.; Rigden, D.J.; et al. Improving Cry8Ka toxin activity towards the cotton boll weevil (*Anthonomus grandis*). *BMC Biotechnol.* 2011, 11, 85.
73. Shao, E.; Lin, L.; Chen, C.; Chen, H.; Zhuang, H.; Wu, S.; Sha, L.; Guan, X.; Huang, Z. Loop replacements with gut-binding peptides in Cry1Ab domain II enhanced toxicity against the brown planthopper, *Nilaparvata lugens* (Stål). *Sci. Rep.* 2016, 6, 20106.
74. Vílchez, S. Making 3D-cry toxin mutants: Much more than a tool of understanding toxins mechanism of action. *Toxins* 2020, 12, 600.

75. Velásquez, L.-F.; Rojas, D.; Cerón, J. Proteínas de *Bacillus thuringiensis* con actividad citotóxica: Parasporinas. *Rev. Colomb. Biotecnol.* 2018, 20, 89–100.

3. Computational study, synthesis and evaluation of active peptides derived from Parasporin-2 and spike protein from Alphacoronavirus against colorectal cancer cells

Jenniffer Cruz

Miguel Orlando Suárez-Barrera

Paola Rondón-Villarreal

Andrés Olarte-Díaz

Fanny Guzmán

Lydia Visser

Nohora Juliana Rueda-Forero

Bioscience Reports

2021, 41 BSR20211964 <https://doi.org/10.1042/BSR20211964>

Author Contributions: Conceptualization, J.C., M.O.S.-B. and N.J.R.-F.; A.O.-D writing—original draft preparation J.C., M.O.S.-B., P.R.-V., and N.J.R.-F; writing—review and editing J.C., P.R.-V., F.G., M.O.S.-B., L.V., F.G., and N.J.R.-F.; supervision J.C., M.O.S.-B. and N.J.R.-F. All authors have read and agreed to the published version of the manuscript. **Funding:** The work has been funded by the Universidad de Santander, Colombia, and MINCIENCIAS, MINEDUCACIÓN, MINCIT and ICETEX, through the Program Ecosistema Científico Cod. FP44842-211-2018, Project number 58668.

This chapter is linked to the aims: - To design engineering strategies for Parasporin PS2Aa1, combining directed evolution methodologies, site-specific mutagenesis, structural bioinformatics tools, and the structural and functional knowledge described in the literature to obtain proteins with different potentials to control cancer cell lines growing.- To analyze the PS2Aa1-APN receptor interactions using computational strategies involving molecular docking and dynamics to explore the possible potential of this membrane receptor to bind to the domain I of this parasporin.- To produce novel parasporal proteins with enhanced activity against colon cancer cell lines and determine

the cytotoxic activity of selected mutant proteins of *Bacillus thuringiensis* based on their binding affinity to membrane receptors by computational approaches.

In this study, it was begun to investigate how computational tools provide insight into some regions of the PS2Aa1 domain I that interact with the APN receptor, based on this information a synthesis of peptides belonging to loops 1 and 2 of this anticancer protein was performed. This chapter allowed to determine what region can be selected as the candidate for obtaining new variants of PS2Aa1, based on the results of cytotoxicity and binding assays. The results of this work were utilized to create PS2Aa1 variants, some of which are described in Chapter 4.

3.1 Abstract

Parasporin-2Aa1 (PS2Aa1) is a toxic protein of 37 kDa (30 kDa, activated form produced by proteolysis) that was shown to be cytotoxic against specific human cancer cells, although its mechanism of action has not been elucidated yet. In order to study the role of some native peptide fragments of proteins on anticancer activity, here we investigated the cytotoxic effect of peptide fragments from domain-1 of PS2Aa1 and one of the loops present in the binding region of the virus spike protein from Alphacoronavirus (HCoV-229E), the latter according to scientific reports, who showed interaction with the human APN (h-APN) receptor, evidence corroborated through computational simulations, and thus being possible active against colon cancer cells. Peptides namely P264-G274, Loop1-PS2Aa, and Loop2-PS2Aa were synthesized using the Fmoc solid-phase synthesis and characterized by mass spectrometry (MS). Additionally, one region from loop 1 of HCoV-229E, Loop1-HCoV-229E, was also synthesized and characterized. The A4W-GGN5 anticancer peptide and 5-fluorouracil (5-FU) were taken as a control in all experiments. Circular dichroism revealed an α -helix structure for the peptides derived from PS2Aa1 (P264-G274, Loop1-PS2Aa, and Loop2-PS2Aa) and β -laminar structure for the peptide derived from Alphacoronavirus spike protein Loop1-HCoV-229E. Peptides showed a hemolysis percentage of less than 20% at 100 μ M concentration. Besides, peptides exhibited stronger anticancer activity against SW480 and SW620 cells after

exposure for 48 h. Likewise, these compounds showed significantly lower toxicity against normal cells CHO-K1. The results suggest that native peptide fragments from Ps2Aa1 may be optimized as a novel potential cancer-therapeutic agent.

3.2 Introduction

In the world, colorectal cancer (CRC) is one of the major causes of death, among the most common cancers types, CRC is currently ranked fourth, after female breast, lung, and prostate cancer, with 1.93 million new cases and almost 935,000 deaths in 2020 according to the World Health Organization GLOBOCAN [1], representing about 10% of cancer cases and deaths. Overall, colorectal cancer ranks third in terms of incidence but second in terms of mortality. It is predicted that in the year 2035, the number of new cases of CRC may increase to nearly 2.5 million [2]. The annual prevalence for colon cancer in Colombia also.

Places it as the third most frequent cancer type, after prostate and breast cancer, accounting for 8.3% of the total malignant neoplasms and with a mortality rate that locates it in the fourth place [3]. Surgery, radiotherapy, and chemotherapy are the most common treatments for colon cancer, which are very invasive and with a large number of side effects [4–8]. The development of new strategies to combat colon cancer has become urgent, and anticancer peptides (ACPs) are proposed as promising molecules. Compared with other small organic molecules and proteins, ACPs have several outstanding properties, such as small size, high activity, low immunogenicity, good biocompatibility, diversity of sequences, and multiple modification sites for the functional molecules [9]. Initially, according to their mechanism of action, ACPs were considered membrane-active peptides (necrosis) regarding their primary activity [10]. However, over the years, it was clarified that they could also be linked to different processes such as mitochondrial membrane lytic activity (apoptosis), angiogenesis inhibition, inhibition/activation of essential proteins, or recruitment of immune cells to attack cancer cells [11,12]. From a structural point of view, most ACPs have either α -helical or β -sheet conformation but some extended structures have also been reported [13]. Concerning cell targets, they can be classified into two major groups. The first one includes peptides, such as cecropins and

magainins, which are active against microbial and cancer cells while being harmless to healthy mammalian cells. The second group contains ACPs, such as human neutrophil defensins HNP-1 to 3 that act against all three types of cells: microbial, normal, and cancerous [11,14]. For the design of ACPs, *in silico* techniques have been useful to save time and reduce costs in experimental tests by predicting, screening, and designing peptides with potential anticancer activity [15]. Equipments such as Support Vector Machines, and methods like molecular docking and molecular dynamics have been used in the design of ACPs [16], and also in the identification of potential anticancer molecules that inhibit important targets such as CDK2 [17], CDK5, CDK7, and CDK9 [18]. Similarly, fragmentation is a strategy to obtain short bioactive peptides from the bioactive proteins [19], e.g., HPRP-A1 exhibited a broad-spectrum anticancer activity and it is derived from the N-terminus of the ribosomal protein L1 of *Helicobacter pylori* [20]. Furthermore, Liu et al. [21] designed the ABH3 peptide, derived from the BH3 protein, and the data indicated that the ABH3 peptide induces cell death through the lytic properties of the peptide that disrupts cell membrane. Among others, a cyclo [EMTOVNOGQ] peptide from alpha-fetoprotein (AFP), a human protein produced during pregnancy, was tested for activity against cancer cells [22]. An interesting protein with anticancer properties is PS2Aa1, also classified as Cry46Aa1, which is produced by the Gram-positive bacterium *Bacillus thuringiensis* (Bt) during sporulation. This protoxin (37 kDa) is activated by serine proteases, such as proteinase K and trypsin, producing a highly toxic fragment (30 kDa) active against cancer cells [23–27]. Nevertheless, its mechanism of action or the receptors involved in its interaction with cells is still mostly unknown in detail. PS2Aa1 shares a remarkable structural similarity with Epsilon (ETX) and β -type aerolysin toxins, which are recognized as β -pore-forming toxins (β -PFTs). This similarity suggests a possible mechanism of pore action for this type of toxins [28]. Another study [24] proposed the induction of apoptosis as a mechanism of cell death together with the identification of multiple survival pathways, inhibitions including AKT, XIAP, ERK1/2, and the induction of the tumor suppressor PAR-4 after treatment with PS2Aa1. Abe et al. [29] proposed that PS2Aa1 toxins are capable of producing oligomerization, which in turn induce cell death by their binding to areas rich in membrane lipids, such as lipid rafts. It is important to note that for many of the Cry insecticidal toxins, protein receptors present in lipid rafts have

been recognized, such as aminopeptidases including human aminopeptidase (h-APN) or alkaline ALP phosphatases, proteins anchored to GPI (glucosyl-phosphatidyl-inositol) [30]; hence, receptor proteins of this type may induce the activity of toxins. Structurally, PS2Aa1, has three different domains. Domain I is rich in aromatic amino acid residues with structural diversity; it has an extended conformation of β sheets, with hydrophobic regions in the distal surface of the domain, and it is involved in the processes of insertion in the membrane and monomer oligomerization. Domain I is attributed to the primary function of recognizing membrane receptors, such as the GPI and APN anchor proteins in the glycan region. Domain II is linked to amphipathic hairpins through β chains, which are essential for pore formation. The domain III segment probably contains an amphipathic elongation consisting of a β sheet and α helix and tends to be organized similarly to aerolysins [23,28,31,32]. Therefore, the main goal of the present study was the evaluation of the anticancer activity of three native sequences derived from PS2Aa1 domain-1, P264-G274, Loop1-PS2Aa, and Loop2-PS2Aa against colon cancer cells SW680 and SW480 using the strategy of fragmentation for the search of new bioactive compounds. These fragments were chosen based on computational analysis of the possible regions of interactions in the PS2Aa1 domain-1. Peptides sequences from the most promising regions were selected as peptides, and molecular docking simulations were performed with the APN receptor. Additionally, one fragment derived from Alphacoronavirus, Loop1-HCoV-229E, was selected because it is well-known that according to its mechanism of action, the virus interacts with the APN receptor [33]. Peptides showed to be bioactive in a dose-dependent concentration. Besides, for the most active peptide against each evaluated cancer cell line, the cellular adhesion percentage and fluorescence microscopy were evaluated to propose a possible explanation of the mechanism involved in the anticancer activity.

The present study constitutes a basis for the development of new analogs peptides or else conducting site-directed mutations of the PS2 protein to increase its anticancer potential. Additionally, Loop1-PS2Aa and P264-G274, peptides that exhibited stronger anticancer activity against SW480 and SW620 respectively and demonstrated high effectiveness and selectivity, are proposed as possible alternative as therapeutic agents for the treatment of colon cancer.

3.3 Materials and Methods

3.3.1 Materials and reagents

5-Fluorouracil (5-FU), fetal bovine serum (FBS) and sulforhodamine B (SFB) were purchased from Sigma (Sigma Aldrich, U.S.A.). Dulbecco's modified Eagle's medium (DMEM), L-glutamine, and penicillin/streptomycin were purchased from Lonza (Walkersville, MD, U.S.A.). Trypsin-EDTA was purchased from Invitrogen/Gibco.

3.3.2 Peptide synthesis and characterization

All natives' sequences from PS2Aa1 and HCoV-229E were synthesized via F-moc solid-phase peptide synthesis (SPPS) [34] using the tea-bag procedure reported by Houghten [35]. Peptides were purified by Reverse Phase-High Performance Liquid Chromatography (RP-HPLC) (Jasco Corporation, Tokyo, Japan) using a Vydac C-18 preparative column using a mixture of (A) H₂O with 0.1% (v/v) TFA, and (B) acetonitrile (ACN) containing 0.1% (v/v) TFA as mobile phase. For the elution of peptides, the gradient program was: 30 min with 5–70% of B at 1 ml/min and detection at 220 nm. The molar mass of purified peptides was determined by ESI-MS mass spectrometry (MS) [36,37] (Supplementary Figures S1–S5). Circular dichroism (CD) of peptides was carried out at 25°C in a 1 mm path length cuvette and spectra were obtained over 190–260 nm in a CD Spectrometer (J-815 Jasco Corporation, Japan) using a 0.2 mM peptide solution dissolved in a mixture of 50 mM sodium phosphate buffer, pH 7.4, and 30% (v/v) 2,2,2-trifluoroethanol (TFE). Each spectrum was obtained as an average of three scans taken at a rate of 20 (nm/min) with a spectral band of 1 nm. Each experiment was repeated four times and averages were taken of the resulting data [38].

3.3.3 Hemolytic activity assay

The hemolytic activity of the peptides was determined by measuring the hemolysis in sheep erythrocytes induced by them, as reported in previous studies [39]. A suspension

containing the erythrocytes and 0.1% Triton X-100 was used as a positive control. The percentage of hemolysis was calculated using the following (eqn 1):

$$\text{Hemolysis (\%)} = \frac{A_s - A_0}{A_{100} - A_0} * 100 \quad (1)$$

where A_s is the absorbance of the sample, A_{100} is the absorbance of erythrocytes completely lysed in 0.1% Triton X-100, and A_0 is the absorbance in the complete absence of hemolysis. All tests were performed independently in triplicate.

3.3.4 Cell and culture conditions

All cell lines (SW480, SW620 and CHO-K1) used in this research were obtained from the Programa de Nanobiocáncer de Colombia Científica. Human epithelial colorectal adenocarcinoma cells from line SW480 and SW620 have grown in 75 cm² flasks 10ml and maintained in 10ml of Dulbecco's Modified Eagle Medium (DMEM) containing 10% fetal bovine serum (FBS), 2mM glutamine, 1% MEM of non-essential amino acids, 10.000U/ml of penicillin, 10.000 µg/ml of streptomycin and 25 µg/ml of amphotericin B. Cells were cultured at 37°C in a 5% CO₂ atmosphere. CHO-K1, cell line derived from a biopsy of an ovary of an adult Chinese hamster, was taken as control of normal cells.

3.3.5 Cytotoxicity assay

Assessment of cytotoxicity of tested peptides (P264-G274, Loop1-PS2Aa, Loop2-PS2Aa, and Loop1-HCoV-229E) and 5-FU in non-cancerous (CHO-K1) cell line and human colon cancer cells, SW480 and SW620, were performed by the SFB assay [40]. 5-FU, an established chemotherapeutic drug, and peptide A4W-GGN5, a potent antimicrobial and anticancer peptide derived from Gaegurin 5, were used as positive control. Briefly, CHO-K1, SW480, and SW620 cells at a density of 2×10^5 cells/well were seeded into 96-well plates. After 24 h of incubation, the medium was removed, and cells were exposed to different concentrations of peptides and chemotherapeutic drug (from 0 to 150 µM) with the control being replaced with phosphate buffer saline (PBS). After 12 and 48 h of peptides and 5-FU treatment, without removing the medium, 50 µl of TCA (50% p/v) were added to each well, and the plates were incubated by 1 h at 4°C. After the

plates were washed five times with water, they were dried at room temperature. Then 100 μ l of SRB (0.4% p/v) was added to each well and the plates were incubated for 30 min. Later on, the plates were washed five times with (1% v/v) acetic acid and dried at room temperature, and the colorant SRB was dissolved in 200 μ L of buffer Tris 10 mM (pH 10.5). Finally, after gently mixing, the absorbance of each well was evaluated at 450 nm in a Varioskan™ LUX multimode microplate reader (Thermo Fisher Scientific, Waltham, MA, U.S.A.). Experiments were done in triplicate and results are presented as the percentage of inhibition of non-treated CHO-K1 or SW480 and SW620 cells. Data represent the mean and standard deviation of three independent experiments (n=3). The concentration at which the chemotherapeutic agent and the peptides effectively reduced cell viability by 50% (EC50) for each cell line, was calculated in GraphPad Prism 4.03 software (GraphPad Software, Inc., La Jolla, CA, U.S.A.) using non-linear regression.

3.3.6 *In vitro* binding assay

SW480 and SW620 cells at a density of 2×10^5 cells/well were seeded into 24-well plates. After 24 h of incubation, cell binding was examined by inoculating the suspension with 750 μ l of the rhodamine-labeled peptide at different concentrations (from 0 to 150 μ M). After 1 h of incubation at 37°C and 5%CO₂ atmosphere, a constant volume of the supernatant (containing non-adherent peptides) was collected from the well, and the fluorescence of the supernatant was measured in a Varioskan™ LUX multimode microplate reader (Thermo Fisher Scientific, Waltham, MA, U.S.A.) (λ_{ex} = 546 nm; λ_{em} = 568 nm). The assay was performed using six replicates for each peptide in SW620 and SW480 cells from the same number of passes. The adherent fraction of the peptide was measured by interpolation with a calibration curve for each peptide. The test results were expressed as percent binding, taking into account the relationship between the initial concentration of the peptide and the concentration of adherent peptide [41].

3.3.7 Fluorescence microscopy

The assays for determining the localization of the peptides in the SW620 and SW480 cells were carried out as previously published [42]. In detail, the cells were seeded into chamber slides (2×10^5 cells/well) for 24 h, washed twice with PBS, and then incubated in the absence and presence of the most active rhodamine-labeled peptides for each of cell line, at a concentration twice the EC50 for 1 h at 37°C in the dark. After that, the monolayers were washed three times with PBS (1 mM, pH 7.2) to remove the excess peptide, and the cells were fixed with a 4% (v/v) solution of p-formaldehyde in PBS for 30 min. The cell monolayers were washed with PBS and the core was stained with 1 mg/ml of Hoechst for 2 min at room temperature. The monolayers were analyzed in a Nikon Eclipse TE2000-E fluorescence microscopy.

3.3.8 Annexin V-Cy3 staining

The presence of phosphatidylserine at the cell surface was detected by phosphatidylserine binding protein annexin V conjugated with Cy3 using the commercially available Annexin V-Cy3 apoptosis detection kit (APOAC, Apoptosis Detection Kit, Sigma). The cells (2.0×10^5 ml⁻¹) were seeded into chamber slides for 24 h, washed twice with PBS, and then incubated in the absence and presence of the most active peptides with the respective EC50 concentrations of the most active peptides for each of cell line (SW480 and SW620) for 24 and 48 h. The PBS and binding buffer were used to wash the adherent cells and the washed cell adherents were suspended in 50 µl of Ann-Cy3 and 6-CFDA. Then, the plates were incubated for 10 min in the dark. Afterwards, the excess label was removed by washing the cells with binding buffer. EVOS M7000 digital inverted fluorescence microscope (Thermo Fisher Scientific; Waltham, MA, U.S.A.) was used to observe Ann-Cy3 and 6-CFDA-labeled cells. This assay allowed one to differentiate live cells (green), necrotic cells (red), and apoptotic cells (red nuclei and green cytoplasm). The percentage of cells reflecting apoptotic and necrotic cells was manually calculated. Data were collected for three replicates and used to calculate the respective means and standard deviations [24].

3.3.9 Caspase 3-7 assay

To measure the specific activity of caspase 3 and 7, an assay kit named CellEvent™ Caspase-3/7 Green Detection Reagent (Invitrogen™) was used. This assay provides a proluminescent caspase-3/7 substrate containing a sequence (DEVD) specific to caspase 3 and 7. If caspases 3 and/or 7 are active, the substrate is cleaved and aminoluciferin will be emitted. Briefly, chamber slides were seeded with 50 µl of cancer cells (for SW480 and SW620, 20000 cells/well) resuspended in the culture medium. Plates were incubated at 37°C, 5% CO₂ for 24 h. Cells were loaded with 7.5 µM CellEvent™ Caspase-3/7 Green Detection Reagent then treated at EC₅₀ concentration of more active peptide for each cell and incubated for another 4 h. After that, the monolayers were washed three times with PBS (1 mM, pH 7.2) to remove the excess peptide, and the cells were fixed with a 4% (v/v) solution of p-formaldehyde in PBS for 30 min. About 10 µL of Entellan were added each sample and mounted with a glass coverslip. The monolayers were analysed in a Nikon Eclipse TE2000-E fluorescence microscopy [43].

3.3.10 LDH assay

Lactate dehydrogenase (LDH) is a cytosolic enzyme present in many different cell types that is released into the cell culture medium upon damage to the plasma membrane. The CyQUANT LDH Cytotoxicity Assay was used to accurately and quantitatively measure this extracellular LDH. For this test 10.000 cells/100 µl (the optimal number) were plate in triplicate wells in a 96-well tissue culture plate with additional wells for controls (Spontaneous LDH Activity and Maximum LDH Activity). Cells were incubated overnight at 37°C with the appropriate level of CO₂. After overnight incubation, samples were prepared according to the following: was added 10 µl of sterile, ultrapure water to one set of triplicate wells of cells, was added nothing to one set of triplicate wells of cells and was added 10 µl of the peptides to one set of triplicate wells of cells. To the set of triplicate wells serving as the Maximum LDH Activity Controls, was added 10 µl of 10× Lysis Buffer, then mix by gentle tapping. The plate was incubated at 37°C with the appropriate level of CO₂ for 45 min. Then, 50 µl of the supernatant were transferred of each sample

(Spontaneous LDH Activity, Maximum LDH Activity, and Chemical-treated LDH activity) to a 96-well flat-bottom plate in triplicate wells. Aliquot of 50 μ l of reaction mixture was placed to each sample well, then mixed well. The plate was incubated at room temperature for 30 min protected from light. About 50 μ l of Stop Solution was added to each sample, then the absorbance at 490 and 680 nm was measured [44].

3.3.11 Molecular docking of peptides and APN receptor

The 3D structure of the peptides was predicted using the software PEP-FOLD 3.5 [45], and the 3D structure of the APN receptor was obtained from the Protein Data Bank [46] (PDB ID: 6ATK), keeping only the A chain. For the two peptides that produced the best experimental results, two rounds of molecular docking simulations were performed to predict their binding with the APN receptor by using the software tool Rosetta (version 3.12) [47]. In the first round, 500 models were obtained by using a global simulation, i.e., the peptide could move around the APN receptor. For this round, the flags used in Rosetta were set as follows: -nstruct 500, -dock pert 3 3, -spin, -randomize1, -randomize2, -ex1 and -ex2aro. Later on, the number of possible hydrogen bonds between the peptide and the APN was obtained for each of the 500 models, and the most frequent residues involved in hydrogen bond interactions were identified. Additionally, for each peptide, the model with the highest number of hydrogen bonds, and the peptide located near to the most frequent residues, were selected to be used in the refinement step by using the FlexPepDock protocol of Rosetta with the following flags: -nstruct 100, -flexPepDocking:flexpep score only, -flexPepDocking:pep refine, and the Rosetta FlexPepDock web server [48] (version 3.2) was also used with the number of low and high-resolution structures equal to 100. Finally, the resulting models were analyzed in terms of hydrogen bonds with the APN receptor.

3.3.12 Statistical analysis

All experiments were repeated at least three times. Results were expressed as mean values \pm standard error (mean \pm SE). Significant differences between the

treatments and their respective controls were determined based on one-way ANOVA followed by Tukey's test. A level of $P < 0.05$ was considered to be significant.

3.4 Results

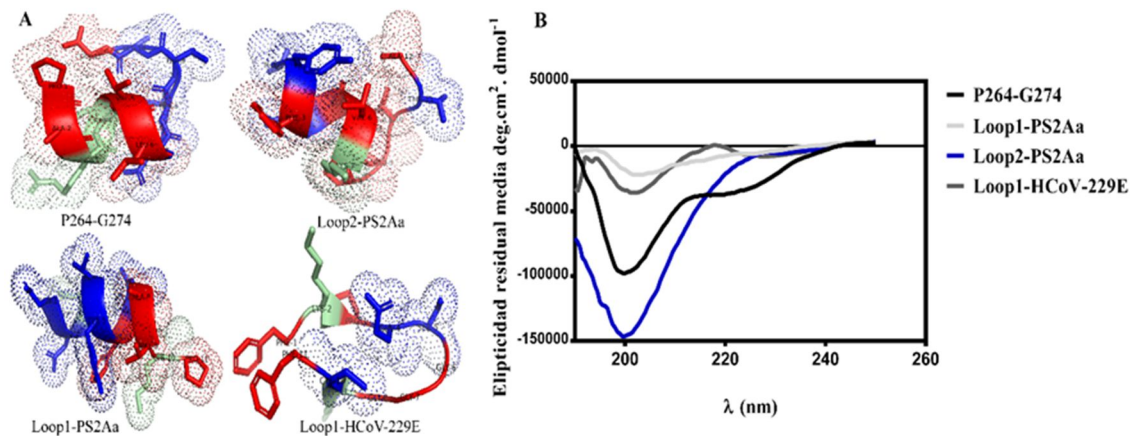
3.4.1 Design and characterization of the peptides

Based on previous journal publications [49] and results obtained by a computational analysis in our research group, it was possible to identify some probable regions of PS2Aa1 that can interact with the h-APN receptor. Based on these considerations, the PS2Aa1 was fragmented, and three peptides, namely P264-G274, Loop1-PS2Aa and Loop2-PS2Aa, were derived from this toxin, and their synthetic forms were synthesized by Fmoc methodology. Additionally, one region from loop 1 of HCoV-229E, Loop1-HCoV-229E, was synthesized to use as a control, since it has been shown that the HCoV-229E acts through its interaction with the h-APN receptor [33]. Here, the biological activity of peptides derived from different loops in the PS2Aa1 and HCoV-229E was evaluated against colon cancer cells. Peptides presented different physicochemical properties, as shown in Table 1. The net positive charge of peptides varies from +1 to +3. According to Heliquist [50], P264-G274 peptide has 63.64% of polar residues and 36.36% of non-polar residues, a hydrophobicity (H) value of 0.19, and a hydrophobic moment (μH).

Table 7. Peptides sequence, molecular characterization and physicochemical properties (net positive charge) (<https://www.bachem.com/service-support/peptide-calculator/>), H (hydrophobicity), μH (hydrophobic moment).

Peptide	Sequence	Number of residues	z	Molecular weight (Da)		H	μH
				Theoretical	Observed		
P264-G274	PARDVLNTTSG-NH ₂	11	+1	1129.29	1130.23	0.19	0.38
Loop1-PS2Aa	NNETYFNAVKP-NH ₂	11	+1	1295.47	1295.49	0.17	0.23
Loop2-PS2Aa	TYFNAVKPPITA-NH ₂	12	+2	1320.61	1320.63	0.56	0.34
Loop1-HCoV-229E	FKPQSGGGKCF-NH ₂	11	+3	1154.41	1154.44	0.33	0.35
A4W-GGN5	FLGWLFKVASK-NH ₂	11	+3	1294.67	1294.68	0.80	0.50

Figure 13. Secondary structure of peptides. A) theoretical in silico secondary structure of P264-G274, Loop1-PS2Aa, Loop2-PS2Aa, and Loop1-HCoV-229E. B) circular dichroism spectra of the peptides in TFE (30% p/V). CD was recorded after four accumulations at 20 °C, using a 1mm path length quartz cell, between 190 and 250 nm at 100 nm min⁻¹, with a bandwidth of 0.5 nm. Peptide concentration: 1 mg/mL.



value of 0.30; besides, it is an uncharged peptide. Loop1-PS2Aa and Loop2-PS2Aa peptides presented H values of 0.17 and 0.56, respectively. μ H values of Loop1-PS2Aa and Loop2-PS2Aa peptides were 0.23 and 0.34, respectively. Loop1-PS2Aa peptide presented a net positive charge of +1, while Loop2-PS2Aa peptide presented a net positive charge of +2. Loop1-HCoV-229E, a unique peptide derived from HCoV-229E spike protein, presented an H value of 0.33 and a μ H value of 0.35. Additionally, this was the peptide with the highest net positive charge (+2) along with the control peptide A4W-GGN5. Peptides were characterized by MS, and all the peptides presented the same theoretical and experimental mass (m/z), as shown in Table 1.

On the other hand, the theoretical in silico secondary structures of the peptides obtained with the software PEP-FOLD 3.5 [45] were compared with the CD spectra. All the peptides exhibited a theoretical α -helix secondary structure (see Figure 1), except for the Loop1-HCoV-229E peptide that exhibited a theoretical β -lamellar secondary structure. The secondary structure of the peptides was also confirmed by the determination of their CD spectra. Figure 1 shows the CD spectra of all the synthesized compounds, in which all PS2Aa1 derivatives exhibited a maximum absorption band at 190 nm and two minimum absorption bands between 205 and 220nm (see Figure 1A,B). On the other hand, the CD spectra for alphacoronavirus-derived peptides exhibited a secondary structure of β -

sheets, with a maximum absorption band at 195 nm and a minimum absorption band at 216 nm.

3.4.2 Anticancer and hemolytic activities

The anti-proliferative response of the peptides and the chemotherapeutic drug (5-FU) on SW480 and SW620 were examined using the SRB assay. The anticancer activities P264-G274, Loop1-PS2Aa, Loop2-PS2Aa, and Loop1-HCoV-229E peptides against two different cancer colon cell lines are shown in Table 2. For all cell lines tested, Loop1-PS2Aa exhibited a stronger anticancer activity against SW480 after exposure for 48 h, whereas the most active peptide against SW620 was P264-G274 at the same exposure time.

Table 8. *EC₅₀ and HC₅₀ values of the anticancer and hemolytic activity of the peptides.*

Peptide	EC ₅₀ (μM)		CHO-K1	%HC ₅₀ at 150 (μM)
	SW480	SW620		
P264-G274	90.98±0.75	11.28±0.52	---	12.2
Loop1-PS2Aa	23.76±1.25	106.2±1.67	----	18.1
Loop2-PS2Aa	92.99±0.98	15.95±0.69	----	9.4
Loop1-HCoV-229E	125.0±1.32	>150.0	----	9.2
A4W-GGN5	98.63±1.17	22.07±1.63	----	23.0
5-FU	24.38±0.82	11.92±1.20	----	-----

--- Undetermined

The results show dose-dependent inhibition of cell growth at 48 h, as illustrated in Figure 2A–C. The ability of all peptides to inhibit the growth of SW480 and SW620 cells is significant from the concentration of 4 μM. Within all cell lines tested, Loop1-PS2Aa exhibited stronger anticancer activity against SW480 after exposure for 48 h, whereas the most active peptide against SW620 was P264-G274 at the same time of exposure. At 48 h of exposure, the peptides did not exhibit significant inhibition of normal CHO-K1 cells (Figure 2C). Furthermore, the peptides were more active against SW620 cells than against SW480 cells. 5-FU exhibited significant inhibition of the growth from 48 h of treatment in both cell lines.

The percentages of viability SW480 cells at the highest peptides concentration (150 μM) were as follows: Loop1-PS2Aa peptide 16%; Loop2-PS2Aa peptide 39.5%; peptide

P264-G274 41.6%; Loop1-HCoV-229E peptide 56.2%. In this case, the Loop1-PS2Aa peptide was more active than the positive controls 5-FU (18.9% viability) and A4W-GGN5 (41.8% viability) (Figure 2A). In the case of SW620 cells, the percentages of cell viability at the same peptide concentration were: P264-G274 16.5%; Loop2-PS2Aa peptide 24.1%; Loop1-PS2Aa peptide 46.8%; Loop1-HCoV-229E peptide 55.2%. 5-FU exhibited strong activity on SW480 cells with a viability percentage of 2.8%, while the value for the A4W-GGN5 peptide was of 32.2% (Figure 2B). The anticancer activities of P264-G274, Loop1-PS2Aa, Loop2-PS2Aa, and Loop1-HCoV-229E peptides against two different colon cancer cell lines are shown in Table 2. The peptides presented anticancer activity with EC₅₀ values ranging from 11.28 μM to more than 150 μM . Loop1-PS2Aa peptide showed higher activity (EC₅₀ 23.76 μM) than 5-FU (EC₅₀ 24.38 μM)- against SW480, while the EC₅₀ values of P264-G274, Loop2-PS2Aa, Loop1-HCoV-229E, and A4W-GGN5 peptides were 90.98 μM , 92.99 μM , 125.0 μM , and 98.63 μM , respectively. Moreover, the peptide P264-G274 showed the highest EC₅₀ value of 11.28 μM , followed by 5-FU (11.92 μM), Loop2-PS2Aa (15.95 μM), A4W-GGN5 (22.07 μM) Loop1-PS2Aa (106.2 μM) and Loop1-HCoV-229E peptides (>150.0 μM).

The peptides were more active against the SW620 cells than against SW480 cells after 48h of exposure. The degree of hemolysis of the peptides derived from PS2Aa1 was determined on human erythrocytes. The results presented in Figure 3 and Table 2 show that all evaluated peptides exhibited an HC₅₀ value of less than 150 μM , with a percentage of hemolysis less 24% lower than the positive control (TX-100 0.1%). These results indicate that all compounds evaluated may be promising candidates as anticancer agents, without producing a negative effect on red blood cells.

3.4.3 *In vitro* binding assay

In vitro cell binding of the most active peptides was evaluated at an 1 h incubation period with the compounds labeled with rhodamine fluorochrome. The concentration of the attached peptide was calculated indirectly by quantifying the fluorescence of each of the supernatants of the peptides at different concentrations and by performing the

calibration curve of each of the most active peptides against the SW480 cell lines and SW620.

The results show that at low peptide concentrations, the percentages of cell binding are high, but as the concentration increases, they decrease probably when approaching the saturation level of the molecules in contact with the cell membrane (Figure 4). In Figure 4, the Loop1-Ps2Aa peptide, the most active against the SW480 cell line, showed that at its highest concentration (150 μM) 19.3% of it has bound (37.4 μM). In contrast, at low concentrations, 4 , 8, and 16 μM , the percentages of binding were 100%, 95.3%, and 63.5%, respectively. On the other hand, the P264-G274 peptide presented a very low level of cell binding at all the concentrations evaluated with SW620 cells. At 4 μM concentration, only 35.3% of the cells binding, while at the highest peptide concentration (150 μM) only 4% had adhered or penetrated the cell. These results show a greater difficulty of adhesion or entry of the P264-G274 peptide on the SW620 cells when compared with the binding of the Loops1-PS2Aa peptide to the SW480 cells. The number of residues with which the peptide chain of P264-G274 can interact with the receptors present in SW620 cells may be less.

Figure 14. Effect of peptides (P264-G274, Loop1-PS2Aa, Loop2-PS2Aa, Loop1-HCoV-229E, and A4W-GGN5) and the chemotherapeutic drug (5-FU), on the viability of -cancerous and non-cancerous cells measured by the SRB assay. A4W-GGN5 and 5-FU were used as a positive control. (A-C) SW480, SW620, and CHO-K1 cells were incubated with peptides in the concentration range of 0-150 μM for 48 h. Dosages that caused a statically significant decrease in cell growth compared to the untreated control at each time point were indicated by asterisks (* $p < 0.05$; one-way ANOVA followed by Tukey's test).

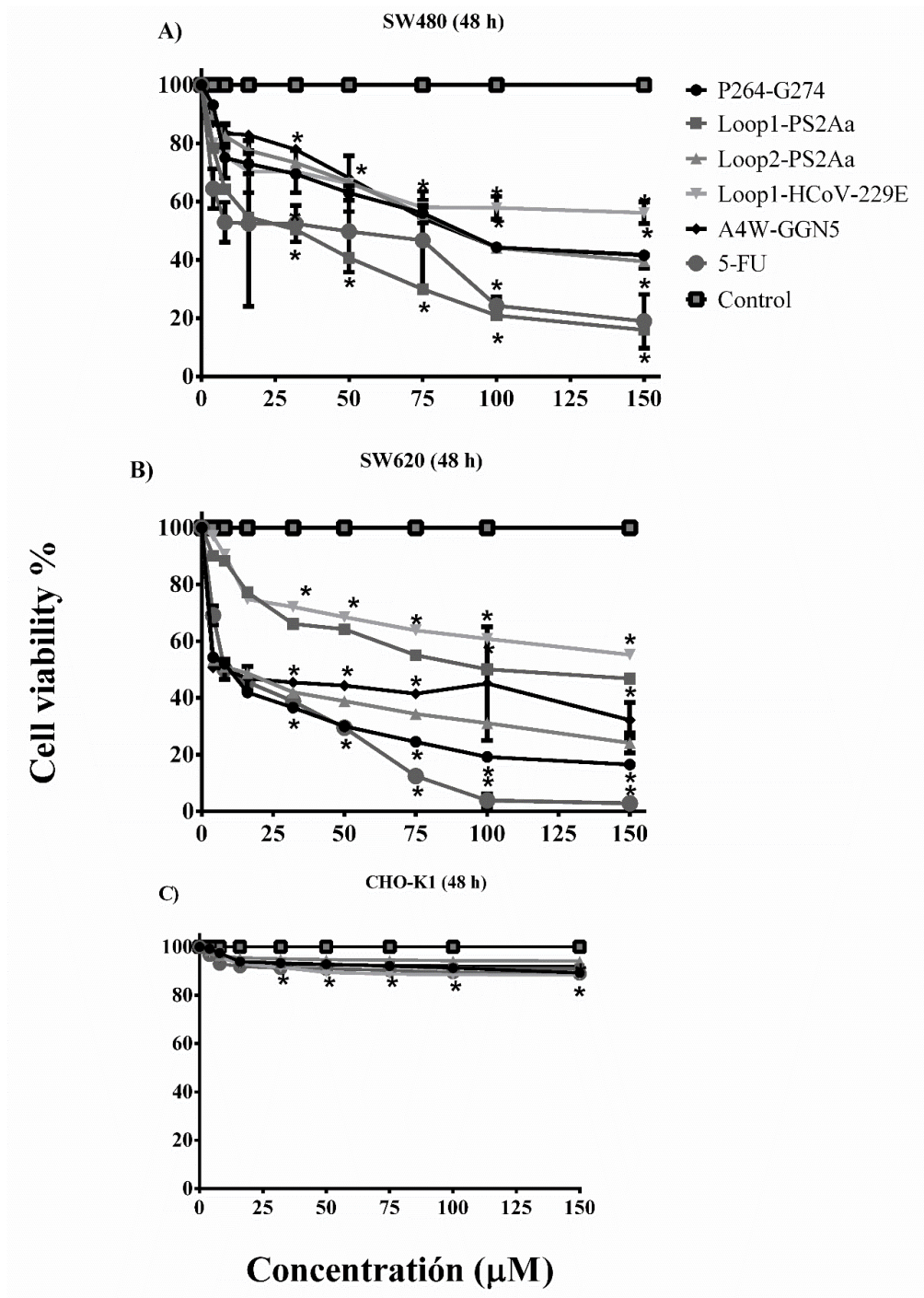
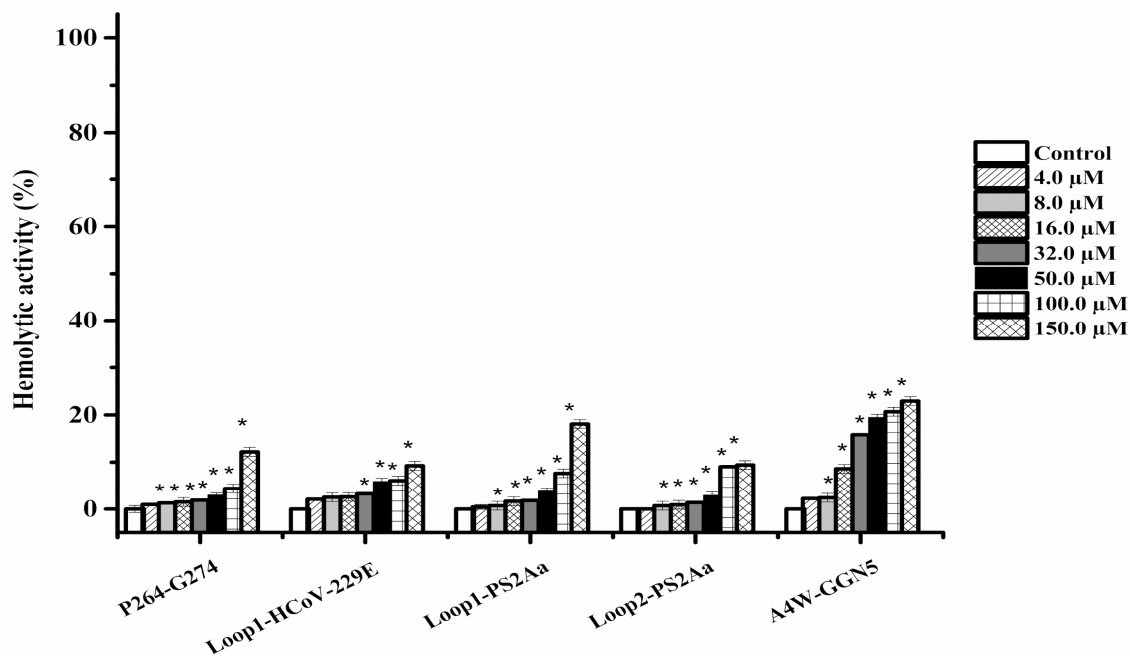


Figure 15. Hemolytic activity of peptides (P264-G274, Loop1-PS2Aa, Loop2-PS2Aa, Loop1-HCoV-229E, and A4W-GGN5). Hemolytic activity of peptides against human red blood cells at different peptide concentrations (4-100 μM), in Hank's glucose at 37°C for 4h of exposure. Experiments were performed in three independent replicates. Dosages that caused a statically significant decrease in cell growth compared to the untreated control at each time point were indicated by asterisks (* $p < 0.05$; one-way ANOVA followed by Tukey's test).



3.4.4 Fluorescence morphological evaluation

The Hoechst double staining of SW480 and SW620 cells is represented in Figure 5. Under fluorescence microscopy, more uniformly blue live cells with normal morphology were observed in the control of untreated cells than in the peptides treated cells. The colocalization of the peptide Rho-Loop1-PS2Aa at 47.5 μM resulted in the entering of compounds into the nucleus of SW480 cells, while the peptide Rho-P24-G274 was located in cytoplasmic regions, without affecting the nucleus. These results were observed after 1 h of exposure. These findings suggest that Rho-Loop1-PS2Aa and Rho-P24-G274 can be able to interact with nuclear and cytoplasmic proteins on SW480 and SW620 colon cancer cells.

3.4.5 Annexin V-CY3 staining

The early apoptotic cells are differentiated using the combination of annexin V-Cy3 (red emission) and 6-CFDA (green emission). In the case of early apoptosis, both annexin V-Cy3 and 6-CFDA are positive (green and red emission), whereas in necrosis only annexin V-Cy3 is positive (only red emission) and in viable cells, only 6-CFDA is positive (only green emission). The results are given in Figure 6. When the cells were treated with most active peptides for each of the cell lines, Loop1-PS2Aa and P264-G274, both annexin V-Cy3 and 6-CFDA are positive which clearly indicates the early stage of apoptosis. Same results were observed with the control of chemotherapeutic drug 5-FU.

Figure 16. In vitro cell binding of the most active peptides (A) Cell binding of Loop1-PS2Aa peptide on the cancerous cell line SW480. (B) Cell binding of P264-G274 peptide on the cancerous cell line SW620. Experiments were performed in three independent replicates.

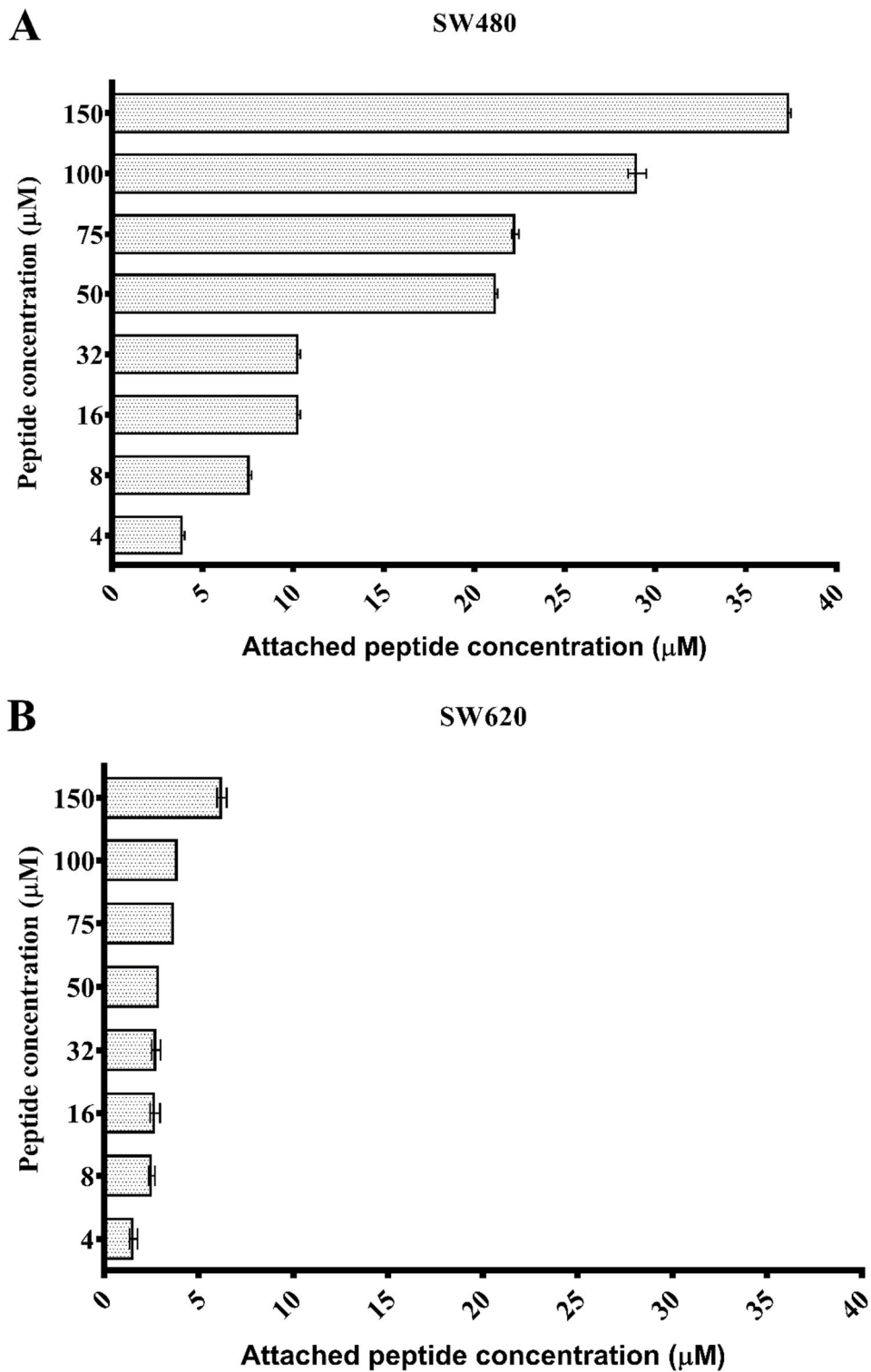


Figure 17. SW480 and SW620 colon cancer cells were stained by Hoechst and observed under fluorescence microscopy (20X). Cell morphology was observed under fluorescence microscopy, the bar represent 100 μ m.

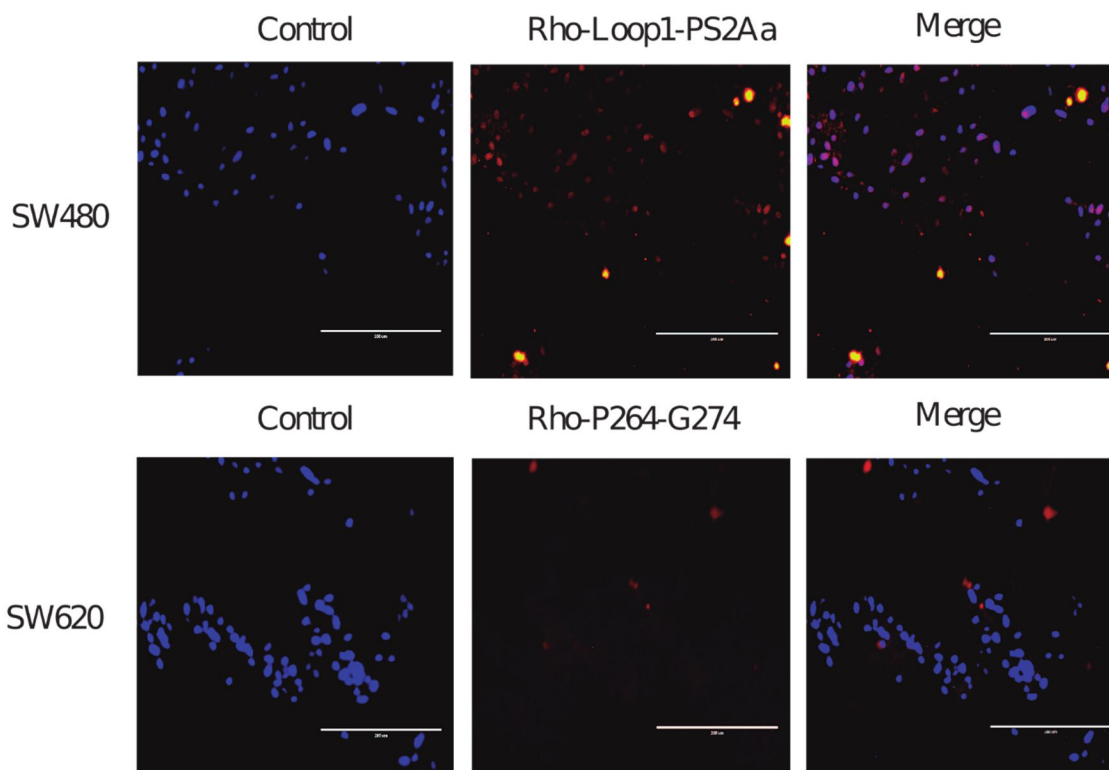


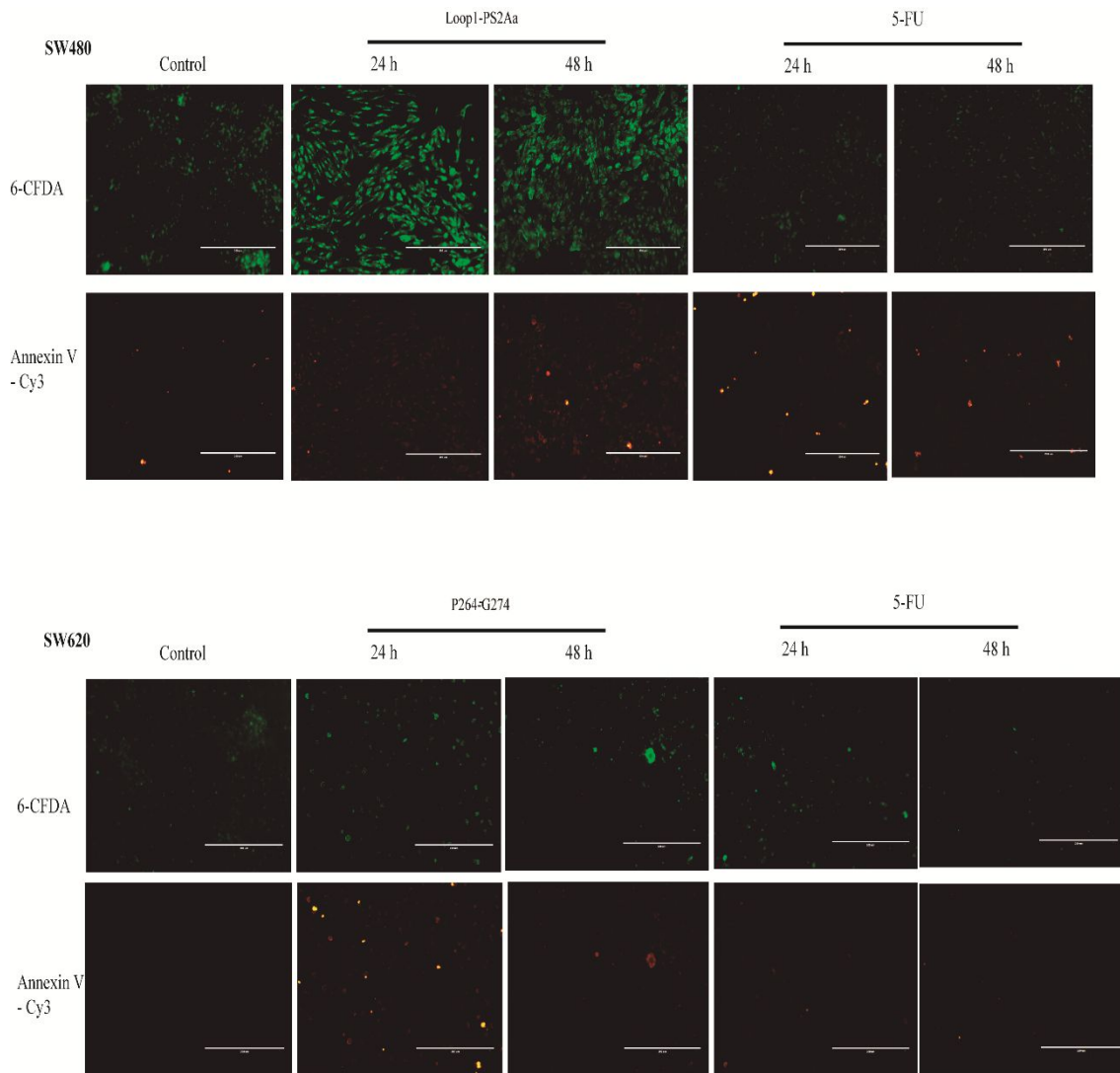
Table 9. Top 10 of the APN residues that were found to interact with peptide P264-G274 through hydrogen bonds.

Residue	Number of hydrogen bonds in 500 models	Residue	Number of hydrogen bonds in 100 refined models
Arg ⁶⁹⁰	15	Asp ⁷⁴⁹	126
Gln ⁹⁰⁸	12	Gln ⁶⁹¹	38
Gln ⁹¹²	11	Arg ⁶⁹⁰	31
Asp ⁷⁴⁹	10	Glu ⁶⁸⁹	20
Glu ¹⁵⁷	9	Arg ⁶⁵⁸	3
Glu ⁹⁰⁴	7	Glu ⁶⁸⁸	3
Glu ⁶⁸⁸	7	His ⁶⁵⁰	3
Gln ⁵³¹	7	His ⁷³²	2
Gln ⁹⁵²	7	Ser ⁶⁵¹	1
Glu ¹⁵⁴	7	Asn ⁷³⁶	1

3.4.6 Caspase and LDH mechanism

Recent data suggest that caspase-3 and caspase-7 must have distinct functions. Caspase-3 can inhibit ROS production and is the effector caspase necessary for efficient cell killing. In contrast, caspase-7 has no significant role in sensitivity to intrinsic cell death, but it is responsible for ROS production and cell detachment. The action mechanism of Peptides Loop1-PS2Aa and P264-G274 against SW480 and SW620, respectively, is mediated by intrinsic apoptosis (green cells Figure 7A,B). Likewise, for the effect of the peptides over SW480 and SW620 in the extracellular medium no LDH enzyme was detected (Figure 7C).

Figure 18. Photomicrographs of control and Annexin V-Cy3/6-CFDA stained SW480 and SW620 colon cancer cells treated with the peptides Loop1-PS2Aa and P264-G274, respectively for 24 h and 48 h. 5-FU was taken as a positive control, the bar represent 100µm.



3.4.7 Molecular docking of peptides and h-APN receptor

The computational results obtained suggest that peptide P264-G274 has a preference for interacting with amino acid residues such as Gln and Glu when it is free to move around the h-APN monomer. In the refinement step, where this peptide could only move in a specific region of the APN, the preferred residues were Asp749, Gln691, Arg690, and Glu689. Table 3 shows the top 10 residues in the APN with their

corresponding number of hydrogen bonds found in the 500 models obtained in the global simulations, and the top 10 of APN residues found in the 100 models predicted in the refinement step. Moreover, Figure 8 shows the top 10 residues in the 3D structure of the APN for both rounds of simulation, and Figure 9 shows the interactions of the resulting complex between the peptide P264-G274 and the APN. Similarly, the peptide Loop1-PS2Aa peptide shows a preference to interact with residues such as Asp, Gln, and Glu in global simulations, and a preference for Asn746, Arg658, and Asp423 in the refinement round. Table 4 shows the top 10 of the APN residues involved in hydrogen bonds with this peptide in both, global and refinement simulations.

Moreover, Figure 10 shows these top residues highlighted in red color, and Figure 11 shows the interactions of the resulting complex between the peptide Loop1-PS2Aa and APN. Finally, Table 5 summarizes of the APN and peptides residues involved in the hydrophobic and hydrogen bond interactions for the best complexes found for P264-G274 and Loop1-PS2Aa peptides.

3.5 Discussion

Current cancer treatment is often accompanied by several detrimental side effects; for instance, toxic effects of 5-FU, a chemotherapeutic drug that is usually used for metastatic colon cancer treatment [51]. Besides, the development of drug resistance by cancer cells has limited the success of chemotherapeutic drugs. Therefore, a safe and selective anticancer agent with a new mode of action has been evaluated. Parasporin-2Aa1 (PS2Aa1) was shown to be cytotoxic against specific human cancer cells. In order to study the role of some native peptide fragments of proteins on anticancer activity, here we investigated the cytotoxic effect of peptide fragments from domain-1 of PS2Aa1 and one of the loops present in the binding region of the virus spike protein from Alphacoronavirus (HCoV-229E). In this respect, P264-G274 (PARDVLNTTSG-NH₂) and Loop1-PS2Aa (NNETYFNAVKP-NH₂)- amphipathic cationic ACPs, could be a choice. The reported results demonstrate that P264-G274 and Loop1-PS2Aa peptides exhibit time and concentration-dependent manner of growth inhibition of SW620 and SW480 cells, respectively. These may be due to the electrostatic interaction of positive charges

(from +1 to +3) in the peptides with the negative charge of anionic molecules, such as phosphatidylserines, and glycosaminoglycans, which make the cancer cell membranes similar in composition to the bacterial membranes [52]. The initial electrostatic interactions between the cationic.

Figure 19. Caspase and LDH assay. A) intrinsic apoptosis of Loop1-PS2Aa peptide on the cancerous cell line SW480 after 4 hours of exposure. B) intrinsic apoptosis of P264-G274 peptide on the cancerous cell line SW620 after 4 hours of exposure. C) No detection of LDH enzyme in the extracellular medium after 4 hours of exposure with the peptides Loop1-PS2Aa peptide on the cancerous cell line SW480 and P264-G274 peptide on the cancerous cell line SW620. Experiments were performed in three independent replicates.

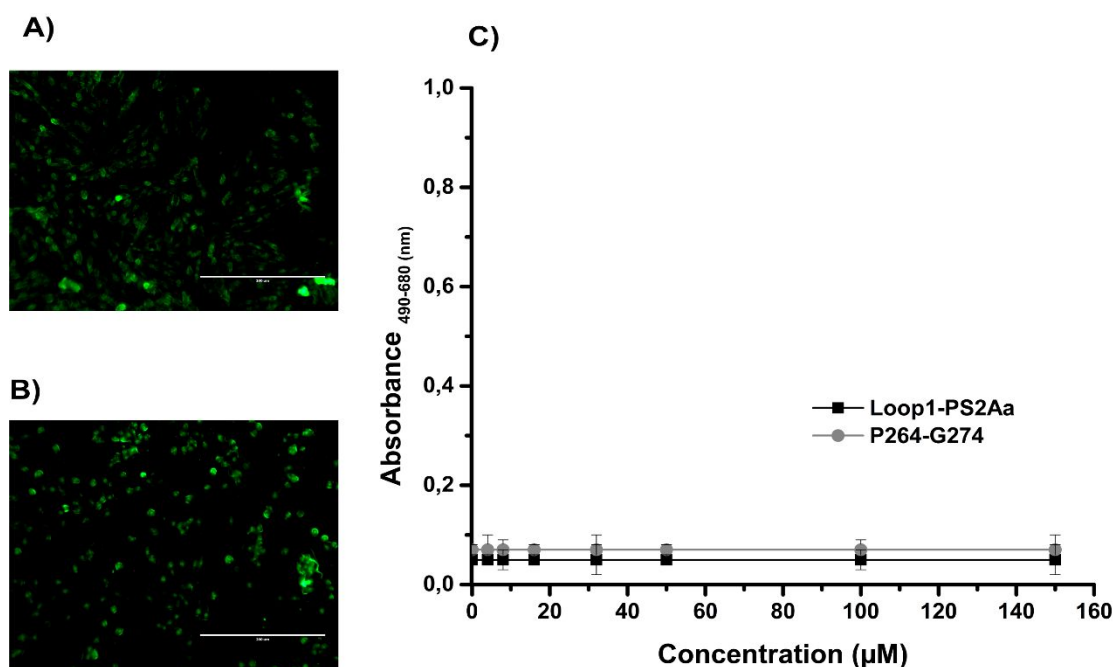


Table 10. Top 10 of the APN residues that were found to interact with peptide Loop1-PS2Aa through hydrogen bonds.

Residue	Number of hydrogen bonds in 500 models	Residue	Number of hydrogen bonds in 100 refined models
Asp ⁸⁷⁸	7	Asn ⁷⁴⁶	165
Gln ⁶⁹¹	7	Arg ⁶⁵⁸	162
Glu ⁷⁸¹	6	Asp ⁴²³	14
Asp ¹¹⁸	5	Ser ⁶⁵¹	6
Arg ⁸¹⁷	5	Gln ⁶⁹¹	4
Gln ²⁹³	5	Asn ⁴³⁰	1
Gln ⁹⁵²	5	Pro ⁴²⁷	1
Gln ⁶⁰⁸	5	Gly ⁵⁹⁴	1

Residue	Number of hydrogen bonds in 500 models	Residue	Number of hydrogen bonds in 100 refined models
His ²⁷⁰	5	Arg ⁶⁹⁰	1
Glu ¹⁸¹	5	Asp ⁷⁴⁹	1

Figure 20. APN residues involved in hydrogen bonds with P264-G274 peptide. This figure shows the top 10 of the APN residues involved in hydrogen bonds with peptide P264-G274, in 500 models obtained in global simulations (left) and 100 models obtained in the refinement round (right).

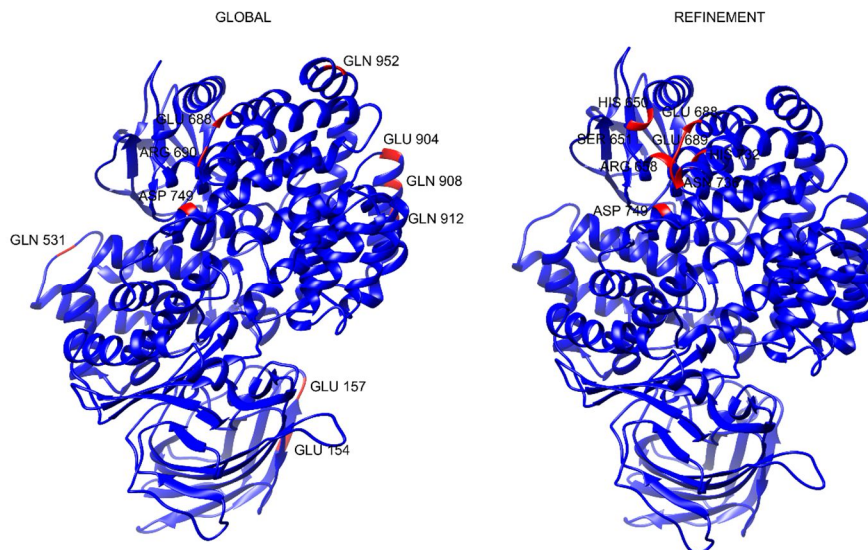


Table 11. Summary of APN and peptides residues involved in molecular interactions in the best complexes.

Peptide	Hydrogen Bonds*	Hydrophobic Interactions*
P264-G274	Arg3(B) - Asp749(A) Asp4(B) - Asn746(A) Asn7(B) - Asp749(A) Asn7(B) - Gln691(A)	A: Asn430, Pro744. B: Thr8.
Loop1-PS2Aa	Asn1(B) - Asn746(A) Asn7(B) - Arg658(A) Tyr5(B) - Gln691(A)	A: Asp649, Ser651, Ala652, Pro654, Val655, Asp749. B: Thr4, Ala8, Lys10, Pro11.

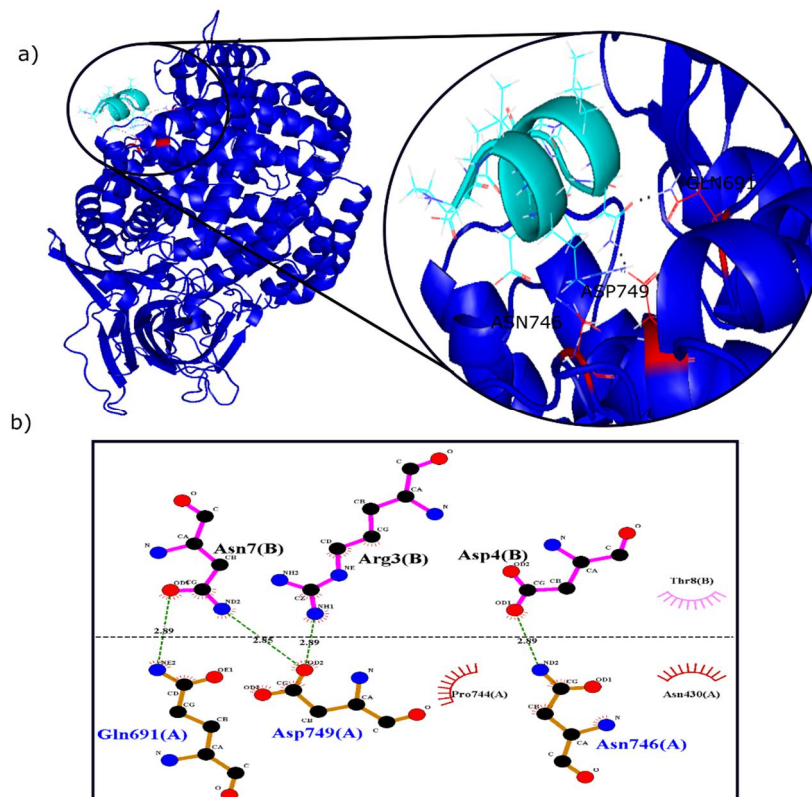
*A= APN, B=Peptide.

peptide with the negatively charged cancer cell membranes are important to destabilize the membrane [53]. Subsequently, peptides may rapidly penetrate the cancer cells with a hydrophobic property (36.36% of nonpolar residues in P264-G274 and 45.45% in Loop1-PS2Aa peptides). The other peptides, like Loop2-PS2Aa and Loop1-HCoV-

229E, were not significantly inhibited despite having a higher net positive charge than the more active peptides (Table 1).

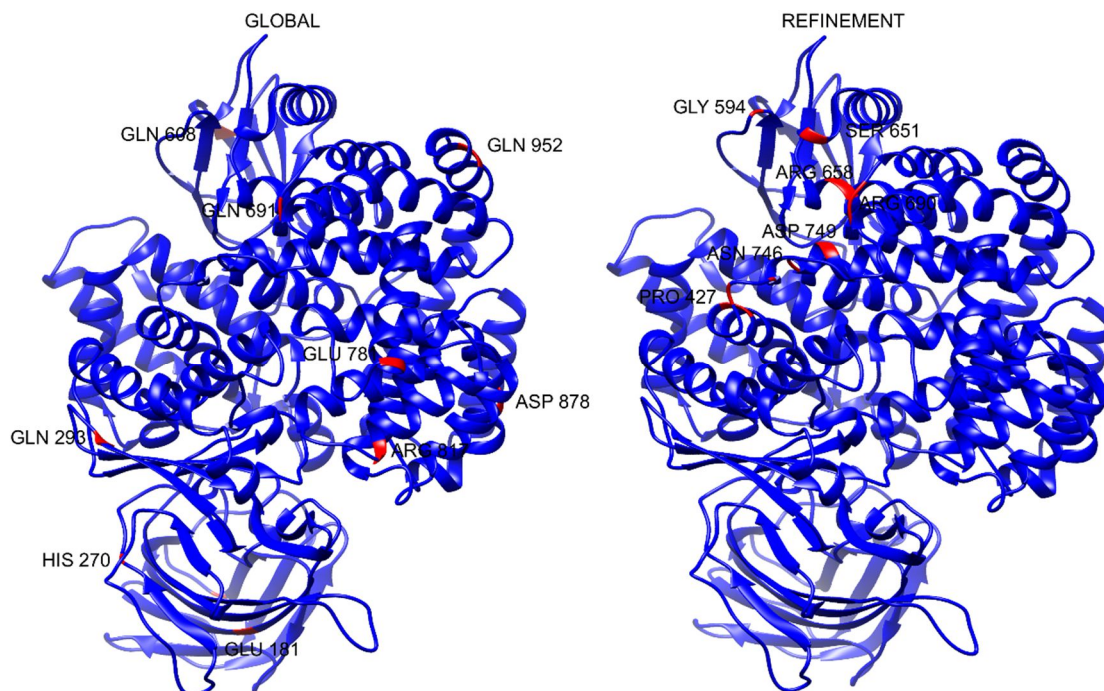
So also, the presence of some residues such as Trp becomes essential in the sequence. Therefore, our results suggest that a combination of P264-G274 and Loop1-PS2Aa peptides with 5-FU can exert a synergistic effect and enhance the efficacy of therapeutics. Peptides structure plays a central role in their activity. It is commonly accepted that most ACPs do not fold in a well-defined structure when free in solution but adopt α -helix or β -sheet structure when electrostatic interactions with membranes occur [53]. Differences in terms of structure were the first method for the classification of ACPs. Examples of some AMPs, lately defined as α -ACPs, are cecropin, magainin, melittin, and buforin II, with lactoferricin B, HNP-1/3, and games in being classified as β -ACPs W [54]. More recently, it was noticed that, independently of the secondary structure that the peptide adopts, a classification considering the mechanisms of action.

Figure 21. Interactions in the resulting complex between P264-G274 peptide and the APN. a) Complex between the P264-G274 peptide and APN, b) Hydrogen bonds and hydrophobic interactions found in the complex.



in the target cancer cells was more suitable [54]. Initially, ACPs were related to necrosis processes as their primary activity. However, over the years, it was clarified that they could also target different processes, such as mitochondrial membrane lytic activity (apoptosis), targeting essential cell proteins, inhibiting angiogenesis or recruiting immune cells to attack cancer cells and non-membrane activities [54]. These ACPs have high selectivity toward cancer cell membranes and develop low resistance compared to conventional chemotherapeutic drugs. From a structural point of view, P264-G274 ($EC_{50} = 11.28$ against SW620) and Loop1-PS2Aa ($EC_{50} = 23.76$ against SW480) peptides with the alpha-helix secondary structure were found to be more active compared with the peptide derived from alpha-coronavirus Loop1-HCoV-229E ($EC_{50} = 125.0 \mu\text{M}$ and higher than $150.0 \mu\text{M}$ against SW480 and SW620, respectively). Furthermore, these compounds presented a lower EC_{50} value compared with the 5-FU positive control and the A4W-GGN5 peptide for each of the cell lines where they were most active (Table 2).

Figure 22. APN residues involved in hydrogen bonds with Loop1-PS2Aa peptide. This figure shows the top 10 of APN residues involved in hydrogen bonds with peptide P264-G274, in 500 models obtained in global simulations (left) and 100 models obtained in the refinement round (right).

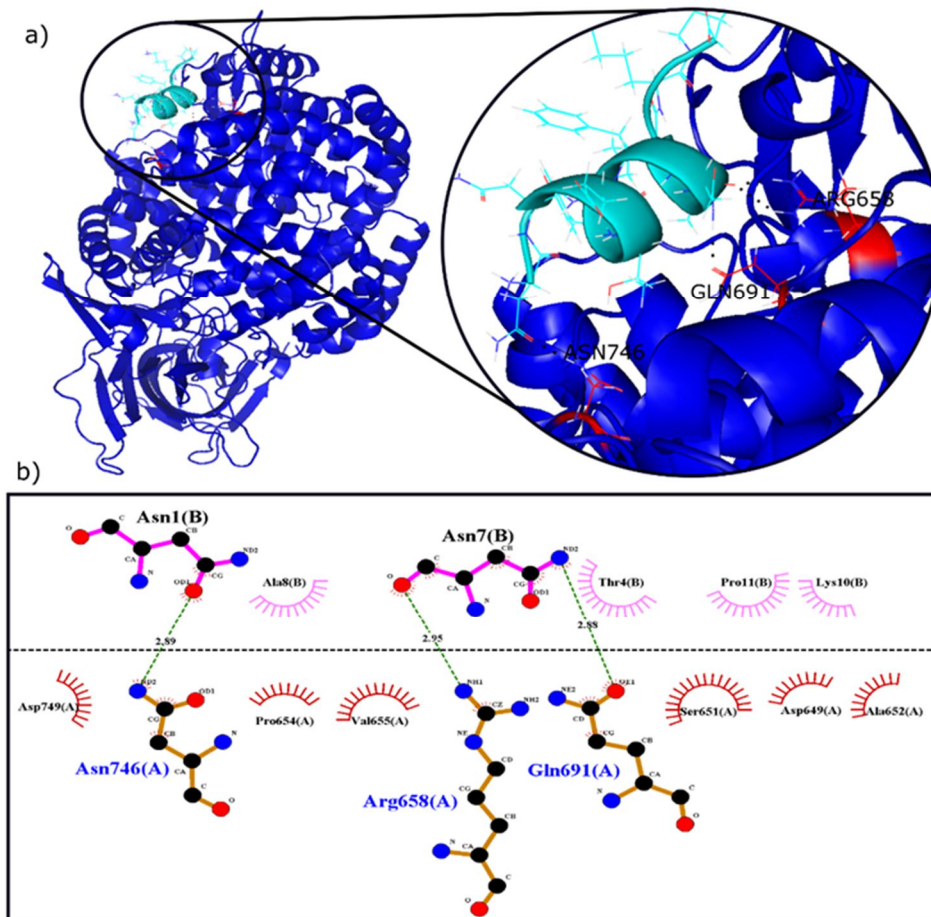


The present study is the first one carrying out the fragmentation of the toxic protein PS2Aa to understand the role of some regions of domain I, knowing in advance that the protein has exhibited high anticancer activity [17]. This domain is composed of four short alpha-helices and beta antiparallel sheets, which is also characterized by being rich in exposed aromatic amino acid residues (Phe, Trp, and Tyr), suggesting a possible site of binding of PS2 to susceptible cancer cells. Recently, the role of GPI-anchored proteins in the mechanism of action of PS2 toxins has been studied. In the CHO (Chinese hamster ovary) cell lines, it was observed that the glucan present in the GPI proteins induces oligomerization processes in the PS2 toxins but has a co-receptor function in the toxic action because it is also present in resistant cells to PS2Aa1 peptide [55]. Therefore, the APN is another very interesting receptor to investigate. The h-APN receptor has been shown to have a high affinity to HCoV-229E. The HCoV-229E receptor-binding domain (RBD) binds at a site on h-APN called H-site. The HCoV-229E RBD binds to h-APN in its closed conformation, and structural comparison shows that the H-site does not differ between the open and closed conformations. It was also studied that there are three extended loops responsible for the binding of the receptor and the evolution of HCoV-229, and their close relatives are accompanied by changing loop-receptor interactions. Within loop 1, residues Cys317 and Cys320 form a disulfide bond that makes a stacking interaction with the side chains of residues Tyr289 and Glu291 in hAPN. The most prominent of the remaining RBD–hAPN interactions are the salt bridge between residue Arg359 in loop 2 and residue Asp315 in hAPN and the interactions between residues Trp404 and Ser407 in loop 3 with residues Asp315 and Lys292 in hAPN; the importance of Trp404 in loop 3 as evidenced by the fact that mutating it also ablated binding [56].

The entry of the most active peptides into the cell may be mediated by interaction with receptors such as hAPN. Figure 5 shows that the colocalization of the peptide Loop1-PS2Aa peptide at 47.5 μ M was in the nucleus of SW480 cells after 1 h of exposure, while the peptide P24-G274 was located in cytoplasmic regions in the same time of exposure, without affecting the nucleus. Likewise, results obtained at higher levels of cell adhesion demonstrated that the Loop1-PS2Aa peptide enters SW480 cells much faster than P24-G274 peptide in SW620 cells. Slater et al. [57] compared in an in vitro model of cancer progression, the SW480 and SW620 paired cell lines derived from a colon

adenocarcinoma and its lymph node metastasis, respectively. Their chemosensitivity and the cancer stem cell (CSC) properties were investigated. The mentioned study determined that the SW480 and SW620 cells exhibited similar

Figure 23. Interactions in the resulting complex between Loop1-PS2Aa peptide and the APN. a) Complex between the Loop1-PS2Aa peptide and APN, b) Hydrogen bonds and hydrophobic interactions found in the complex.



growth rates, although the SW480 cells were more migratory in wound healing assays on collagen and fibronectin matrices. SW480 and SW620 cells displayed similar CSC profiles, although, SW480 cells demonstrated significantly greater tumor sphere forming efficiency over SW620 cells. Tumor spheres derived from SW480 and SW620 cells also displayed differential sensitivity to 5-FU, oxaliplatin, geldanamycin, and novobiocin, which was not apparent when cells were grown under adherent conditions.

These results suggest that although the two cell lines have similar levels of putative CSC populations, there are differences in their physiology that cannot be explained by these CSC levels. Finally, according to the molecular docking simulations performed, an interaction is possible between the best experimental peptides, i.e., P264-G274 and Loop1-PS2Aa, and the h-APN receptor which is overexpressed in cancer cells. Even though the number of possible hydrogen bonds revealed the global simulations is low for the top residues, the situation changes significantly with the refinement models, where residues with more than 100 possible hydrogen bonds were found in 100 predicted models. Our results demonstrate that some regions of the domain I of PS2Aa1, represented in small peptide fragments of the protein, may be related to anticancer activity and initial adhesion with receptors. The latter results could be remarkable, in finding the main cell membrane receptor who interacts with the parasporins in human cancer cells.

This strategy of protein fragmentation can give insights about the mechanism of action of PS2Aa1 and the role that each of its domains plays in the cytotoxic effect in different cancer cell lines.

3.6 References

1. Sung, H.; Ferlay, J.; Siegel, R. L.; Laversanne, M.; Soerjomataram, I.; Jemal, A.; Bray, F. Global Cancer Statistics 2020: GLOBOCAN Estimates of Incidence and Mortality Worldwide for 36 Cancers in 185 Countries. *CA. Cancer J. Clin.* 2021, 71 (3), 209–249. <https://doi.org/10.3322/caac.21660>.
2. Xie, Y.; Chen, Y.; Fang, J. Comprehensive Review of Targeted Therapy for Colorectal Cancer. *Signal Transduct. Target. Ther.* 2020, No. November 2019. <https://doi.org/10.1038/s41392-020-0116-z>.
3. Ferlay, J.; Soerjomataram, I.; Dikshit, C.; Eser, S.; Mathers, C.; Rebelo, M.; Parkin, D.; Forman, D.; Bray, F. Cancer Incidence and Mortality Worldwide Sources, Methods and Major Patterns in GLOBOCAN 2012. *Int. J. Cancer* 2015, 136, E359–E386. <https://doi.org/10.1002/ijc.29210>.
4. Modest, D. P.; Pant, S.; Sartore-Bianchi, A. Treatment Sequencing in Metastatic Colorectal Cancer. *Eur. J. Cancer* 2019, 109, 70–83. <https://doi.org/10.1016/j.ejca.2018.12.019>.

5. Xu, Z.; Becerra, A. Z.; Fleming, F. J.; Aquina, C. T.; Dolan, J. G.; Monson, J. R.; Temple, L. K.; Jusko, T. A. Treatments for Stage IV Colon Cancer and Overall Survival. *J. Surg. Res.* 2019, 242 (301), 47–54. <https://doi.org/10.1016/j.jss.2019.04.034>.
6. Xu, J.; Zhang, Y.; Xu, J.; Wang, M.; Liu, G.; Wang, J.; Zhao, X.; Qi, Y.; Shi, J.; Cheng, K.; Li, Y.; Qi, S.; Nie, G. Reversing Tumor Stemness via Orally Targeted Nanoparticles Achieves Efficient Colon Cancer Treatment. *Biomaterials* 2019, 119247. <https://doi.org/10.1016/j.biomaterials.2019.119247>.
7. Wang, D.; Li, Y. Bimetallic Nanocrystals: Liquid-Phase Synthesis and Catalytic Applications. *Adv. Mater.* 2011, 23 (9), 1044–1060. <https://doi.org/10.1002/adma.201003695>.
8. Kaleta-Richter, M.; Kawczyk-Krupka, A.; Aebisher, D.; Bartusik-Aebisher, D.; Czuba, Z.; Cieślak, G. The Capability and Potential of New Forms of Personalized Colon Cancer Treatment: Immunotherapy and Photodynamic Therapy. *Photodiagnosis Photodyn. Ther.* 2019, 25, 253–258. <https://doi.org/10.1016/j.pdpdt.2019.01.004>.
9. Felício, M. R.; Silva, O. N.; Gonçalves, S.; Santos, N. C.; Franco, O. L. Peptides with Dual Antimicrobial and Anticancer Activities. *Front. Chem.* 2017, 5 (February), 1–9. <https://doi.org/10.3389/fchem.2017.00005>.
10. Hancock, R. E. W.; Haney, E. F.; Gill, E. E. The Immunology of Host Defence Peptides: Beyond Antimicrobial Activity. *Nat. Rev. Immunol.* 2016, 16 (5), 321–334. <https://doi.org/10.1038/nri.2016.29>.
11. Hoskin, D. W.; Ramamoorthy, A. Studies on Anticancer Activities of Antimicrobial Peptides. *Biochimica et Biophysica Acta - Biomembranes.* 2008, pp 357–375. <https://doi.org/10.1016/j.bbamem.2007.11.008>.
12. Nantasenamat, C. Review Article: UNRAVELING THE BIOACTIVITY OF ANTICANCER PEPTIDES AS. 2018, No. Thundimadathil 2012, 734–752.
13. Hammami, R.; Fliss, I. Current Trends in Antimicrobial Agent Research: Chemo- and Bioinformatics Approaches. *Drug Discov. Today* 2010, 15 (13–14), 540–546. <https://doi.org/10.1016/j.drudis.2010.05.002>.
14. Papo, N.; Shai, Y. Host Defense Peptides as New Weapons in Cancer Treatment. *Cell. Mol. Life Sci.* 2005, 62 (7–8), 784–790. <https://doi.org/10.1007/s00018-005-4560-2>.
15. Droin, N.; Hendra, J. B.; Ducoroy, P.; Solary, E. Human Defensins as Cancer Biomarkers and Antitumour Molecules. *J. Proteomics* 2009, 72 (6), 918–927. <https://doi.org/10.1016/j.jprot.2009.01.002>.
16. Kumar, S.; Hui, L. In Silico Design of Anticancer Peptides. *Proteomics Drug Discov.* 2017, 1647, 245–254. <https://doi.org/10.2307/j.ctt1ffjgqc.21>.

17. Singh, R.; Bhardwaj, V. K.; Sharma, J.; Das, P.; Purohit, R. Identification of Selective Cyclin-Dependent Kinase 2 Inhibitor from the Library of Pyrrolone-Fused Benzosuberene Compounds: An in Silico Exploration. *J. Biomol. Struct. Dyn.* 2021, 0 (0), 1–9. <https://doi.org/10.1080/07391102.2021.1900918>.
18. Singh, R.; Bhardwaj, V.; Das, P.; Purohit, R. Natural Analogues Inhibiting Selective Cyclin-Dependent Kinase Protein Isoforms: A Computational Perspective. *J. Biomol. Struct. Dyn.* 2020, 38 (17), 5126–5135. <https://doi.org/10.1080/07391102.2019.1696709>.
19. Hu, C.; Chen, X.; Zhao, W. Design and Modification of Anticancer Peptides. *Drug Des. Open Access* 2017, 05 (03). <https://doi.org/10.4172/2169-0138.1000138>.
20. Hao, X.; Yan, Q.; Zhao, J.; Wang, W.; Huang, Y.; Chen, Y. TAT Modification of Alpha-Helical Anticancer Peptides to Improve Specificity and Efficacy. *PLoS One* 2015, 10 (9), 1–13. <https://doi.org/10.1371/journal.pone.0138911>.
21. Liu, Q.; Zhao, H.; Jiang, Y.; Wu, M.; Tian, Y.; Wang, D.; Lao, Y.; Xu, N.; Li, Z. Development of a Lytic Peptide Derived from BH3-Only Proteins. *Cell Death Discov.* 2016, 2 (1). <https://doi.org/10.1038/cddiscovery.2016.8>.
22. Mesfin, F. B.; Zhu, S.; Bennett, J. A.; Andersen, T. T.; Jacobson, H. I. Development of a Synthetic Cyclized Peptide Derived from α -Fetoprotein That Prevents the Growth of Human Breast Cancer. *J. Pept. Res.* 2001, 58 (3), 246–256. <https://doi.org/10.1034/j.1399-3011.2001.00922.x>.
23. Akiba, T.; Okumura, S. Parasporins 1 and 2: Their Structure and Activity. *J. Invertebr. Pathol.* 2017, 142, 44–49. <https://doi.org/10.1016/j.jip.2016.10.005>.
24. Brasseur, K.; Auger, P.; Asselin, E.; Parent, S.; Côté, J. C.; Sirois, M. Parasporin-2 from a New *Bacillus Thuringiensis* 4r2 Strain Induces Caspases Activation and Apoptosis in Human Cancer Cells. *PLoS One* 2015, 10 (8), 1–22. <https://doi.org/10.1371/journal.pone.0135106>.
25. Mizuki, E.; Park, Y. S.; Saitoh, H.; Yamashita, S.; Akao, T.; Higuchi, K.; Ohba, M. Parasporin, a Human Leukemic Cell-Recognizing Parasporal Protein of *Bacillus Thuringiensis*. *Clin. Diagn. Lab. Immunol.* 2000, 7 (4), 625–634.
26. Kitada, S.; Abe, Y.; Shimada, H.; Kusaka, Y.; Matsuo, Y.; Katayama, H.; Okumura, S.; Akao, T.; Mizuki, E.; Kuge, O.; Sasaguri, Y.; Ohba, M.; Ito, A. Cytocidal Actions of Parasporin-2, an Anti-Tumor Crystal Toxin from *Bacillus Thuringiensis*. *J. Biol. Chem.* 2006, 281 (36), 26350–26360. <https://doi.org/10.1074/jbc.M602589200>.
27. Velásquez Cardona, L. F.; Rojas Torres, D. S.; Cerón Salamanca, J. TOXINAS DE *Bacillus Thuringiensis* CON ACTIVIDAD ANTICANCERÍGENA: PARASPORINAS. *Rev. Colomb. Biotecnol.* 2018, 20 (2), 89–100. <https://doi.org/10.15446/rev.colomb.biote.v20n2.73668>.

28. Akiba, T.; Abe, Y.; Kitada, S.; Kusaka, Y.; Ito, A.; Ichimatsu, T.; Katayama, H.; Akao, T.; Higuchi, K.; Mizuki, E.; Ohba, M.; Kanai, R.; Harata, K. Crystal Structure of the Parasporin-2 Bacillus Thuringiensis Toxin That Recognizes Cancer Cells. *J. Mol. Biol.* 2009, 386 (1), 121–133. <https://doi.org/10.1016/j.jmb.2008.12.002>.
29. Abe, Y.; Shimada, H.; Kitada, S. Raft-Targeting and Oligomerization of Parasporin-2, a Bacillus Thuringiensis Crystal Protein with Anti-Tumour Activity. *J. Biochem.* 2008, 143 (2), 269–275. <https://doi.org/10.1093/jb/mvm220>.
30. Bravo, A.; Gómez, I.; Porta, H.; García-Gómez, B. I.; Rodríguez-Almazan, C.; Pardo, L.; Soberón, M. Evolution of Bacillus Thuringiensis Cry Toxins Insecticidal Activity. *Microb. Biotechnol.* 2013, 6 (1), 17–26. <https://doi.org/10.1111/j.1751-7915.2012.00342.x>.
31. Abe, Y.; Inoue, H.; Ashida, H.; Maeda, Y.; Kinoshita, T.; Kitada, S. Glycan Region of GPI Anchored-Protein Is Required for Cytocidal Oligomerization of an Anticancer Parasporin-2, Cry46Aa1 Protein, from Bacillus Thuringiensis Strain A1547. *J. Invertebr. Pathol.* 2017, 142, 71–81. <https://doi.org/10.1016/j.jip.2016.11.008>.
32. Moniatte, M.; Van Der Goot, F. G.; Buckley, J. T.; Pattus, F.; Van Dorselaer, A. Characterisation of the Heptameric Pore-Forming Complex of the Aeromonas Toxin Aerolysin Using MALDI-TOF Mass Spectrometry. *FEBS Lett.* 1996, 384 (3), 269–272. [https://doi.org/10.1016/0014-5793\(96\)00328-6](https://doi.org/10.1016/0014-5793(96)00328-6).
33. Luan, Y.; Xu, W. The Structure and Main Functions of Aminopeptidase N. *Curr. Med. Chem.* 2007, 14 (6), 639–647. <https://doi.org/10.2174/092986707780059571>.
34. Palomo, J. M. Solid-Phase Peptide Synthesis: An Overview Focused on the Preparation of Biologically Relevant Peptides. *RSC Adv.* 2014, 4 (62), 32658–32672. <https://doi.org/10.1039/C4RA02458C>.
35. Houghten, R. A. General Method for the Rapid Solid-Phase Synthesis of Large Numbers of Peptides: Specificity of Antigen-Antibody Interaction at the Level of Individual Amino Acids *Immunology*: Houghten. 1985, 82 (August), 5131–5135.
36. Aguilar, M. TM HPLC of Peptides and Proteins. 2004, 251.
37. Dave, K. a; Headlam, M. J.; Wallis, T. P.; Gorman, J. J. Preparation and Analysis of Proteins and Peptides Using MALDI TOF/TOF Mass Spectrometry. *Curr. Protoc. Protein Sci.* 2011, Chapter 16 (February), Unit 16.13. <https://doi.org/10.1002/0471140864.ps1613s63>.
38. Bakshi, K.; Liyanage, M.; Volkin, D.; Middaugh, C. Circular Dichroism of Peptides. In *Therapeutic peptides; Methods Mol Biol.*, 2014; pp 247–253. <https://doi.org/10.1007/978-1-62703-673-3>.

39. Kim, H. K.; Lee, D. G.; Park, Y.; Kim, H. N.; Choi, B. H.; Choi, H.; Hahm, K. Antibacterial Activities of Peptides Designed as Hybrids of Antimicrobial Peptides. 2002, 347–353.
40. Orellana, E.; Kasinski, A. Sulforhodamine B (SRB) Assay in Cell Culture to Investigate Cell Proliferation. *Bio-Protocol* 2016, 6 (21). <https://doi.org/10.21769/bioprotoc.1984>.
41. Maijaroen, S.; Jangpromma, N.; Daduang, J.; Klaynongsruang, S. KT2 and RT2 Modified Antimicrobial Peptides Derived from *Crocodylus Siamensis* Leucocin I Show Activity against Human Colon Cancer HCT-116 Cells. *Environ. Toxicol. Pharmacol.* 2018, 62 (July), 164–176. <https://doi.org/10.1016/j.etap.2018.07.007>.
42. Manojkumar, Y.; Ambika, S.; Arulkumar, R.; Gowdhami, B.; Balaji, P.; Vignesh, G.; Arunachalam, S.; Venuvanalingam, P.; Thirumurugan, R.; Akbarsha, M. A. Synthesis, DNA and BSA Binding, In Vitro Anti-Proliferative and in Vivo Anti-Angiogenic Properties of Some Cobalt(II) Schiff Base Complexes. *New J. Chem.* 2019, 43 (28), 11391–11407. <https://doi.org/10.1039/c9nj01269a>.
43. Hastings, J.; Kenealey, J. Avenanthramide-C Reduces the Viability of MDA-MB-231 Breast Cancer Cells through an Apoptotic Mechanism. *Cancer Cell Int.* 2017, 17 (1). <https://doi.org/10.1186/s12935-017-0464-0>.
44. Kaja, S.; Payne, A. J.; Naumchuk, Y.; Koulen, P. Quantification of Lactate Dehydrogenase for Cell Viability Testing Using Cell Lines and Primary Cultured Astrocytes. *Curr. Protoc. Toxicol.* 2017, 2017, 1–10. <https://doi.org/10.1002/cptx.21>.
45. Shen, Y.; Maupetit, J.; Derreumaux, P.; Tufféry, P. Improved PEP-FOLD Approach for Peptide and Miniprotein Structure Prediction. *J. Chem. Theory Comput.* 2014, 10 (10), 4745–4758. <https://doi.org/10.1021/ct500592m>.
46. Rose, P. W.; Prlić, A.; Bi, C.; Bluhm, W. F.; Christie, C. H.; Dutta, S.; Green, R. K.; Goodsell, D. S.; Westbrook, J. D.; Woo, J.; Young, J.; Zardecki, C.; Berman, H. M.; Bourne, P. E.; Burley, S. K. The RCSB Protein Data Bank: Views of Structural Biology for Basic and Applied Research and Education. *Nucleic Acids Res.* 2015, 43 (D1), D345–D356. <https://doi.org/10.1093/nar/gku1214>.
47. Fleishman, S. J.; Leaver-Fay, A.; Corn, J. E.; Strauch, E. M.; Khare, S. D.; Koga, N.; Ashworth, J.; Murphy, P.; Richter, F.; Lemmon, G.; Meiler, J.; Baker, D. Rosettascripts: A Scripting Language Interface to the Rosetta Macromolecular Modeling Suite. *PLoS One* 2011, 6 (6), 1–10. <https://doi.org/10.1371/journal.pone.0020161>.
48. London, N.; Raveh, B.; Cohen, E.; Fathi, G.; Schueler-Furman, O. Rosetta FlexPepDock Web Server - High Resolution Modeling of Peptide-Protein Interactions. *Nucleic Acids Res.* 2011, 39 (SUPPL. 2), 249–253. <https://doi.org/10.1093/nar/gkr431>.

49. Xu, C.; Wang, B. C.; Yu, Z.; Sun, M. Structural Insights into Bacillus Thuringiensis Cry, Cyt and Parasporin Toxins; 2014; Vol. 6. <https://doi.org/10.3390/toxins6092732>.
50. Gautier, R.; Douguet, D.; Antony, B.; Drin, G. HELIQUEST: A Web Server to Screen Sequences with Specific α -Helical Properties. *Bioinformatics* 2008, 24 (18), 2101–2102. <https://doi.org/10.1093/bioinformatics/btn392>.
51. de Angelis, P. M.; Fjell, B.; Kravik, K. L.; Haug, T.; Tunheim, S. H.; Reichelt, W.; Beigi, M.; Clausen, O. P.; Galteland, E.; Stokke, T. Molecular Characterizations of Derivatives of HCT116 Colorectal Cancer Cells That Are Resistant to the Chemotherapeutic Agent 5-Fluorouracil. *Int. J. Oncol.* 2004, 24 (5), 1279–1288. <https://doi.org/10.3892/ijo.24.5.1279>.
52. Alves, A. C.; Ribeiro, D.; Nunes, C.; Reis, S. Biophysics in Cancer: The Relevance of Drug-Membrane Interaction Studies. *Biochim. Biophys. Acta - Biomembr.* 2016, 1858 (9), 2231–2244. <https://doi.org/10.1016/j.bbamem.2016.06.025>.
53. Hoskin, D. W.; Ramamoorthy, A. Studies on Anticancer Activities of Antimicrobial Peptides. *Biochim. Biophys. Acta* 2008, 1778 (2), 357–375. <https://doi.org/10.1016/j.bbamem.2007.11.008>.
54. Wu, D.; Gao, Y.; Qi, Y.; Chen, L.; Ma, Y.; Li, Y. Peptide-Based Cancer Therapy: Opportunity and Challenge. *Cancer Lett.* 2014, 351 (1), 13–22. <https://doi.org/10.1016/j.canlet.2014.05.002>.
55. Abe, Y.; Inoue, H.; Ashida, H.; Maeda, Y.; Kinoshita, T.; Kitada, S. Glycan Region of GPI Anchored-Protein Is Required for Cytocidal Oligomerization of an Anticancer Parasporin-2, Cry46Aa1 Protein, from Bacillus Thuringiensis Strain A1547. *J. Invertebr. Pathol.* 2017, 142, 71–81. <https://doi.org/10.1016/j.jip.2016.11.008>.
56. Wong, A. H. M.; Tomlinson, A. C. A.; Zhou, D.; Satkunarajah, M.; Chen, K.; Sharon, C.; Desforgues, M.; Talbot, P. J.; Rini, J. M. Receptor-Binding Loops in Alphacoronavirus Adaptation and Evolution. *Nat. Commun.* 2017, 8 (1), 1–9. <https://doi.org/10.1038/s41467-017-01706-x>.
57. Slater, C.; De La Mare, J. A.; Edkins, A. L. In Vitro Analysis of Putative Cancer Stem Cell Populations and Chemosensitivity in the SW480 and SW620 Colon Cancer Metastasis Model. *Oncol. Lett.* 2018, 15 (6), 8516–8526. <https://doi.org/10.3892/ol.2018.8431>.

3.7 Supporting information

Figure S1. Chromatogram and mass spectra of P264-G274 peptide.

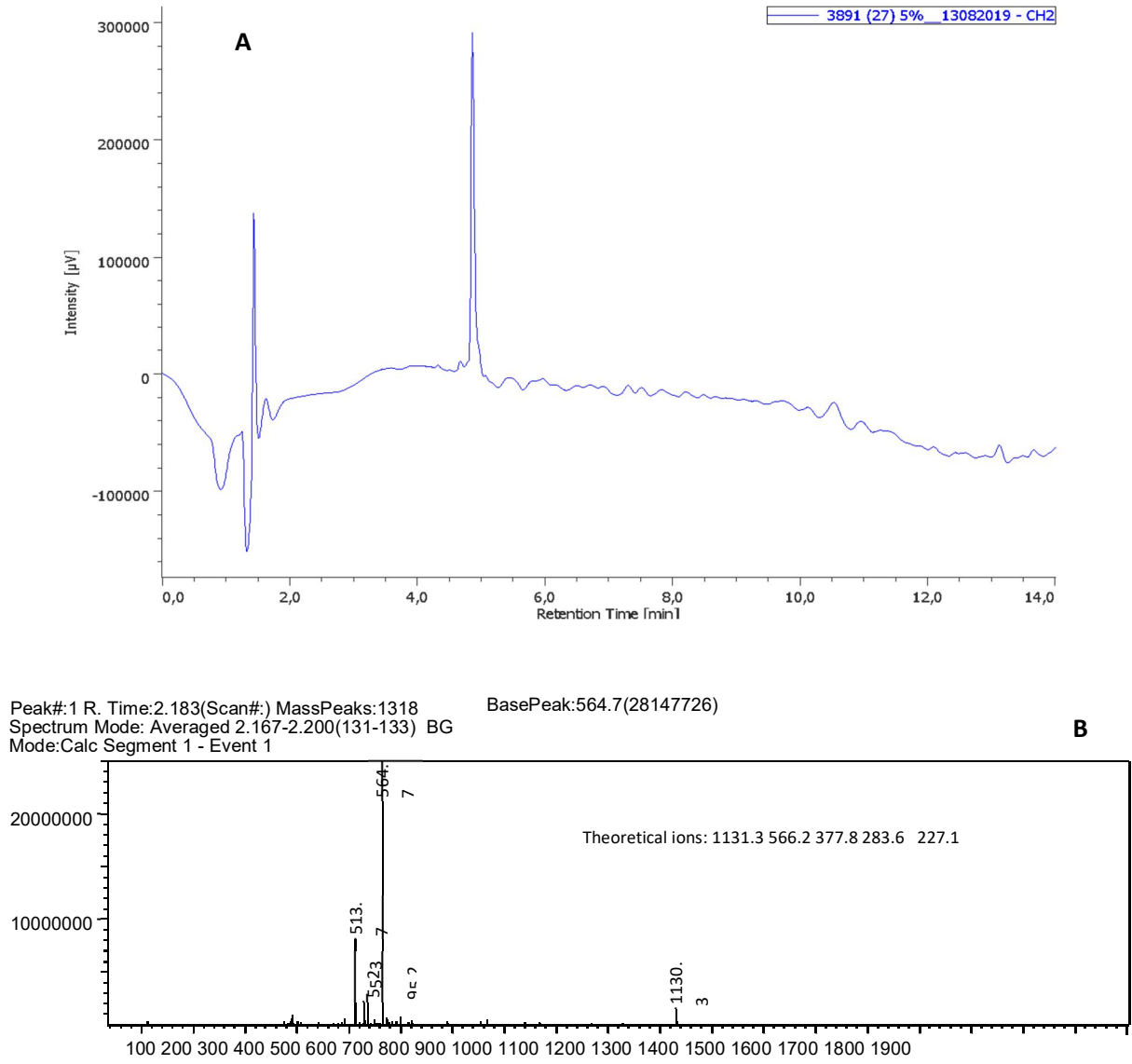


Figure S2. Chromatogram and mass spectra of Loop1-Ps2Aa peptide.

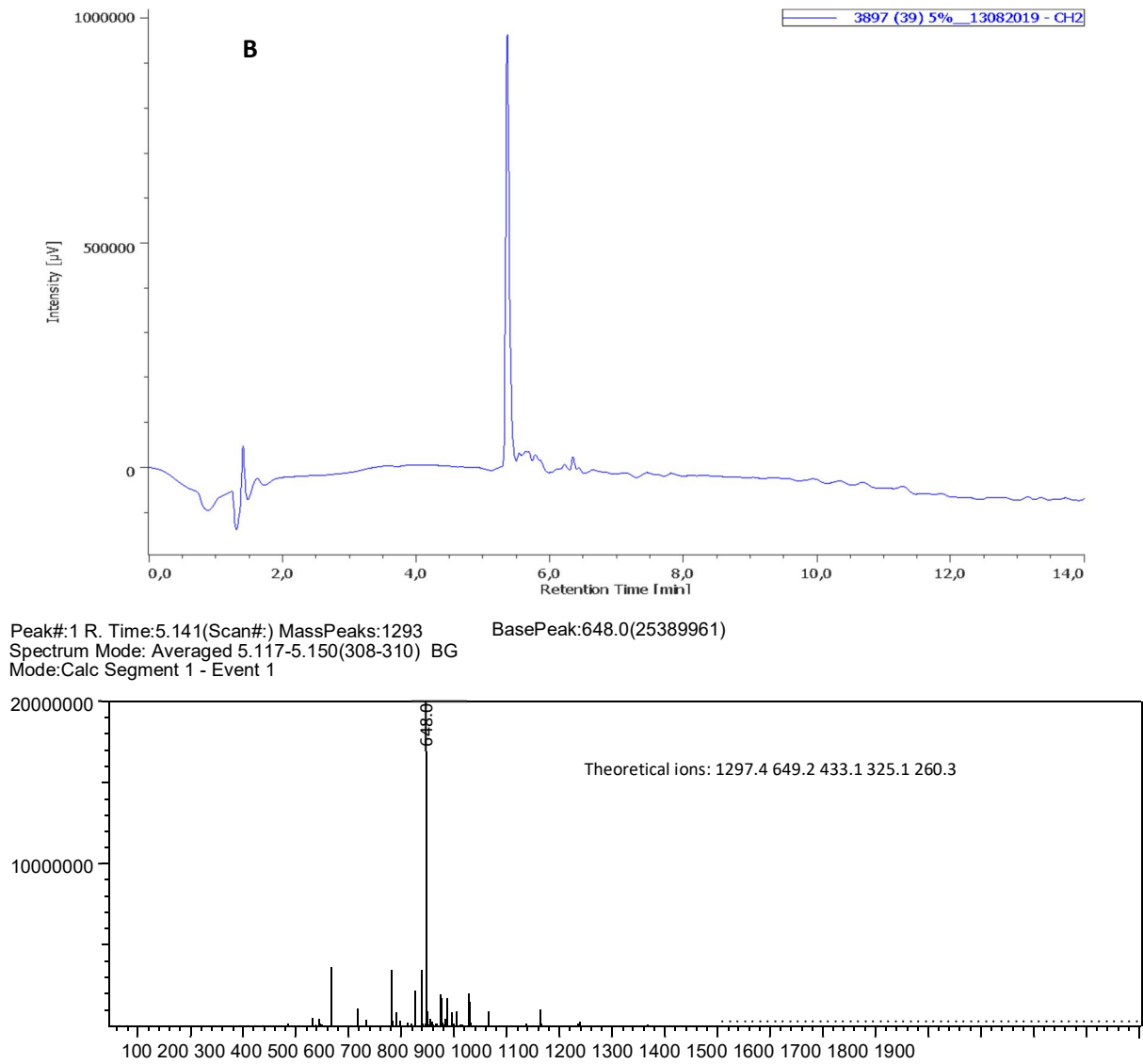


Figure S3. Chromatogram and mass spectra of Loop2-Ps2Aa peptide.

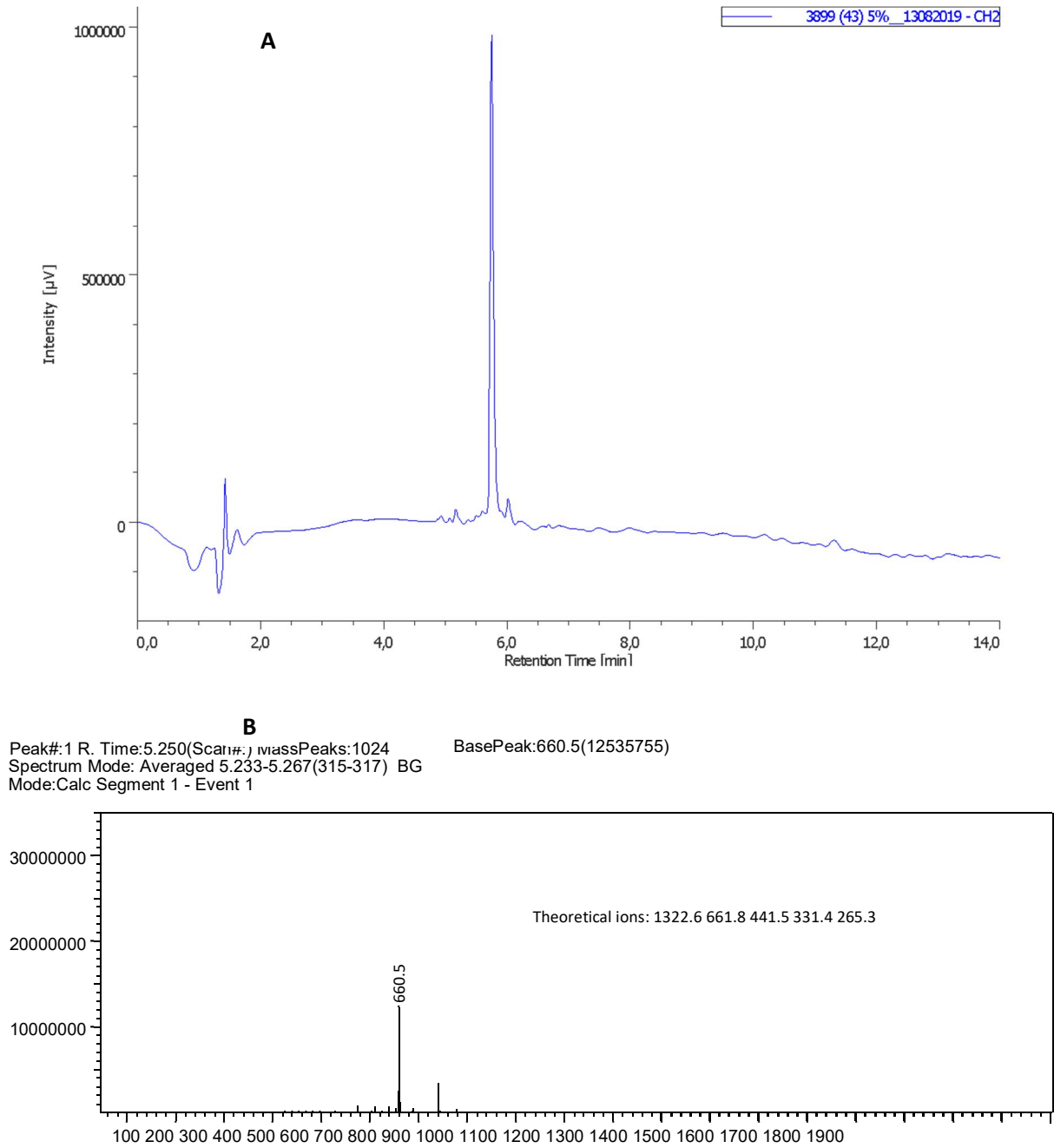


Figure S4. Chromatogram and mass spectra of Loop1-HCoV-229E peptide.

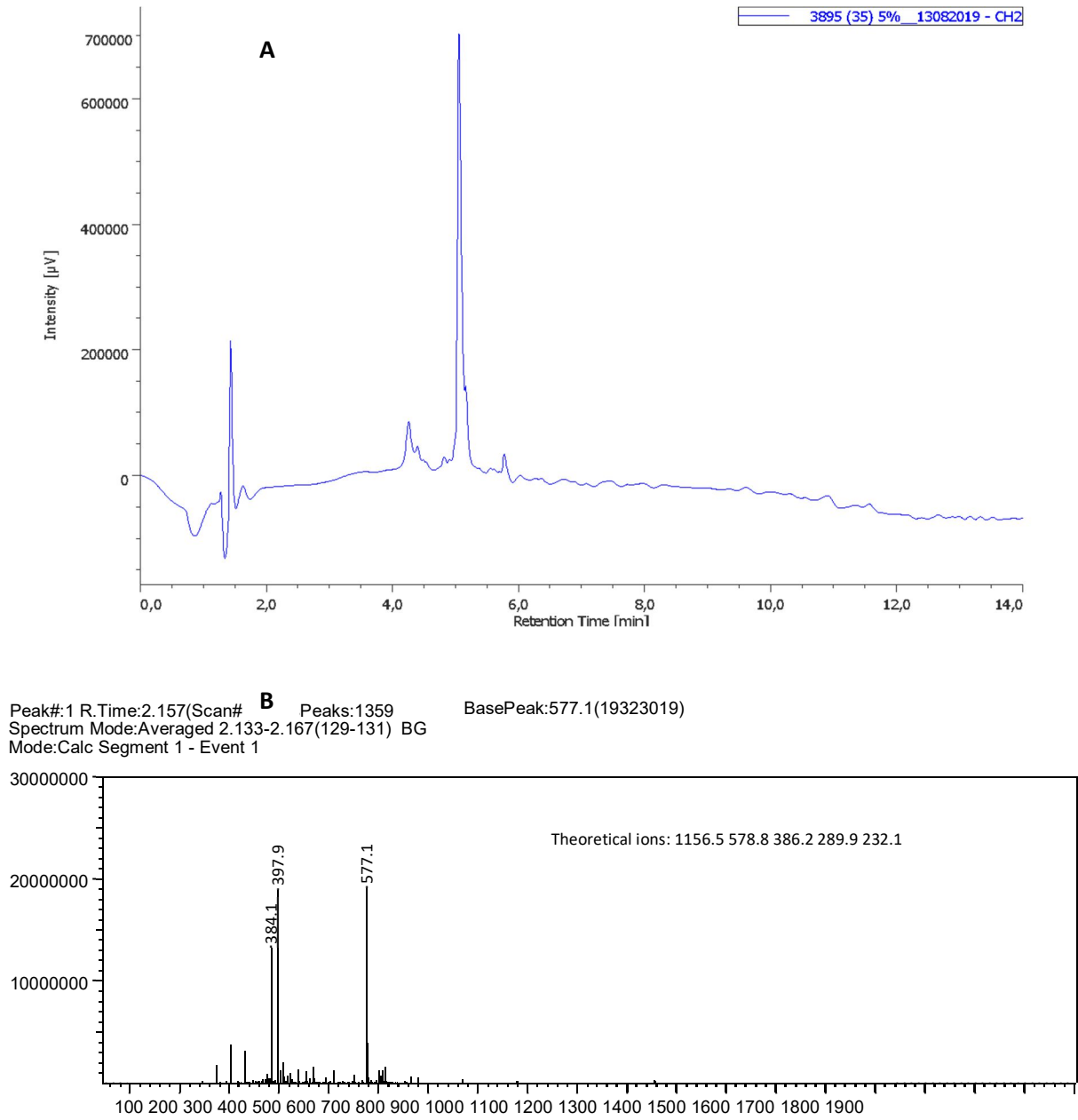
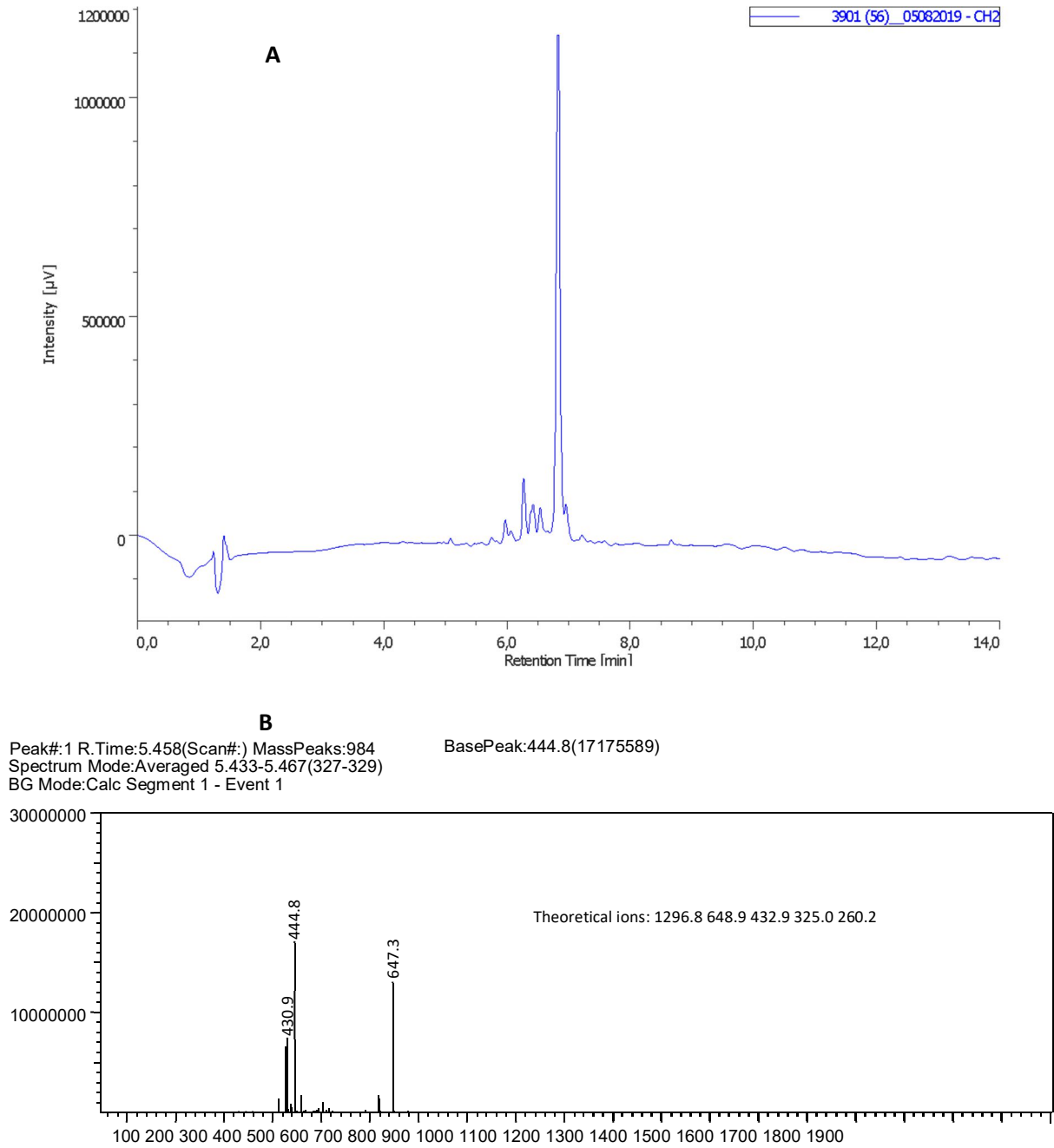


Figure S5. Chromatogram and mass spectra of A4W-GGN5 peptide



4. Site-Directed Mutants of Paraspurin PS2Aa1 with Enhanced Cytotoxic Activity in Colorectal Cancer Cell Lines

Miguel Orlando Suárez-Barrera

Lydia Visser

Efraín Hernando Pinzón-Reyes

Paola Rondón-Villarreal

Juan Sebastián Alarcón-Aldana

Nohora Juliana Rueda-Forero

Molecules

2022, *27*, 7262. <https://doi.org/10.3390/molecules27217262>

Author Contributions: Conceptualization, M.O.S.-B., L.V., E.H.P.-R., P.R.V. and N.J.R.-F.; Investigation, M.O.S.-B., L.V., E.H.P.-R., P.R.V., J.S.A.-A. and N.J.R.-F.; Methodology, M.O.S.-B., L.V., E.H.P.-R., P.R.V. and N.J.R.-F.; Project administration, N.J.R.-F.; Writing—original draft, M.O.S.-B., L.V., E.H.P.-R., P.R.V., J.S.A.-A. and N.J.R.-F.; Writing—review and editing, M.O.S.-B., L.V. and N.J.R.-F. All authors have read and agreed to the published version of the manuscript. **Funding:** The work has been funded by MINCIENCIAS, MINEDUCACIÓN, MINCIT, and ICETEX, through the Program Ecosistema Científico Cod. FP44842-211-2018 Project number, 58668. **This chapter is linked to the aims:** - To design engineering strategies for Paraspurin PS2Aa1, combining directed evolution methodologies, site-specific mutagenesis, structural bioinformatics tools, and the structural and functional knowledge described in the literature to obtain proteins with different potentials to control cancer cell lines growing.- To analyze the PS2Aa1-APN receptor interactions using computational strategies involving molecular docking and dynamics to explore the possible potential of this membrane receptor to bind to the domain I of this parasporin.- To produce novel parasporal proteins with enhanced activity against colon cancer cell lines and determine

the cytotoxic activity of selected mutant proteins of *Bacillus thuringiensis* based on their binding affinity to membrane receptors by computational approaches.

This work is a continuation of Chapter 3, and it describes a site-directed mutagenesis strategy for obtaining PS2Aa1 variants with aminoacid substitutions in Loop 1 of Domain I, with the variant 3-35 showing an increased potential in the control of colorectal cancer cell lines. Furthermore, it was discovered that the residue 256 is crucial in the interaction of this protein with the receptor APN.

4.1 Abstract

Parasporin 2 has cytotoxic effects against numerous colon cancer cell lines, making it a viable alternative to traditional treatments. However, its mechanism of action and receptors remain unknown. In this study, site-directed mutagenesis was used to obtain PS2Aa1 mutants with variation in domain I at positions 256 and 257. Variants 015, 002, 3-3, 3-35, and 3-45 presented G256A, G256E, G257A, G257V, and G257E substitutions, respectively. Cytotoxicity tests were performed for the cell viability of cell lines SW480, SW620, and CaCo-2. Mutants 3-3, 3-35, and 3-45 efficiently killed the cell lines. It was found that the activated forms of caspase-3 and PARP were in higher abundance as well as increased production of γ H2AX when 3-35 was used to treat CaCo-2 and SW480. To assess possible membrane-binding receptors involved in the interaction, an APN receptor blocking assay showed reduced activity of some parasporins. Hence, we performed molecular docking and molecular dynamics simulations to analyze the stability of possible interactions and identify the residues that could be involved in the protein–protein interaction of PS2Aa1 and APN. We found that residues 256 and 257 facilitate the interaction. Parasporin 3-35 is promising because it has higher cytotoxicity than PS2Aa1.

Keywords: Anticancer; Parasporin; Site-directed mutagenesis; Apoptosis; APN receptor

4.2 Introduction

The use of bacteria and their byproducts, i.e., attenuated or genetically modified, has begun to increase in recent decades based on their ability to recognize specific characteristics of cancer cells. They can act directly on mechanisms involved in the proliferation and growth of tumor cells [1]. Additionally, their use as antitumor agents represent a promising strategy because of the ease of their genetic manipulation, which allows biomolecules with improved toxic activity and specificity to be obtained [1–4]. Mizuki et al., in the first report on Parasporin (PS) in 2000 [5], described its potential as an anticancer molecule, specifically in leukemia. Subsequently, most studies have focused on the characterization and screening of new proteins identified from *Bacillus thuringiensis* (*Bt*) strains and isolates [6–10]. Akiba and Okumura proposed in 2017 that the mechanism of action of this protein is in inducing apoptosis [11], but many unknowns persist up to now, especially regarding the identity of the major PS receptor, with N-aminopeptidase (APN) and GPI-anchored proteins having been proposed as candidates [6,7,12,13]. Parasporin 2Aa1 (PS2Aa1) has shown cytotoxic effects against several human cancer cells, being highly specific for human liver and colon cancer cells [7–9], thus representing an additional treatment alternative for colorectal cancer. This protein is a polypeptide that requires proteases such as proteinase K to switch from a pro-toxin of 37 kDa to its active form of 30 kDa, which is shown to be highly cytotoxic and selective toward different cancer cell lines [10]. Furthermore, this protein is believed to act specifically on the membrane of target cells through domain I, which indicates the presence of a specific PS2Aa1 receptor whose identity is so far unknown [12]. Once PS2Aa1 is bound to the receptor, through domains II and III, it forms oligomers that permeabilize the membrane and lead to the formation of pores, which induces structural cytoskeletal alterations, organelle fragmentation, alterations in cell morphology, and finally lysis of susceptible cells [8]. Considering this scenario, our research group is studying the structure–function relationship of Parasporin 2, while exploring its possible use as a therapeutic alternative. This is how we recently designed and prepared peptides in which loop 1 of domain I was mutated, and the selection of this site in the design was supported by in silico modeling with APN. In that study, the Loop1–PS2Aa and P264–G274, peptides

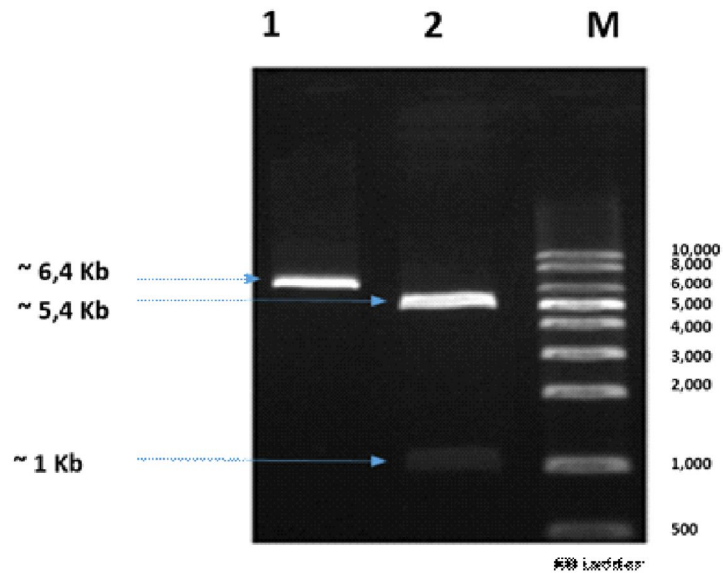
exhibited stronger anticancer activity than the wild type against SW480 and SW620, respectively, and demonstrated high effectiveness and selectivity; hence, they were proposed as possible alternative therapeutic agents for the treatment of colon cancer. In this sense, we decided to take domain I of PS2Aa1, mutate the residues that presented differentiated activities in the reported peptides, and consider additional positions for the modification of these peptides to generate the libraries of PS2Aa1 mutants, which we describe below [6]. The goal of this work was to obtain a characterized set of PS2Aa1 mutants with modifications in domain I and assess its cytotoxicity in colon cancer cells. Moreover, we used molecular docking and molecular dynamics simulations to analyze the possible interactions between PS2Aa1 and APN receptor, which have been proposed as a possible interacting protein. Additionally, our work contributes to the understanding of the relation between the structure and function of these proteins and their possibilities of being used as new treatments in the future.

4.3 Results

4.3.1 Cloning and Obtention of PS2Aa1 Mutants

The gene *ps2Aa1* (NCBI accession number AB099515.1) was cloned in the plasmid pET30a to generate the construct *pET-30a/ps2Aa1*, which was corroborated by restriction assays with a band of ~1 Kb for PS2Aa1 and a band of ~5.4 Kb for pET30 (Figure 1). Then, the construct was transformed into *E. coli* strain DE3BL21 for the production of plasmid and subsequent site-direct mutagenesis to create four libraries, one for each primer set.

Figure 24. Agarose gel showing the construct pET-30a/ps2Aa1 treated with the restriction enzymes KpnI and HindIII; Lane 1: construct pET-30a/ps2Aa1; Lane 2: construct pET-30a/ps2Aa1 treated with the restriction enzymes KpnI and HindIII; Lane M: molecular weight marker.



A low mutation rate was obtained, whereby only 12 of the 71 selected mutants had mutations in their sequences. Therefore, from the 12 PS2Aa1 mutants, 6 were chosen for cytotoxicity assays. Mutant 0-2 presented an amino acid change from glycine (G) to aspartic acid (D) at position 256 of its amino acid chain corresponding to position 1000 of the nucleotide sequence; mutant 0-6 had an amino acid change from glycine to valine (V) in the same position; mutant 0-15, like the previous proteins, presented an amino acid change at position 256 to become alanine (A); therefore, these three mutants were obtained from the primer set flanking nucleotide position 1000. On the other hand, mutants 3-35 and 3-45 presented amino acid changes in their sequences at position 257 (position 1003 in the nucleotide chain), changing from glycine (G) to valine (V) and glutamic acid (E), respectively. It is, therefore, assumed that these mutants were obtained from the primer set targeting position 1003.

4.3.2 Description of Parasporins Obtained from PS2Aa1 Using Site-Directed Mutagenesis

From the libraries in *E. coli*, 103 colonies were sequenced. Mutagenesis was successful, although not in all the colonies because of the randomness attributed to the reaction by adding equimolar conditions of adenine, guanine, cytosine, or thymine. The sequence analysis showed 99.9% identity with parasporin 2 of *Bt*, determined by BLASTn searching of the contigs for each variant, and MatGat, similarity/identity matrices for DNA [14]. The contigs were translated to their respective amino acid sequence and a multiple sequence alignment was performed comparing each of these sequences with the native parasporin reported in the PDB (code: 2ztb). The substitutions obtained at residues 256 and 257 were mostly glycine for alanine (A), aspartic acid (D), valine (V), and glutamic acid (E), as described in Table 1.

Table 12. Description of parasporins obtained from PS2Aa1 using site-directed mutagenesis.

ID (Library)	Type/Site of the Mutation	Mutant Name	Amino Acid Sequencing
Wt.	PS2Aa1 (PDB 2ZTB)	-	251-KRVGPGGHYF-260
02	SUS/256	G256D	251-KRVGPDGHYF-260
015	SUS/256	G256A	251-KRVGPAGHYF-260
3-3	SUS/257	G257A	251-KRVGPGAHYF-260
3-35	SUS/257	G257V	251-KRVGPGVHYF-260
3-45	SUS/257	G257E	251-KRVGPGEHYF-260

4.3.3 Cytocidal Activities of PS2Aa1 Variants in Human Colorectal Cancer Cells

We first compared the native *Bt* protein 4R2 with the recombinant PS2Aa1 and found that the activities were comparable in SW480 and SW620, but PS2Aa1 was more effective than 4R2 in CaCo-2 (Figure S1). Cell line NCM460 was used as a control. In this normal colorectal cell line, none of the parasporins showed any relevant effect, consistent with previous reports of specificity of the parasporin to cancer cells (Figure S1). The variants showed different patterns in the cell lines. In SW480, the protein with the highest cytotoxic activity was 3-35 with an IC₅₀ of 0.32 µg/mL, more than three times that of PS2Aa1 (IC₅₀ = 1 µg/mL). All of the variants were effective, with 002 having the lowest

cytotoxicity ($IC_{50} = 4.68 \mu\text{g/mL}$). In SW620, 3-35 was also the most cytotoxic ($IC_{50} 2.06 \mu\text{g/mL}$), while 3.45 was the least ($IC_{50} 17.77 \mu\text{g/mL}$). Against CaCo-2 cells, the mutant 3-35 was the most cytotoxic ($IC_{50} 0.96 \mu\text{g/mL}$), with similar results observed for 3-3 and 3.45, whereas 0015 and 002 were not effective (Table 2).

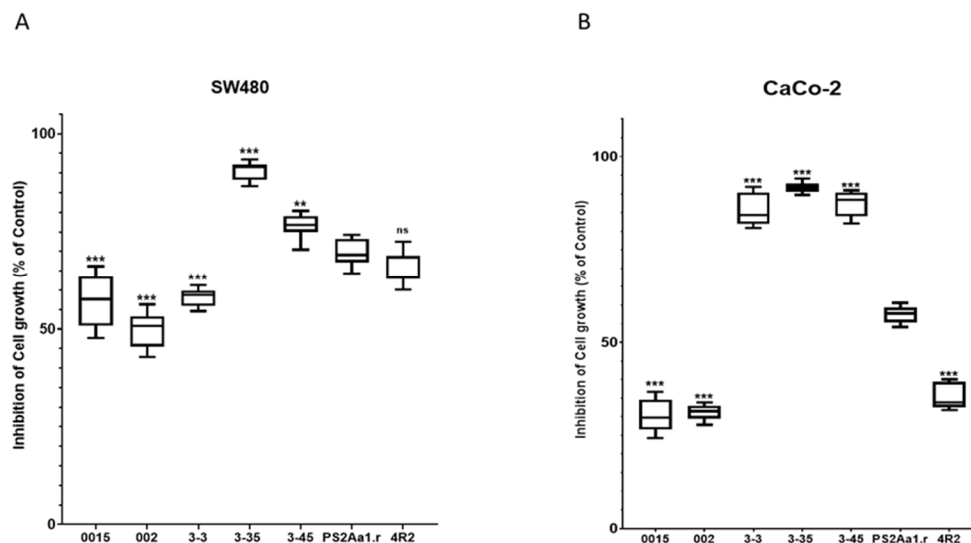
Table 13. Cytocidal activities of PS2Aa1 variants in human colorectal cancer cells.

Parasporin	IC_{50} Parasporin $\mu\text{g}\cdot\text{mL}^{-1}$ (95% CI)		
	SW480	SW620	CaCo-2
0015	2.42 (1.59–4.70)	ND	ND
002	4.68 (2.57–17.74)	ND	ND
3-3	2.02 (1.51–2.96)	ND	0.98 (0.83–1.16)
3-35	0.32 (0.22–0.43)	2.46 (2.07–3.00)	0.88 (0.81–0.95)
3-45	0.78 (0.65–0.92)	ND	0.96 (0.84–1.09)
P2SAa1	1.00 (0.65–1.55)	5.70 (4.10–9.50)	2.57 (1.84–4.15)
4R2	0.62 (0.41–0.86)	ND	ND

ND: non-detectable.

Comparisons with PS2Aa1 were based on ordinary one-way ANOVA employing Tukey's multiple comparison test for SW480 and CaCo-2. All the comparisons were significantly different (**, ***), except between the activity of PS2Aa1 and the native strain 4R2 in SW480 (Figure 2).

Figure 25. Tukey's multiple comparison test for (A) SW480 and (B) CaCo-2. The results for the percentage of cell growth inhibition correspond to $5 \mu\text{g}\cdot\text{mL}^{-1}$ for each parasporin. PS2Aa1 was used as a control. ** $p \leq 0.01$, and *** $p \leq 0.001$, ns (non-significant)



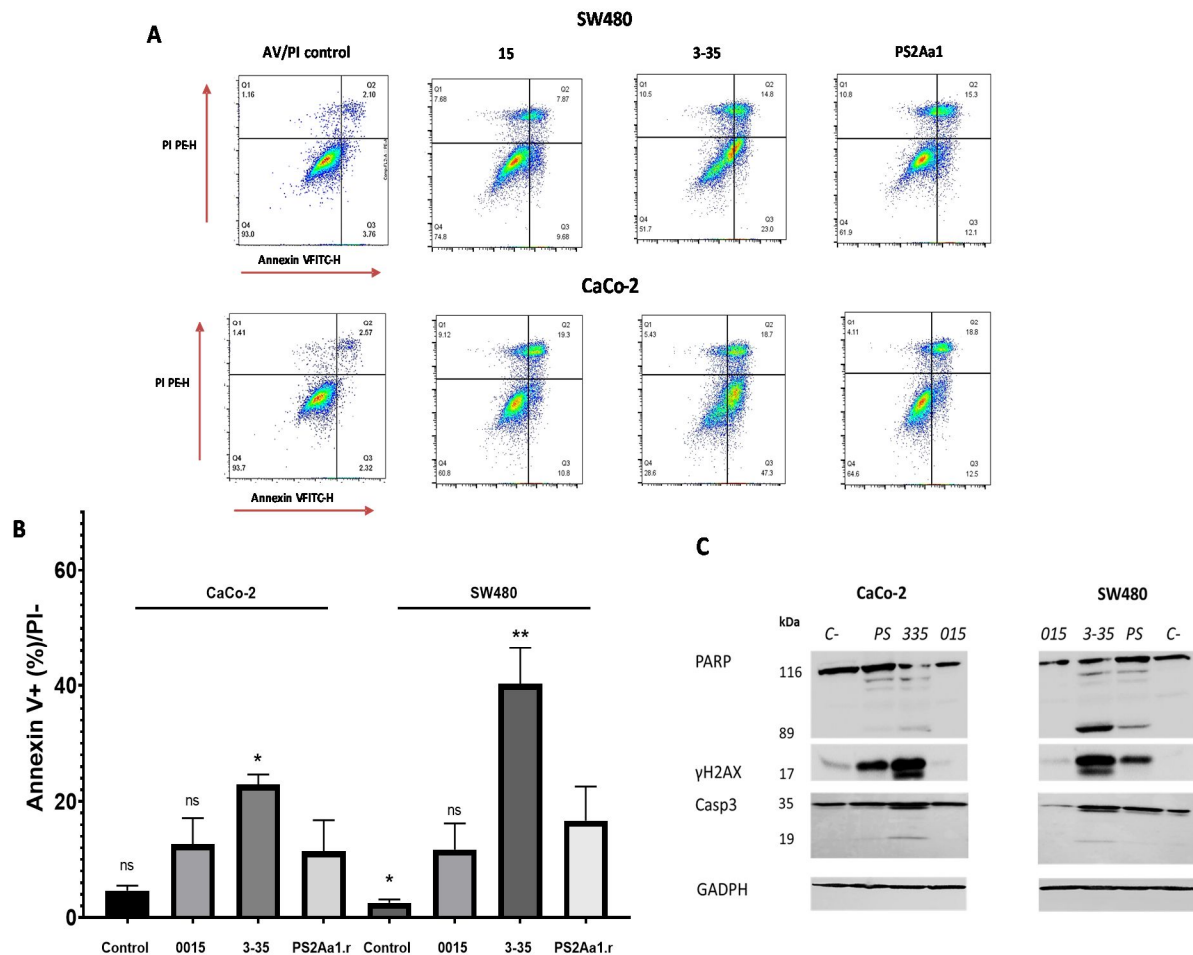
4.3.4 Variants of PS2Aa1 Induce Apoptosis in Human Colorectal Cancer Cells

To expand our results, we performed an analysis with annexin V (AV) and propidium iodide (PI) to characterize the percentage of cells in apoptosis and death. For this part of the study, the cell lines SW480 and CaCo-2 and the parasporins 015, 3-35, and PS2Aa1 were selected, owing to the observation of relevant cytotoxic activity.

After the treatment of CaCo-2 and SW480 with 5 µg/mL of each parasporin, higher percentages of apoptotic cells, 25% and 37%, respectively, were observed for both cell lines when treated with parasporin 3-35 followed by PS2Aa1 and, lastly, 015 (Figure 3A,B), which is similar to the cytotoxicity results, where 3-35 also excels. The differences between PS2Aa1 and 015 were not remarkable, and no differences in dead cells were detected in all of the treatments, suggesting the late activation of apoptosis in the cell lines by parasporin 2Aa1 and its variants as an effect of the pore-forming action of these proteins, which was previously suggested to be the mechanism of action [13,15–17]. HSD Tukey testing was performed with the results of annexin V-positive cells, showing that there are significant differences between PS2Aa1.r and 3-35 in the treatment of CaCo-2 (*). For SW480, it was shown that there are differences between PS2Aa1.r and 3-35 (**), and Ps2Aa1.r and the control (*); $p \leq 0.05$ (Figure 3B).

To further investigate the induction of apoptosis, we also measured different markers using Western blot analysis, such as cleaved caspase-3, cleaved poly (ADP-ribose) polymerase-1 (PARP), and Histone 2 family member, phosphorylated on serine 139 (γ-H2AX). For both CaCo-2 and SW480, activation of caspase-3 and PARP was more induced by the treatment with parasporin 3-35, with multiple bands obtained for both proteins. PARP cleavage is more pronounced in SW480 and corresponds with the lowest IC_{50} ($0.32 \mu\text{g} \cdot \text{mL}^{-1}$) in the cytotoxicity assay (Table 2). We did not see differences between the results of caspase-3 and γH2AX in the cell lines. In the case of γH2AX, the band intensity in the treatment with 3-35 is the highest. The presence of a slightly higher molecular weight band at 17 kDa indicates the phosphorylated form of this modified histone involved in the repair of DNA damage (Figure 3C).

Figure 26. Cytotoxic effects of parasporins to CaCo-2 and SW480. Detection of annexin V/PI (A), statistical analysis of induction of apoptosis by parasporins (B). Western blot of PARP, caspase-3 (Casp3), and γ H2AX in SW480 and CaCO-2 after treatment with the indicated parasporins (C). GAPDH was used as a loading control. The amount of toxins used for each treatment was 5 μ g/mL over 48 h. * $p \leq 0.05$, ** $p \leq 0.01$, ns (non-significant)

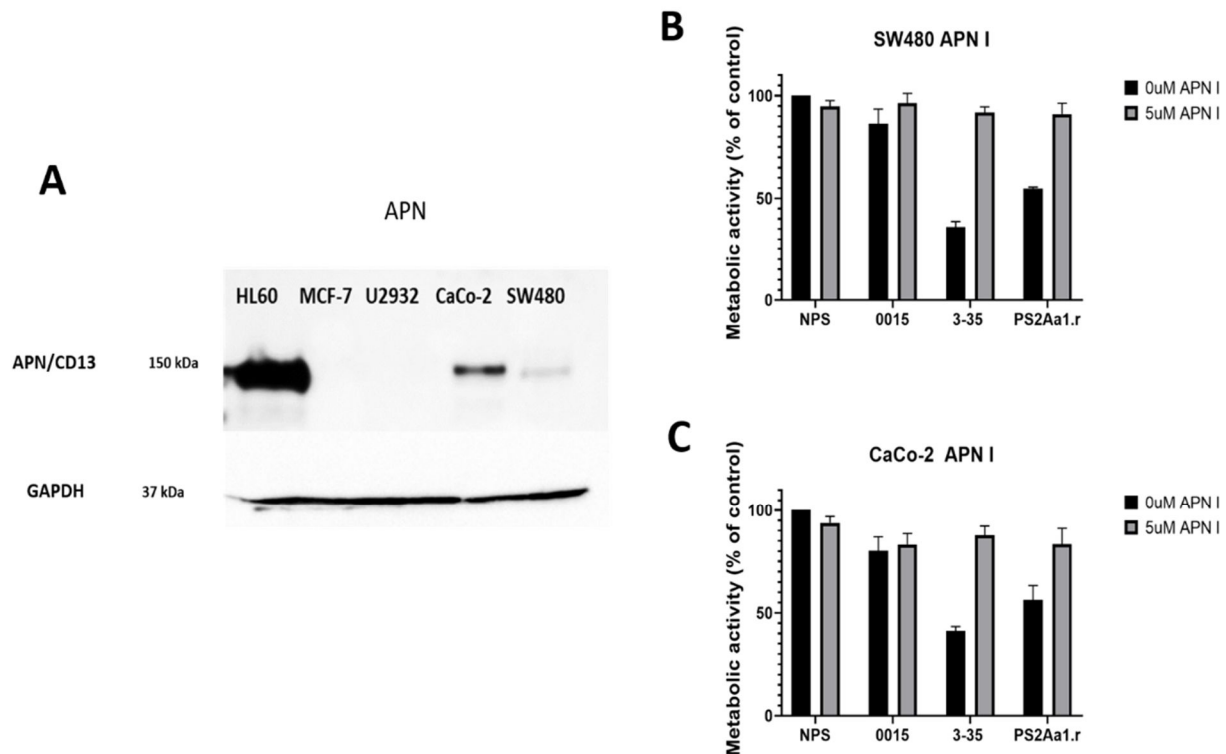


4.3.5 Cytotoxic Activity of PS2Aa1 Variants Is Affected by APN Receptor Inhibition

We next checked for the presence of APN as a possible receptor for PS2Aa1. The highest level of expression of the APN receptor was obtained in the positive control cell line HL60, and the protein was not present in negative controls MCF-7 and U2932 (Figure 4A). In the case of colorectal cancer cells, the amount of APN is higher in CaCo-2 compared with SW480. We next blocked APN with an inhibitor and tested the effect of the different parasporins at 5 μ g·mL⁻¹. The effect of 3-35 and PS2Aa1 on SW480 and CaCo-2 was diminished to the point of no cytotoxicity at the lowest concentration of APN inhibitor

(5 μM) (Figure 4B, C), which strongly suggest that the effect of 3-35 and PS2Aa1 is presumably dependent on binding to APN. To further understand these results, *in silico* analysis was performed via docking and molecular dynamics simulations.

Figure 27. (A) Detection of APN receptor in different cell lines HL60, MCF-7, U2932, CaCo-2, and SW480. Metabolic activity of (B) SW480 and (C) CaCO-2 without parasporin (NP), parasporin 0015, 3-35, and the recombinant of PS2Aa1 (PS2Aa1.r) at 5 $\mu\text{g}\cdot\text{mL}^{-1}$ in the presence or absence of the APN inhibitor.



4.3.6 Molecular Docking and Molecular Dynamics Analysis Highlight Residues 256 and 257 of Domain I of PS2Aa1

The predicted models were ranked based on the number of hydrogen bonds in the interface, with the top 10 shown in Table 3. After visual inspection, model number 560 was selected to perform the molecular dynamics simulations. Figure 5 shows the selected complex between PS2Aa1 and APN with the relevant residues in the interaction.

Table 14. Top 10 models according to the number of hydrogen bonds in the interface.

Top	Model	Number of Hydrogen Bonds in the Interface
1	560	9
2	3413	9
3	105	9
4	819	8
5	994	8
6	2079	8
7	3521	8
8	1015	8
9	1742	8
10	708	8

Figure 28. Relevant residues for PS2Aa1–APN interaction. Relevant residues for interacting with the APN receptor are displayed. GLY256, ARG76, ARG266, and SER273. PS2Aa1 and APN are colored blue and teal, respectively.

The 560-model selected by molecular docking analysis was subjected to molecular dynamics computational simulations to identify possible residues of wild-type PS2Aa1, which showed preference in protein–protein interaction (PS2Aa1–APN). As shown in Table 4, after three molecular dynamics simulation replicates, some of the PS2Aa1 residues were in contact with APN for the longest simulation time and at a smaller average distance from the center of mass of the PS2Aa1 residue and the closest APN residues. Table 4 records the wild-type PS2Aa1 residues, for each of the three simulation replicates, that were in contact for more than 80% of the simulation time and that also maintained inter-action distances of less than 5 Å. These two conditions suggest *in silico* that these residues could be of interest in the PS2Aa1–APN interaction.

Table 15. Residues in contact with APN receptors.

MD	Contact Residues (>80%) *
Replicate 1	PRO255, GLY256
Replicate 2	ARG76, PRO238, ILE239, THR240, VAL241, ARG266, GLY256, GLY257, THR272, SER273, GLY274
Replicate 3	ARG76, PRO238, ILE239, THR240, VAL241, ASP242, PRO255, GLY256, GLY257, ARG266, ASP267, ASN270, THR272, SER273, GLY274, THR275

* The residues in contact with APN receptors at 80% frequency are shown for each independent MD.

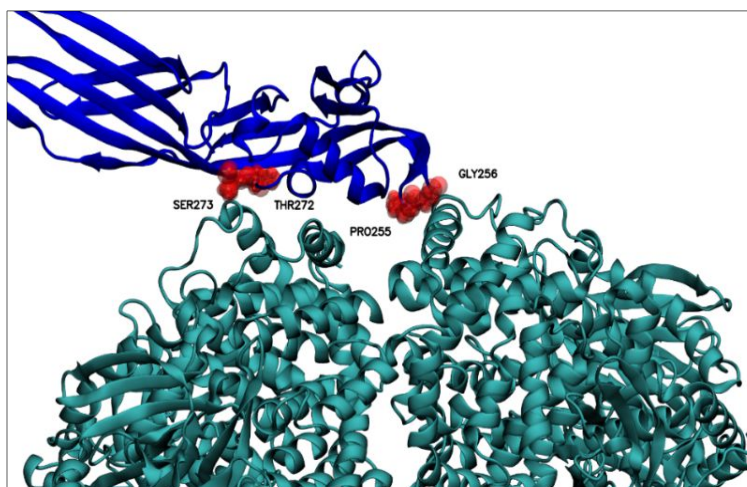
Table 5 below presents a review of these residues from their prevalence in the three replicates, that is, the frequency with which these residues were identified as preferential for interaction in the molecular dynamic simulations (Table 4). There, GLY256 seems to be the residue of conspicuous importance, as it is the only residue recorded in all three replicas of molecular dynamics; the importance of this residue could be explained based on its position, because GLY256 is in a PS2Aa1 loop (Figure 5), a mobile and flexible part of the protein. Moreover, GLY256 presents stable dynamics (SD 0.21 Å), with an average minimum distance of 4.44 Å to APN (Figure 6), and is the closest residue.

Table 16. Prevalence of PS2Aa1 residues among MD replicates.

MD	PS2Aa1 Residues
Replicate 3	GLY256
Replicate 2	ARG76*, PRO238, ILE239, THR240, VAL241, PRO255, GLY257, ARG266*, THR272, SER273*, GLY274
Replicate 1	ASP267, ASN270, THR275

* Residues with the highest frequency in the MD replicates.

Figure 29. Residues relevant for the interaction with APN at distances less than 6 Å between the center of mass of the relevant PS2Aa1 residues and the nearest APN residue. Above, PS2Aa1 and APN are colored blue and teal, respectively.



Residues ARG76, PRO238, ILE239, THR240, VAL241, PRO255, GLY257, ARG266, THR272, SER273, and GLY274 had high prevalence in two MD replicates (Table 6), highlighting the significant prevalence (frequency) of residues ARG76, ARG266, and SER273 that were close to the APN receptor. These three residues are

found within the beta-sheet secondary structure of PS2Aa1 (Figure 5), which could limit their interacting with APN.

There are also some residues that could have had a modest role in the PS2Aa1–APN interaction because they appeared in only one MD replicate (ASP267, ASN270, and THR275) and were the farthest residues from APN. Likewise, the previous group of residues were located in the beta-sheet secondary structure of PS2Aa1, which reduced their chance to interact with APN.

Lastly, some high-prevalence residues have an average distance of less than 6 Å (Table 6). These were PRO255, GLY256, THR272, and SER273, with GLY256 having the shortest distance and significant relevance in all the simulations (Table 6, Figure 6).

Table 17. Distances of the residues of PS2Aa1 relevant to interacting with APN.

Comparison	Mean	SD
GLY256	4.44	0.21
THR272	5.53	0.61
SER273	5.58	0.09
PRO255	5.77	0.26
THR240	6.04	0.27
ARG266	6.29	0.70
PRO238	6.30	0.58
GLY274	6.33	0.23
ASP267	6.49	0.44
ARG76	6.58	0.55
GLY257	6.64	0.69
ASN270	7.04	0.79
THR275	7.59	0.45
VAL241	7.64	0.75
ILE239	7.74	0.25

These results also suggest the participation of amino acids PRO255 and GLY256 as part of the loop of domain I of PS2Aa1 in the interactions with the APN receptor (Figure 6), being within the top 4 of the residues with the shortest interaction distance (Table 6).

4.4 Discussion

In this study, genetic modification was used to obtain mutants with substitutions in residues 256 and 257 of PS2Aa1. These modifications allowed us to build a library of new parasporins with different activities against colorectal cancer cell lines. Site-directed

mutagenesis was performed considering the results of Cruz et al. [6], where peptides from loop 1 of PS2Aa1 had remarkable activity and adherence with SW480. It was established that the oligonucleotides with the mutations incorporated for site-directed mutagenesis should be present at the N-terminal end (variable region), specifically in domain I of PS2Aa1 because, based on previous molecular docking studies, this region is the one presumably responsible for specific binding to membrane receptors [14]. The search for conserved domains found that PS2Aa1 shares conserved domains with aerolysin-type β PFT proteins, which comprises a highly conserved region corresponding to the chain of the C-terminal end and a highly variable region at the N-terminal end of the protein, which usually contains recognition signals [11] and corresponds to domain I of the β PFT proteins. Its high variability means that this family of proteins has various binding receptors that are highly specific.

For the mutants, we obtained a selectivity index of 18.9 and 17.5 for PS2Aa1 against SW480 and SW620, respectively, and 46.4 and 34.4 for variant 3-35 against SW480 and SW620, respectively (data not shown). PS2Aa1 is described as an aerolysin and beta-pore-forming protein type because of their shared homology [15]. Parasporins and aerolysins are anticancer proteins [16] and the cytogenetic effects of aerolysin produced by *Aeromonas hydrophila* on normal and tumor cells have been studied; however, the latter present a toxic effect upon normal cell lines, unlike parasporins, which have an undetectable or only slight effect on normal cell lines [7,8] and a greater effect on several cancer cell lines.

Concerning the IC_{50} , $40.15 \mu\text{g}\cdot\text{mL}^{-1}$ PS2Aa1 and $39.93 \mu\text{g}\cdot\text{mL}^{-1}$ 3-35 were noted for CHOK-1 and $>100 \mu\text{g}\cdot\text{mL}^{-1}$ for both against NCM460 presenting the parasporins and their variants as potential candidates for cancer treatment in the future. Moreover, in this study, we decided to analyze the possible interaction between PS2Aa1 and the designed mutants with the membrane receptor APN. Our results were like those found by Periyasamy et al. (2016) [7], where the use of an APN inhibitor reduced the cytotoxic activity of PS2Aa1. We found that the lowest concentration of APN inhibitor led to the loss of the cytotoxic activity of 3-35 and PS2Aa1 with CaCo-2 and SW480. Although not conclusive, our results showed that variant 3-35 requires, to some extent, APN receptor for its cytotoxic activity against Caco-2 and SW480. However, it is interesting to note that

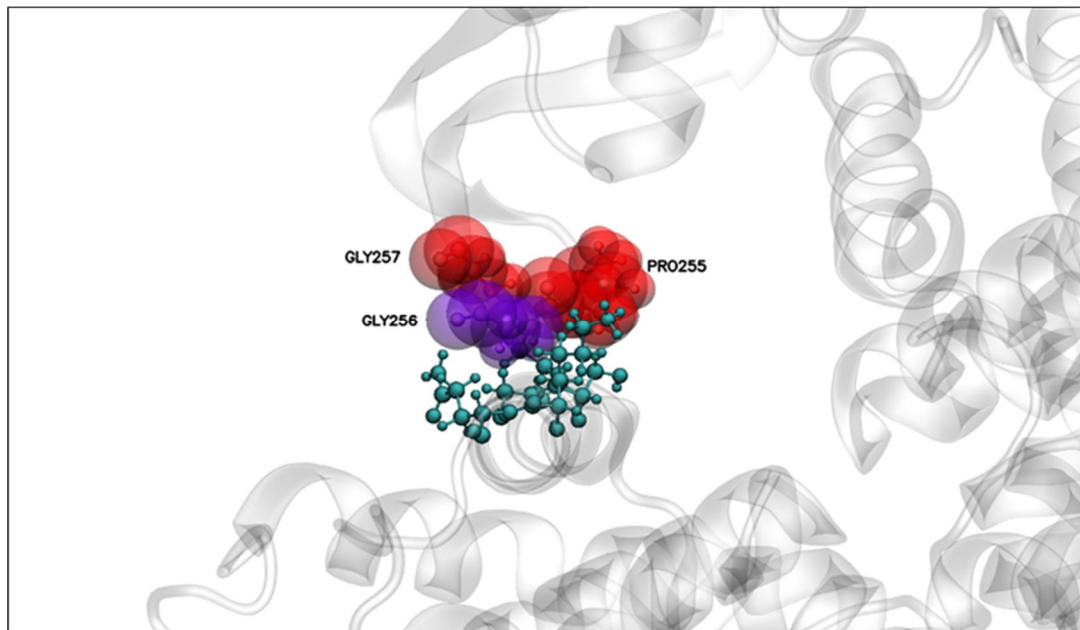
the mutant 3-35 achieved the highest cytotoxicity with cell line SW480, despite the CaCo-2 cell line having higher amounts of APN. Hence, it is likely that APN is not the only receptor directly involved in the mechanism of action of these toxins [6,17]. As previously mentioned, GPI-anchored proteins play a crucial role in the interaction with the cell membrane. These receptors seem to be more relevant in the activity of the PS in cancer cell lines because cell lines such as MCF-7 lack APN, but PS2Aa1 has strong activity against this line [18]. It has been suggested that APN could be a receptor in the mechanism of action of PS2Aa1 because parasporin activity decreased substantially in HCT116 cells, a colorectal cancer cell line, when treated with an APN inhibitor [7]. In addition, it is known that PS2Aa1 is related to the Cry proteins, which use APN as a receptor in the midgut of insects [17,19–23]; in this scenario, APN receptor is important for parasporin activity. The data indicate that, although there was a decrease in cytotoxic activity, it was not completely lost, which leads to the assumption that APN is important, but it is not the only receptor involved. Considering another binding receptor for PS2Aa1, the GPI-anchored proteins have also been suggested as relevant to the binding to the cell membrane. It was determined that the glycan core, which is part of CD59, is essential for the recognition of the aerolysin-type parasporin [6,7,12].

PS2Aa1 in its native form can induce apoptosis in mammalian cancer cells [24] like PS produced by *B. thuringiensis* A1519, which induces the mitochondrial apoptosis pathway in Jurkat cells via caspase-3 and -9 cleavage followed by the release of cytochrome C [25]. In this study, we showed through cytotoxicity assays that the mutant 3-35 had a more remarkable effect on cancer cell lines, and the amount of cleaved caspase-3 and PARP and the production of γ H2AX were reported for the first time. We also presented the effect of this mutant in early and late apoptosis with respect to recombinant PS2Aa1; these results suggest that the point variation G257V on Loop 1 can alter the behavior of the protein measured by its differentiated cytotoxicity and apoptosis induction when compared with the native PS2Aa1.

The molecular docking and dynamics simulations showed that it is likely that a stable interaction between domain I of PS2Aa1 and APN receptor could take place. Moreover, the mutation of mutant 3-35 was performed in the region of amino acids involved in interactions during the molecular dynamics simulations (Figure 7). Residue

256 was present in all three replicates, with the smallest interaction distance between its center of mass and the APN contact surface (Figure 7). The experimental results showed that its mutation reduced the interaction and cytotoxicity, so the G in position 256 seems relevant for the cytotoxic effects of PS2Aa1. In contrast, the mutation of position 257, which was involved in two replicates of molecular dynamic simulation, led to an improved interaction and cytotoxicity, i.e., the change of glycine for valine improved the cytotoxic activity of the designed mutant 3-35 by creating a more nonpolar amino acid, suggesting that it feasibly conferred more stability on the protein. This mutant outperformed native Ps2Aa1 and 4R2 in terms of cytotoxicity in all three tested cell lines: SW480, SW620, and CaCo-2.

Figure 30. PS2Aa1–APN interaction. Relevant residues for interaction with APN are analyzed in Figure 6. Distances were computed between the center of mass of the relevant residues of PS2Aa1 and the closest residue from APN.



Finally, the use of site-directed mutagenesis might be helpful to obtain a clearer understanding of how parasporin 2 works and to shed some light on understanding the action mechanism while generating proteins with enhanced activity like variant 3-35. This study reveals interesting features of domain I and highlights the relevance of residues 256

and 257 in the interaction with possible receptors that might be interacting with PS2Aa1, such as APN, and membrane-anchored receptors or GPI-anchored proteins [12].

4.5 Materials and Methods

4.5.1 Bacterial Strains and Culture Conditions

E. coli strain DE3BL21 harboring the construct pET30a + PS2Aa1 and *Bacillus thuringiensis* (*Bt*) BMB171 were cultured in Luria Bertani (LB) broth incubated at 37 °C with constant agitation for 24 h.

4.5.2 Parasporin Site-Directed Mutagenesis

Mutagenesis assays were carried out using the Gene-Art Site-Directed Mutagenesis Plus kit according to the manufacturer's instructions and four sets of designed primers (Table 7). Reaction and amplification conditions were developed according to the kit specifications.

Each of the mutation reactions was directly transformed into chemically competent TOP10F and DH5 α T1 cells, 70 μ L of the transformed cells was then inoculated on plates with LB + kanamycin agar (25 μ g/mL) + X-gal + Isopropyl β -D-1-thiogalactopyranoside (IPTG) and incubated for 18 h at 37 °C, and white/blue cell screening was performed.

Table 18. Primers designed for site-directed mutagenesis of PS2Aa1.

Primer Id.	Sequence
-Pet100Ps2a_994_FW	5'-TTC CCA AAA GAG TAG <u>NGC</u> CAG GTG GGC ATT A-3'
-Pet100Ps2a_994_RV	5'-TAA TGC CCA CCT GGC <u>NCT</u> ACT CTT TTG GGA A-3'
-Pet100Ps2a_997_FW	5'-CCA AAA GAG TAG GGC <u>NAG</u> GTG GGC ATT ATT T-3'
-Pet100Ps2a_997_RV	5'-AAA TAA TGC CCA CCT <u>NGC</u> CCT ACT CTT TTG G-3'
-Pet100Ps2a_1000_FW	5'-AAA GAG TAG GGC CAG <u>NTG</u> GGC ATT ATT TTT G-3'
-Pet100Ps2a_1000_RV	5'-CAA AAA TAA TGC CCA <u>NCT</u> GGC CCT ACT CTT T-3'
-Pet100Ps2a_1003_FW	5'-GAG TAG GGC CAG GTG <u>NGC</u> ATT ATT GGT T-3'
-Pet100Ps2a_1003_RV	5'-AAC CAA AAA TAA TGC <u>NCA</u> CCT GGC CCT ACT C-3'

4.5.3 Library Verification

The positive clones (blue colonies) were cultured in LB plates with kanamycin (25 µg/mL). A single colony was selected and cultured in 5 mL LB broth at 37 °C overnight with agitation at 200 rpm. The plasmid pET-30PS2-Variant was isolated using the Wizard Plus SV Minipreps DNA purification system (Promega®) according to the manufacturer's instructions. Sanger sequencing of the desired fragments using universal T7 primers was performed by Macrogen® (Seoul- Korea). The ~1000 bp contig was assembled using DNA Baser version 5.15 (Sequence assembly software) and used in BLASTn search (National Center for Biotechnology Information; www.ncbi.nlm.nih.gov) URL (accessed on 19- September-2022). The protein sequence was deduced using the Translate tool available at Expasy (<https://web.expasy.org/translate/>) URL (accessed on 20- September-2022) followed by multiple alignment sequence analysis of the variants in comparison with native PS2Aa1 using Bio-Edit Software [26]. Finally, variants with non-silent mutations were transformed into *Bt* BMB171 via electroporation using two consecutive electric pulses of 1.5 kV during 4.5 ms. Following this procedure, four PS2Aa1 mutant libraries were created.

4.5.4 Preparation of Activated Parasporin Proteins

Bt BMB171 variants were cultivated in LB broth and incubated for 5 days at 30 °C. The cells were then harvested by centrifugation at 10,000 rpm for 10 min; the pellet containing the precipitated parasporin proteins was solubilized in 5 mL of solubilization buffer (56 mM Na₂CO₃ (pH: 11.4) and 11 mM of dithiothreitol (DTT) (pH: 11.4)) for 2 h at 37 °C. Insoluble material was removed by centrifugation at 10,000 rpm for 10 min and the supernatant was passed through a 0.22 µm membrane filter. The filtrate (70 mL) pH was adjusted to 8 using 1 M Tris-HCl (pH 8).

The solubilized proteins were digested using proteinase K (final concentration of 185 µg/mL) for 1 h at 37 °C. Phenylmethylsulfonyl fluoride (PMSF) was added (final concentration 1 mM) to stop proteolytic processing. To confirm the presence of the parasporin proteins, SDS-PAGE analysis was performed as previously described [19].

The protein concentration was determined using the Bio-Rad Protein Assay (Bio-Rad Laboratories, Mississauga, ON, Canada).

4.5.5 Colon Cancer Cell Lines

Colon cancer cell lines were obtained from the American Type Culture Collection (ATCC). Lines SW-480 and CaCo-2 were cultured in Dulbecco's modified Eagle's medium (DMEM) with 25 mM glucose and 2 mM L-glutamine, supplemented with 10% fetal bovine serum (FBS), 10,000 µg/mL penicillin and streptomycin, and 1% non-essential amino acids; SW620 and NCM460 were cultured in RPMI supplemented with 10% FBS. The cultures were incubated in a humidified incubator at 37 °C under a 5% CO₂ atmosphere.

4.5.6 Cytotoxicity Assays of PS2Aa1 Mutants in Colon Cancer Cells

To characterize the anti-proliferative activity of the toxins PS2Aa1 and mutants, concentrations ranging from 0.25 to 5 µg/mL of the activated protein were prepared. The cells were incubated with parasporin for 72 h, and anticancer activity was assessed on the basis of cell viability following incubation with alamar blue (BioRad) for 5 h at 37 °C under a 5% CO₂ atmosphere. Emission at 560 nm and excitation at 590 nm were measured using a CLARIOstar reader. IC₅₀ concentrations were calculated from these data.

4.5.7 APN Detection and Blocking Assay

Western blot detection of APN was carried out using antibody CD13/APN (Cell Signaling Technology®) and GAPDH was used as a loading control. The proteins extracted from HL60 and MCF-7 were used as the positive and negative control, respectively. The blocking assay was performed as reported by Periyasamy et al. 2016 [7]. Briefly, CaCo-2 and SW480 cells were used, but, because of the presence of APN receptors, the concentration of the APN blocker Dinitroflavone (Santa Cruz Biotechnology, Inc., Dallas, TX, USA) was diluted from 5 to 50 µM and added to the cells, with triplication

of samples. This was followed by incubation for 72 h at 37 °C under a 5% CO₂ atmosphere using 3 µg of parasporin. The results of metabolic activity were analyzed using the alamar blue assay, as previously described [7].

4.5.8 Molecular Docking and Molecular Dynamics Analysis

Molecular docking analysis was performed to determine possible interactions between PS2Aa1 and the APN receptor. The 3D structures of PS2Aa1 and APN were downloaded from the Protein Data Bank with PDB ID 2ZTB and 6ATK, respectively. The simulations were performed using the protein–protein global docking protocol of Rosetta [27] with flags `construct-5000`, `-spin`, `-randomize1`, and `-randomize2`, and simulations were run in the software version 3.9. Later, the Interface Analyzer protocol of Rosetta [28] was used to analyze the interaction between PS2Aa1 and APN. Next, the top 10 models were visually inspected for the selection of a suitable model in which the amino acids corresponding to domain I of PS2Aa1 were interacting with a valid region of APN. Subsequently, the selected model was used to perform molecular dynamics (MD) simulations, in triplicate, for PS2Aa1–APN complexes. The MD simulation protocol included solvation with TIP3P water molecules, and Na⁺ and Cl⁻ ions were added to ensure the neutrality of the system at an ion concentration of 150 mM. The Amber ff19SB force field for proteins was implemented for all systems.

The system was first minimized and equilibrated using Amber18 software. For the parasporin–APN complexes, stepped minimization, heating, and balancing were performed. Complexes were first minimized for 5000 (steepest descent) and 10,000 (conjugate gradient) followed by heating for 1 ns and then in an NVT to 300 K. For all simulations, an 8 Å cutoff was used for unbounded Coulombic and Lennard–Jones interactions and for periodic boundary conditions with a particle mesh Ewald treatment of long-range Coulombic interactions. A 2 fs time-step was employed by the SHAKE algorithm and the production steps were 100 ns for both systems.

4.5.9 Statistical Analysis

Type 1 ANOVA and Tukey's test was performed using Graphad Prism 8. Statistical significance was indicated as * $p \leq 0.05$, ** $p \leq 0.01$, and *** $p \leq 0.001$, with an IC of 95%.

4.6 References

1. Laliani, G.; Ghasemian Sorboni, S.; Lari, R.; Yaghoubi, A.; Soleimanpour, S.; Khazaei, M.; Hasanian, S.M.; Avan, A. Bacteria and cancer: Different sides of the same coin. *Life Sci.* 2020, *246*, 11739. <https://doi.org/10.1016/j.lfs.2020.117398>.
2. Desbats, M.A.; Giacomini, I.; Prayer-Galetti, T.; Montopoli, M. Metabolic Plasticity in Chemotherapy Resistance. *Front. Oncol.* 2020, *10*, 281. <https://doi.org/10.3389/FONC.2020.00281>.
3. Shriwas, O.; Mohapatra, P.; Mohanty, S.; Dash, R. The Impact of m6A RNA Modification in Therapy Resistance of Cancer: Implication in Chemotherapy, Radiotherapy, and Immunotherapy. *Front. Oncol.* 2021, *10*, 3220. <https://doi.org/10.3389/FONC.2020.612337>.
4. Baidara, P.; Mandal, S.M. Bacteria and bacterial anticancer agents as a promising alternative for cancer therapeutics. *Biochimie* 2020, *177*, 164–189. <https://doi.org/10.1016/j.biochi.2020.07.020>.
5. Mizuki, E.; Park, Y.S.; Saitoh, H.; Yamashita, S.; Akao, T.; Higuchi, K.; Ohba, M. Parasporin, a Human Leukemic Cell-Recognizing Parasporal Protein of *Bacillus thuringiensis*. *Clin. Vaccine Immunol.* 2000, *7*, 625–634. <https://doi.org/10.1128/CDLI.7.4.625-634.2000>.
6. Cruz, J.; Suárez-Barrera, M.O.; Rondón-Villarreal, P.; Olarte-Díaz, A.; Guzmán, F.; Visser, L.; Rueda-Forero, N.J. Computational study, synthesis and evaluation of active peptides derived from Parasporin-2 and spike protein from Alphacoronavirus against colorectal cancer cells. *Biosci. Rep.* 2021, *41*, 1964. <https://doi.org/10.1042/BSR20211964>.
7. Periyasamy, A.; Kkani, P.; Chandrasekaran, B.; Ponnusamy, S.; Viswanathan, S.; Selvanayagam, P.; Rajaiah, S. Screening and characterization of a non-insecticidal *Bacillus thuringiensis* strain producing parasporal protein with selective toxicity against human colon cancer cell lines. *Ann. Microbiol.* 2016, *66*, 1167–1178. <https://doi.org/10.1007/s13213-016-1204-8>.

8. Abe, Y.; Shimada, H.; Kitada, S. Raft-targeting and oligomerization of parasporin-2, a *Bacillus thuringiensis* crystal protein with anti-tumour activity. *J. Biochem.* 2008, *143*, 269–275. <https://doi.org/10.1093/jb/mvm220>.
9. Ito, A.; Sasaguri, Y.; Kitada, S.; Kusaka, Y.; Kuwano, K.; Masutomi, K.; Mizuki, E.; Akao, T.; Ohba, M. A *Bacillus thuringiensis* crystal protein with selective cytotoxic action to human cells. *J. Biol. Chem.* 2004, *279*, 21282–21286. <https://doi.org/10.1074/jbc.M401881200>.
10. Mendoza-Almanza, G.; Esparza-Ibarra, E.L.; Ayala-Luján, J.L.; Mercado-Reyes, M.; Godina-González, S.; Hernández-Barrales, M.; Olmos-Soto, J. The cytotoxic spectrum of *Bacillus thuringiensis* toxins: From insects to human cancer cells. *Toxins* 2020, *12*, 1–22. <https://doi.org/10.3390/toxins12050301>.
11. Akiba, T.; Okumura, S. Parasporins 1 and 2: Their structure and activity. *J. Invertebr. Pathol.* 2017, *142*, 1–6. <https://doi.org/10.1016/j.jip.2016.10.005>.
12. Abe, Y.; Inoue, H.; Ashida, H.; Maeda, Y.; Kinoshita, T.; Kitada, S. Glycan region of GPI anchored-protein is required for cytotoxic oligomerization of an anticancer parasporin-2, Cry46Aa1 protein, from *Bacillus thuringiensis* strain A1547. *J. Invertebr. Pathol.* 2017, *142*, 71–81. <https://doi.org/10.1016/j.jip.2016.11.008>.
13. Soberón, M.; Portugal, L.; Garcia-Gómez, B.I.; Sánchez, J.; Onofre, J.; Gómez, I.; Pacheco, S.; Bravo, A. Cell lines as models for the study of Cry toxins from *Bacillus thuringiensis*. *Insect Biochem. Mol. Biol.* 2018, *93*, 66–78. <https://doi.org/10.1016/j.ibmb.2017.12.008>.
14. Al-Baidani, S.J.; Moyet Al-Faisal, A.H.; Ali, N.A. Study of some cytogenetic effects of Aerolysin Produced by *Aeromonas hydrophila* on normal and tumor cells in vitro. *J. Biotechnol. Res. Cent.* 2010, *4*, 11–16. <https://doi.org/10.24126/jobrc.2010.4.1.83>.
15. Ohba, M.; Mizuki, E.; Uemori, A. Parasporin, a new anticancer protein group from *Bacillus thuringiensis*. *Anticancer Res.* 2009, *29*, 427–433.
16. Katayama, H.; Kusaka, Y.; Yokota, H.; Akao, T.; Kojima, M.; Nakamura, O.; Mekada, E.; Mizuki, E. Parasporin-1, a novel cytotoxic protein from *Bacillus thuringiensis*, induces Ca²⁺ influx and a sustained elevation of the cytoplasmic Ca²⁺ concentration in toxin-sensitive cells. *J. Biol. Chem.* 2007, *282*, 7742–7752.
17. Borin, D.B.; Castrejón-Arroyo, K.; Cruz-Nolasco, A.; Peña-Rico, M.; Rorato, M.S.; Santos, R.C.V.; de Baco, L.S.; Pérez-Picaso, L.; Camacho, L.; Navarro-Mtz, A.K. Parasporin a13-2 of *Bacillus thuringiensis* isolates from the papaloapan region (Mexico) induce a cytotoxic effect by late apoptosis against breast cancer cells. *Toxins* 2021, *13*, 476. <https://doi.org/10.3390/toxins13070476>.
18. Akiba, T.; Abe, Y.; Kitada, S.; Kusaka, Y.; Ito, A.; Ichimatsu, T.; Katayama, H.; Akao, T.; Higuchi, K.; Mizuki, E.; et al. Crystal structure of the parasporin-2 *Bacillus thuringiensis* toxin that recognizes cancer cells. *J. Mol. Biol.* 2009, *386*, 121–133.

19. Brasseur, K.; Auger, P.; Asselin, E.; Parent, S.; Cote, J.C.; Sirois, M. Parasporin-2 from a New *Bacillus thuringiensis* 4R2 Strain Induces Caspases Activation and Apoptosis in Human Cancer Cells. *PLoS ONE* 2015, *10*, e0135106. <https://doi.org/10.1371/journal.pone.0135106>.
20. Inagaki, Y.; Tang, W.; Zhang, L.; Du, G.; Xu, W.; Kokudo, N. Invasion of Hepatocellular Carcinoma Cells As Well As Angiogenesis. *Biosci. Trends* 2010, *4*, 56–60.
21. Liao, C.; Jin, M.; Cheng, Y.; Yang, Y.; Soberón, M.; Bravo, A.; Liu, K.; Xiao, Y. *Bacillus thuringiensis* Cry1Ac Protoxin and Activated Toxin Exert Differential Toxicity Due to a Synergistic Interplay of Cadherin with ABCC Transporters in the Cotton Bollworm. *Appl. Environ. Microbiol.* 2022, *88*, e02505-21. <https://doi.org/10.1128/aem.02505-21>.
22. Karlova, R.; Weemen-Hendriks, M.; Naimov, S.; Ceron, J.; Dukiandjiev, S.; de Maagd, R.A. *Bacillus thuringiensis* delta-endotoxin Cry1Ac domain III enhances activity against *Heliothis virescens* in some, but not all Cry1-Cry1Ac hybrids. *J. Invertebr. Pathol.* 2005, *88*, 169–172.
23. Okumura, S.; Ohba, M.; Mizuki, E.; Crickmore, N.; Côté, J.-C.; Nagamatsu, Y.; Kitada, S.; Sakai, H.; Harata, K.; Shin, T. *Parasporin Classification and Nomenclature*; Publisher: location, 2010.
24. Melo, A.L.D.A.; Soccol, V.T.; Soccol, C.R. *Bacillus thuringiensis*: Mechanism of action, resistance, and new applications: A review. *Crit. Rev. Biotechnol.* 2016, *36*, 317–326.
25. Kitada, S.; Abe, Y.; Maeda, T.; Shimada, H. Parasporin-2 requires GPI-anchored proteins for the efficient cytotoxic action to human hepatoma cells. *Toxicology* 2009, *264*, 80–88. <https://doi.org/10.1016/J.TOX.2009.07.016>.
26. Hall, T.A. BIOEDIT: A user-friendly biological sequence alignment editor and analysis program for Windows 95/98/ NT. *Nucleic Acids Symp. Ser.* 1999, *41*, 95–98.
27. Ehrlich, L.P.; Wade, R.C. Protein-protein docking. *Rev. Comput. Chem.* 2001, *17*, 61–97. <https://doi.org/10.1002/0471224413.ch2>.
28. Lewis, S.; Stranges, P.B.; Jared, A.-B. InterfaceAnalyzer. Available online: https://www.rosettacommons.org/docs/latest/application_documentation/analysis/interface-analyzer (accessed on 15 October 2022).

4.7 Supplementary information

Figure S1: Cytocidal activities of variants of Parasporin 2 (PS2Aa1) obtained with site directed mutagenesis to CaCo2 cell lines. the toxin activated with proteinase K was added (final concentrations, 0.2 μ g/mL to 5 μ g/mL).

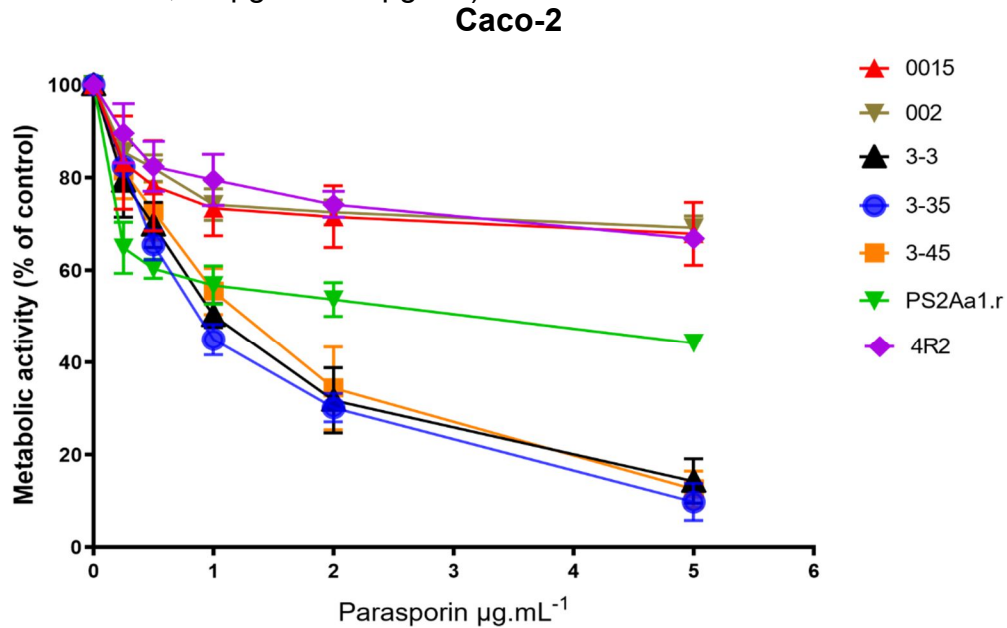


Figure S2: Cytocidal activities of variants of Parasporin 2 (PS2Aa1) obtained with site directed mutagenesis to SW620 cell lines. the toxin activated with proteinase K was added (final concentrations, 0.2 μ g/mL to 5 μ g/mL).

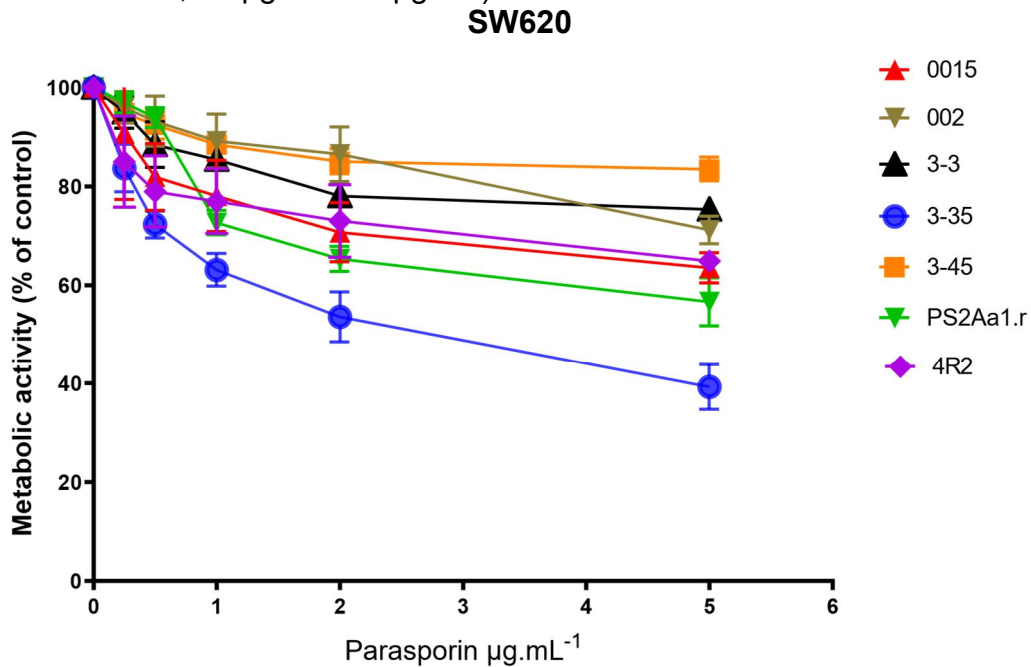


Figure S3: Cytocidal activities of variants of Parasporin 2 (PS2Aa1) obtained with site directed mutagenesis to SW480 cell lines. the toxin activated with proteinase K was added (final concentrations, 0.2 μ g/mL to 5 μ g/mL).

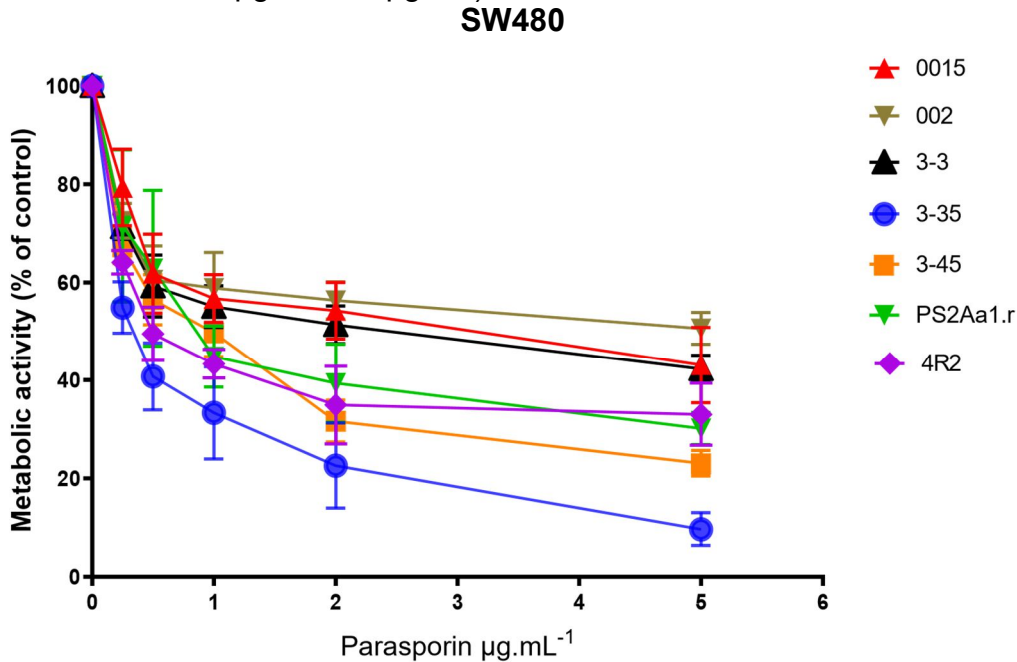
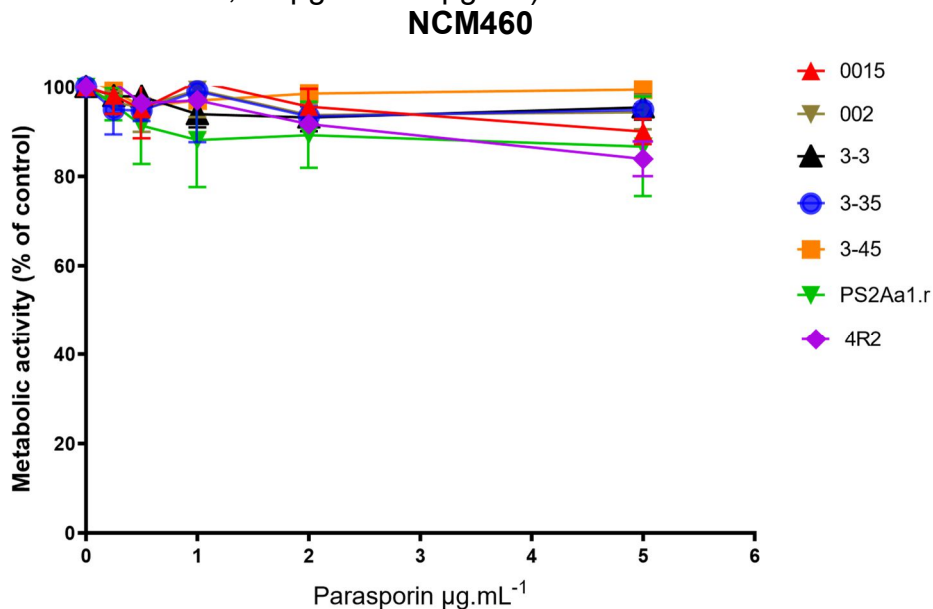


Figure S4: Cytocidal activities of variants of Parasporin 2 (PS2Aa1) obtained with site directed mutagenesis to NCM460 cell lines. the toxin activated with proteinase K was added (final concentrations, 0.2 μ g/mL to 5 μ g/mL).



5. Toxic Determination of Cry11 Mutated Proteins Obtained Using Rational Design and Its Computational Analysis

Miguel O. Suárez-Barrera
Diego F. Herrera-Pineda
Paola Rondón-Villarreal
Efraín Hernando Pinzón-Reyes
Rodrigo Ochoa
Lydia Visser
Nohora Juliana Rueda-Forero

International Journal of Molecular Sciences

2023, 24, 9079. <https://doi.org/10.3390/ijms24109079>

Author Contributions: Conceptualization, M.O.S.-B., P.R.-V., E.H.P.-R., R.O., L.V. and N.J.R.-F.; methodology, M.O.S.-B., P.R.-V., E.H.P.-R., R.O., L.V. and N.J.R.-F.; software, P.R.-V., E.H.P.-R. and R.O.; validation, M.O.S.-B., P.R.-V., E.H.P.-R., R.O., D.F.H.-P. and N.J.R.-F.; formal analysis, M.O.S.-B., P.R.-V., E.H.P.-R. and L.V.; investigation, M.O.S.-B., D.F.H.-P., P.R.-V., E.H.P.-R., R.O. and L.V.; resources, N.J.R.-F.; writing—original draft preparation, M.O.S.-B., D.F.H.-P., P.R.-V., E.H.P.-R., R. O., L.V. and N.J.R.-F.; writing—review and editing, M.O.S.-B. and N.J.R.-F.; project administration, N.J.R.-F.; and funding acquisition, N.J.R.-F. All authors have read and agreed to the published version of the manuscript. **Funding:** The work has been funded by MINCIENCIAS, MINEDUCACIÓN, MINCIT, and ICETEX, through the Program Ecosistema Científico Cod. FP44842-211-2018 Project number, 58668. Universidad de Talca, Chile.

This chapter is linked to the aim:- To produce novel parasporal proteins with enhanced activity against colon cancer cell lines and determine the cytotoxic activity of selected mutant proteins of *Bacillus thuringiensis* based on their binding affinity to membrane receptors by computational approaches.

5.1 Abstract

Cry11 proteins are toxic to *Aedes aegypti*, the vector of dengue, chikungunya, and Zika viruses. Cry11Aa and Cry11Bb are protoxins, which when activated present their active-toxin form in two fragments between 30 and 35 kDa respectively. Previous studies conducted with Cry11Aa and Cry11Bb genes using DNA shuffling generated variant 8, which presented a deletion in the first 73 amino acids and one at position 572 and 9 substitutions including L553F and L556W. In this study, variant 8 mutants were constructed using site-directed mutagenesis, resulting in conversion of phenylalanine (F) and tryptophan (W) to leucine (L) at positions 553 and 556, respectively, producing the mutants 8F553L, 8W556L, and 8F553L/8W556L. Additionally, two mutants, A92D and C157R, derived from Cry11Bb were also generated. The proteins were expressed in the non-crystal strain BMB171 of *Bacillus thuringiensis* and subjected to median-lethal concentration (LC_{50}) tests on first-instar larvae of *A. aegypti*. LC_{50} analysis showed that the 8F553L, 8W556L, 8F553L/8W556L, and C157R variants lost their toxic activity (>500 ng·mL⁻¹), whereas the A92D protein presented a loss of toxicity of 11.4 times that of Cry11Bb. Cytotoxicity assays performed using variant 8, 8W556L and the controls Cry11Aa, Cry11Bb, and Cry-negative BMB171 on the colorectal cancer cell line SW480 reported 30–50% of cellular viability except for BMB171. Molecular dynamic simulations performed to identify whether the mutations at positions 553 and 556 were related to the stability and rigidity of the functional tertiary structure (domain III) of the Cry11Aa protein and variant 8 showed the importance of these mutations in specific regions for the toxic activity of Cry11 against *A. aegypti*. This generates pertinent knowledge for the design of Cry11 proteins and their biotechnological applications in vector-borne disease control and cancer cell lines.

Keywords: *Bacillus thuringiensis*; Cry11; site-directed mutagenesis; *Aedes aegypti*; cancer cell lines

5.2 Introduction

The use of insecticidal proteins based on *Bacillus thuringiensis* (*Bt*) formulations is a promising approach to controlling different disease-transmitting vectors. Additionally, these toxins are ecosystem-friendly, offering an efficient and equally effective alternative to chemical treatments, and they do not present a risk to other living organisms, including humans. However, the resistance acquired by insects against Cry toxins is becoming a challenge [1]. Hence, current research has been focused on the development of more robust and stable Cry toxins to better control vector-borne diseases.

Cry11 proteins have three active domains that act against vector-borne diseases in the Dipteran order [2]. The best-characterized member of this family is Cry11Aa, a protein of approximately 70 kDa produced by *Bt* subsp. *israelensis* (*Bti*), in which proteolytic activation removes approximately 28 amino acids from the N-terminus. The resulting protein is cleaved into two fragments of 32 and 34 kDa. These fragments remain associated and exhibit insecticidal activity against *A. aegypti* [3,4]. Cry11Bb, produced by *Bt* subsp. *Medellin* (*Btmed*) [2] has the distinction of having toxic effects on mosquito genera such as *Culex* and *Anopheles*. This toxin weighs 94 kDa, and its toxic effects result from solubilization and proteolytic processing into fragments of 30 and 35 kDa in the midguts of insects [5].

Protein engineering has emerged as a tool for developing modified Cry proteins with novel activities. Directed evolution methodologies focus on amino acid substitution and the insertion or elimination of DNA sequences [6]. For the improvement of Cry toxins, strategies related to rational approaches such as protein engineering [7], domain exchanges [8], use of synthetic peptides involved in the enhancement of protein stability [9], and site-directed mutagenesis [10], as well as non-rational approaches such as DNA shuffling, error-prone PCR, and microarrays with phage libraries have also been used [7]. These approaches, in addition to obtaining improved variants, have allowed the identification of insect-dependent toxin activation mechanisms, stability, oligomerization, and the modulation of interactions with membrane receptors in the epithelial cells of the midgut of insects [11]. Simultaneously, mutagenesis studies have enabled the development and/or conditioning of new molecular biology techniques, providing

alternatives to overcome the resistance acquired by insects and the development of green biotechnology that could reduce the negative environmental impact [12].

It has been reported that small changes in amino acid residues of the three-domain Cry proteins provided an improvement in their toxicity or target changes [7]; for example, the change of a residue (V171C) in the δ -Cry1Ab endotoxin showed a loss of toxic activity against *Manduca sexta*, an insect susceptible to this toxin, while increasing its toxicity (25-fold) against *Lymandria dispar*, since this modification probably contributed to greater protein stability and a better binding rate to the midgut receptors [13]. Additionally, some studies have reported genetic improvements in Cry11 using DNA-shuffling techniques or site-directed mutagenesis [7]. Our group is focused on the directed evolution of Cry11 and Parasporin proteins through DNA shuffling [10], thermodynamics and secondary structure formation analysis [14], and the development of an *in silico/in vitro* workflow [15]. Previous reports highlighted that variant 8 obtained via DNA shuffling from Cry11Aa and Cry11Bb exhibited up to 3.78- and 6.09-fold higher toxicity to *A. aegypti* than Cry11Aa and Cry11Bb, respectively [10]. Mutations in variant 8 are responsible for the increase in toxicity; however, it is important to assess the role of each mutation to understand the mechanism of action of Cry11. Simultaneously, Cry proteins have been described as possible adjuvants because of their resistance and stability in highly alkaline environments during the development of vaccines [16], making these bioproducts relevant not only in environmental applications but also in the biomedical field. Our group is currently focused on generating new proteins with anticancer activity, considering the possibilities with the mutations obtained with variant 8 and subsequent proteins. We also assessed whether mutations in these proteins influence the anticancer activities. Therefore, molecular analysis and determination of toxicity were performed using *A. aegypti* larvae with the colorectal cancer cell line SW480 as targets. Mutants 8F553L, 8W556L, and 8F553L/8W556L were used to analyze mutations in variant 8 at these positions. Furthermore, the A92D and C157R variants were used to analyze mutations at residues 92 and 157 in the Cry11Bb toxin. Finally, a computational analysis of the possible implications of the mutations at positions 553 and 556 in the three-dimensional structure of the Cry11Bb toxin was performed.

The results presented here elucidate the role of induced mutations in proteins with insecticidal and anticancer activities. This work provides new insights into the structure–function relationship of the parasporal proteins of Bt and their applications as insecticidal toxins and anticancer proteins.

5.3 Results

5.3.1 Variants Were Successfully Obtained from Variant 8 and Cry11Aa

The designed primers were effective in obtaining each variant. The constructs pSV2-L553F, pSV2-L556W, and pSV2-L553F/L556W were verified using a restriction enzyme assay with *HindIII* and *SacI*, and were observed in an agarose gel; a double band was obtained, of which one of 5 kb corresponds to the size of the plasmid and the other one of approximately 2 kb corresponds to the size of the Cry gene (Figure S1). Simultaneously, the constructs pSV2-A92D and pSV2-C157R showed a linearized vector pSV2 digested with *HindIII* and *SacI* (5 kb) and bands of the inserts between 2 and 3 kb. Each construct was used to transform the crystalline strain BMB171; the transformation efficiency was established at $\approx 10^9$ CFU· μg^{-1} of the DNA (construct). Sequencing of these constructs revealed that the individual mutants, L553F and L556W, were successfully reversed from cytosine to adenine and from guanine to thymidine, respectively.

5.3.2 Cry 11 Proteins and Variants Are Produced in Bt BMB171

The viable cell count for each mutant and control was $> 1 \times 10^9$ CFU·mL⁻¹. Dry weight estimates ranged from 0.023 to 0.061 g·mL⁻¹. The protein concentration obtained was between 12.32 and 40.74 mg·mL⁻¹ as measured using the Bradford method.

The electrophoretic protein pattern was verified using 10% SDS-PAGE. The samples stained with Coomassie R-250 blue showed a protein pattern with a recognizable band close to 70 kDa for the L553F, L556W, L553F/L556W, and Cry11Aa proteins, whereas for the mutants A92D, C157R, and Cry11Bb, the observed band was close to 90 kDa. For the specific case of BMB171, the banding of the Cry11 protein was not shown.

After activation with proteinase K, a double band was observed for each of the mutant and native proteins, with molecular weights of 30 and 35 kDa, confirming the activation of the protoxin to the toxin (Figure S2).

5.3.3 The Residues Phenylalanine (553) and Tryptophan (556) Are Relevant to the Insecticidal Activity of the Variant 8 Protein

Variant 8, obtained via DNA shuffling, presented insecticidal activity approximately five times higher than that of the parental genes Cry11Aa and Cry11Bb. By reversing the mutations in residues 553, 556, and 553/556, no toxic activity was detected with an LC_{50} of up to $500 \text{ ng}\cdot\text{mL}^{-1}$ (Table 1), indicating the importance of these residues (F and W) for the toxicity of this protein. Similarly, no toxic activity was detected for C157R; the mutant A92D showed a decrease in the activity of 11.44 compared with Cry11Bb.

Table 19. LC_{50} for each of the variants obtained in this study.

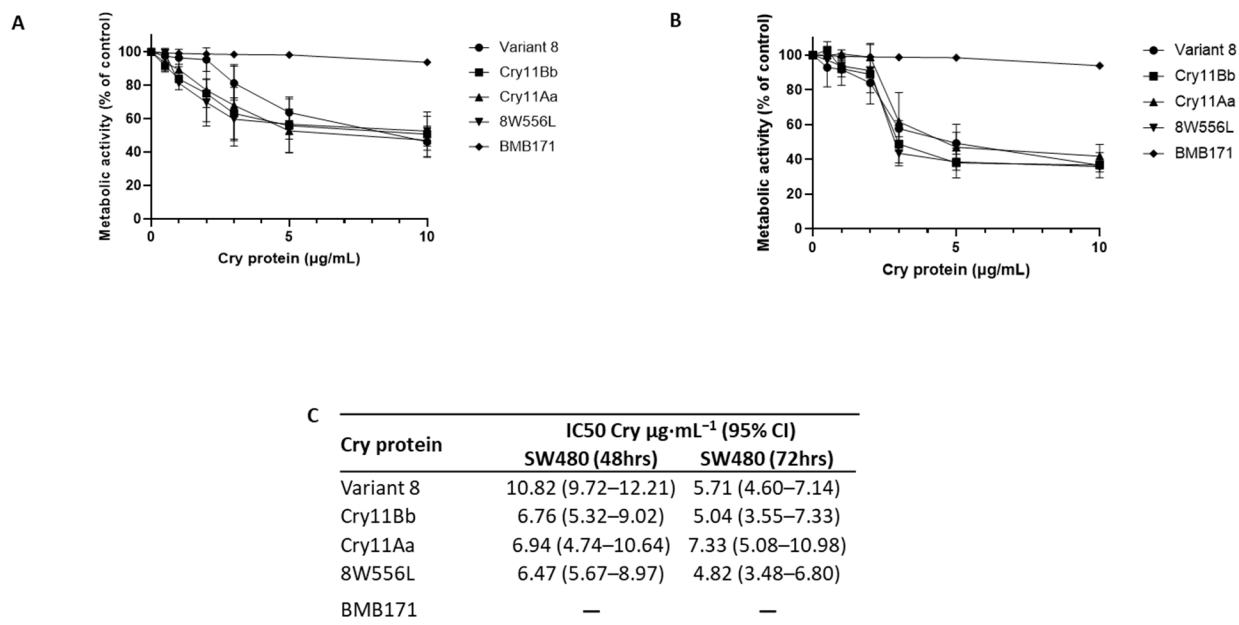
Origin of <i>Bt</i> Protein	Strain	LC_{50} ($\text{ng}\cdot\text{mL}^{-1}$) (95% CI) <i>Aedes aegypti</i>
Variant8 Derivatives	8F553L	>500
	8W556L	>500
	8F553L/8W556L	>500
Cry11Bb Derivatives	C157R	>500
	A92D	313.71 (158.73–317.46)
Controls	Cry11Aa	39.20 (20.04–45.12)
	Cry11Bb	27.40 (15.64–31.47)
	Variant 8	8.22 (2.01–9.33)

5.3.4 Cry Proteins Have an Antiproliferative Effect on the SW480 Cell Line

We used strain BMB171 as a Cry-expressing negative control, which showed no detectable or slight activity against SW480 cells. The activities of all Cry proteins, including the controls Cry11Aa and Cry11Bb, were similar, measured at $10 \mu\text{g}\cdot\text{mL}^{-1}$ for 48 and 72 h, with metabolic activities of 50% and 30%, respectively (Figure 1A,B). Furthermore, the calculated IC_{50} showed no differences between the controls Cry11Aa and Cry11Bb, and 8W556L, with an IC_{50} of $6.5\text{--}7.0 \mu\text{g}\cdot\text{mL}^{-1}$. Surprisingly, 8W556L was 1.6 times more active

for this cell line than Variant 8. This suggests that residue 556 might be relevant for anticancer activity.

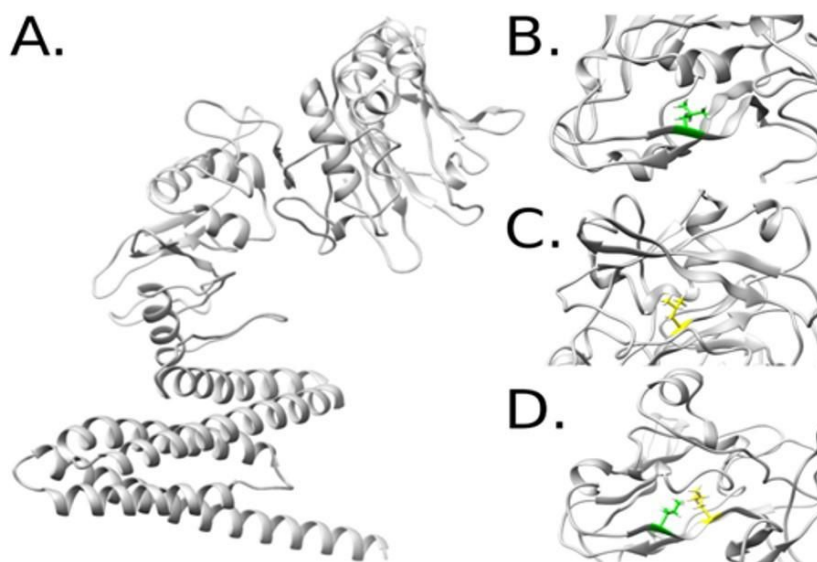
Figure 31. Cytotoxicity activity of the Cry proteins on the colorectal cancer cell line SW480 at 48 h (A) and 72 h (B). The measurements were determined with Alamar Blue staining. The IC₅₀ was calculated with different concentrations of Cry proteins (0.5–10 $\mu\text{g}\cdot\text{mL}^{-1}$) at 48 and 72 h (C). No IC₅₀ was calculated for BMB171.



5.3.5 Modeled Structures by De Novo Methodology

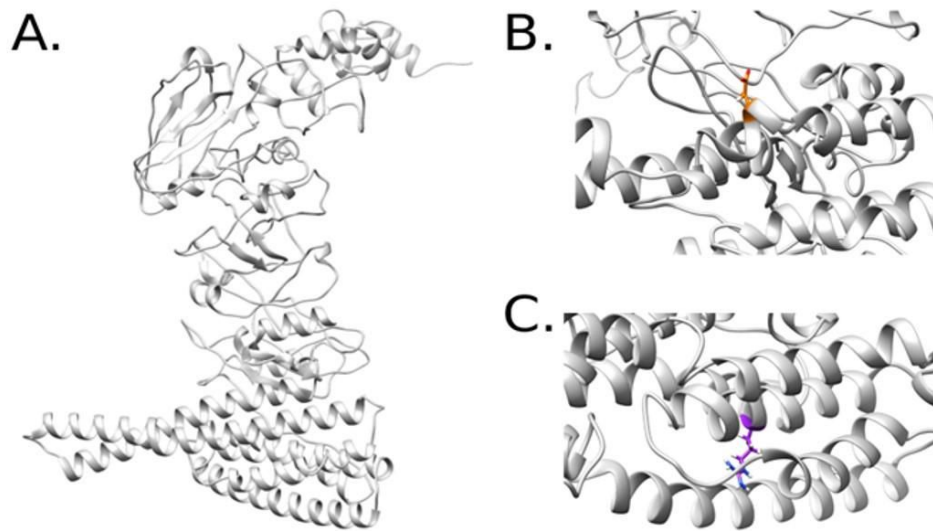
Owing to the lack of available homologous structures for the designed variant 8, de novo methodology was used to obtain energetically favorable models for further analysis. The highest identity percentage for Cry11Bb was 25% for related structures reported in the Protein Data Bank (PDB) [17] and similar results were obtained for the variant 8 protein sequence. Following de novo contact-based modeling, a structural view of variant 8 and the mutants 8F553L, 8W556L, and 8F553L/8W556L is shown in Figure 2.

Figure 32. Structural model of variant 8 (A). Representations of the variants 8F553L (B), 8W556L (C), and the combination of 8F553L and 8W556L (D) after running MD simulations of the mutated complexes.



The structure of variant 8 was modeled based on a sequence of 571 amino acids, which were initially subjected to other modeling methods with unsuccessful results. The selected mutations were located in a domain with non-representative matches to other proteins with available structures. However, this region still folds into a representative backbone that confers stability and is crucial for subsequent interactions with other molecular entities. A similar analysis was performed after modeling de novo Cry11Bb and sampling its variants for convergence purposes (Figure 3).

Figure 33. Structural model of Cry11Bb (A). Representations of the variants A92D (B) and C157R (C) after running MD simulations of the mutated complexes.



For this isoform, the variants are located in a region composed of multiple helices but pointing in opposite directions from a group of helices (Figure 3B,C). This set of models was more challenging to predict owing to the larger sequence size (750 amino acids). However, with the proposed method and energy evaluations, we conclude that the models are suitable for additional computational analysis.

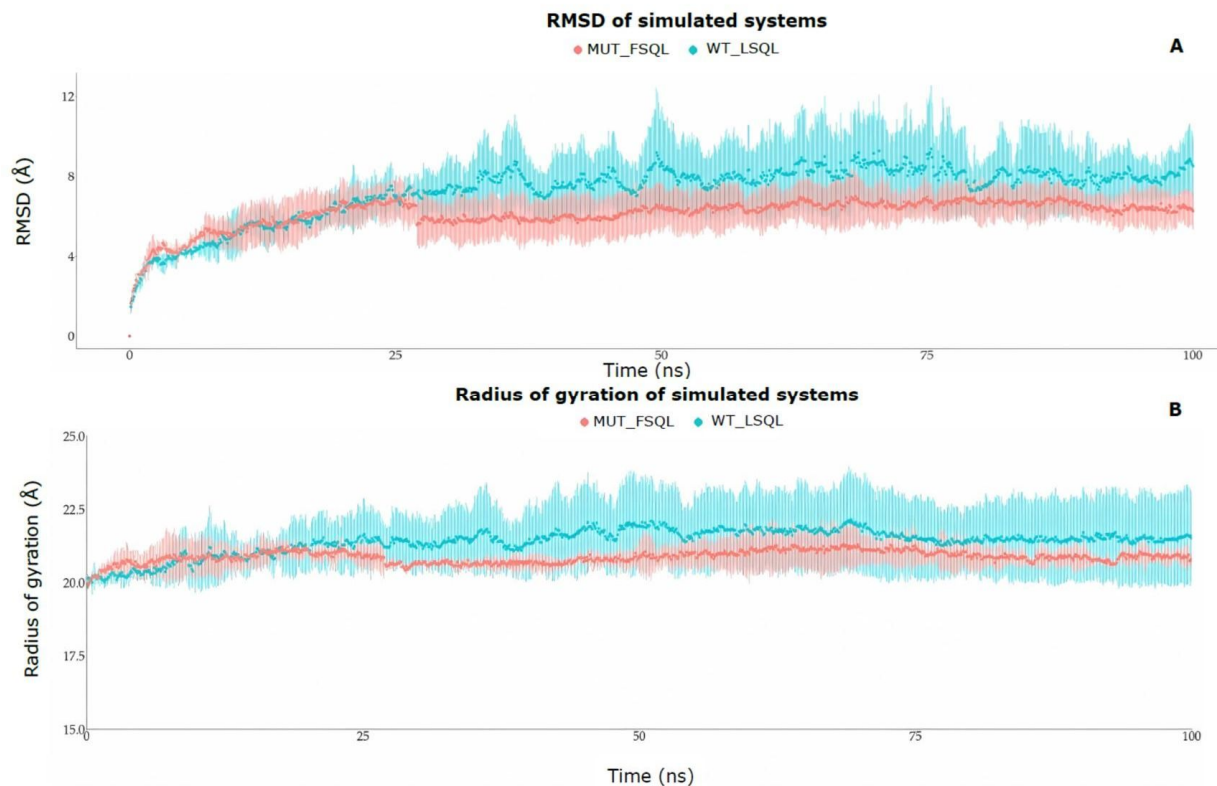
Molecular dynamics simulations were performed with an implicit solvent in triplicate for domain II of variant 8 and Cry11 wild-type molecules, where amino acid mutations were performed based on the results, trajectory, root-mean-square deviation of atomic position (RMSD), root-mean-square fluctuation (RMSF), and radius of gyration.

RMSD analysis (Figure 4A) showed that the mutant molecule (variant 8) registered greater stability when exposed to solvent than the wild-type molecule (Cry11). This stability can be attributed as a consequence of the two mutations made at positions 553 and 556; in the same way, the greater stability of the mutant molecule seems to favor the interaction of the molecule in the toxicity process.

The radius of gyration analysis (Figure 4B) shows that the wild-type protein (Cry11) retains a less rigid structure after the first quarter of the DM simulation has elapsed, while the mutated protein, although it starts with a less rigid structure, is presented in the course of the rest of the interaction to the more compact solvent. This preferentially compact

conformation of the mutant after a small non-rigid interval seems to favor the interaction of the molecule in the process that desiccates the toxicity of the mutant. The RMSD and radius of gyration calculations between the systems showed a statistically significant difference in the t-test, with a p -value of 0.000 (<0.05).

Figure 34. RMSD of simulated (A): red color (variant 8) and blue color (Cry11). The radius of gyration of the simulated (B): red color (variant 8) and blue color (Cry11).



RMSF analysis allowed us to observe some amino acids that presented average differences greater than 2 Å (Table 2) between the wild and mutant systems; the amino acids with the greatest difference could explain the increase in the toxicity of the mutant. Some amino acids of interest present differences greater than 3 Å in the mutant: LEU59, SER70, LEU87, and TRP265; the latter shows the greatest difference of 5.78 Å and corresponds to one of the mutated amino acids (Table 2). These amino acids that significantly change their spatial conformation with respect to their initial positions in the wild-type protein could be determining factors in the increase in the toxicity of the mutant

protein. It is highlighted that the amino acid LEU556, one of the mutated amino acids, has a very high conformational difference.

Table 20. *The difference in RMSF is the difference in Å of the spatial position of the same amino acid in the two systems, wild-type (Cry11), and mutant (Variant 8).*

Amino Acids	Position	The Difference in RMSF between the Two Systems (Å)
LEU	350	3.71 Å
SER	361	3.72 Å
LEU	378	3.84 Å
PRO	512	2.40 Å
PHE	524	2.18 Å
THR	534	2.00 Å
LEU	556	5.78 Å
SER	562	2.32 Å

5.4 Discussion

The efficiency of Cry proteins produced by Bt is high, and only small amounts are generally necessary to cause toxicity [7]. Over time, the target insects for these proteins have developed various resistance mechanisms associated with the alteration of intestinal proteins that activate Cry proteins, modification of receptor-binding sites in the midgut, and synthesis of oligosaccharides, among others [18–20]. Therefore, there is a need to apply various genetic improvement strategies such as DNA shuffling, domain swapping, and/or truncation [7]. These approaches will aid in controlling resistant mosquito populations and in elucidating the structure, function, and mechanisms of action of these proteins [11].

In the present study, a site-directed mutagenesis approach was used to explore the role of positions 553 and 556 in the differential activity of variant 8, a mutant obtained via DNA shuffling of Cry11Aa and Cry11Bb [10]. Herein, we present a molecular analysis of the lethality of these mutated variants in *A. aegypti* larvae. The LC₅₀ values obtained for the mutants were >500 ng·mL⁻¹, suggesting that the reversal of amino acids located at positions 553 and 556 directly affected the lethality of these variants and that the chemical nature of these residues probably plays a significant role in their structural function. Additionally, the 556 variant was tested in SW-480 colon cancer cell lines, as Cry proteins that lack insecticidal activity could be candidates for anticancer proteins. The

results indicated that the insecticidal activity of 8W556L was null, but when tested against SW480, its cytotoxic activity was almost two times higher than that of variant 8 at 48 h and similar to the cytotoxic activity of Cry11Aa and Cry11Bb. At 72 h, the activities of all Cry proteins were similar. This difference in activity against both targets indicates that the mechanism of action probably depends on the composition of the cell membrane [20–22], and the mutation of 8W556L is located in domain III; this region is involved in the processes of oligomerization and stabilization of the Cry proteins [3,21].

It is not the first time that Cry proteins or peptides obtained from Cry proteins have been used to control cancer cell lines. In 2022, it was reported that the co-administration of inactivated and activated forms of Cry1Ac with doxorubicin in a triple-negative breast cancer mouse model enhanced tumor immunity [22]. In 2021, Rendon-Marín et al. evaluated the activity of peptides obtained from Cry11Bb and found that the peptide BTM-P1 had a toxic effect on Caco-2 and MCF-7 cells, inducing apoptosis in MCF-7 cells with low hemolytic activity [23]. The background of the reported information and the study presented in this paper make exploring new targets for Cry proteins a promising approach for biotechnology and human medicine.

Computational simulations of molecular dynamics allowed us to establish hypotheses about the influence of the amino acids at positions 553 and 556 (mutants 8F553L, 8W556L, and 8L553F/8 L556W) on the structural behavior of domain II arranged in a solvent for the Cry11 and variant 8 proteins. Molecular simulation studies demonstrated that the structure of domain II in the mutated variant 8 protein remained with greater energy stability, showing a compact structure throughout the simulation time; 3% of the amino acids in the mutated domain changed their initial configuration at a distance greater than 2 Å, at the positions LEU350, SER361, LEU378, and LEU556. Amino acids such as phenylalanine and tryptophan have chemical characteristics that differ from leucine. For leucine, its conformation is given by aliphatic side chains, whereas [24,25] phenylalanine and tryptophan are made up of aromatic rings [24] that are involved in hydrophobic interactions and tend to be positioned at the center of a protein, excluded from the solvent, allowing better stability and function. Electron delocalization also plays an important role. These results suggest that the indolyl NH functional group in the tryptophan residue may be associated with protein–receptor interactions. Previous studies

on chemical modifications of tryptophan, such as sulfenylation, led to a loss of toxicity in mice and apparent binding affinity for rat brain and cockroach synaptosomal preparations [24]. Currently, different scientific fields are exploring the role of tryptophan in the photon-sensing capabilities of living organisms through the resonance delocalization of π -electrons [25].

Cry proteins are highly conserved within their three domains; any changes in any residues either enhance activity, induce loss of activity, or change the target, depending on the domain affected. Studies conducted by Fernandez et al. [3] showed that the toxicity of Cry11Aa is affected by amino acid substitutions via site-directed mutagenesis of hydrophobic residues (alanine) to hydrophilic residues, such as glutamic acid. The loops responsible for binding to membrane receptors have a greater binding affinity as they are hydrophobic regions; their chemical properties continue to be preserved because they are not exposed to the solvent. Similarly, in studies based on loop 3 of the Cry1Ab protein where a substitution of phenylalanine for alanine was made, a significant reduction in the toxic activity (3.5 times) towards insects of the order Lepidoptera was observed since binding to the receptors present in the insect membrane did not occur because alanine, having an aliphatic chain within its chemical characteristics, hinders the generation of hydrogen bonds between the protein and the receptor [26]. This result is different from others because phenylalanine is an amino acid with aromatic chemical characteristics. In contrast, Tiewisiri and Angsuthanasombat reported a high decrease in toxicity against *A. aegypti* when making alanine substitutions in the positions where aromatic amino acids (tryptophan, tyrosine, and phenylalanine) were found at residues 243, 249, and 264, respectively, located in the α -7 helix, which confirmed that aromatic residues are involved in the increase or decrease in toxicity [27].

The receptor binding capacity of Cry toxins is attributed primarily to domain II rather than domain III, although the latter may be involved in the binding processes [28]. Several studies have shown that domain III of various Cry toxins is involved in receptor binding [28,29]. For example, the substitution of domain III in Cry1Ab and Cry1Ac with domain III of Cry1Ca resulted in an approximately 10-fold increase in toxicity towards *Spodoptera exigua* and the recognition of receptor proteins present in insect membranes [30]. Moreover, Mushtaq et al. designed a hybrid toxin that shared domains I and II of Cry1Ac

(active sites for *Anticarsia gemmatalis* and *Chrysodeixis includens*) and domain III of Cry2Ac7 to generate a new protein with increased toxicity against both species [31]. The results indicated that the toxicity against *A. gemmatalis* and the binding to its membrane receptors were maintained; a different case occurred with *C. includens*, where no toxicity was found [31].

The A92D and C157R variants obtained by site-directed mutagenesis of Cry11Bb were intended to demonstrate the significance of the amino acid residues located at positions 92 and 157 in domain I. The results obtained for the LC₅₀ assays against *A. aegypti*

showed a 13- and 21.8-fold decrease in toxicity for the A92D and C157R variants, respectively, compared with the parental Cry11Bb (Table 1). Genetic manipulation of domain I is mainly focused on studying or improving the toxic activity of Cry proteins against the formation of pores or ion channels in the midgut membranes of insects. This domain comprises various polar amino acids that directly participate in the formation of hydrogen bonds or salt bridges [7,32]. Wu and Aronson reported that the substitution of specific residues at position A92D of the Cry1Ab protein caused a reduction in toxic activity due to the substitution of the negatively charged amino acid residues at this position, which caused detrimental effects on pore formation in *M. sexta* [33]. Additionally, Álzate in 2010 reported a three-fold decrease in the insecticidal activity of the Cry1Ab toxin against *M. sexta* when modifying the L157R position, which correlated with the degree of loss of transport activity of ions generated by the chemical nature of the modified amino acids [13].

This work is promising for the study of the structure–function relationship of Cry11 proteins as a valuable biotechnological asset that, in the future, might be an alternative to the use of chemical insecticides in the control of mosquitoes, and may aid in preventing the spread of vector-borne diseases, and simultaneously, in the collecting of information to enhance modeling and in the obtaining of biomolecules directed to the control of mosquito-borne diseases considered a problem of public health worldwide [34]. This work also explored the potential biomedical applications of this parasporal protein in controlling the proliferation of primary adenocarcinomas. Further research is required to elucidate

whether these mutations broaden the targets of these proteins while contributing to a deeper understanding of the structure–function relationship in the Cry11 protein family.

5.5 Materials and Methods

5.5.1 Culture Media, Strains, and DNA Extraction

The bacterial strains were cultured in Luria Bertani (LB) broth supplemented with ampicillin $50 \mu\text{g}\cdot\text{mL}^{-1}$ for the transformants of *Escherichia coli* DE3BL21 strain and chloramphenicol $10 \mu\text{g}/\text{mL}$ for the transformants of the non-crystal producing Bt BMB171 strain; Plasmid DNA was extracted using the Wizard Minipreps kit (Promega®, Madison, WI, USA) following the manufacturer's instructions. Agarose gel electrophoresis was performed at a concentration of 0.8% and stained with SYBR-safe 10 \times .

5.5.2 Synthesis and Design of Cry11Bb and Variant 8 Mutants

5.5.2.1 Cry11Bb Mutant Library

Variants obtained using rational approximations for Cry11Bb were designed based on the toxin–receptor interaction analyzed in previous studies [7,13,33,35,36]; the Cry11Bb sequence was modified at position 92, changing an alanine for aspartic acid (A92D), and in the second variant, changing the cysteine for arginine at position 157 (C157R). The genes were synthesized at Genescript (Piscataway, NJ, USA) and cloned into the expression vector pSV2, followed by electroporation in *E. coli* DE3BL21. The transformation was verified using plasmid extraction, followed by a restriction assay using HindIII/SacI (NEB, Manchester UK), and then visualized using agarose gel electrophoresis.

5.5.2.2 Variant 8 Mutant Library

Primers were designed using the web service <https://www.lifetechnologies.com/order/oligoDesigner/mutagenesis> (accessed on 8 January 2021). The pSV2 plasmid harboring the variant 8 gene was used as the template; the selected positions for mutations were 553, 556, and a double mutation 553 and 556. The primers used are listed in Table S1 (Supplementary Material). The GeneArt™ Site-Directed Mutagenesis System kit (Thermo Fisher Scientific, Waltham, MA USA) was used for amplification, following the manufacturer's instructions. The constructs were amplified, transformed into chemically competent *E. coli* TOP10 cells, and electroporated into *Bt* BMB171 cells. The library was verified via sequencing the constructs; for this, 20 $\mu\text{g}\cdot\mu\text{L}^{-1}$ were sent to Macrogen (Seoul, Republic of Korea) and sequenced using the oligos: 8MDF (CTGCTGGAATACGGGTACA) and 8MDR (AATTCGGTTGTTCAATAAGT).

5.5.3 Obtaining Final Complete Culture (FCC) of *Bt*

Mutants L553F, L556W, L553F-L556W, A92D, and C157R and recombinants expressing Cry11Aa and Cry11Bb toxins, together with the non-crystal-forming strain *Bt* BMB171, were grown in 10 mL of LB broth with chloramphenicol at 10 $\mu\text{g}\cdot\text{mL}^{-1}$ and incubated at 30 °C with shaking at 300 rpm for 7 d. After 48 h of incubation, spore and crystal formation were examined using malachite green staining. To obtain FCC, 5 mL of each culture was centrifuged at 10,000 rpm for 5 min at 4 °C. The supernatant was discarded, and 1 mL of 1M NaCl was added. The preparation was incubated for 1 h at 30 °C with stirring at 50 rpm. Subsequently, it was centrifuged at 12,000× g for 5 min at 4 °C. The supernatant was discarded, 1 mL of 1× phosphate buffered saline (PBS) was added, and the pellet was homogenized and centrifuged under the above-mentioned conditions. This procedure was repeated twice, and cells were frozen in 1 mL of PBS.

5.5.4 Protein Electrophoresis on Sodium Dodecyl Sulfate-Polyacrylamide Gel Electrophoresis (SDS-PAGE)

The samples were run on a 10% acrylamide gel. The gel and electrophoretic run were prepared following the instructions in the protocol book by Sambrook [37]. Coomassie blue R-250 and destaining solution were used for gel development for 30 min. The samples were treated with proteinase K at $10 \mu\text{g}\cdot\text{mL}^{-1}$ to verify the characteristic activated fragments of Cry11 proteins.

5.5.5 Protein Preparation and Half-Lethal Concentration (LC_{50})

The cultures of each mutant dissolved in PBS 1× were subjected to heat stress, which was performed as follows: 100 μL of each culture was incubated at 72 °C for 20 min followed by incubation at 4 °C for 10 min. Dilutions of 10^{-1} to 10^{-5} were made with a final volume of 100 μL , and then the dilutions were plated on LB agar with chloramphenicol ($10 \mu\text{g}\cdot\text{mL}^{-1}$) and incubated at 30 °C for 24 h. The results were reported in spores/mL of culture. Proteins were solubilized by taking 200 μL of the final culture of each mutant and parental strain and adding 800 μL of crystal solubilization buffer (50 mM NaOH and 10 mM EDTA; pH 11.7). This solution was incubated overnight at 4 °C, followed by centrifugation at 27,000× g for 5 min at 4 °C. The supernatant was collected, and the volume was adjusted to 1 mL with 0.1 M Tris-base pH 7.4. To quantify the proteins, the Bradford micro-technique was used at 540 nm with a NanoDrop 2000. Three measurements were performed for each variant.

To establish the amount corresponding to the total protein of the cell mass, a dry weight estimation was performed by taking 500 μL of the FCC of each variant and centrifuging at 15,000 rpm at 4 °C for 30 min. The supernatant was discarded, and the pellet dried for 48 h at 20 °C. Subsequently, dry weight measurements were performed. Lethality tests were performed on each of five larvae of *A. aegypti* in instar I in triplicate with three replicates. To estimate lethality, live larvae were counted and translated into the percentage of dead larvae. Statistical analyses were performed using the ProBit

function, and the mean lethal concentration (LC₅₀) was calculated using R-Project Software v4.2.0. [38].

5.5.6 Variants of Cry in the Control of the Human Colorectal Cancer Cells

The solubilized proteins were activated using proteinase K (185 µg·mL⁻¹) for 1 h at 37 °C. Phenylmethylsulphonyl fluoride was added (final concentration: 1 mM) to inhibit the proteolytic activity. SDS-PAGE was performed to confirm the presence of Cry proteins. Protein concentration was determined using the Bio-Rad Protein Assay (Bio-Rad Laboratories, Mississauga, ON, Canada).

$$\% \text{ metabolic activity} = \frac{\text{cell absorbance with treatment}}{\text{cell absorbance without treatment}} \times 100 \quad (1)$$

Colorectal cancer cells (20,000/well) of SW480 (obtained from American Type Culture Collection-ATCC-Accession number CCL-228) were plated, and RPMI culture medium (Sigma Aldrich®, St. Louis, CO, USA) supplemented with 10% fetal bovine serum was added to make a final volume of 100 µL. Subsequently, 100 µL of culture medium with activated proteins at twice the concentration to be evaluated (0.5, 1, 2, 3, 5, and 10 µg/mL) were added and incubated for 48 and 72 h at 37 °C. Finally, 10 µL of Alamar blue was added to each well and incubated for 4–6 h to measure the fluorescence (Ex 560 nm and Em 590 nm) and thus determine the IC₅₀. The results are expressed in terms of metabolic activity using the following formula:

5.5.7 Structural Modeling of Cry11 Variants

To design the Cry11 mutants, a protocol was prepared to model two Cry11 variant structures: variant 8 and Cry11Bb. To fit the model, we applied a de novo prediction method called trRosetta [39], which was built using direct energy minimization with Rosetta Commons functionalities [40], including inter-residue distances and orientation restraints predicted by a deep neural network (<https://yanglab.nankai.edu.cn/trRosetta/>), accessed on 10 April 2022.

The best model per sequence was subjected to energy and geometrical evaluations using the ProSa web server

(<https://prosa.services.came.sbg.ac.at/prosa.php>) accessed on 15 April 2022 and the structural assessment pipeline available on the SwissModel portal (<https://swissmodel.expasy.org/assess>) accessed on 15 April 2022.

5.5.8 Generation of Additional Variants and Sampling of the Models

Based on the initial models, a subsequent set of variants was predicted by performing single-point mutations on the variant 8 and Cry11Bb structures. The first variation consisted of mutations at positions 553 and 556 (mutants F553L, W556L, and F553L/W556L) of the variant 8 model. Single-point mutations were performed using UCSF Chimera [41] through the prediction of rotamers using Dunbrack backbone-dependent libraries [42], in which the Cry11Bb structure was used to generate the variants A92D and C157R. Molecular Dynamics (MD) was performed in triplicate for Cry11 and variant 8 in periods of 100 ns. The simulation protocol for all systems was solvated with TIP3P63 water molecules with a margin of at least 14 Å from the protein, and Na⁺ and Cl⁻ ions were added to ensure the neutrality of the system. At an ion concentration of 150 mM, the Amber ff1464 and GAFF65 force fields for the proteins were implemented for all systems. The system's energy was first minimized and balanced using Amber18.67 software for complexes, and stepped minimization, heating, and balancing were performed. Complexes were first minimized for 1000 conjugate gradient steps, followed by 10,000 unrestricted steps, heated in 200 ps unrestricted steps, and then in an NPT set (7 ns) up to 300 K. The protocol for the setup of the protein system simulations on the GPU was followed. Finally, simulations were performed under NPT conditions (Langevin thermostat with Berendsen Barostat) to ensure the balance of the entire system.

5.6 References

1. Badran, A.H.; Guzov, V.M.; Huai, Q.; Kemp, M.M.; Vishwanath, P.; Kain, W.; Nance, A.M.; Evdokimov, A.; Moshiri, F.; Turner, K.H.; et al. Continuous evolution of *Bacillus thuringiensis* toxins overcomes insect resistance. *Nature* 2016, 533, 58–63. <https://doi.org/10.1038/NATURE17938>.

2. Arias, M.; Orduz, S.; Lemeshko, V.V. Potential-dependent permeabilization of plasma membrane by the peptide BTM-P1 derived from the Cry11Bb1 protoxin. *Biochim. Biophys. Acta* 2009, 1788, 532–537. <https://doi.org/10.1016/J.BBAMEM.2008.12.009>.
3. Fernández, L.E.; Pérez, C.; Segovia, L.; Rodríguez, M.H.; Gill, S.S.; Bravo, A.; Soberón, M. Cry11Aa toxin from *Bacillus thuringiensis* binds its receptor in *Aedes aegypti* mosquito larvae through loop alpha-8 of domain II. *FEBS Lett.* 2005, 579, 3508–3514. <https://doi.org/10.1016/J.FEBSLET.2005.05.032>.
4. Sauka, D.H.; Monella, R.H.; Benintende, G.B. Detection of the mosquitocidal toxin genes encoding Cry11 proteins from *Bacillus thuringiensis* using a novel PCR-RFLP method. *Rev. Argent. Microbiol.* 2010, 42, 23–26. <https://doi.org/10.1590/S0325-75412010000100005>.
5. Orduz, S.; Realpe, M.; Arango, R.; Murillo, L.A.; Delécluse, A. Sequence of the cry11Bb11 gene from *Bacillus thuringiensis* subsp. medellin and toxicity analysis of its encoded protein. *Biochim. Biophys. Acta* 1998, 1388, 267–272. [https://doi.org/10.1016/S0167-4838\(98\)00168-X](https://doi.org/10.1016/S0167-4838(98)00168-X).
6. Marcos, M.L.; Echave, J. Too packed to change: Side-chain packing and site-specific substitution rates in protein evolution. *PeerJ* 2015, 3, e911. <https://doi.org/10.7717/peerj.911>.
7. Vílchez, S. Making 3D-Cry Toxin Mutants: Much More Than a Tool of Understanding Toxins Mechanism of Action. *Toxins* 2020, 12, 600. <https://doi.org/10.3390/toxins12090600>.
8. Sun, Y.; Zhao, Q.; Xia, L.; Ding, X.; Hu, Q.; Federici, B.A.; Park, H.W. Identification and characterization of three previously undescribed crystal proteins from *Bacillus thuringiensis* subsp. *Jegathesan*. *Appl. Environ. Microbiol.* 2013, 79, 3364–3370. <https://doi.org/10.1128/AEM.00078-13>.
9. Mehlo, L.; Gahakwa, D.; Nghia, P.T.; Loc, N.T.; Capell, T.; Gatehouse, J.A.; Gatehouse, A.M.; Christou, P. An alternative strategy for sustainable pest resistance in genetically enhanced crops. *Proc. Natl. Acad. Sci. USA* 2005, 102, 7812–7816. <https://doi.org/10.1073/pnas.0502871102>.
10. Florez, A.M.; Suarez-Barrera, M.O.; Morales, G.M.; Rivera, K.V.; Orduz, S.; Ochoa, R.; Guerra, D.; Muskus, C. Toxic Activity, Molecular Modeling and Docking Simulations of *Bacillus thuringiensis* Cry11 Toxin Variants Obtained via DNA Shuffling. *Front. Microbiol.* 2018, 9, 2461. <https://doi.org/10.3389/fmicb.2018.02461>.
11. Deist, B.R.; Rausch, M.A.; Fernandez-Luna, M.T.; Adang, M.J.; Bonning, B.C. Bt Toxin Modification for Enhanced Efficacy. *Toxins* 2014, 6, 3005–3027. <https://doi.org/10.3390/toxins6103005>.

12. Lucena, W.A.; Pelegrini, P.B.; Martins-de-Sa, D.; Fonseca, F.C.A.; Gomes, J.E., Jr.; De Macedo, L.L.P.; Da Silva, M.C.M.; Oliveira, R.S.; Grossi-de-Sa, M.F. Molecular Approaches to Improve the Insecticidal Activity of *Bacillus thuringiensis* Cry Toxins. *Toxins* 2014, 6, 2393–2423. <https://doi.org/10.3390/toxins6082393>.
13. Alzate, O.; Osorio, C.; Florez, A.M.; Dean, D.H. Participation of valine 171 in alpha-Helix 5 of *Bacillus thuringiensis* Cry1Ab delta-endotoxin in translocation of toxin into *Lymantria dispar* midgut membranes. *Appl. Environ. Microbiol.* 2010, 76, 7878–7880. <https://doi.org/10.1128/AEM.01428-10>.
14. Pinzon, E.H.; Sierra, D.A.; Suarez, M.O.; Orduz, S.; Florez, A.M. DNA secondary structure formation by DNA shuffling of the conserved domains of the Cry protein of *Bacillus thuringiensis*. *BMC Biophys.* 2017, 10, 4. <https://doi.org/10.1186/s13628-017-0036-7>.
15. Pinzón-Reyes, E.H.; Sierra-Bueno, D.A.; Suarez-Barrera, M.O.; Rueda-Forero, N.J.; Abaunza-Villamizar, S.; Rondón-Villareal, P. Generation of Cry11 Variants of *Bacillus thuringiensis* by Heuristic Computational Modeling. *Evol. Bioinform.* 2020, 16, 1176934320924681. <https://doi.org/10.1177/1176934320924681>.
16. Gonzalez-Vazquez, M.C.; Vela-Sanchez, R.A.; Rojas-Ruiz, N.E.; Carabarin-Lima, A. Importance of Cry Proteins in Biotechnology: Initially a Bioinsecticide, Now a Vaccine Adjuvant. *Life* 2021, 11, 999. <https://doi.org/10.3390/life11100999>.
17. Berman, H.M.; Westbrook, J.; Feng, Z.; Gilliland, G.; Bhat, T.N.; Weissig, H.; Shindyalov, I.N.; Bourne, P.E. The Protein Data Bank. *Nucleic Acids Res.* 2000, 28, 235–242. <https://doi.org/10.1093/nar/28.1.235>.
18. Soberon, M.; Pardo-Lopez, L.; Lopez, I.; Gomez, I.; Tabashnik, B.E.; Bravo, A. Engineering modified Bt toxins to counter insect resistance. *Science* 2007, 318, 1640–1642. <https://doi.org/10.1126/science.1146453>.
19. Fabrick, J.A.; Wu, Y. Roles of insect midgut cadherin in Bt intoxication and resistance. In *Bt Resistance: Characterization and Strategies for GM Crops Producing Bacillus thuringiensis Toxins*; CABI: Wallingford, UK, 2015; pp. 69–86. <https://doi.org/10.1079/9781780644370.0069>.
20. Batool, K.; Alam, I.; Jin, L.; Xu, J.; Wu, C.; Wang, J.; Huang, E.; Guan, X.; Yu, X.Q.; Zhang, L. CTLGA9 Interacts with ALP1 and APN Receptors To Modulate Cry11Aa Toxicity in *Aedes aegypti*. *J. Agric. Food Chem.* 2019, 67, 8896–8904. <https://doi.org/10.1021/acs.jafc.9b01840>.
21. Jiménez, A.I.; Reyes, E.Z.; Cancino-Rodezno, A.; Bedoya-Pérez, L.P.; Caballero-Flores, G.G.; Muriel-Millan, L.F.; Likitvivatanavong, S.; Gill, S.S.; Bravo, A.; Soberón, M. *Aedes aegypti* alkaline phosphatase ALP1 is a functional receptor of *Bacillus thuringiensis* Cry4Ba and Cry11Aa toxins. *Insect Biochem. Mol. Biol.* 2012, 42, 683–689. <https://doi.org/10.1016/J.IBMB.2012.06.001>.

22. Raúl, S.G.R.; Damaris, I.A.; de Jesús, J.C.Á.; Leticia, M.F. Cry1Ac Protoxin Confers Antitumor Adjuvant Effect in a Triple-Negative Breast Cancer Mouse Model by Improving Tumor Immunity. *Breast Cancer* 2022, 16, 11782234211065154. <https://doi.org/10.1177/11782234211065154>.
23. Rendon-Marin, S.; Quintero-Gil, C.; Lemeshko, V.V.; Orduz, S. Cytolytic activity of peptides derived from the Cry11Bb insecticidal toxin of *B. thuringiensis* subsp. *Medellin*. *Arch. Biochem. Biophys.* 2021, 704, 108891. <https://doi.org/10.1016/J.ABB.2021.108891>.
24. Li, J.; Jiang, X.; Dick, A.; Sharma, P.P.; Chen, C.H.; Rathi, B.; Kang, D.; Wang, Z.; Ji, X.; Lee, K.H.; et al. Design, synthesis, and antiviral activity of phenylalanine derivatives as HIV-1 capsid inhibitors. *Bioorganic Med. Chem.* 2021, 48, 116414. <https://doi.org/10.1016/J.BMC.2021.116414>.
25. Alachkar, A. Aromatic patterns: Tryptophan aromaticity as a catalyst for the emergence of life and rise of consciousness. *Phys. Life Rev.* 2022, 42, 93–114. <https://doi.org/10.1016/J.PLREV.2022.07.002>.
26. Rajamohan, F.; Alzate, O.; Cotrill, J.A.; Curtiss, A.; Dean, D.H. Protein engineering of *Bacillus thuringiensis* delta-endotoxin: Mutations at domain II of CryIAb enhance receptor affinity and toxicity toward gypsy moth larvae. *Proc. Natl. Acad. Sci. USA* 1996, 93, 14338–14343. <https://doi.org/10.1073/pnas.93.25.14338>.
27. Tiewisiri, K.; Angsuthanasombat, C. Structurally conserved aromaticity of Tyr249 and Phe264 in helix 7 is important for toxicity of the *Bacillus thuringiensis* Cry4Ba toxin. *J. Biochem. Mol. Biol.* 2007, 40, 163–171. <https://doi.org/10.5483/BMBREP.2007.40.2.163>.
28. Likitvivatanavong, S.; Aimanova, K.G.; Gill, S.S. Loop residues of the receptor binding domain of *Bacillus thuringiensis* Cry11Ba toxin are important for mosquitocidal activity. *FEBS Lett.* 2009, 583, 2021–2030. <https://doi.org/10.1016/J.FEBSLET.2009.05.020>.
29. Naimov, S.; Weemen-Hendriks, M.; Dukiandjiev, S.; De Maagd, R.A. *Bacillus thuringiensis* Delta-Endotoxin Cry1 Hybrid Proteins with Increased Activity against the Colorado Potato Beetle. *Appl. Environ. Microbiol.* 2001, 67, 5328–5330. <https://doi.org/10.1128/aem.67.11.5328-5330.2001>.
30. de Maagd, R.A.; Kwa, M.S.; Van der Klei, H.; Yamamoto, T.; Schipper, B.; Vlak, J.M.; Stiekema, W.J.; Bosch, D. Domain III substitution in *Bacillus thuringiensis* delta-endotoxin CryIA(b) results in superior toxicity for *Spodoptera exigua* and altered membrane protein recognition. *Appl. Environ. Microbiol.* 1996, 62, 1537–1543. <https://doi.org/10.1128/aem.62.5.1537-1543.1996>.
31. Mushtaq, R.; Shakoori, A.R.; Jurat-Fuentes, J.L. Domain III of Cry1Ac Is Critical to Binding and Toxicity against Soybean Looper (*Chrysodeixis includens*) but Not to

- Velvetbean Caterpillar (*Anticarsia gemmatalis*). *Toxins* 2018, 10, 95. <https://doi.org/10.3390/toxins10030095>.
32. Li, J.; Carroll, J.; Ellar, D.J. Crystal structure of insecticidal delta-endotoxin from *Bacillus thuringiensis* at 2.5 Å resolution. *Nature* 1991, 353, 815–821. <https://doi.org/10.1038/353815A0>.
 33. Wu, D.; Aronson, A.I. Localized mutagenesis defines regions of the *Bacillus thuringiensis* δ -endotoxin involved in toxicity and specificity. *J. Biol. Chem.* 1992, 267, 2311–2317. [https://doi.org/10.1016/s0021-9258\(18\)45879-6](https://doi.org/10.1016/s0021-9258(18)45879-6).
 34. Tetreau, G.; Sawaya, M.R.; De Zitter, E.; Andreeva, E.A.; Banneville, A.S.; Schibrowsky, N.A.; Coquelle, N.; Brewster, A.S.; Grünbein, M.L.; Kovacs, G.N.; et al. De novo determination of mosquitocidal Cry11Aa and Cry11Ba structures from naturally-occurring nanocrystals. *Nat. Commun.* 2022, 13, 4376. <https://doi.org/10.1038/s41467-022-31746-x>.
 35. Alzate, O.; Hemann, C.F.; Osorio, C.; Hille, R.; Dean, D.H. Ser170 of *Bacillus thuringiensis* Cry1Ab δ -endotoxin becomes anchored in a hydrophobic moiety upon insertion of this protein into *Manduca sexta* brush border membranes. *BMC Biochem.* 2009, 10, 25. <https://doi.org/10.1186/1471-2091-10-25/FIGURES/8>.
 36. Sheng-Jiun, W.; Alvaro, M.F.; Bradley, J.H.; Donald, H.D.; Oscar, A. Two disulfide mutants in domain I of *Bacillus thuringiensis* Cry3Aa δ -endotoxin increase stability with no effect on toxicity. *Adv. Biol. Chem.* 2012, 2, 123–131. <https://doi.org/10.4236/ABC.2012.22015>.
 37. Sambrook, J.; Russell, D.W. SDS-Polyacrylamide Gel Electrophoresis of Proteins. *Cold Spring Harb. Protoc.* 2006, 2006, pdb.prot4540. <https://doi.org/10.1101/pdb.prot4540>.
 38. R: The R Project for Statistical Computing. Available online: <https://www.r-project.org/> (accessed on 15 April 2023).
 39. Yang, J.; Anishchenko, I.; Park, H.; Peng, Z.; Ovchinnikov, S.; Baker, D. Improved protein structure prediction using predicted interresidue orientations. *Proc. Natl. Acad. Sci. USA* 2020, 117, 1496–1503. https://doi.org/10.1073/PNAS.1914677117/SUPPL_FILE/PNAS.1914677117.SAPP.PDF.
 40. Kuhlman, B. Designing protein structures and complexes with the molecular modeling program Rosetta. *J. Biol. Chem.* 2019, 294, 19436–19443. <https://doi.org/10.1074/JBC.AW119.008144>.
 41. Pettersen, E.F.; Goddard, T.D.; Huang, C.C.; Couch, G.S.; Greenblatt, D.M.; Meng, E.C.; Ferrin, T.E. UCSF Chimera—A visualization system for exploratory research and analysis. *J. Comput. Chem.* 2004, 25, 1605–1612. <https://doi.org/10.1002/jcc.20084>.

42. Dunbrack, R.L. Rotamer libraries in the 21st century. *Curr. Opin. Struct. Biol.* 2002, 12, 431–440. [https://doi.org/10.1016/S0959-440X\(02\)00344-5](https://doi.org/10.1016/S0959-440X(02)00344-5).

6. Summary, Conclusions, and Future Perspectives

Miguel Orlando Suárez Barrera

6.1 Summary and Conclusions

Bacillus thuringiensis was first identified in the 20th century by Ishiwata in 1901, who reported that this microorganism had the ability to infect *Bombyx mori* plague. This plague caused severe damage to the silk industry in Japan and the authors called these bacteria *Bacillus sotto*. A decade later, Berliner isolated the same (Gram-positive) bacterium from the larvae of *Ephesitia kuehniella* in Thuringia (Germany) and called it *Bacillus thuringiensis* (Bt), this name is currently the most preferred name for this bacterium [1]–[5]. Bt is a ubiquitous Gram-positive aerobic bacterium that is highly resistant to high temperatures and desiccation leads to the formation of endospores (1 to 1.2 micrometers wide and 3 to 5 micrometers long). It has been isolated from various parts of the earth, mainly in niches such as soil, plant leaves, and dead insects. Its genome is about 2.4 to 5.7 million base pairs, and most strains have extrachromosomal elements, some of which are circular and others linear, varying in size from two to hundreds of kilobases [2]. Bt belongs to the *B. cereus* group, which includes 5 species: *B. cereus*, *B. anthracis*, *B. mycoides*, *B. pseudomycoides*, and *B. weihenstephanensi* [3].

Bt parasporal toxins have been described as crystal-shaped proteins that have therapeutic effects on a broad range of diseases and toxic effects on pest vector organisms. Two of these crystals, i.e. the Cry and Cyt proteins, also have cytotoxic activity against human cancer cell lines; these proteins have been named parasporins (PS) [4]. Currently, PSs have gained attention in biotechnology and medicine, with Bt as one of the most important microorganisms used as a biocontrol agent and, more recently, as a producer of noninsecticidal parasporin proteins [5].

To date, the study of proteins produced by Bt has focused only on quantifying their insecticidal potential, ignoring their potential uses in other areas of biotechnology and

health. However, in recent years, several new properties have been discovered in crystals extracted from different Bt strains, such as anticancer cell activity, anti-protozoal activity, and lectin activity [6]– [8]. In particular, the anticancer cell activity represents a novel opportunity for further research on the parasporin application in cancer therapy and diagnosis [7].

Chapter 1 describes current knowledge on Bt-derived parasporal proteins, including Cry and PS toxins, their classification, structure, mechanism of action, and target cells, as well as the scientific progress made in nearly two decades of work. The focus is on Cry11 and the aerolysin-type parasporin PS2Aa1 and their prospects as approaches to combat diseases related to public health. Next, it describes the potential of these toxins to become the subject of genetic improvement studies leading to producing biomolecules with an enhanced toxic effect. Finally, it helps to define the specific mechanism of action of Bt PS proteins and elucidate their biotechnological and medical utility.

Chapter 2 is a compilation of studies from different research groups related to describing and characterizing PS to explore new applications of these proteins. In this chapter, we present the classification of PS according to their molecular weight (i.e. high and low molecular weight), which resulted in six different families of PS1-PS6. Overall, knowledge about these PS at the molecular level, including the mechanism of action and the receptors targeted by cancer cells, is limited. For example, the PS2Aa1 protein, a member of the PS2 family, is known as a β pore-forming toxin, which induces apoptosis in several human cancer cell lines.

In this chapter, we explored the options of applying genetic modifications to PS, including a broad spectrum of site-directed mutagenesis approaches, e.g., generation of truncated proteins and phage display experiments. This allowed the generation of PS variants with a different spectrum of activities against human cancer cells aiming at obtaining biomolecules with enhanced toxicity and stability. We determined its structural properties and mechanism of action using in vivo studies to take the next step toward developing valuable products for human health. In addition, it is important to identify new native Bt strains with improved cytotoxic activity against cancer cells to obtain promising candidates for further genetic improvement leading to toxins with enhanced activity. It has become evident that PS proteins are emerging as a viable alternative for cancer treatment.

Compared to other currently applied approaches, PSs have the potential to cause fewer side effects with improved treatment outcomes and quality of life of cancer patients.

In **Chapter 3**, It was investigated the cytotoxic effect of peptide analogs from domain I of PS2Aa1, where through a rational design, the conserved regions were identified and changed to increase the charge and hydrophobicity. Peptides were synthesized using the Fmoc solid-phase synthesis and characterized by mass spectrometry (MS). The peptide derived from PS2Aa1 (P264-G274) was taken as a native control. Peptides showed a hemolysis extent of less than 20% at a concentration of 100 μ M compared with the TritonX-100 positive control, which was set to 100%. P264-G274, showed EC50 value of 11.28 ± 0.52 , like the control peptide Loop2-PS2Aa (15.95 ± 0.69) on SW620 cell line. Likewise, these peptides showed significantly lower toxicity against CHO-K1 normal cells. The Loop1-PS2Aa peptide at 47.5 μ M was in the nucleus of SW480 cells after 1 h, whereas the P24-G274 peptide was localized in cytoplasmic regions during the same exposure time without affecting the nucleus. Similarly, the results obtained at higher levels of cell adhesion showed that the Loop1-PS2Aa peptide penetrated SW480 cells much faster than the P24-G274 peptide in SW620 cells. The molecular docking simulations also showed an interaction between the best experimental peptides, i.e. P264-G274 and Loop1-PS2Aa, and the APN receptor.

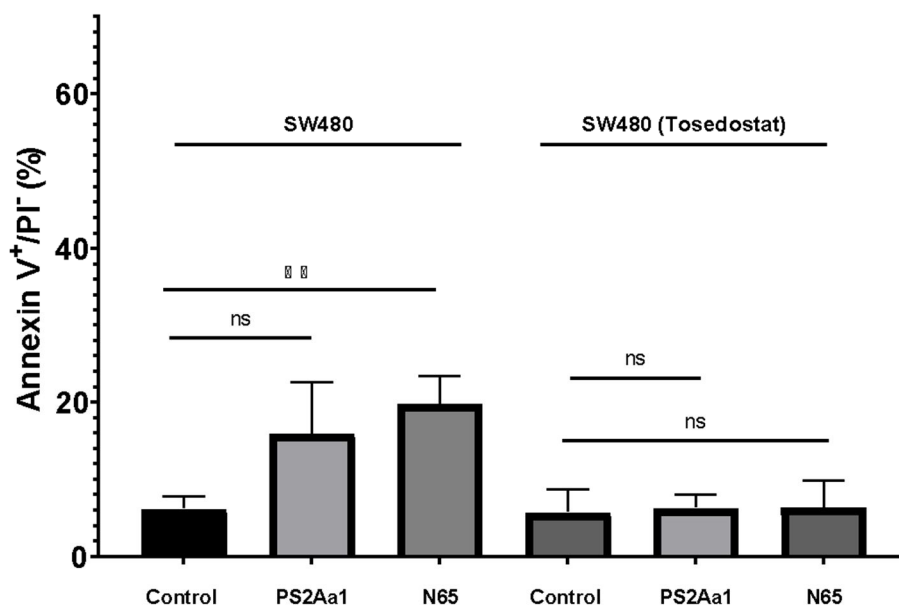
This study provides a foundation for generating novel analog peptides or site-directed alterations of the PS2 protein to boost its anticancer potential. Furthermore, Loop1-PS2Aa and P264-G274, peptides that have shown more significant anticancer action against SW480 and SW620, respectively, as well as good efficacy and selectivity, are proposed as potential therapeutic agents for the treatment of colon cancer.

In **Chapter 4**, the site-directed mutagenesis assays aimed to obtain variants with mutations in domain I of PS2Aa1 because it is the most variable region among proteins and its potential role in binding to receptors (Akiba & Okumura, 2017). We generated a library containing numerous potential domain I mutants by site-directed mutagenesis. After sequence validation, only 12 clones had a mutation leading to an amino acid change, of which 6 were selected because they had mutations in domain I. The expected variants were not generated for most of the the side-directed mutagenesis primers (n=997). A potential explanation for not generating these mutants could be the formation of dimers

(data not shown in the paper), which significantly reduces the yield of transformants (Edelheit et al., 2009).

From the cytotoxicity assays, it could be deduced that the 3-35 mutant had the best cytotoxic effect against the cell lines. This variant was characterized by an amino acid change at position 257, where valine replaced glycine. It is well known that mutations can alter protein function by improving or decreasing their stability and interactions with ligands of other biomolecules (Studer et al., 2013). For example, the hydrophobicity of nonpolar aliphatic amino acids, such as glycine, valine, proline, isoleucine, and leucine, may be involved in maintaining the three-dimensional structure of proteins. In other studies, the authors found that amino acid substitutions of Glutamic Acid and Asparagine residues to alanine in Cry4Ba mutants (PS-related) reduced toxicity to *A. aegypti* mosquito larvae. In this chapter, we found that using a Dinitroflavone which acts as an APN inhibitor, resulted in the loss of the cytotoxic activity of PS2Aa1 G257V and PS2Aa1 against CaCo-2 and SW480. Additionally, to corroborate these results, the Tosedostat antiproliferative APN inhibitor and a loss of cytotoxic activity were observed up to 5 times against SW480 using the mutated parasporin N65, similar to the results presented in Chapter 4 (**Figure 11**).

Figure 35. The activity of PS2Aa1 and the mutant N65 against SW480 in the presence (10nM) or absence of Tosedostat.



Our results suggest the role of APN in ensuring the anticancer activity of PS, potentially by identification of the cell membrane and their oligomerization. These data support the findings of Periyamy et al. (2016) [6], showing a reduction in the cytotoxic activity of PS2Aa1 by an APN inhibitor. Therefore, it is likely that APN is not the only receptor directly involved in the mechanism of action of these toxins [6,16]. The Molecular dynamic results of the mutant 3-35 showed residue 256 of PS2Aa1 was present in all three replicates and exhibited the smallest interaction distance between its center of mass and the APN contact area compared to the results of the Native PS2Aa1. Experimental results showed that mutation of this amino acid residue reduced the interaction and cytotoxicity, so the G at position 256 appears essential for the cytotoxic effects of PS2Aa1. The potential use of APN as a receptor by the Bt PS protein is not new; Cry proteins are known to deliver this receptor to target cells in the insect midgut. It should be noted that PS was earlier classified as Cry proteins, and PS2Aa1 was initially referred to as Cry46Aa1. There is a lack of proof to show that the APN receptor is relevant for the action of PS2Aa1, and the absence of this receptor in MCF-7 cells sensitive to PS2Aa1 further complicates this issue. Nevertheless, the evidence from this study and others related to the mechanism of action of PS awakens curiosity and indicates to gain more knowledge about PS proteins, including the use of mutant PS.

Furthermore, novel Bt native strains with improved cytotoxic action against cancer cells must be identified and evaluated, as well as candidates for future genetic development to acquire toxins with increased activity. PS proteins are being established as a potential alternative for cancer treatment. They have the potential to cause fewer adverse effects than other current techniques, increasing both treatment outcomes and cancer patients' quality of life.

In **Chapter 5**, site-directed mutagenesis was performed to investigate the role of single amino acids at positions 553 and 556 and of the 4 amino acids covering positions 553-556 in defining the enhanced activity of variant 8 (14). The results showed a decreased lethality of the mutant variants against *A. aegypti* larvae compared to the original variant 8. The LC50 values obtained for the mutants were >500 ng/ml, indicating that the reversal of amino acids at positions 553 and 556 significantly affected their activity

against *A. aegypti* larvae. The properties of these amino acid residues probably play a critical role in the functionality of this protein.

Computer molecular dynamics simulations allowed us to hypothesize the influence of amino acids at positions 553 and 556 and the two amino acids on the structure of domain II of Cry11Aa and variant 8 proteins. The molecular simulations' conclusions indicated that the domain II structure was energetically more stable in variant 8 than the original protein Cry11Aa, maintaining a compact structure throughout the simulation period. Moreover, 3% of the amino acids in the mutant domain changed their original configuration at a distance of more than 2 Å.

Site-directed mutagenesis of Cry11Bb revealed the importance of amino acid residues at positions 92 and 157 in domain I. LC50 assays against *A. aegypti* showed a 13-fold and 21.8-fold reduction in toxicity of the A92D and C157R variants, respectively, compared with the parental Cry11Bb. This work revealed promising data and novel insights into the importance of specific amino acids in defining the functionality of Cry11 and represented a valuable biotechnological asset in the control of vector-borne diseases, a public health problem around the world.

This research is pertinent to analyzing the structure-function relationship of Cry11 proteins as a significant biotechnological resource that could offer an alternative to using chemical insecticides in mosquito control. Furthermore, this protein's potential biomedical applications in limiting the proliferation of primary adenocarcinomas have been studied. More research is needed to determine whether these mutations broaden these proteins' targets and contribute to a better understanding of the structure-function link in the Cry11 protein family.

6.2 Discussion and future perspectives

There is a need to find and evaluate new native Bt strains with improved cytotoxic activity against cancer cells and to find candidates for future genetic improvement to obtain toxins with enhanced activity. PS Proteins are being established as a potential alternative for cancer treatment. They can potentially cause fewer adverse effects than other current homologous, improving both treatment outcomes and quality of life for

cancer patients. Parasporins have attracted the interest of researchers due to their selective toxic activity against different types of cancer cells and have therefore been proposed as a treatment option. In this context, it is crucial to understand how these proteins function, what they do in affected cells, and why they affect only certain types of cells. PS2Aa1 (Mpp46Aa1) is one of the parasporins with the broadest anti-cancer spectrum. Therefore, its mechanism of action was investigated in this study by characterizing variations acquired by site-directed mutagenesis.

It was found that some residues, such as Trp, play an important role in the sequence of PS2Aa1. This discovery implies that combining P264-G274 and Loop1-PS2Aa peptides with 5-FU may synergistically impact and improve therapeutic efficacy. Peptide structure is important to their efficacy. When free in solution, most ACPs do not fold into a well-defined form but acquire a α -helical or β -sheet structure when electrostatic interactions with membranes occur. A library of mutants with a differential activity was created using PS2Aa1 as a template and based on preliminary studies showing mutants with random substitutions in G256 and G257 amino acids to study different specific protein regions of PS2Aa1. Genetic modification was used to obtain mutants with substitutions in residues 256 and 257 of PS2Aa1. Therefore, these modifications allowed us to build a library of new parasporins with different activities against colorectal cancer cell lines. In this context, several studies had documented changes in the activity of Bt proteins when critical amino acid substitutions were made by site-directed mutagenesis, as in the case of Cry9Ca, where variants L186D and V189D with mutations in the same loop were virtually inactive against *Manduca sexta* in vitro assays [13]. Similarly, replacing valine 171 in Cry1Ab with a cysteine increased its toxicity to *Lymantria dispar* while decreasing its toxicity [13]. It is consistent with the activity of the 0-35 variant, as it gains activity over all cell lines compared to PS2Aa1.

Based on previous molecular docking studies, it was determined that the oligonucleotides with mutations incorporated for site-directed mutagenesis should be present at the N-terminal end, specifically in domain I of PS2Aa1, as this region is thought to be responsible for specific binding to membrane receptors [14]. PS2Aa1 has domains in common with aerolysin-type PFT proteins. It includes a highly conserved area corresponding to the C-terminal chain and a highly variable section at the protein's N-

terminus that generally contains recognition signals [11] and corresponds to the domain I of PFT proteins. Due to its tremendous diversity, this protein family contains a diverse spectrum of highly specialized binding receptors. Molecular docking and dynamics simulations revealed the possibility of a permanent link between PS2Aa1 domain I and the APN receptor. Moreover, mutant 3-35 was mutated in the region of amino acids critical for the interactions in the molecular dynamics simulations. The shortest interaction distance between its center of mass and the APN contact region was identified in all three replicates, with residue 256 having the shortest interaction distance between its center of mass and the APN contact region.

PS2Aa1 can induce apoptosis in cancer cells in its native state, comparable to PS4, which is produced by *B. thuringiensis* A1519 and activates the mitochondrial apoptosis pathway in Jurkat cells via cleavage of caspase-3 and -9 and subsequent release of cytochrome C [25]. Using cytotoxicity assays, it was found that mutant 3-35 has a more pronounced effect on cancer cell lines, and we quantified for the first time the amount of caspase-3 and PARP cleaved and the formation of γ H2AX [24]. In addition, we demonstrated how this mutation affects early and late apoptosis in recombinant PS2Aa1. These results demonstrate that the point mutation G257V on loop 1 can alter the activity of the protein, which is characterized by differential cytotoxicity and apoptosis.

On the other hand, cry proteins and Cry protein-derived peptides have been used to target cancer cell lines. In a triple-negative breast cancer model in mice, co-administration of inactivated and activated versions of Cry1Ac with doxorubicin improved tumor immunity in 2022 [22]. Rendon-Marin et al. investigated the effect of Cry11Bb-derived peptides in 2021 and discovered that the BTM-P1 peptide was hazardous to Caco-2 and MCF-7 cells and caused MCF-7 cell death with moderate hemolytic activity [23]. The influence of amino acids at positions 553 and 556 (mutants 8F553L, 8W556L, and 8L553F/8 L556W) on the structural behavior of the solvent-arranged domain II for Cry11 and variation 8 proteins was hypothesized using molecular dynamics simulations. Molecular simulation studies revealed that the II domain structure in the mutant variation 8 protein was more energy stable and compact throughout the simulation period. At positions LEU350, SER361, LEU378, and LEU556, 3% of the amino acids in the mutant domain modified their initial structure by more than 2 positions.

6.2.1 Parasporal proteins: anticancer biomolecules

6.2.1.1 New studies of the interaction of PS2Aa1 (Mpp46Aa1) with the cell-membrane receptor GPI-Ap

GPI-anchored proteins were confirmed to be expressed on four cell lines that exhibited differential cytotoxicity by parasporin 2. However, the expression of GPI-anchored proteins was similar in cells. Therefore, PS2 requires some GPI-anchored proteins for effective cytolysis [14]. We took this into account to start the new in silico phase using X-ray crystallography of GPI-Ap CD59 and PDB of PS2Aa1, recently named Mpp46Aa1, to generate the coordinate file for mutant N65, which has increased cytotoxic activity against various cancer cell lines. Furthermore, in the new molecular dynamics' simulations, at least one of the substitutions in N65 mutant parasporin was involved in interaction with CD59, to be more specific with the glycan core.

6.2.1.2 Colorectal cancer (CRC) as a target of Parasporin strategies

CRC is one of the leading causes of cancer mortality, responsible for 655.000 deaths per year worldwide [23]. In Colombia, incidence and deaths are also high. According to reports from the Global Cancer Observatory, the disease accounted for one-third of all cancer cases in both sexes and all age groups and had a significant psycho-affective, social, and economic impact, challenging the health system [24]. Current treatment of CRC relies mainly on surgery, chemotherapy, radiotherapy, and targeted therapy; thus, combining two or more approaches is often recommended.

The most optimal treatment approach depends on the stage of cancer development and the histopathological and clinical characteristics. Therapeutic agents for the treatment of CRC include cytotoxic agents (5-fluorouracil, oxaliplatin, capecitabine, and irinotecan), targeted therapies (antibodies against endothelial growth factor A –bevacizumab, and antibodies against epidermal growth factor receptor -cetuximab and panitumumab). In the 1980s, many scientists tested drug combinations with 5-fluorouracil (5-FU), and in the mid-1990s, the combination of 5-FU and leucovorin became a standard therapeutic

adjuvant for stage III CRC patients [25]. Furthermore, the addition of oxaliplatin to 5-FU and leucovorin soon improved survival rates compared with treatments containing only 5-FU and leucovorin. It argues for using combinations of therapeutic approaches with synergistic effects on CRC. However, these molecules and hybrids often exhibit low solubility and/or limited bioavailability and may induce toxic severe side effects on the gastrointestinal tract, bloodstream, nerves, heart, and skin. Therefore, there is a need to develop delivery systems for molecules and hybrids to achieve better therapeutic efficacy with fewer side effects [26].

As an alternative to synthetic active ingredients, in recent years, there has been a growth in the use of proteins and peptides as therapeutic molecules in drug development [27]. For example, the anticancer activity of PS proteins from Bt has been demonstrated, and genetic modification of PS can lead to molecules with improved anticancer action as a therapeutic alternative against CRC. However, in the case of oral administration, on its journey to the therapeutic target, these molecules are subject to enzymatic degradation, have a short half-life, display a limited permeability through biological membranes, and can provoke immune responses. Together, these diminish efficient and specific delivery [27], [28].

The use of nanosystems for the administration of active ingredients has been explored to transport anticancer agents as a treatment for CRC. Compared to conventional drug delivery, nanobioconjugates can be designed to protect drugs from first-pass metabolism and enzymatic degradation in the stomach and small intestine, which leads to an increase in the amount of drug available for localized release in the colon [29]. Currently, most drug-loaded nano Particles (NPs) have been designed for intravenous administration, accumulating in blood vessels and subsequently eradicating cancer cells [29], [30]. However, releasing NPs directly into the colorectal region can lower the physiological barriers to successfully targeted chemotherapy and improve the efficacy of the active ingredients proposed as a preventive and therapeutic strategy. Therefore, nanobioconjugates based on hybrids of molecules and PS and peptides should be developed to allow their site-specific delivery and targeting to optimize the treatment of CRC and protect interaction with the physiological environment to maintain their stability and reduce the immune response.

6.2.1.3 Personalized medicine using parasporins, and other molecules in the control of CRC

Under personalized medicine, avant-garde technologies, devices, therapeutic approaches, and practices are used according to the patient's particular biology and molecular basis as a more efficient and effective way to diagnose and intervene in the disease, especially cancer [31]. Personalized medicine is expected to play a fundamental role in assessing disease risk or predicting response to treatment to understand a person's health status and thus inform healthcare decisions. Unlike trial and error, once a disease is diagnosed, the best treatment alternative follows the statement "therapy with the right drug at the right dose for the right patient" [32], promoted by personalized medicine.

A potential treatment can be designed and tailored based on the patient's response, considering their genome and biology, and can therefore be more effective, precise, and profitable; this is an accepted practice within the concept of personalized medicine, which is on its way to replacing mass-produced single-dose or fixed-dose combinations of conventional treatments. In this context, the development of functional nanocarriers [29], [33], [34] for controlled, site-specific drug delivery is a branch of personalized medicine that promises to revolutionize healthcare. Developing therapeutic alternatives for CRC based on nanoconjugates of hybrid molecules and proteins could provide new avenues to fight this disease. However, advanced and consolidated knowledge regarding efficacy, mechanisms of action, biosafety, in vivo pharmacokinetics, and biodistribution of Parasporin PS2Aa1 and Hybrid 5-Fluoracil/Curcumin, will be necessary before they can be used against CRC as personalized medicine.

6.2.1.4 Variant 8 peptide-based nanoconjugates as a new resource

The mutations within variant 8 could make them an asset in preventing the spread of cancer, like their counterparts, the parasporins. It has also been shown that coupling nanomaterials to biomolecules can increase their activity and stabilization against cancer cell lines [9]. However, this part requires further studies.

Optimization of Cry proteins has led to a functional approach to increase their efficacy in targeting vectors that have shown low susceptibility and resistance to native Bt toxins over time, and even to solve problems that affect them, such as environmental conditions. Nanobioremediation techniques have contributed to the development of a new field of research based on interaction phenomena between nanomaterials and microorganisms, and the synthesis of nanoparticles is of great interest. [19]. The synthesis of bioconjugates has evolved through experiments on bioreduction and biosorption of nanomaterials by microorganisms that assimilate and/or reduce inorganic materials [22].

Variant 8 is the protagonist of the Cry part described in this work, and our in-depth work contributed to understanding how and why this protein has an enhanced effect in the control of mosquito disease vectors, but since this work, new approaches have emerged about the use of variant 8 in the control of cancer cell lines. The development and recovery of variant 8 peptides conjugated to nanoparticles as a new source for the control of cancer cell lines represents a novel and attractive approach.

6.3 References.

1. G. N. Pandian *et al.*, "Bombyx mori midgut membrane protein P252, which binds to Bacillus thuringiensis Cry1A, is a chlorophyllide-binding protein, and the resulting complex has antimicrobial activity," *Appl Environ Microbiol*, vol. 74, no. 5, pp. 1324–1331, 2008, [Online]. Available: http://www.ncbi.nlm.nih.gov/entrez/query.fcgi?cmd=Retrieve&db=PubMed&dopt=Citation&list_uids=18192432
2. N. M. Rosas-Garcia, M. Mireles-Martinez, J. L. Hernandez-Mendoza, and J. E. Ibarra, "Screening of cry gene contents of Bacillus thuringiensis strains isolated from avocado orchards in Mexico, and their insecticidal activity towards *Argyrotaenia* sp. (Lepidoptera: Tortricidae) larvae," *J Appl Microbiol*, vol. 104, no. 1, pp. 224–230, 2008, [Online]. Available: http://www.ncbi.nlm.nih.gov/entrez/query.fcgi?cmd=Retrieve&db=PubMed&dopt=Citation&list_uids=17887987
3. G. Sanahuja, R. Banakar, R. M. Twyman, T. Capell, and P. Christou, "Bacillus thuringiensis: a century of research, development and commercial applications," *Plant Biotechnol J*, vol. 9, no. 3, pp. 283–300, 2011, [Online]. Available: http://www.ncbi.nlm.nih.gov/entrez/query.fcgi?cmd=Retrieve&db=PubMed&dopt=Citation&list_uids=21375687

4. E. Moazamian, N. Bahador, N. Azarpira, and M. Rasouli, "Anti-cancer Parasporin Toxins of New *Bacillus thuringiensis* Against Human Colon (HCT-116) and Blood (CCRF-CEM) Cancer Cell Lines," *Curr Microbiol*, vol. 75, no. 8, pp. 1090–1098, 2018, doi: 10.1007/s00284-018-1479-z.
5. R. Ammons *et al.*, "Anti-cancer Parasporin Toxins are Associated with Different Environments: Discovery of Two Novel Parasporin 5-like Genes," *Curr Microbiol*, vol. 72, no. 2, pp. 184–189, 2016, doi: 10.1007/s00284-015-0934-3.
6. T. Akiba *et al.*, "Nontoxic crystal protein from *Bacillus thuringiensis* demonstrates a remarkable structural similarity to β -pore-forming toxins," *Proteins: Structure, Function and Genetics*, vol. 63, no. 1, pp. 243–248, Apr. 2006, doi: 10.1002/prot.20843.
7. Aldeewan, Y. Zhang, and L. Su, "Bacillus thuringiensis Parasporins Functions on Cancer Cells," *Int J Pure Appl Biosci*, vol. 2, no. 4, pp. 67–74, 2014.
8. O. Horstick, Y. Tozan, and A. Wilder-Smith, "Reviewing dengue: still a neglected tropical disease?," *PLoS Neg Trop Dis*, vol. 9, no. 4, p. e0003632, 2015, doi: 10.1371/journal.pntd.0003632
9. Thammasittirong, K. Prigyai, and S. N. R. Thammasittirong, "Mosquitocidal potential of silver nanoparticles synthesized using local isolates of *Bacillus thuringiensis* subsp. israelensis and their synergistic effect with a commercial strain of *B. thuringiensis* subsp. israelensis," *Acta Trop*, vol. 176, pp. 91–97, Dec. 2017, doi: 10.1016/j.actatropica.2017.07.020.
10. X. Pan *et al.*, "Adsorption of Insecticidal Crystal Protein Cry11Aa onto Nano-Mg(OH)₂: Effects on Bioactivity and Anti-Ultraviolet Ability," *J Agric Food Chem*, vol. 65, no. 43, pp. 9428–9434, Nov. 2017, doi: 10.1021/acs.jafc.7b03410.
11. R. Deist, M. A. Rausch, M. T.eresa Fernandez-Luna, M. J. Adang, and B. C. Bonning, "Bt toxin modification for enhanced efficacy," *Toxins (Basel)*, vol. 6, no. 10, pp. 3005–3027, 2014, doi: 10.3390/toxins6103005.
12. M. Florez *et al.*, "Toxic Activity, Molecular Modeling and Docking Simulations of *Bacillus thuringiensis* Cry11 Toxin Variants Obtained via DNA Shuffling," *Front Microbiol*, vol. 9, no. 2461, 2018, doi: 10.3389/fmicb.2018.02461.
13. Fernández-Chapa, J. Ramírez-Villalobos, and L. Galán-Wong, "Toxic Potential of *Bacillus thuringiensis*: An Overview," *Protecting Rice Grains in the Post-Genomic Era*, Jun. 2019, doi: 10.5772/INTECHOPEN.85756.
14. Okassov, A. Nersesyan, S. Kitada, and A. Ilin, "Parasporins as new natural anticancer agents: a review," *J BUON*, vol. 20, no. 1, pp. 5–16, 2015, [Online]. Available: <http://www.ncbi.nlm.nih.gov/pubmed/25778289>

15. W. P. Donovan, J. M. Gonzalez Jr., M. P. Gilbert, and C. Dankocsik, "Isolation and characterization of EG2158, a new strain of *Bacillus thuringiensis* toxic to coleopteran larvae, and nucleotide sequence of the toxin gene," *Mol Gen Genet*, vol. 214, no. 3, pp. 365–372, 1988, [Online]. Available: <http://www.ncbi.nlm.nih.gov/pubmed/3146015>
16. L. E. Fernandez *et al.*, "Cry11Aa toxin from *Bacillus thuringiensis* binds its receptor in *Aedes aegypti* mosquito larvae through loop alpha-8 of domain II," *FEBS Lett*, vol. 579, no. 17, pp. 3508–3514, 2005, [Online]. Available: http://www.ncbi.nlm.nih.gov/entrez/query.fcgi?cmd=Retrieve&db=PubMed&dopt=Citation&list_uids=15963509
17. L. E. Fernandez *et al.*, "Cloning and epitope mapping of Cry11Aa-binding sites in the Cry11Aa-receptor alkaline phosphatase from *Aedes aegypti*," *Biochemistry*, vol. 48, no. 37, pp. 8899–8907, 2009, doi: 10.1021/bi900979b.
18. L. E. Fernandez *et al.*, "Cloning and epitope mapping of Cry11Aa-binding sites in the Cry11Aa-receptor alkaline phosphatase from *Aedes aegypti*," *Biochemistry*, vol. 48, no. 37, pp. 8899–8907, Sep. 2009, doi: 10.1021/bi900979b.
19. S. Marimuthu, A. A. Rahuman, A. v Kirthi, T. Santhoshkumar, C. Jayaseelan, and G. Rajakumar, "Eco-friendly microbial route to synthesize cobalt nanoparticles using *Bacillus thuringiensis* against malaria and dengue vectors," *Parasitol Res*, vol. 112, no. 12, pp. 4105–4112, [Online]. Available: http://www.ncbi.nlm.nih.gov/entrez/query.fcgi?cmd=Retrieve&db=PubMed&dopt=Citation&list_uids=24013343
20. N. Banu, C. Balasubramanian, and P. v Moorthi, "Biosynthesis of silver nanoparticles using *Bacillus thuringiensis* against dengue vector, *Aedes aegypti* (Diptera: Culicidae)," *Parasitol Res*, vol. 113, no. 1, pp. 311–316, 2014, [Online]. Available: http://www.ncbi.nlm.nih.gov/entrez/query.fcgi?cmd=Retrieve&db=PubMed&dopt=Citation&list_uids=24173811
21. W. Rao *et al.*, "Flowerlike Mg(OH)₂ Cross-Nanosheets for Controlling Cry1Ac Protein Loss: Evaluation of Insecticidal Activity and Biosecurity," *J Agric Food Chem*, vol. 66, no. 14, pp. 3651–3657, Apr. 2018, doi: 10.1021/ACS.JAFC.8B00575/ASSET/IMAGES/LARGE/JF-2018-005754_0005.JPEG.
22. Prakash, S. Sharma, N. Ahmad, A. Ghosh, and P. Sinha, "Bacteria mediated extracellular synthesis of metallic nanoparticles," 2010. [Online]. Available: <http://www.interestjournals.org/IRJOB>
23. S. P. Chandran, S. B. Natarajan, S. Chandraseharan, and M. S. B. Mohd Shahimi, "Nano drug delivery strategy of 5-fluorouracil for the treatment of colorectal cancer," *Journal of Cancer Research and Practice*, vol. 4, no. 2, pp. 45–48, Jun. 2017, doi: 10.1016/J.JCRPR.2017.02.002.

24. M. L. Ospina M, J. A. Huertas, J. I. Montaña C, and J. C. Rivillas G, "Observatorio Nacional de Cáncer Colombia," *Revista Facultad Nacional de Salud Pública*, vol. 33, no. 2, pp. 262–276, Jun. 2015, doi: 10.17533/UDEA.RFNSP.V33N2A13.
25. Pardini *et al.*, "5-Fluorouracil-based chemotherapy for colorectal cancer and MTHFR/MTRR genotypes," *Br J Clin Pharmacol*, vol. 72, no. 1, p. 162, Jul. 2011, doi: 10.1111/J.1365-2125.2010.03892.X.
26. Y. H. Cho *et al.*, "5-FU promotes stemness of colorectal cancer via p53-mediated WNT/ β -catenin pathway activation," *Nature Communications* 2020 11:1, vol. 11, no. 1, pp. 1–13, Oct. 2020, doi: 10.1038/s41467-020-19173-2.
27. Q. Zhu, Z. Chen, P. K. Paul, Y. Lu, W. Wu, and J. Qi, "Oral delivery of proteins and peptides: Challenges, status quo and future perspectives," *Acta Pharm Sin B*, vol. 11, no. 8, pp. 2416–2448, Aug. 2021, doi: 10.1016/J.APSB.2021.04.001.
28. S. Marqus, E. Pirogova, and T. J. Piva, "Evaluation of the use of therapeutic peptides for cancer treatment," *J Biomed Sci*, vol. 24, no. 1, Mar. 2017, doi: 10.1186/S12929-017-0328-X.
29. Sánchez, S. P. Mejía, and J. Orozco, "Recent Advances in Polymeric Nanoparticle-Encapsulated Drugs against Intracellular Infections.," *Molecules*, vol. 25, no. 16, pp. E3760–E3760, Aug. 2020, doi: 10.3390/MOLECULES25163760.
30. Colorado *et al.*, "Metabolic Activity of Anthocyanin Extracts Loaded into Non-ionic Niosomes in Diet-Induced Obese Mice," *Pharm Res*, vol. 37, no. 8, Aug. 2020, doi: 10.1007/S11095-020-02883-Z.
31. V. Vásquez and J. Orozco, "Detection of COVID-19-related biomarkers by electrochemical biosensors and potential for diagnosis, prognosis, and prediction of the course of the disease in the context of personalized medicine," *Anal Bioanal Chem*, p. 1, 2022, doi: 10.1007/S00216-022-04237-7.
32. L. Mancinelli, M. Cronin, and W. Sadée, "Pharmacogenomics: the promise of personalized medicine," *AAPS PharmSci*, vol. 2, no. 1, pp. 29–41, 2000, doi: 10.1208/PS020104.
33. P. Mena-Giraldo, J. Orozco, K. Kumar Sadasivuni, T. Kovářík, and M. Planck, "Polymeric Micro/Nanocarriers and Motors for Cargo Transport and Phototriggered Delivery.," *Polymers (Basel)*, vol. 13, no. 22, pp. 3920–3920, Nov. 2021, doi: 10.3390/POLYM13223920.
34. S. P. Mejía, A. Sánchez, V. Vásquez, and J. Orozco, "Functional Nanocarriers for Delivering Itraconazole Against Fungal Intracellular Infections," *Front Pharmacol*, vol. 12, p. 1520, Jun. 2021, doi: 10.3389/FPHAR.2021.685391/BIBT

7. Appendices

7.1 Author affiliations

Miguel O. Suárez-Barrera¹⁻⁴

Lydia Visser¹

Anke van den Berg¹

Paola Rondón-Villarreal²

Efraín H. Pinzón-Reyes²

Jenniffer Cruz²

Nohora J. Rueda-Forero²

Diego F. Herrera-Pineda²

Juan S. Alarcón-Aldana²

Jahir Orozco³

Ernesto Moreno⁴

Alvaro Mauricio Florez⁵

Gloria M. Morales²

Karen Viviana Rivera²

Sergio Orduz⁶

Rodrigo Ochoa⁷

Diego Guerra⁷

Carlos Muskus⁷

Fanny Guzman⁹

[1] Department of Pathology and Medical Biology, University Medical Center Groningen, University of Groningen, Groningen, The Netherlands.

[2] Facultad de Ciencias Médicas y de la Salud, Instituto de Investigación Masira, Universidad de Santander, Bucaramanga, Colombia.

[3] Max-Planck Tandem Group in Nanobioengineering, Institute of Chemistry, Faculty of Natural and Exact Sciences, University of Antioquia, Medellin, Colombia;

-
- [4] Escuela de Medicina, Facultad de Salud, Universidad Industrial de Santander, Bucaramanga, Colombia.
- [5] Facultad de Ciencias Básicas, Universidad de Medellín, Medellín, Colombia.
- [6] RG Microbial Ecology: Metabolism, Genomics & Evolution, Microbiomas Foundation, Chía, Colombia.
- [7] Grupo Biología Funcional, Laboratorio de Prospección y Diseño de Biomoléculas, Escuela de Biociencias, Universidad Nacional, Sede Medellín, Colombia.
- [8] Programa de Estudio y Control de Enfermedades Tropicales PECET, Unidad de Biología Molecular y Computacional-UBMC, Universidad de Antioquía, Medellín, Colombia.
- [9] 4NBC Núcleo de Biotecnología Curauma, Pontificia Universidad Católica de Valparaíso, Campus Curauma, Av. Universidad 330, Valparaíso, Chile.

7.2 Acknowledgements

Well, we come to this part of the book, where all the people who accompanied me in this process are mentioned. Each step I have taken in my training as a **Ph.D.** is guided by several people who, in one way or another, have been elemental to get to my defence day.

I would like to begin this section by formally thanking all the members of my advisory committee, which includes my **tutors Jahir Orozco and Anke Van den Berg**, my **co-tutors Ernesto Moreno and Lydia Visser**, and my **asesors Ewing Duque and Tonny Naranjo**; for contributing to my education, for giving me the right advice, and for their commitment at every stage of my PhD. For your information, the work started about 4 years ago in Colombia, between my hometown Bucaramanga and Medellín.

So many experiences that I have had so far, all relevant, I have always been optimistic, and in the long run, I know that any experience collected contributes significantly to my life. To 'mi **mentor Lydia**. Where do I start? 2019 was the first time I met the one who today is a strong reference for me in terms of professional training as a leader. Thank you for everything I have learned from you for 3 years, for all those words of motivation, for being a constant guarantor in my evolution as a researcher, and for

teaching me not only to be a more self-critical and objective person with my work but also to be a better human being, rescuing from you values such as empathy, fairness, honesty, among others; in a world where values do not have much relevance in modern research, where this is usually left aside, due to the number of publications, ego, and journals to be published I appreciate your charisma and your humanity in the execution of science. To my **tutor, Anke**, thanks for the accompaniment from the beginning of my double degree at RUG, a commitment that has been working for 3 years, your character and objectivity in the construction of more solid scientific documents, as well as the detailed review of parts of experiments were of vital help in the creation of new knowledge embodied in this Book. To my **tutor, Jahir**, thank you for being part of my training as a guide and for your timely contributions and questions that gave way to the execution and design in decisive phases of the experimentation and analysis of results.

A special recognition to the Assessment Committee members Prof. **A.J. Moshage**, Prof. **J.M. van Dijl**, and Prof. **M.A. Bravo De La Parra**, for dedicating time and giving some valuable suggestions about the book.

To all the members of the **O and O Laboratory** of the UMCG, especially to **Bea Rutgers**, thank you for every teaching and for being a great teacher at many times. Your kindness is one of the best qualities I have seen in someone to my '*parcera*' **Nienke Smith**. Thank you for being my youngest teacher, thanks for your advice and friendship, "*We are the winner team*", for those pleasant talks, and for always being willing to help me. Some time ago, a student of mine said, "*Anyone who teaches you something, and you learned it, this person becomes your teacher*", you are and always will be my teacher.

To my dear Ph.D. colleagues and friends **Marcelo, Nick, Weiting, Xing, Zainab, Penny**, and **Yuji**, thank you for those talks and good times shared, for going out, and for sharing recipes and sweets from time to time.

To my co-workers in Colombia who, at the same time, have the fortune to be my friends **Paola** and **Hernando**, thank you for all that hard work, for believing in this project, for your friendship, and for being there in every moment I have travelled for years. You are always in my heart for being part of my life and, more importantly, being there when I need someone the most. To my Foshis, **Nohora**, I do not know what would become of me without the presence of your life in mine since we were two teenagers full of goals and

dreams. We have shared this path. I owe you a lot, and I know that none of this would be happening without you in my life. Thank you for always believing in me, never losing trust, supporting me unconditionally, and being a professional and personal role model. To the entire **BIOMOL** team, a special thanks.

To my '*parceros*' **Rodrigo**, **Gonzalo**, and **Roza**, thank you for giving me your friendship, for having become people I can trust in many ways, and for sharing many experiences. To **Rodrigo**, I wish you the best in your life in Groningen. I always go to every moment of chat and support, my first friend in this city of bicycles and Stroop waffles. To **Gonzalo**, whom I met two years ago, thank you for spreading that joy, for teaching me the value of friendship, and even more so in being able to learn to continue maintaining that soul of a child that we all must preserve regardless of the time lived. Thanks to **Roza** for always having something to talk about and for taking an interest in my things, my friend, thanks for those outings, like the one on King's Day; that one is unforgettable. I will never forget that the end of my life as a Ph.D. student is not the end of our friendship. Finally, to my '*cariñin*', **Karime** thank you for being my friend in European adventures and beyond. To your family, a warm hug; I always feel at home in Switzerland, and to **my Family**, especially to my parents **Orlando** and **Claudia**, who are mainly responsible for my achievements, thank you for always guiding me on this path and for being part of me despite the distance, this achievement is for you, for those who live in my heart even if I cannot see you.

Last but not least, thanks to **one of my favourite people**, none of this would be happening without you. I owe you practically everything. I must confess that I still think of you. You appear in my dreams, memories of when we went out to conquer the world, living every second as if it were the last, risky, without fear of consequences. You don't know how much I miss you. Sometimes I want to have fun like before, but I know that everything is better this way. I feel very proud of you, as you will be when you read this paragraph and know I achieved it.

To all the people who believed in me and still... '*Gracias*'.

7.3 About Me: Miguel Orlando Suárez Barrera (MOSB)

I was born on October 3rd, 1986 in Bucaramanga Colombia. I began my studies at the Universidad de Santander UDES as an industrial microbiologist, graduating in 2009, and from that point, I began my career as a researcher working with *Bacillus thuringiensis* and as a university professor. In 2016, I graduated with a master's degree in basic biomedical sciences, and a new phase of my life began. I worked at other universities, served as a training member for the Colombian government on biosafety topics, and received several national awards and grants. I continued my studies on site-directed mutagenesis of Cry proteins and published several mutant proteins that serve as models to consolidate this model of biocontrol of mosquitoes transmitting tropical diseases and authored academic articles about its mechanism of action.

At the same time, I participated in *quorum sensing* inhibition work using enzymes extracted from *Bacillus thuringiensis* to control multidrug-resistant bacteria, identifying microbiomes of different soils for tropical fruit cultivation, and participating in bio-projects on remediation and bioremediation. In 2018 I started my Ph.D. studies at the Universidad de Antioquia U.de.A with a project on anticancer proteins from *Bacillus thuringiensis* called Parasporins. This project is part of the most ambitious initiative of the Colombian Ministry of Science and Technology that aims to find and design new molecules to treat colorectal cancer. This program was called NanoBiocancer. After two years, I started my double Ph.D. at the University of Groningen RUG, where I worked in the Department of Pathology and Biological Medicine, where I conducted my studies on new *Bacillus thuringiensis* proteins and their activity in different cancer cell lines, their characterization, and construction of models for the initiation of possible steps in the mechanism of action. Nowadays, I am the PI of a new project funded by the Colombian government focused on the continuation of parasporin-mutated proteins, the target of this call is the creation of combinatory treatments between the parasporin and other natural molecules, including plant and fungi, reaching future preclinic assays on mice, all these directed in the control of colorectal cancer. I am preparing myself to receive next year a position as the director of the '*grupo de Biología molecular y Biotecnología de la Universidad de Santander*', and the head teacher of the laboratory under the same name. Additionally, I will participate in

different projects with the Colombian government related to training, conferences, and workshops on different topics.

7.4 Funding

This work has been funded by MINCIENCIAS, MINEDUCACIÓN, MINCIT, and ICETEX, through the Program Ecosistema Científico Cod. FP44842-211-2018 Project number 58668: Characterization and structural analysis of new parasporins derived from PS2Aa1 obtained by directed evolution.

This thesis was financially supported by the University of Groningen and the **Graduate School of Medical Sciences, University of Groningen.**

7.5 List of publications

Suárez-Barrera, M.O.; Herrera-Pineda, D.F.; Rondón-Villarreal, P.; Pinzón-Reyes, E.H.; Ochoa, R.; Visser, L.; Rueda-Forero, N.J. Toxic Determination of Cry11 Mutated Proteins Obtained Using Rational Design and Its Computational Analysis. *Int. J. Mol. Sci.* **2023**, *24*, 9079. <https://doi.org/10.3390/ijms24109079>

Suárez-Barrera, M.O.; Visser, L.; Pinzón-Reyes, E.H.; Rondón Villarreal, P.; Alarcón-Aldana, J.S.; Rueda-Forero, N.J. Site-Directed Mutants of Parasporin PS2Aa1 with Enhanced Cytotoxic Activity in Colorectal Cancer Cell Lines. *Molecules* **2022**, *27*, 7262. <https://doi.org/10.3390/molecules27217262>

Suárez-Barrera, M.O.; Visser, L.; Rondón-Villarreal, P.; Herrera-Pineda, D.F.; Alarcón-Aldana, J.S.; Van den Berg, A.; Orozco, J.; Pinzón-Reyes, E.H.; Moreno, E.; Rueda-Forero, N.J. Genetic Modification Approaches for Parasporins *Bacillus thuringiensis* Proteins with Anticancer Activity. *Molecules* **2021**, *26*, 7476. <https://doi.org/10.3390/molecules26247476>

Jenniffer Cruz, Miguel Orlando Suárez-Barrera, Paola Rondón-Villarreal, Andrés Olarte-Díaz, Fanny Guzmán, Lydia Visser, Nohora Juliana Rueda-Forero; Computational study, synthesis, and evaluation of active peptides derived from Parasporin-2 and spike

protein from Alphacoronavirus against colorectal cancer cells. *Biosci Rep* 22 December 2021; 41 (12): BSR20211964. doi: <https://doi.org/10.1042/0BSR20211964>

7.6 Other publications derived from the work.

Pinzón-Reyes EH, Sierra-Bueno DA, Suarez-Barrera MO, Rueda-Forero NJ, Abaunza-Villamizar S, Rondón-Villareal P. Generation of Cry11 Variants of *Bacillus thuringiensis* by Heuristic Computational Modeling. *Evolutionary Bioinformatics*. 2020;16. doi:10.1177/1176934320924681

Mantilla K, Suárez-Barrera M, Rueda-Forero NJ, Guarín OD, Gómez FR, Durán SM, et al. Characterization of biodeteriorating microorganisms in buildings in Bucaramanga, Colombia. *J Phys Conf Ser*. 2019;1386:12104

Florez AM, Suarez-Barrera MO, Morales GM, Rivera KV, Orduz S, Ochoa R, et al. Toxic activity, molecular modeling and docking simulations of *Bacillus thuringiensis* Cry11 toxin variants obtained via DNA shuffling. *Front Microbiol*. 2018 Oct 17;9(OCT):2461.

Pinzon, E.H., Sierra, D.A., Suarez, M.O. et al. DNA secondary structure formation by DNA shuffling of the conserved domains of the Cry protein of *Bacillus thuringiensis*. *BMC Biophys* **10**, 4 (2017). <https://doi.org/10.1186/s13628-017-0036-7>

7.7 Paper: Toxic Activity, Molecular Modeling and Docking Simulations of *Bacillus thuringiensis* Cry11 Toxin Variants Obtained via DNA Shuffling

Alvaro Mauricio Florez
Miguel Orlando Suarez-Barrera
Gloria M. Morales
Karen Viviana Rivera
Sergio Orduz
Rodrigo Ochoa
Diego Guerra
Carlos Muskus

Frontiers in Microbiology

2018 9:2461 doi: 10.3389/fmicb.2018.02461

Author Contributions: AF conceived the study, was in charge of overall direction and planning and wrote the manuscript with input from all authors. MS-B carried out the experiments and worked out almost all of the technical details. GM performed directed evolution techniques and sequencing analysis. KR assisted with MS-B measurements and bioassays. SO contributed to electronic microscopy analysis and devised the project. RO carried out the molecular docking analysis. DG contributed to the analysis of 3D structure prediction and validation and secondary structure analysis of non-conserved regions. CM contributed to the interpretation of the 3D structure prediction and docking results. **Funding:** This work was supported by grants from the Colombian Department of Science, Technology and Innovation, COLCIENCIAS, 1299-12-16813 and 5201-545-31565

7.7.1 Abstract

The Cry11 family belongs to a large group of δ -endotoxins that share three distinct structural domains. Among the dipteran-active toxins referred to as three-domain Cry11

toxins, the Cry11Aa protein from *Bacillus thuringiensis* subsp. *israelensis* (Bti) has been the most extensively studied. Despite the potential of Bti as an effective biological control agent, the understanding of Cry11 toxins remains incomplete. In this study, five Cry11 variants obtained via DNA shuffling displayed toxic activity against *Aedes aegypti* and *Culex quinquefasciatus*. Three of these Cry11 variants (8, 23, and 79) were characterized via 3D modeling and analysis of docking with ALP1. The relevant mutations in these variants, such as deletions, insertions and point mutations, are discussed in relation to their structural domains, toxic activities and toxin-receptor interactions. Importantly, deletion of the N-terminal segment in domain I was not associated with any change in toxic activity, and domain III exhibited higher sequence variability than domains I and II. Variant 8 exhibited up to 3.78- and 6.09-fold higher toxicity to *A. aegypti* than Cry11Bb and Cry11Aa, respectively. Importantly, variant 79 showed an α -helix conformation at the C-terminus and formed crystals retaining toxic activity. These findings indicate that five Cry11 variants were preferentially reassembled from the cry11Aa gene during DNA shuffling. The mutations described in loop 2 and loop 3 of domain II provide valuable information regarding the activity of Cry11 toxins against *A. aegypti* and *C. quinquefasciatus* larvae and reveal new insights into the application of directed evolution strategies to study the genetic variability of specific domains in cry11 family genes.

Keywords: *Bacillus thuringiensis*, Cry11, DNA shuffling, docking, *Aedes aegypti*, *Culex quinquefasciatus*

7.7.2 Introduction

Bacillus thuringiensis (Bt), a Gram-positive bacterium characterized by the production of Cry δ -endotoxins capable of killing insects, has been used since the late 1930s as a biological control agent (Melo et al., 2016). A total of 308 holotype toxins are clustered into 75 Cry proteins (Crickmore et al., 2014) (revised February, 2018). The tertiary structures of nine Cry toxins determined via X-ray crystallography to date contain three conserved domains with specific functions and implicated in the structural stability of the protein. The domain I is a bundle of 7–8 α helices involved in pore formation, domain II is a β -prism with exposed loops regions involved in receptor binding and, domain III is

a β -sandwich and has influence on receptor binding, ion channel formation and insect specificity (Li et al., 1991; Grochulski et al., 1995; Derbyshire et al., 2001; Galitsky et al., 2001; Morse et al., 2001; Guo et al., 2009; Hui et al., 2012; **Figure 1A**).

The mechanisms by which *Bt* induces death in insects are controversial and have not been completely elucidated (Vachon et al., 2012). Currently, there are two mechanisms related to *Bt*- induced toxicity in insects that have been accepted; the sequential binding and signaling pathways (Zhang Q. et al., 2017). The sequential binding mechanism has been extensively studied and is based on the formation of pores in epithelial cells in the midgut of targeted insects, which results in toxin-receptor interactions, osmotic imbalance and cell death (Bravo et al., 2007; Pardo- Lopez et al., 2013). After crystal ingestion, Cry toxins become solubilized, and specific proteases present in the lumen of the midgut activate the toxins, which then bind to specific receptors located in the insect midgut. In some Cry toxins, this event induces the proteolytic removal of helix $\alpha 1$ (Aronson, 2000), triggering Cry toxin oligomerization, insertion of oligomeric structures altering membrane stability, receptor and production of channels or pores, ultimately leading to cell lysis and insect death (Bravo et al., 2004; **Figure 1B**). The signaling pathways is a recent proposed mechanism in which the activation of signaling cascades, leads to increased cyclic AMP and protein kinase activities, resulting in cell death (Zhang et al., 2006). Both of these mechanisms contain gaps. In the sequential binding mechanism, the presence of several types of resistance and the link between proteolysis and pore formation are not understood (Melo et al., 2016). In the signaling pathway mechanism, how Cry toxin-receptor interactions mediate toxic activity is unclear (Melo et al., 2016). In this context, it has been suggested that Cry toxins can cause death based on their ability to induce both pore formation and ion channel activation (Zhang Q. et al., 2017).

The pBtoxis megaplasmid from *Bt* subsp. *israelensis* (*Bti*) contains four Cry proteins encoded by the *cry4Aa*, *cry4Ba*, *cry10Aa*, and *cry11Aa* genes and two Cyt proteins encoded by the *cyt1Aa* and *cyt2Ba* genes (Berry et al., 2002). The *cry* genes produce 134, 128, 78, and 72 kDa polypeptides, respectively, all of which possess larvicidal activity higher than of the Cyt's proteins (Ben-Dov, 2014). However, the high toxic activity of *Bti* is the result of synergistic interactions between all of them (Ben-Dov,

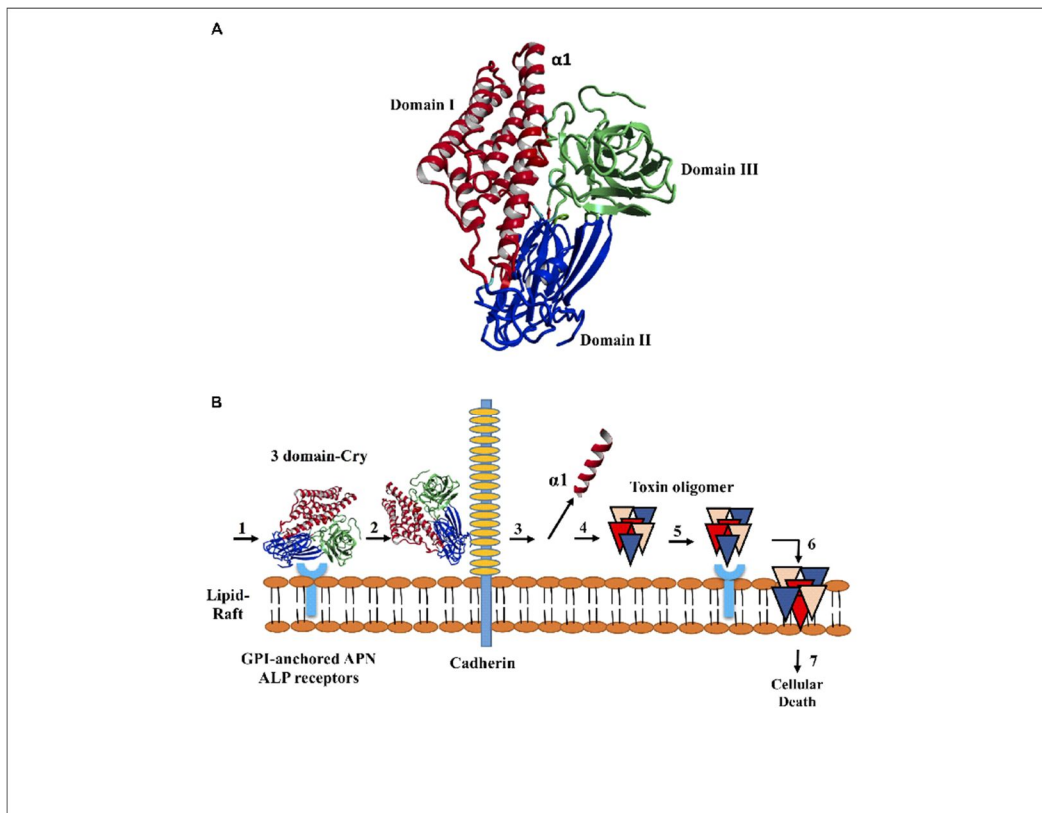
2014). That is the case of Cyt1Aa that despite the low toxicity, it is highly synergistic with *Bti* Cry toxins and aids to overcome resistance in mosquitoes to Cry toxins (Wirth et al., 1997). Due to the synergistic interactions of *Bt* subsp. *israelensis* toxins, this bacterium has been used worldwide to control mosquito larvae of the genera *Aedes*, *Culex* and *Anopheles*, which are involved in the transmission of diseases including malaria, hemorrhagic fever, dengue fever, lymphatic filariasis, yellow fever (Ben-Dov, 2014), Chikungunya and Zika (Chouin- Carneiro et al., 2016; Gardner et al., 2016; Tsetsarkin et al., 2016).

Cry11Aa from *Bti* is a 72 kDa protoxin that is activated by gut enzymes via the proteolytic removal of 28 residues from its N-terminus and proteolytic cleavage into two fragments of 38 and 30 kDa that remain associated and retain toxicity (Dai and Gill, 1993; Revina et al., 2004; de Barros Moreira Beltrao and Silva-Filha, 2007). The Cry11Aa toxin has higher activity against *Aedes* and *Culex* than against *Anopheles* (Revina et al., 2004; Otieno-Ayayo et al., 2008). In *A. aegypti*, this toxin interacts with two midgut brush border membrane receptors; a GPI anchored and alkaline phosphatase (ALP1) (Fernandez et al., 2006) and also binds to Cyt1Aa as a kind of membrane-bound receptor of Cry11Aa increasing the toxic activity (Perez et al., 2005). Other midgut proteins different to the receptor alkaline phosphatase (ALP1) such as ATP binding protein, increases the toxicity of Cry11Aa against *C. quinquefasciatus* (Zhang L. et al., 2017). Other two toxins, Cry11Bb (94 kDa) and Cry11Ba (81 kDa), share a similar insect specificity and are phylogenetically related to Cry11Aa. Cry11Bb and Cry11Ba are produced by *Bt* subsp. *medellin* and *Bt* subsp. *jegathesan*, respectively (Delecluse et al., 1995; Orduz et al., 1998).

Although the tertiary structure of Cry11 toxins have not been determined by X-ray crystallography, Cry11Aa have been the most studied among this group using protein engineering tools. Several mutations haven been introduced into different domains that are implicated in its toxicity. Therefore, studies have focused on domain I developing N-terminally truncated forms of Cry11Aa (Pang et al., 1992) or modifications in domains II and III altering the interactions with its receptor in the midgut, confirming the importance of these domains for Cry11Aa-mediated toxicity (Fernandez et al., 2005, 2009). Based on phage display libraries and site-directed mutagenesis, the exposed regions of loop α 8, β 4 and loop 3 in domain II of Cry11Aa have been shown to be involved in the interaction of

Cry11Aa with *A. aegypti* brush border membrane vesicles (BBMVs). Specifically, two mutations in loop $\alpha 8$, V262E and E266A, reduced the toxic activity of Cry11Aa against *A. aegypti* (Fernandez et al., 2005). There are also mutations in loop α -8 that are involved in Cry11Aa–ALP1 receptor interaction, that affect the Cyt1Aa and Cry11Aa interaction reducing the synergism between these proteins and decreasing their toxic activity (Perez et al., 2005). Other binding sites have been described for the interaction of Cry11Aa with the receptor ALP1 as an important secondary receptor for Cry11Aa and Cry11Ba (Chen et al., 2017). The involved regions are located in loop 2 of domain II and $\beta 18$ – $\beta 19$ of domain III of Cry11Aa, which interact with ALP1 regions R⁵⁹–G¹⁰² and N²⁵⁷–I²⁹⁶, respectively (Fernandez et al., 2009).

Figure 36. Structure of the Cry toxins, domains, and their mode of action. (A) Ribbon diagram of Cry deduced 3D structure. Three domains are colored in red blue and green, respectively. (B) Sequential binding mechanism. 1. The toxin binds to GPI-anchored APN and ALP receptors in the lipid rafts; 2. Binding to cadherin receptor 3. Proteolytic cleavage of the helix $\alpha 1$ at N-terminal end; 4. N-terminal cleavage induces the formation of pre-pore oligomer 5. Increasing of the oligomer binding affinity to GPI-anchored APN and ALP receptors; 6. Oligomer inserts into the membrane, leading to pore-formation and cell lysis; and 7. Cellular death.



Since the three Cry11 toxins are phylogenetically related and exhibit similar specificity to insect species, it is possible to infer similarities at structural level that can be analyzed after mixing their genes in order to create novel proteins with improved properties. Therefore, considering the lack of studies focused on this approach, we designed a DNA shuffling strategy to obtain variants with increased toxicity to *A. aegypti* and *C. quinquefasciatus*. DNA shuffling has been used alone or in combination with phage display and the staggered extension process via homologous recombination to increase the activity of Cry toxins against specific insect pests (Lucena et al., 2014). This technique is a powerful approach based on recombination between parental genes in a single DNA shuffling reaction following random fragmentation (Stemmer, 1994).

Here, we report five variants that were reassembled from the *cry11Aa* gene that exhibit from moderate to high toxic activities against *A. aegypti* and *C. quinquefasciatus* mosquito larvae. Variant 8 was the most toxic to the mosquito larvae, and variants 23 and 79 displayed important differences in 3D structure, toxin-ALP1 interactions and toxicity in which are implicated domains II and III preferably.

7.7.3 Materials and methods

7.7.3.1 Microbial Strains, Clone Selection and Gene Constructs

For DNA manipulation, *Escherichia coli* DH5 α , JM109 (Promega) and DH5 α TOP10 $\text{\textcircled{C}}$ (Life Technologies) cells were grown at 37°C in Luria Bertani (LB) culture medium supplemented with ampicillin (50 $\mu\text{g/ml}$) and X-gal (50 mg/ml). A Bt 4Q2-81 strain carrying the pBTM3 plasmid and expressing the *cry11Bb* gene from Bt subsp. medellin (Restrepo et al., 1997) and a second Bt 4Q2-81 strain carrying the pJEG90.1 plasmid and expressing the *cry11Ba* gene from Bt subsp. jegathesan (Delecluse et al., 1995) were cultured as previously described (Restrepo et al., 1997) in M1 medium supplemented with 30 $\mu\text{g/ml}$ tetracycline and 20 $\mu\text{g/ml}$ erythromycin. Crystal production was evaluated via phase contrast microscopy. *E. coli* DH5 α cells harboring the pSV2 plasmid, which carried the p19 gene upstream of *cry11Aa* from *Bt subsp. israelensis*, were cultured in M1 medium supplemented with 20 $\mu\text{g/ml}$ chloramphenicol; this strain was obtained from Dr.

Neil Crickmore from the University of Sussex. The pTOAa, pTOBa-1, pTOBa-2, and pTOBb plasmids carrying the *cry11Aa*, *cry11Ba-1*, *cry11Ba-2*, and *cry11Bb* genes, respectively, were amplified via PCR and cloned using the TOPO TA Cloning® system (Life Technologies) (**Supplementary Table 1**). To obtain pGEBb-1, the pTOBb vector was digested with *EcoRI* and *BamHI*, releasing an insert of 3.5 kb that was ligated into pGEM7zf (+) (Promega). The DNA shuffling library was cloned into the TA TOPO cloning system. Selected variants were subcloned into the pSV2 expression vector using *HindIII* and *SacI* and transformed into BMB171 cells in LB supplemented with 6 µg/ml chloramphenicol. The acrysaliferous strain BMB171 was used to produce the variants and was donated by Dr. Ziniu Yu from the State Key Laboratory of Agricultural Microbiology, Huazhong Agriculture University, Wuhan, Hubei, China.

7.7.3.2 Isolation of *cry11* Genes via PCR

The *cry11* genes were amplified via PCR using specific primers and plasmid DNA from constructs pBTM3, pSV2 and pJEG90.1 as templates. Briefly, reactions were conducted in a final volume of 50 µl that contained 20 ng of plasmid DNA, 0.5 µM primers, 1× *Taq* polymerase buffer, 0.4 mM dNTPs, 1.5 mM MgCl₂ and 0.5 U *GoTaq* polymerase (Promega). The amplification conditions were denaturation at 94°C for 5 min followed by 35 cycles of 45 s at 94°C, 45 s at 55°C, and 4 min 30 s at 72°C, and a final extension at 72°C for 10 min. The PCR products were separated via electrophoresis and purified using the PCR Clean- Up System (Promega). The *cry11Ba* gene was obtained via two independent PCRs, producing a 1.8-kb product (denoted Ba1) corresponding to *cry11Ba* with a deletion of 246-bp downstream of the ATG start site and a 0.9-kb fragment (denoted as Ba-2) that contained a 0.75-kb fragment of *cry11Ba* including the stop codon and a 249-bp segment homologous to the multiple cloning site (MCS) of the pHT315 shuttle vector.

7.7.3.3 *cry11* Gene Cloning, Insert Validation, and Sequencing

The *cry11* genes obtained via PCR were cloned using the TOPO TA system. Recombinant variants for each product were selected, and plasmid DNA was extracted using the Wizard Plus Minipreps kit (Promega). Verification of each insert was performed via digestion of 50 ng of DNA with *EcoRI*, followed by separation via agarose gel electrophoresis. The released inserts were also used as templates for PCR to confirm the presence of the *cry11* genes in the inserts. Each reaction was conducted in a final volume of 25 μ l that contained 0.4 μ M each of the forward primer 5'-TTAGAAGATACGCCAGATCAAGC-3' and the reverse primer 5'-CATTGTACTTGAAGTTGTAATCCC-3' (Bravo, 1997; Bravo et al., 1998) in 1 \times *Taq* polymerase buffer, 0.4 mM dNTPs, 2.5 mM MgCl₂ and 0.12 U *GoTaq* polymerase. The amplification conditions were 5 min at 94°C followed by 35 cycles of 45 s at 94°C, 45 s at 51°C, and 1 min at 72°C and a final extension step of 6 min at 72°C. pTOAa containing a 2.5-kb insert, pTOBa-1 containing a 1.6-kb insert, pTOBa-2 containing a 0.78-kb insert and pTOBb containing a 3.5-kb insert were sequenced by MacroGen, Inc. (Seoul, South Korea) using M13/T7 primers and the primer pair pCR4F (5'-GATAACAATTTACACAGGA-3') and pCR4R (5'-TTGTAAAACGACGGCCAGTG-3').

7.7.3.4 Test Primers for Reassembly via PCR

The pTOAa, pTOBa-1 and pTOBa-2 constructs were used as templates in 50- μ l PCRs that contained 0.32 μ M PCR4 primers as described in **Supplementary Table 1**, 1 \times *Pfx* polymerase buffer, 0.4 mM dNTPs, 2.5 mM MgCl₂ and 0.5 U *Pfx50* polymerase (Life Technologies) in 1 \times reaction buffer that contained 1 mM MgSO₄. The amplification conditions were denaturation at 94°C for 4 min followed by 35 cycles of 45 s at 94°C, 45 s at 59–67°C, and 4 min 30 s at 68°C and a final extension step of 10 min at 68°C. The PCR products were separated via electrophoresis and purified using the Wizard purification system (Promega). To generate the pGE7 construct, 50 ng of pGEBb-1 plasmid DNA was used as a template. The PCR was performed in a final volume of 50 μ l that contained 0.32 μ M of each primer as described in **Supplementary Table 1**, 1 \times *Pfx* polymerase buffer,

0.3 mM dNTPs, 1 mM MgSO₄ and 0.5 U *Pfx50* polymerase. The PCR conditions were denaturation for 4 min at 94°C followed by 35 cycles of 94°C for 45 s, 68°C for 45 s, and 68°C for 4 min 30 s and a final extension step at 68°C for 10 min. The PCR products were separated via agarose gel electrophoresis and purified using the Wizard® SV Gel and PCR Clean-Up System (Promega).

7.7.3.5 DNA Shuffling

Three micrograms of each PCR product obtained from the TA cloning constructs and from pGEBb with lengths of 2.5 kb (*cry11Aa*), 1.6 kb (*cry11Ba-1*), 0.78 kb (*cry11Ba-2*), and 3.5 kb (*cry11Bb*) were mixed in 25 µl of 50 mM Tris–HCl, pH 7.4, and 10 mM of MnCl₂. In the same tube, 0.0006 U DNase I (Life Technologies) was added to a final volume of 50 µl. The reaction was incubated between 5 and 20 min at room temperature to optimize production of fragments ranging between 25 and 250 bp. The reaction was stopped by adding 25 µl of 25 mM EDTA. The DNase I digestion products were separated via electrophoresis and purified with the QIAEX II Gel Extraction Kit (QIAGEN). Forty microliters of the pooled of purified fragments were used as template for a PCR without primers in 1× *Pfx* buffer, 0.3 mM dNTPs, and 2.5 U *Pfx50* polymerase in a final volume of 50 µl under the following conditions: 94°C for 3 min, 45 cycles of 94°C for 30 s, 48°C for 3 min and 68°C for 1 min (with a 12-s increase in extension time per cycle), and a final extension step at 68°C for 7 min. The products for reassembly were validated via agarose gel electrophoresis and purified using the Wizard PCR Clean-Up system.

The full-length sequences were amplified using two sets of primers, PCR4F/R and PGE7F/R, and the combination of these primers, PCR4F/PGE7R, along with a template of 1 µl of the products of the primerless PCR, to a final volume of 50 µl. The PCR was conducted in 1× *Pfx50* buffer, 0.3 µM dNTPs, 0.3 µM primers, and 5 U *Pfx50* under the following conditions: 4 min at 94°C, 25 cycles of 94°C for 45 s, 55°C for 1 min, and 68°C for 4 min (with a 20-s increase in extension time per cycle), and a final extension step at 68°C for 10 min. The second PCR product, corresponding to the DNA shuffling product, was analyzed via agarose gel electrophoresis and purified using the Wizard PCR Prep DNA Purification System.

7.7.3.6 Cloning, DNA Sequencing and Homology Analysis

The shuffled PCR products were cloned using the TOPO Zero Blunt PCR cloning kit (Life Technologies) according to the manufacturer's instructions and chemically competent *E. coli* DH5 α TOP10 cells (Life Technologies). Sequencing data were used to select clones according to their open reading frame (ORF) and DNA identity to the parental genes. Plasmid DNA from each clone was isolated using a Wizard Minipreps kit, and the DNA was sent to Macrogen, Inc., South Korea, for sequencing. The forward and reverse primers used for sequencing were as follows: M13 forward (-20): 5'-GTAAACGACGGCCAG-3'; M13 reverse, 5'-CAGGAAACAGCTATGAC-3'. Gene homology analysis was performed using BLASTn and BLASTx, available at¹. Sequence alignments were performed using ClustalW (Thompson et al., 1994), available on the web².

7.7.3.7 Transformation of *Bacillus thuringiensis*

The PCR products were cloned using TOPO Zero Blunt PCR cloning kit and then subcloned into the pSV2 expression vector using *Hind*III and *Sac*I. The resulting vectors were transformed into BMB171 cells via electroporation using a Bio- Rad MicropulserTM. BMB171 cells were grown in LB-glycine 0.12% up to an OD₆₀₀ of 0.15, corresponding to the early exponential phase, and then transformed with 500 ng of the constructs. The electroporation conditions were 2 kV/cm, 200 μ s, and 25 μ F for 4 ms. Transformed cells were revitalized via

incubation in 500 μ l of LB for 2 h at 30°C at 50 rpm. Two hundred microliters of transformed cells were plated on 60-mm Petri dishes containing LB agar supplemented with 6 μ g/ml chloramphenicol. Colony counts and percent efficiency of transformation were calculated after 48 h. Endospore and crystal formation was evaluated via scanning electron microscopy (SEM).

7.7.3.8 Cultures, Solubilization, Cry Protein Quantification, and SDS–PAGE

Cultures expressing variants 1, 8, 23, 79, and 81 and recombinant Cry11Aa and Cry11Bb, including the *Bt* acrystiferous BMB171 strain, were grown in 10 ml of LB supplemented with chloramphenicol (6 µg/ml) for 7 days at 30°C and 300 rpm. After 48 h of incubation, the culture purity was confirmed via microscopic observation of spores, crystals, and lysed cells. The final culture was collected via centrifugation at 11,200 × *g* for 15 min at 4°C. The supernatant was discarded, and 1 ml of 1 M NaCl was added to the pellet, which was shaken for 1 h at 30°C and 50 rpm to neutralize protease activity. Then the suspension was washed twice with 1 ml of 1× PBS and centrifuged at 11,200 × *g* for 5 min at 4°C. The number of spores was determined via heat shock using 100 µl of each culture and incubated at 72°C for 20 min. Afterward, the samples were incubated at 4°C for 10 min and were diluted by 10⁻¹ to 10⁻⁵ in a final volume of 100 µl. The dilutions were plated on LB agar supplemented with chloramphenicol (6 µg/ml) and incubated at 30°C for 24 h. To quantify Cry protein production, 200 µl of the final sporulated culture of each variant was solubilized by adding 800 µl of solubilization buffer (50 mM NaOH, 10 mM EDTA, pH 11.7), incubating the culture at 4°C overnight and centrifuging the culture at 25,200 × *g* for 1 h at 4°C. The supernatant was collected, and the volume was adjusted to 1 ml with Tris-base (0.1 M, pH 7.4). The protein concentration was determined using the Bradford protein assay (Bradford, 1976) and was confirmed via SDS–PAGE using bovine serum albumin (BSA) as a standard.

1<http://blast.ncbi.nlm.nih.gov/Blast.cgi>

2<http://www.expasy.org>

3<https://www.r-project.org/>

4<http://zhanglab.ccmb.med.umich.edu/I-TASSER/>

The protein samples were electrophoresed on 10% SDS–PAGE gels at 80 V for 90 min using a Bio-Rad mini protein system (Bio- Rad Laboratories). A total of 5 µg of protein was loaded per lane, and the protein bands were visualized by staining with Coomassie Brilliant Blue R-250 solution for 30 min.

7.7.3.9 SEM

The final cultures were centrifuged at $11,200 \times g$ at 4°C for 10 min, and the precipitate was washed twice in $1\times$ PBS. The pellet was resuspended in 1/10 of the original volume, and 100 μl of the samples were placed on glass slides and dried overnight at room temperature. The samples were coated with a thin layer of gold on a Denton Desk Vacuum IV and analyzed using a JEOL JSM 5010 LV scanning electron microscope.

7.7.3.10 Half Lethal Concentration (LC_{50}) in *A. aegypti* and *C. quinquefasciatus* Larvae

Each bioassay consisted of two replicates using spore/crystal suspensions, each with 30 first instar larvae in 1 ml at 24°C for each variant at 7 different concentrations under the same environmental conditions. A total of 420 larvae were used for each variant. Larval mortality was determined by counting the number of live larvae after 24 and 48 h, and 50% lethal concentrations were determined statistically via Probit analysis which employ a transformation from sigmoid dose-response curve to a straight linear and then analyzed by a regression on the relationship. The calculation of the average lethal concentration (LC_{50}) was made using the R-Project Software³.

7.7.3.11 3D Structure Prediction and Validation and Secondary Structure Analysis of Non-conserved Regions

The amino acid sequences of parental Cry11Aa and variants 8, 23, and 79 were modeled via threading methodology using the free local server I-TASSER⁴. From the five models obtained by the program, the first model of each structure was selected according to the best C and TM scores. These structures were geometrically and energetically validated to assess the quality of the generated 3D model using different servers, such as the Ramachandran SWISS-MODEL⁵, the Z-score and energy graph in the ProSA- web server⁶, ERRAT⁷, and Verify3D⁸. The structures obtained for variants 8, 23, and 79 were aligned with the structure of Cry11Aa. For variant 79, complementary analysis based on the predicted secondary structure of non-conserved regions was performed using JPred⁹.

Subsequently, the *ab initio* method was used to predict the 3D structure of variant 79 using Robetta server¹⁰.

7.7.3.12 Molecular Docking of Cry11 Domains with ALP1

Parental Cry11Aa and variants 8, 23, and 79 were analyzed to identify their interactions with the receptor ALP1 from *A. aegypti* (UniProtKB ID; Q16WV8). For this protein, two regions that interact with Cry11Aa were identified by epitope mapping. These regions are located within R59-G102 and N257-I296 in ALP1, which interact with residues in loop α 8 of Cry11Aa domain II and residues R561-N570 in Cry11Aa domain III, respectively (Fernandez et al., 2009). The structure of ALP1 was modeled using the I-TASSER server taking into account folding recognition by threading. The model was evaluated according to Z-scores obtained using ProSA-web (see text footnote⁶), and a Ramachandran plot was generated using Swiss-MODEL (see text footnote⁵). For docking analysis, the interactions between Cry11Aa and ALP1 regions were analyzed using the Cry11Aa-interacting domains as peptides with rigid conformations based on the predicted 3D structures obtained in the previous step. The ALP1 structure and the peptides obtained from Cry11Aa and each variant were parameterized using AutoDockTools¹¹ via the addition of polar hydrogens to each residue's side chain to facilitate the formation of hydrogen bonds. The structures were also treated with Gasteiger partial charges to facilitate electrostatic interactions among other molecular entities. Docking analysis was performed using AutoDock Vina¹² considering an exhaustiveness set to 80, which is proportional to the length of the ligand. For the simulated interactions with both regions of ALP1, 3D grid cubic boxes with sides of 32 Å in length and a grid space of 1.0Å were located on the defined active site center, covering all the residues of interest and allowing the entrance of the full peptide structures into the protein cavities. Subsequently, the different docking conformations for each variant were illustrated and analyzed using LIGPLOT¹³.

⁵http://swissmodel.expasy.org/workspace/?func=tools_structureassessment1

⁶<https://prosa.services.came.sbg.ac.at/prosa.php>

⁷<http://services.mbi.ucla.edu/ERRAT/>

⁸http://services.mbi.ucla.edu/Verify_3D/

⁹<http://www.compbio.dundee.ac.uk/jpred/>

¹⁰<http://robeta.bakerlab.org/>

¹¹<http://autodock.scripps.edu/resources/adt>

¹²<http://vina.scripps.edu/>

¹³<http://www.ebi.ac.uk/thornton-srv/software/LIGPLOT/>

7.7.4 Results

7.7.4.1 Parental *cry11* Genes

cry11Aa, *cry11Ba*, and *cry11Bb* were used as parental genes to be fragmented in DNA shuffling based on their closely phylogenetical relationship, similarities at structural protein level and toxic specificity to similar insect species. This approach has been used for *in vitro* recombination of families of homologous genes in order to create novel proteins with improved properties and is useful for those in which the three-dimensional structure is unknown. In contrast to other random mutagenesis protocols, this technique introduces mutations by random DNA fragmentation and PCR reassembly in a cyclic process that alternates gene diversification, screening and selection of functional variants (Stemmer, 1994).

Four PCR products of 3.5, 2.7, 1.8, and 0.9 kb corresponding to *cry11* genes were obtained (**Supplementary Figure 1A**), as confirmed via DNA sequencing. The 3.5-kb PCR product contained a 2.2-kb fragment encoding the Cry11Bb protein. Three segments were also identified downstream of the last stop codon. The first segment consisted of 234-bp and showed 93% identity to *cry11Bb2* (accession number HM68615.1). The second segment was a 129-bp fragment that showed 93% identity to the complementary strand of the *IS2140* insertion element (accession number M23740.1) and was used to distinguish the reassembled products from the *cry11Bb* gene. The third segment, a 173-

bp fragment, showed 83% identity to the complementary strand of the *cry30Aa* gene (accession number AJ251978.1).

The 2.7-kb PCR product contained a 1.9-kb fragment encoding the Cry11Aa protein as well as two additional segments of 580- and 90-bp that were identified upstream of the first ATG and downstream from the stop codon, respectively. The 580-bp fragment was homologous to the p19 accessory protein gene (GenBank: CAD30080.1) and was used to distinguish the reassembled products from *cry11Aa* gene. The downstream 90-bp segment was homologous to the MCS of pSV2. Sequence analysis showed that the 1.8-kb and 0.9-kb PCR products from *cry11Ba*, denoted as Ba1 and Ba2, respectively, shared a 407-bp segment. A deletion of 246-bp downstream of ATG start site was used to recognize the reassembled products from *cry11Ba* gene. No mutations were detected in the DNA sequences of the PCR products of any of the parental genes.

7.7.4.2 Assembly of Full-Length *cry11* Genes

The primers used for DNA shuffling were tested via conventional PCR and random fragmentation, and the results indicated that the parental gene amplifications were successful (**Supplementary Figure 1A**). The purified PCR products (**Supplementary Figure 1B**) were mixed and treated with DNase I for 7, 8, or 9 min. However, only the products treated for 8 min (**Supplementary Figure 1C**) generated fragments between 25 and 200-bp. These products were reassembled, resulting fragments between 1 and 10-kb (**Supplementary Figure 1D**). After the final assembly using the PCR4F and pGE7R primers, we observed fragments between 0.25 and 2-kb (**Supplementary Figure 1E**). The assembly reaction products were cloned as described in the Materials and Methods. A total of 94 variants were obtained, and 10 of these variants did not contain an insert. For the remaining variants, 34 were <1.0-kb, 14 were between 1.1 and 2-kb, 22 were >2.1-kb and, and 14 did not show homology.

7.7.4.3 Characteristics and Sequence Homology of *cry11* Variants

According to the sequence analysis of the Cry11 variants, 14 of them did not show homology to any known endogenous Cry11 toxin. Among those 14 variants, six variants were >2.1-kb and eight were between 1 and 2-kb. The 22 variants that displayed sequence homology and a similar size to the full-length parental genes (>2.1-kb) were clustered into three groups. The first group consisted of variants 1, 8, 23, 28, 54, 79, and 81; these variants contained the p19 gene located upstream from the ATG start site and showed homology to *cry11Aa*. A second group of ten variants, including 16, 36, 51, 57, 61, 68, 71, 75, 77, and 85, showed DNA homology to *cry11Aa* but lacked the p19 gene. The third group of variants, 14, 17, 67, 76, and 86, showed homology to the *cry11B* genes.

Among the 22 variants that were between 1 and 2-kb, 14 showed homology to the *cry11B* genes, and eight did not have homology to any of the *cry11* genes used. All 34 variants that were <1-kb showed homology to the *cry11B* genes, and their reassembled products contained only domain III. Among all variants obtained via DNA shuffling, variants 1, 8, 23, 28, 54, 79, and 81 were selected for characterization. Homology analysis of the deduced amino acid sequences of Cry11Aa and variants 1, 8, 23 and 81 showed a high degree of conservation with few amino acid changes, which were preferentially located in domain III (**Supplementary Figure 2A**). Variants 28 and 54 exhibited 100% identity to Cry11Aa. Therefore, these mutants were excluded from further analysis. Comparative analysis of Cry11Aa, variant 23 (aa 1-643), variant 8 (aa 1-568), and variant 79 (aa 1-551) showed that the two first variants are highly conserved in the extension of the sequences. However, many variations relative to Cry11Aa were present in variant 79 at the end of the sequence, particularly beginning from aa 286. In addition to polymorphisms, several insertions/deletions were present at the end of this sequence (**Supplementary Figures 2B,C**).

Finally, secondary structure analysis of the deduced amino acid sequence from variants 8, 23, and 79 predicted the presence of α helix, β -sheets and loops (**Supplementary Figure 2C**). The accession numbers and particular characteristics of the variants 1, 8, 23, 79, and 81 genes are described in **Table 1**.

7.7.4.4 Protein Expression and Crystal Formation

SDS–PAGE revealed that all variants contained a similar pattern of solubilized proteins, and degradation was not observed (**Supplementary Figure 3A**). According to SEM analysis, variants 1, 8, 23, 79, and 81 as well as the parental proteins Cry11Aa and Cry11Bb form crystals (**Supplementary Figure 3B**). Strain BMB171, which was used as the plasmid recipient for protein expression, did not show crystal formation (**Supplementary Figure 3B**).

-The Selected Variants Exhibited Moderate to High Toxic Activity Against *A. aegypti* and *C. quinquefasciatus*.

In accordance with sequence identity, the variants 8, 23, and 79 were reassembled products from the *cry11Aa* parental gene. The toxic activity against *A. aegypti* larvae was up to 3.78- and 6.09-fold higher for variant 8 than for Cry11Bb and Cry11Aa, respectively. No significant differences were observed against *C. quinquefasciatus*. Variants 23 and 79 showed lower and higher mutation rates than Cry11Aa, respectively, although both variants retained toxic activity against *C. quinquefasciatus*. Additionally, variants 23 and 79 exhibited moderate and high toxicity to *A. aegypti*, respectively. Surprisingly, variant 79, despite of high variations still retaining toxic activity. Recombinant Cry11Bb exhibited high toxic activity to both *A. aegypti* and *C. quinquefasciatus* larvae, while variants 23 and 81 exhibited lower toxic activity than control against *A. aegypti*. The results of toxicity assays of five variants for the two types of larvae are shown in **Figure 2**. Based on their mutations and bioassay results, variants 8, 23, and 79 were chosen for analysis of their 3D structure and interaction with ALP1.

-Variants 8 and 23 Are Similar to Their Parental Protein, Whereas Variant 79 Shows Structural Differences

The Z-score, ERRAT and Verify3D results obtained for Cry11Aa and variants 8, 23, and 79 are shown in **Supplementary Table 2**. Multiple alignment including structural alignment of Cry11Aa and its variants showed that variants 8 and 23 are similar to their parental protein due to high sequence conservation (**Supplementary Figures 2A,B**). The similarity of these variants with respect to Cry11Aa was 87.4 and 98.9%, respectively. These variants also showed similar structural conformation to Cry11Aa (**Figures 3A–D**).

However, variant 79 exhibited structural differences in the non-conserved region compared with its parental protein (**Figures 3E,F**). The similarity of variant 79 with respect to Cry11Aa was 55,7%. The predicted secondary structure in the non-conserved region of variant 79 predominantly contains α helices instead of β -sheets, which are found in the corresponding region of Cry11A. This result was also found based on *ab initio* analysis, thus confirming the high prevalence of α helices in this region (**Figure 3G**).

7.7.4.5 The Interactions of Cry11Aa With ALP1 Are Conserved in Variants 8 and 23

The Ramachandran analysis of ALP1 showed that 76% of its residues were in favorable zones according to phi and psi angle positions and were involved in interactions with the parental Cry11Aa protein or its variants. None of the residues of ALP1 positioned in unfavorable zones (**Supplementary Figure 4A**) were involved in interactions with the parental Cry11Aa protein or its variants. The Z-score (-7.27) and the energy obtained from the ProSA-web server were below 0. Both analyses matched the score reported in the PDB crystallographic database, and the interactions were found to be energetically stable (**Supplementary Figures 4B–D**)

Figure 37. Molecular characteristics of Cry11 variants obtained via DNA shuffling.

Variants	GenBank accession number	Identity (%) <i>cry11Aa</i>	Mutation rate (%)	DI		DII		DIII	
				Del. (nt)	Subs. (nt)	Ins. (nt)	Subs. (nt)	Del. (nt)	
Variant 1	MH068786	84,6	15	219	0	73	6	1	
Variant 8	MH068787	87,7	13	219	6	0	13	0	
Variant 23	MH068788	98,9	1	9	6	5	2	0	
Variant 79	MH068789	80,1	20	326	7	42	21	0	
Variant 81	MH068790	90,7	8	153	0	8	2	0	
TOTAL				926	19	128	44	1	

D, domain; *Del*, deletions; *Subs*, substitutions; *Ins*, insertions.

Figure 38. Half lethal concentrations of Cry11 variants obtained via DNA shuffling in *Aedes aegypti* and *Culex quinquefasciatus* larvae. The values are expressed as ng/ml of spore-crystal mixtures, 95% confidence limit (CL).

Protein	LC ₅₀ (ng/ml ⁻¹)(95%CL)	
	<i>Aedes aegypti</i>	<i>Culex quinquefasciatus</i>
Variant 1	26.5 (7.2-28.9)	100.23 (5.8-120.1)
Variant 8	6.0 (1.6-6.4)	49.86 (3.1.-60.2)
Variant 23	254.2 (52.6-263.1)	51.38 (10.0-60.0)
Variant 79	39.7 (7.4-44.7)	66.77 (11.0-72.4)
Variant 81	428.1 (208.3-416.6)	75.48 (10.31-82.3)
Cry11Aa	36.9 (18.8-37.7)	84.64 (10.0-100.2)
Cry11Bb	22.9 (12.1-24.2)	13.13 (1.0-15.6)

The interaction of Cry11Aa with ALP1 involves a peptide of 12 amino acids, ³⁸⁹FTQWFQSTLYGW⁴⁰⁰, within loop 2 in domain II of Cry11Aa that was conserved in variants 8 and 23 (**Supplementary Figure 2A**). However, in variant 79, the only first five amino acids, ²⁸¹FTQWF²⁸⁵, were found (**Supplementary Figure 2B**). The identified interactions of ALP1 with the twelve-amino acid peptide indicated that W³¹⁹ and F³²⁰ of variant 8 form hydrogen bonds with Y⁴⁷⁸ and S³⁸¹ of ALP1, respectively (**Figure 4A**). The protein complex between variant 8 and ALP1 was also stabilized by five and eight hydrophobic interactions, respectively (**Figure 4A**). For variant 23, seven hydrophobic interactions with eleven amino acids of ALP1 were found (**Supplementary Figure 5**). For Cry11Aa, nine hydrophobic interactions with five amino acids and one hydrogen bond with Q³⁹¹ of ALP1 were found (**Figure 4B**). The identified interactions of ALP1 with the five-amino acid peptide of variant 79 described above were also analyzed for the interactions of ALP1 with Cry11Aa as well as variants 8 and 23.

Amino acids F³¹⁶ and W³¹⁹ of variant 8 formed three hydrogen bonds with amino acids E⁹⁸ and Q¹⁰⁰ of ALP1 (**Figure 4C**) in contrast to the two hydrogen bonds found in the interaction between F³⁸⁹ and Q³⁹¹ of the parental Cry11Aa protein with Y⁴⁷⁸ and E¹⁰⁵ of ALP1 (**Figure 4D**). For variant 23, a single hydrogen bond between G³⁸⁸ and Q⁹⁸ of ALP1 was found (**Figure 4E**), whereas variant 79 formed five hydrophobic interactions with nine amino acids of ALP1 (**Figure 4F**).

According to the data for Cry11Aa, the peptide 564RVQSQNSGNN⁵⁷³, located in the β 18 β 19 region of domain III, was found in all variants with exception of variant 79 (**Supplementary Figure 2C**). The LIGPLOT analysis of Cry11Aa showed three hydrophobic interactions of Cry11Aa with surface-exposed amino acids of ALP1 (**Figure 5A**). However, in variant 23, only one stable interaction through a hydrogen bond between R⁵⁶¹ of the variant protein and G²⁶¹ of ALP1 was observed (**Figure 5B**). In variant 8, two hydrogen bonds between R⁴⁹¹ of the variant protein and N²⁵⁹ of ALP1 as well as three hydrophobic interactions of R⁴⁹¹, V⁴⁹², and Q⁴⁹³ of the variant protein with V²⁵⁸, G²⁵⁷, and G²⁶¹ of ALP1 were formed (**Figure 5C**).

Figure 39. Prediction of the 3D Structures of Cry11Aa and Variants 8, 23, and 79. (A) Conserved region of variant 8 in light blue and Cry11Aa in beige, RMSD: 1,084 with 247 aa. (B) Non-conserved region of variant 8 in light blue and Cry11Aa in beige. (C) Conserved region of variant 23 in light blue and Cry11Aa in beige, RMSD: 1,132 with 488 aa. (D) Non-conserved region of variant 23 in light blue and Cry11Aa in beige. (E) Conserved region of variant 79 in light blue and Cry11Aa in beige, RMSD: 1,084 with 247 aa. (F) Non-conserved region of variant 79 in light blue and Cry11Aa in beige. (G) Ribbon representation of the non-conserved region of variant 79 generated using the Robetta server.

A

B

C

D

E

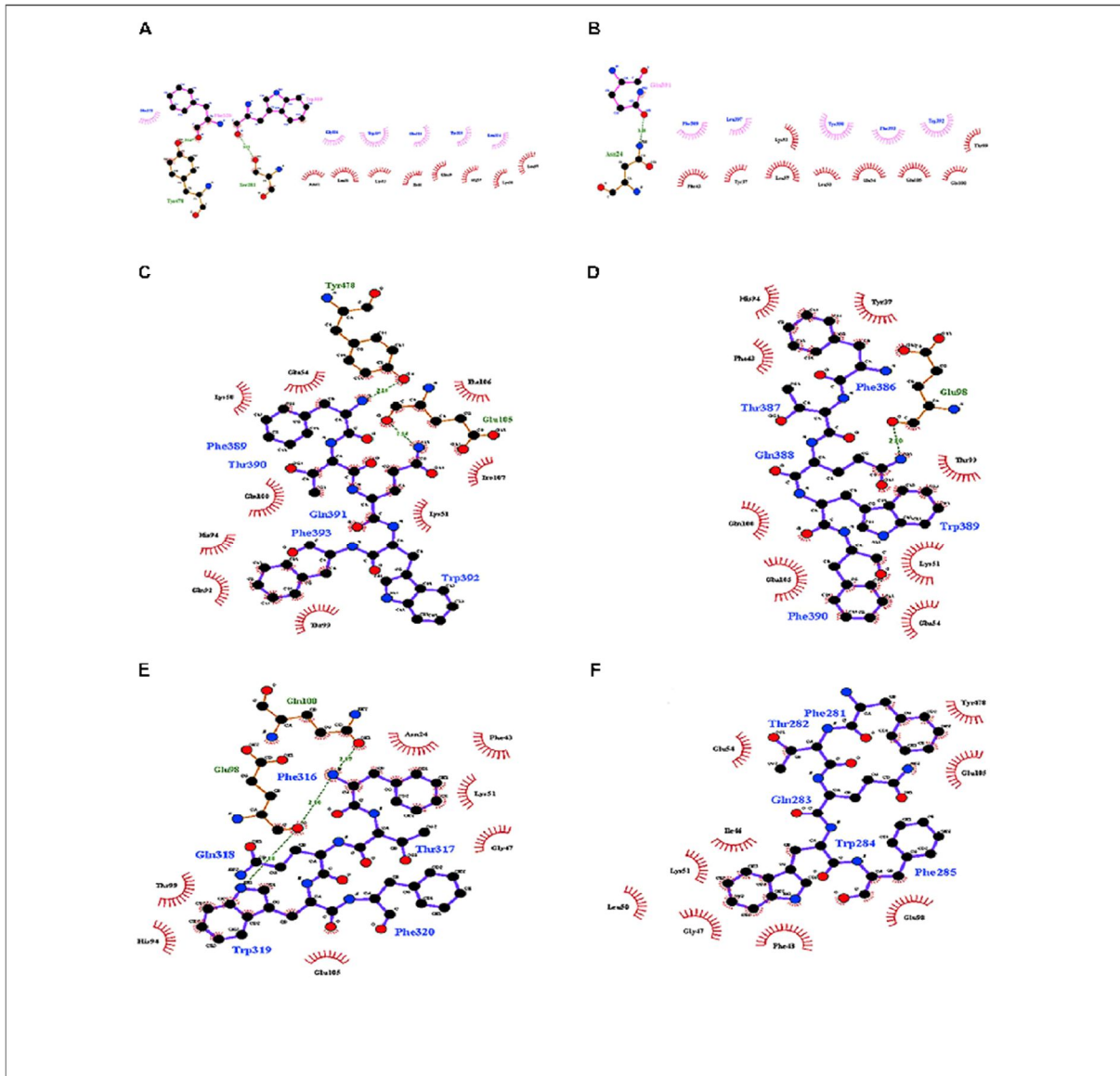
G

7.7.5 Discussion

Directed evolution approaches such as phage display library, DNA shuffling and staggered extension process shuffling combined with Red/Et homologous recombination have been proposed to increase the activity of *Bt* Cry toxins (Lucena et al., 2014). Other approaches based on phage-assisted continuous evolution (PACE) (Badran et al., 2016), *in vitro* template-change PCR (Shu et al., 2016), site-directed mutagenesis, and error-prone PCR have also been used successfully to identify novel receptors expressed on the surface of insect midgut cells and to understand the effects of different *cry* gene mutations on the mechanism of action of Cry toxins (Lucena et al., 2014). In this study, we report five Cry toxin variants produced via reassembly during DNA shuffling of the *cry11Aa* gene that showed toxic activity against *A. aegypti* and *C. quinquefasciatus* larvae.

DNA shuffling was designed using internal sequences in the parental constructs, including the identification of specific sites for priming during reassembly. We used the upstream *p19* gene to identify the genes that were reassembled from *cry11Aa*. A deletion of 246 bp downstream of the ATG start site was used to recognize those genes reassembled from *cry11Ba*, and an internal sequence corresponding to the specific primers was used to reassemble the variants from the construct containing the *cry11Bb* gene. The *p19* gene was present upstream of the first ATG codon in variants 1, 8, 23, 28, 54, 79, and 81. According to sequence analysis, all variants displayed some degree of identity to *cry11Aa*; this observation indicated that all variants were preferentially reassembled from this parental gene during DNA shuffling (**Table 1**).

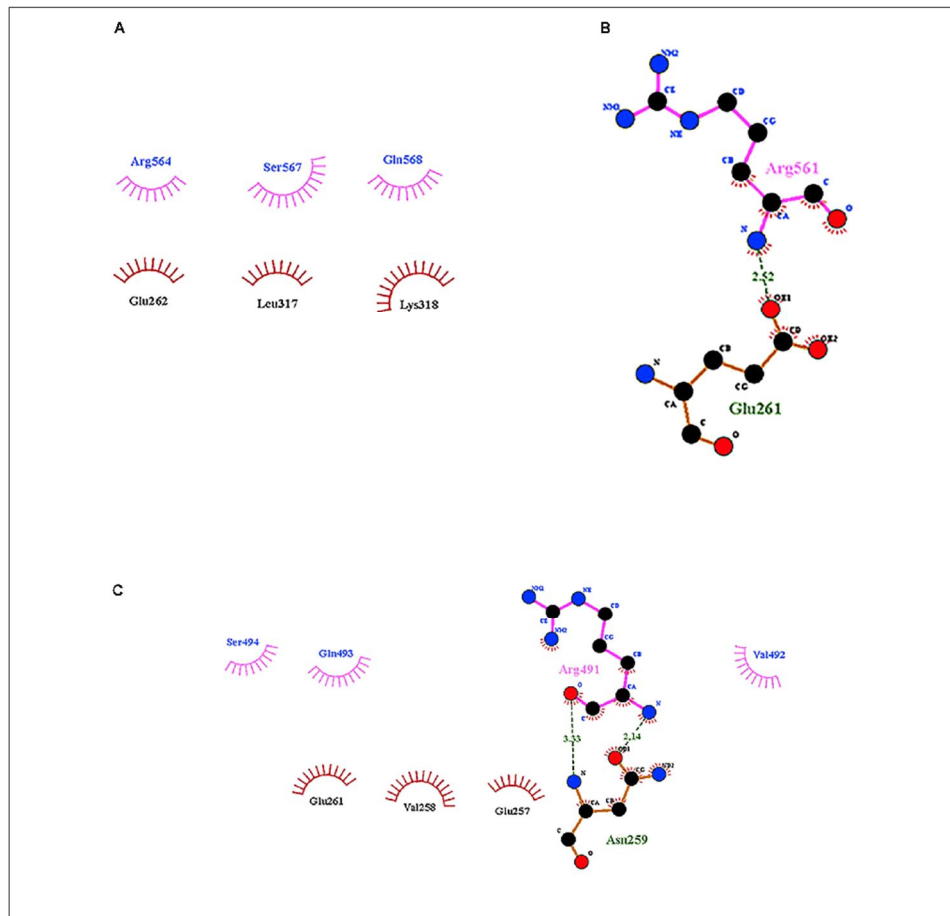
Figure 40. Molecular docking of the interactions of domain II of Cry11Aa and its variants with ALP1. (A,B) Interactions formed by 11-amino acid peptides within domain II of Cry11Aa. (A) Variant 8 (B) Cry11Aa. (C–F) Interactions formed by 5-amino acid peptides within domain II of Cry11Aa (C) variant 8 (D) Cry11Aa (E) Variant 23 (F) Variant 79.



Variants 1 and 79 retained toxic activity against *A. aegypti* and *C. quinquefasciatus* despite lacking 8.0 and 11.9 kDa N-terminal regions, respectively. These variants exhibited the highest mutation rates, 15 and 20%, respectively. The mutations found in variant 1 were not in regions involved in pore formation or toxin-receptor interactions, explaining the toxicity of variant 1 to *A. aegypti* based on bioassays. The insertion of 22 amino acids at the end of the C-terminus with seven substitutions did not affect the toxic

activity of variant 1. The results of the bioassays with *C. quinquefasciatus* larvae showed that variant 1 has similar toxic activity to Cry11Aa but 7.63-fold lower toxic activity than Cry11Bb. In the other hand, toxic activity of variant 79 was unexpected, despite its numerous mutations, its toxic activity against *A. aegypti* and *C. quinquefasciatus* was high (**Figure 2**). The deduced amino acid sequence of variant 79 did not show mutations in helices α -4 and α -5, which are implicated in pore formation, or in regions involved in toxin-receptor interactions, such as loop α 8 and strand β 4 (**Supplementary Figure 2C**). However, among the 260 amino acids at the C-terminus that were modified in variant 79, we found five amino acids located in loop α -2 (F²⁸¹, T²⁸², Q²⁸³, W²⁸⁴, and F²⁸⁵) that generate nine hydrophobic interactions with ALP1 (**Figure 4F**). These five amino acids in Cry11Aa and in variants 8 and 23 also form more stable interactions with ALP1 than hydrogen bonds (**Figures 4C–E**). Additionally, according to 3D and secondary structural analyses, the non-conserved C-terminal region of variant 79 has an unusual α -helix conformation (**Figure 3G**). The structural conformation of domains II and III of variant 79 has not previously been observed in Cry toxins; according to BLASTP analysis, this protein region is completely new. Therefore, we cannot discard the possibility that interactions of loop α 8 in domain I of variant 79 with loop α -2 of ALP1 could be sufficient to explain the toxicity of this variant.

Figure 41. Interactions visualized in LigPlot of ALP1 against peptides of Cry11Aa and its variants 8 and 23. (A) Cry11Aa, (B) Variant 23, and (C) Variant 8.



Variants 23 and 81 contain N-terminal deletions of 0.33 and 5.5 kDa, respectively. The mutation rates of variants 23 and 81 were less than those of other variants, and these two variants displayed 6.8- and 11.6-fold lower toxic activity against *A. aegypti* larvae, respectively, relative to Cry11Aa (**Table 1** and **Figure 2**). However, these variants retained high activity against *C. quinquefasciatus*. The LC_{50} s of variants 23 and 81 for *C. quinquefasciatus* are similar with the values that have been reported for Cry11Aa (van Frankenhuyzen, 2009) and were comparable to those of the parental protein in our bioassays. Loop α_8 , strand β_4 and loop 3 in domain II of these variants did not contain mutations, but differences in docking analysis results for variant 23 compared to the other variants could explain the moderate toxicity of variant 23 to *A. aegypti*. In loop 2, mutation $S^{392}F$ caused loss of the hydrogen bond formed via the interaction between Q^{391} of the wild type protein and N^{24} of ALP1, potentially reducing energetic stability and decreasing

the specificity of the intermolecular interactions. In the same region, in variant 23, four out of the nine amino acids of ALP1 that initially interacted with the wild type Cry11Aa toxin were involved in hydrophobic interactions; this evidence suggests that these changes could affect the stability of the toxin-receptor interaction (**Supplementary Figure 5**). The interaction between the β 18- β 19 region in domain III of variant 23 and ALP1 also appears to be characterized by a lack of hydrophobic interactions and the formation of a stable hydrogen bond between R⁵⁶¹ of variant 23 and Q²⁶¹ of ALP1 (**Figure 5B**). The observed differences in the interaction of ALP1 with wild type Cry11Aa and variant 23 based on docking analysis could be explained by the peptide conformations in the original model (Cry11Aa and variant 23 were considered as rigid peptides folded in the original conformation). In this manner, a technological limitation of docking analysis was overcome by producing interactions with the complete protein. Based on these findings, we suggest that the changes found in loop 2 of domain II and the interactions observed in the β 18- β 19 region of domain III affect the stability of the interaction of variant 23 with ALP1, thereby producing the moderate toxicity of variant 23 to *A. aegypti*.

Variant 8 was the most important of this study despite a deletion of 8.0-kDa at the N-terminus and similar 3D structure to Cry11Aa (**Figures 3A,B**), it showed an increased toxic activity of 6.09 times compared to Cry11Aa toward *A. aegypti* without significant differences against *C. quinquefasciatus* (**Figure 2**). Importantly, this variant did not show substitutions in regions involved in pore formation such as helices α 4 and α 5 neither in regions involved in toxin-receptor interaction such as loop α 8 and strand β 4. However, three substitutions T⁴⁵³A, R⁴⁵⁶G, and P⁴⁶²R in loop 3 located in domain II were found (**Supplementary Figure 2A**). In Cry11Aa, this loop did not show any interaction using the synthetic peptide ⁴⁴⁷LTYNRIEYDSPTTEN⁴⁶¹ in binding assays in the presence of *A. aegypti* BBMV (Fernandez et al., 2009). So far, mutations in loop 3 have been reported in Cry4Ba toxin that produces an increase of toxicity of 1.38 and 700 times toward *A. aegypti* and *C. quinquefasciatus*, respectively (Abdullah et al., 2003). In our study, the interactions found by docking analysis in loop 2 of domain II and strands β 18- β 19 in domain III suggest a role in the stability of the interaction with ALP1. The formation of two hydrogen bonds in loop 2 of domain II produced by W³¹⁹ and F³²⁰ with two amino acids of ALP1 including one hydrophobic interaction (Q³²¹) in the same cavity (**Figure 4A**), as well as two hydrogen

bonds formed in domain III by R⁴⁹¹ with N²⁵⁹ of ALP1 and three hydrophobic interactions, could explain the toxicity toward *A. aegypti* mediated by ALP1 (**Figure 4C**).

The N-terminal deletions found in variants 1, 8, 23, 79, and 81 were between 3 and 108 amino acids in length (0.33 and 11.8 kDa). However, these deletions are not implicated in the differences in toxic activity against *A. aegypti* and *C. quinquefasciatus* larvae between variants. Only one study has reported an N-terminal deletion in the Cry11Aa toxin where a truncated protein lacking 9.6 kDa was non-toxic to *A. aegypti* (Pang et al., 1992). In other Cry toxins such as Cry2a, deletion of 42 amino acids at the N-terminus increased the toxic activity against *Spodoptera littoralis*, *Helicoverpa armigera*, and *Agrotis ipsilon* (Mandal et al., 2007). Furthermore, in Cry1Ac, a deletion of 56 amino acids at the N-terminus, which included helix α -1, increase the toxic activity against *Pectinophora gossypiella* by 107-fold (Mandal et al., 2007) and against *Plutella xylostella* and *Ostrinia nubilalis* by 350-fold (Tabashnik et al., 2011). However, the toxic activity of Cry4Ba against *A. aegypti* was abolished when more than 38 amino acids were removed from the N-terminus (Pao-intara et al., 1988) and, in the case of chimeric proteins formed by a fusion of N-terminus of Cry4Ba and the C-terminus of Cry1Ac, an increase of toxicity against *C. pipiens* larvae was observed (Zghal et al., 2017). Although these findings confirm the importance of the N-terminal region in the toxicity of Cry proteins, the N-terminal deletions found in our variants did not affect their toxic activity against *A. aegypti* or *C. quinquefasciatus* larvae.

The difference in toxicity against *A. aegypti* and *C. quinquefasciatus* (**Figure 2**) could be explained by the presence of compounds either in midgut juice or membranes-bound proteases. Although the roles of these compounds and proteases have not been tested in variants obtained by DNA shuffling, there is evidence that the capacity to processing the protoxin depends on specific proteases located in the larval midgut and favored by alkaline conditions (Ben-Dov, 2014). In Cry11Aa toxin, the treatment with proteases generates fragments with different molecular weight and toxic activity against *Aegypti* (Revina et al., 2004; de Barros Moreira Beltrao and Silva-Filha, 2007), whereas in *C. quinquefasciatus*, the processing pattern differ from those that are active to *A. aegypti* (Dai and Gill, 1993). Therefore, we suggest that the toxicity differences found in *A. aegypti* and *C. quinquefasciatus* could be explained by mechanism that dependent on

the host. Overall, the data presented in this report indicate that the N-terminal deletions observed in all variants did not affect their toxicity to *A. aegypti* or *C. quinquefasciatus*. Variant 8, which contained several substitutions in domains II and III, was the most interesting variant produced in this study due to its high toxicity to the two mosquito species. These findings confirm the importance of these domains in Cry toxin-receptor interactions and in Cry protein toxicity. The substitutions found in variants 8 and 23 provide new information about the role of loops 2 and 3 of domain II in Cry toxin-ALP1 interactions. Importantly, the α helix conformation of the C-terminus of variant 79 based on secondary structure analysis corresponds to a new protein structure with toxic activity. We believe that DNA reassembly via DNA shuffling following random fragmentation could be a good strategy to generate random mutations in specific *cry* genes to design new and more potent toxins.

7.7.6 References

1. Abdullah, M. A., Alzate, O., Mohammad, M., Mcnall, R. J., Adang, M. J., and Dean, D. H. (2003). Introduction of *Culex* toxicity into *Bacillus thuringiensis* Cry4Ba by protein engineering. *Appl. Environ. Microbiol.* 69, 5343–5353. doi: 10.1128/AEM.69.9.5343-5353.2003
2. Aronson, A. (2000). Incorporation of protease K into larval insect membrane vesicles does not result in disruption of integrity or function of the pore-forming *Bacillus thuringiensis* delta-endotoxin. *Appl. Environ. Microbiol.* 66, 4568–4570. doi: 10.1128/AEM.66.10.4568-4570.2000
3. Badran, A. H., Guzov, V. M., Huai, Q., Kemp, M. M., Vishwanath, P., Kain, W., et al. (2016). Continuous evolution of *Bacillus thuringiensis* toxins overcomes insect resistance. *Nature* 533, 58–63. doi: 10.1038/nature 17938
4. Ben-Dov, E. (2014). *Bacillus thuringiensis* subsp. israelensis and Its Dipteran-Specific Toxins. *Toxins* 6, 1222–1243. doi: 10.3390/toxins6041222
5. Berry, C., O'neil, S., Ben-Dov, E., Jones, A. F., Murphy, L., Quail, M. A., et al. (2002). Complete sequence and organization of pBtoxis, the toxin-coding plasmid of *Bacillus thuringiensis* subsp. israelensis. *Appl. Environ. Microbiol.* 68, 5082–5095. doi: 10.1128/AEM.68.10.5082-5095.2002

6. Bradford, M. M. (1976). A rapid and sensitive method for the quantitation of microgram quantities of protein utilizing the principle of protein- dye binding. *Anal. Biochem.* 72, 248–254. doi: 10.1016/0003-2697(76)9 0527-3
7. Bravo, A. (1997). Phylogenetic relationships of *Bacillus thuringiensis* delta-endotoxin family proteins and their functional domains. *J. Bacteriol.* 179, 2793–2801. doi: 10.1128/jb.179.9.2793-2801.1997
8. Bravo, A., Gill, S. S., and Soberon, M. (2007). Mode of action of *Bacillus thuringiensis* Cry and Cyt toxins and their potential for insect control. *Toxicon* 49, 423–435. doi: 10.1016/j.toxicon.2006.11.022
9. Bravo, A., Gomez, I., Conde, J., Munoz-Garay, C., Sanchez, J., Miranda, R., et al. (2004). Oligomerization triggers binding of a *Bacillus thuringiensis* Cry1Ab pore-forming toxin to aminopeptidase N receptor leading to insertion into membrane microdomains. *Biochim. Biophys. Acta* 1667, 38–46. doi: 10.1016/j.bbamem.2004.08.013
10. Bravo, A., Sarabia, S., Lopez, L., Ontiveros, H., Abarca, C., Ortiz, A., et al. (1998). Characterization of cry genes in a Mexican *Bacillus thuringiensis* strain collection. *Appl. Environ. Microbiol.* 64, 4965–4972.
11. Chen, J., Aimanova, K., and Gill, S. S. (2017). Functional characterization of *Aedes aegypti* alkaline phosphatase ALP1 involved in the toxicity of Cry toxins from *Bacillus thuringiensis* subsp. *israelensis* and *jegathesan*. *Peptides* 98, 78–85. doi: 10.1016/j.peptides.2017.05.011
12. Chouin-Carneiro, T., Vega-Rua, A., Vazeille, M., Yebakima, A., Girod, R., Goindin, D., et al. (2016). Differential susceptibilities of *Aedes aegypti* and *Aedes albopictus* from the Americas to Zika Virus. *PLoS Negl. Trop. Dis.* 10:e0004543. doi: 10.1371/journal.pntd.0004543
13. Crickmore, N., Baum, J., Bravo, A., Lereclus, D., Narva, K., Sampson, K., et al. (2014). *Bacillus Thuringiensis Toxin Nomenclature*. Available at: <http://www.btnomenclature.info/>
14. Dai, S. M., and Gill, S. S. (1993). In vitro and in vivo proteolysis of the *Bacillus thuringiensis* subsp. *israelensis* CryIVD protein by *Culex quinquefasciatus* larval midgut proteases. *Insect Biochem. Mol. Biol.* 23, 273–283. doi: 10.1016/0965-1748(93)90008-G
15. de Barros Moreira Beltrao, H., and Silva-Filha, M. H. (2007). Interaction of *Bacillus thuringiensis* svar. *israelensis* Cry toxins with binding sites from *Aedes aegypti* (Diptera: Culicidae) larvae midgut. *FEMS Microbiol. Lett.* 266, 163–169. doi: 10.1111/j.1574-6968.2006.00527.x

16. Delecluse, A., Rosso, M. L., and Ragni, A. (1995). Cloning and expression of a novel toxin gene from *Bacillus thuringiensis* subsp. *jegathesan* encoding a highly mosquitocidal protein. *Appl. Environ. Microbiol.* 61, 4230–4235.
17. Derbyshire, D. J., Ellar, D. J., and Li, J. (2001). Crystallization of the *Bacillus thuringiensis* toxin Cry1Ac and its complex with the receptor ligand *N*-acetyl- D-galactosamine. *Acta Crystallogr. D. Biol. Crystallogr.* 57, 1938–1944. doi: 10.1107/S090744490101040X
18. Fernandez, L. E., Aimanova, K. G., Gill, S. S., Bravo, A., and Soberon, M. (2006). A GPI-anchored alkaline phosphatase is a functional midgut receptor of Cry11Aa toxin in *Aedes aegypti* larvae. *Biochem. J.* 394, 77–84. doi: 10.1042/BJ20051517
19. Fernandez, L. E., Martinez-Anaya, C., Lira, E., Chen, J., Evans, A., Hernandez-Martinez, S., et al. (2009). Cloning and epitope mapping of Cry11Aa- binding sites in the Cry11Aa-receptor alkaline phosphatase from *Aedes aegypti*. *Biochemistry* 48, 8899–8907. doi: 10.1021/bi900979b
20. Fernandez, L. E., Perez, C., Segovia, L., Rodriguez, M. H., Gill, S. S., Bravo, A., et al. (2005). Cry11Aa toxin from *Bacillus thuringiensis* binds its receptor in *Aedes aegypti* mosquito larvae through loop alpha-8 of domain II. *FEBS Lett.* 579, 3508–3514. doi: 10.1016/j.febslet.2005.05.032
21. Galitsky, N., Cody, V., Wojtczak, A., Ghosh, D., Luft, J. R., Pangborn, W., et al. (2001). Structure of the insecticidal bacterial delta-endotoxin Cry3Bb1 of *Bacillus thuringiensis*. *Acta Crystallogr. D. Biol. Crystallogr.* 57, 1101–1109. doi: 10.1107/S0907444901008186
22. Gardner, L. M., Chen, N., and Sarkar, S. (2016). Global risk of Zika virus depends critically on vector status of *Aedes albopictus*. *Lancet Infect. Dis.* 16, 522–523. doi: 10.1016/S1473-3099(16)00176-6
23. Grochulski, P., Masson, L., Borisova, S., Pusztai-Carey, M., Schwartz, J. L., Brousseau, R., et al. (1995). *Bacillus thuringiensis* CryIA(a) insecticidal toxin: crystal structure and channel formation. *J. Mol. Biol.* 254, 447–464. doi: 10.1006/jmbi.1995.0630
24. Guo, S., Ye, S., Liu, Y., Wei, L., Xue, J., Wu, H., et al. (2009). Crystal structure of *Bacillus thuringiensis* Cry8Ea1: An insecticidal toxin toxic to underground pests, the larvae of *Holotrichia parallela*. *J. Struct. Biol.* 168, 259–266. doi: 10.1016/j.jsb.2009.07.004
25. Hui, F., Scheib, U., Hu, Y., Sommer, R. J., Aroian, R. V., and Ghosh, P. (2012). Structure and glycolipid binding properties of the nematocidal protein Cry5B. *Biochemistry* 51, 9911–9921. doi: 10.1021/bi301386q

26. Li, J. D., Carroll, J., and Ellar, D. J. (1991). Crystal structure of insecticidal delta-endotoxin from *Bacillus thuringiensis* at 2.5 Å resolution. *Nature* 353, 815–821. doi: 10.1038/353815a0
27. Lucena, W. A., Pelegrini, P. B., Martins-de-Sa, D., Fonseca, F. C., Gomes, J. E. Jr., de Macedo, L. L., et al. (2014). Molecular approaches to improve the insecticidal activity of *Bacillus thuringiensis* cry toxins. *Toxins* 6, 2393–2423. doi: 10.3390/toxins6082393
28. Mandal, C. C., Gayen, S., Basu, A., Ghosh, K. S., Dasgupta, S., Maiti, M. K., et al. (2007). Prediction-based protein engineering of domain I of Cry2A entomocidal toxin of *Bacillus thuringiensis* for the enhancement of toxicity against lepidopteran insects. *Protein Eng. Des. Sel.* 20, 599–606. doi: 10.1093/protein/gzm058
29. Melo, A. L., Soccol, V. T., and Soccol, C. R. (2016). *Bacillus thuringiensis*: mechanism of action, resistance, and new applications: a review. *Crit. Rev. Biotechnol.* 36, 317–326. doi: 10.3109/07388551.2014.960793
30. Morse, R. J., Yamamoto, T., and Stroud, R. M. (2001). Structure of Cry2Aa suggests an unexpected receptor binding epitope. *Structure* 9, 409–417. doi: 10.1016/S0969-2126(01)00601-3
31. Orduz, S., Realpe, M., Arango, R., Murillo, L. A., and Delecluse, A. (1998). Sequence of the cry11Bb11 gene from *Bacillus thuringiensis* subsp. medellin and toxicity analysis of its encoded protein. *Biochim. Biophys. Acta* 1388, 267–272. doi: 10.1016/S0167-4838(98)00168-X
32. Otieno-Ayayo, Z. N., Zaritsky, A., Wirth, M. C., Manasherob, R., Khasdan, V., Cahan, R., et al. (2008). Variations in the mosquito larvicidal activities of toxins from *Bacillus thuringiensis* ssp. *israelensis*. *Environ. Microbiol.* 10, 2191–2199. doi: 10.1111/j.1462-2920.2008.01696.x
33. Pang, Y., Frutos, R., and Federici, B. A. (1992). Synthesis and toxicity of full-length and truncated bacterial CryIVD mosquitocidal proteins expressed in lepidopteran cells using a baculovirus vector. *J. Gen. Virol.* 73(Pt 1), 89–101. doi: 10.1099/0022-1317-73-1-89
34. Pao-intara, M., Angsuthanasombat, C., and Panyim, S. (1988). The mosquito larvicidal activity of 130 kDa delta-endotoxin of *Bacillus thuringiensis* var. *israelensis* resides in the 72 kDa amino-terminal fragment. *Biochem. Biophys. Res. Commun.* 153, 294–300. doi: 10.1016/S0006-291X(88)81221-X
35. Pardo-Lopez, L., Soberon, M., and Bravo, A. (2013). *Bacillus thuringiensis* insecticidal three-domain Cry toxins: mode of action, insect resistance and consequences for crop protection. *FEMS Microbiol. Rev.* 37, 3–22. doi: 10.1111/j.1574-6976.2012.00341.x

36. Perez, C., Fernandez, L. E., Sun, J., Folch, J. L., Gill, S. S., Soberon, M., et al. (2005). *Bacillus thuringiensis* subsp. *israelensis* Cyt1Aa synergizes Cry11Aa toxin by functioning as a membrane-bound receptor. *Proc. Natl. Acad. Sci. U.S.A.* 102, 18303–18308. doi: 10.1073/pnas.0505494102
37. Restrepo, N., Gutierrez, D., Patino, M. M., Thiery, I., Delecluse, A., and Orduz, S. (1997). Cloning, expression and toxicity of a mosquitocidal toxin gene of *Bacillus thuringiensis* subsp. *medellin*. *Mem. Inst. Oswaldo Cruz* 92, 257–262. doi: 10.1590/S0074-02761997000200021
38. Revina, L. P., Kostina, L. I., Ganushkina, L. A., Mikhailova, A. L., Zalunin, I. A., and Chestukhina, G. G. (2004). Reconstruction of *Bacillus thuringiensis* ssp. *israelensis* Cry11A endotoxin from fragments corresponding to its N- and C-moieties restores its original biological activity. *Biochemistry* 69, 181–187.
39. Shu, C., Zhou, J., Crickmore, N., Li, X., Song, F., Liang, G., et al. (2016). In vitro template-change PCR to create single crossover libraries: a case study with *Bacillus thuringiensis* Cry2A toxins. *Sci. Rep.* 6:23536. doi: 10.1038/srep23536
40. Stemmer, W. P. (1994). DNA shuffling by random fragmentation and reassembly: *in vitro* recombination for molecular evolution. *Proc. Natl. Acad. Sci. U.S.A.* 91, 10747–10751. doi: 10.1073/pnas.91.22.10747
41. Tabashnik, B. E., Huang, F., Ghimire, M. N., Leonard, B. R., Siegfried, B. D., Rangasamy, M., et al. (2011). Efficacy of genetically modified Bt toxins against insects with different genetic mechanisms of resistance. *Nat. Biotechnol.* 29, 1128–1131. doi: 10.1038/nbt.1988
42. Thompson, J. D., Higgins, D. G., and Gibson, T. J. (1994). CLUSTAL W: improving the sensitivity of progressive multiple sequence alignment through sequence weighting, position-specific gap penalties and weight matrix choice. *Nucleic Acids Res.* 22, 4673–4680. doi: 10.1093/nar/22.22.4673
43. Tsetsarkin, K. A., Chen, R., and Weaver, S. C. (2016). Interspecies transmission and chikungunya virus emergence. *Curr. Opin. Virol.* 16, 143–150. doi: 10.1016/j.coviro.2016.02.007
44. Vachon, V., Laprade, R., and Schwartz, J. L. (2012). Current models of the mode of action of *Bacillus thuringiensis* insecticidal crystal proteins: a critical review. *J. Invertebr. Pathol.* 111, 1–12. doi: 10.1016/j.jip.2012.05.001
45. van Frankenhuyzen, K. (2009). Insecticidal activity of *Bacillus thuringiensis* crystal proteins. *J. Invertebr. Pathol.* 101, 1–16. doi: 10.1016/j.jip.2009.02.009
46. Wirth, M. C., Georghiou, G. P., and Federici, B. A. (1997). CytA enables CryIV endotoxins of *Bacillus thuringiensis* to overcome high levels of CryIV resistance in the mosquito, *Culex quinquefasciatus*. *Proc. Natl. Acad. Sci. U.S.A.* 94, 10536–10540. doi: 10.1073/pnas.94.20.10536

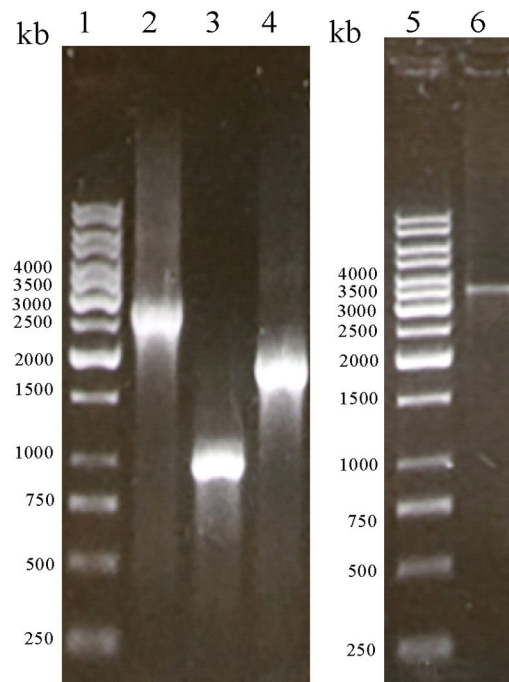
47. Zghal, R. Z., Elleuch, J., Ben Ali, M., Darriet, F., Rebai, A., Chandre, F., et al. (2017). Towards novel Cry toxins with enhanced toxicity/broader: a new chimeric Cry4Ba / Cry1Ac toxin. *Appl. Microbiol. Biotechnol.* 101, 113–122. doi: 10.1007/s00253-016-7766-3
48. Zhang, L., Zhao, G., Hu, X., Liu, J., Li, M., Batool, K., et al. (2017). Cry11Aa interacts with the ATP-binding protein from *Culex quinquefasciatus* to improve the toxicity. *J. Agric. Food Chem.* 65, 10884–10890. doi: 10.1021/acs.jafc.7b04427
49. Zhang, Q., Hua, G., and Adang, M. J. (2017). Effects and mechanisms of *Bacillus thuringiensis* crystal toxins for mosquito larvae. *Insect Sci.* 24, 714–729. doi: 10.1111/1744-7917.12401
50. Zhang, X., Candas, M., Griko, N. B., Taussig, R., and Bulla, L. A. Jr. (2006). A mechanism of cell death involving an adenylyl cyclase/PKA signaling pathway is induced by the Cry1Ab toxin of *Bacillus thuringiensis*. *Proc. Natl. Acad. Sci. U.S.A.* 103, 9897–9902. doi: 10.1073/pnas.0604017103

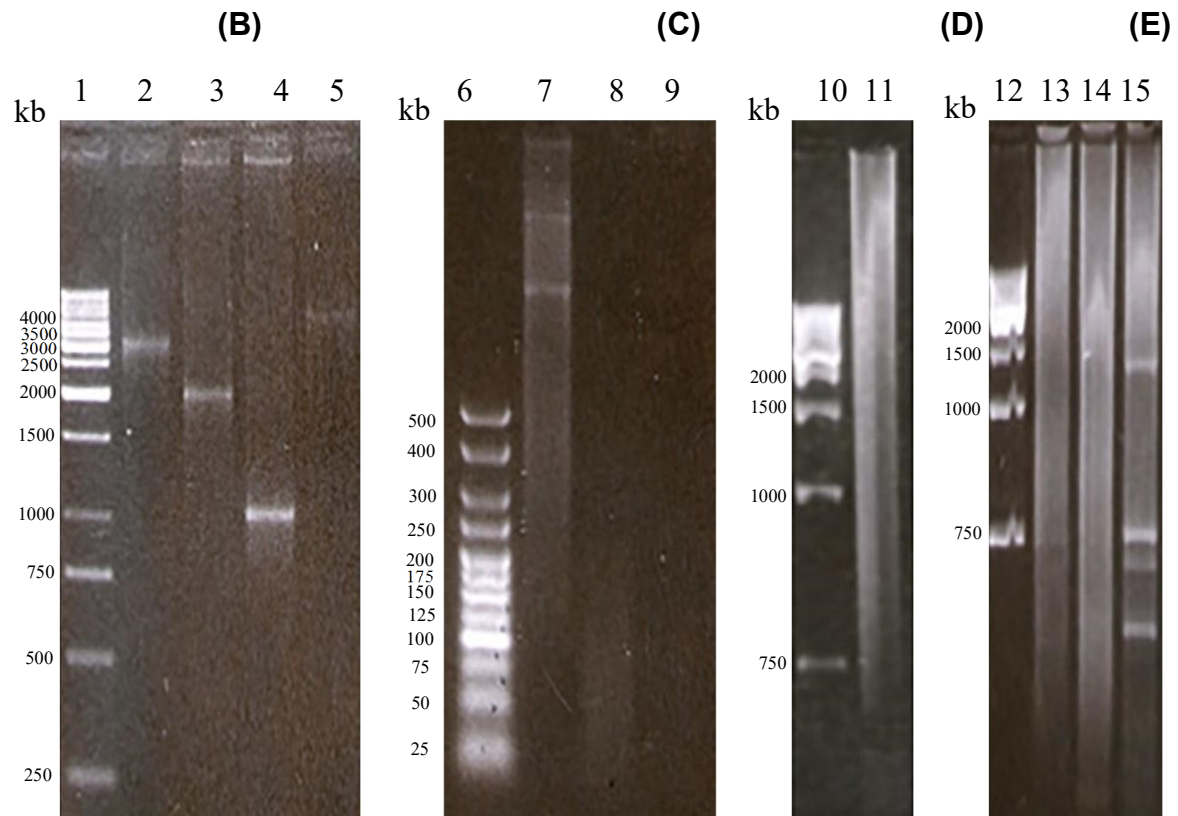
7.7.7 Supplementary Material

Supplementary Figures and Tables

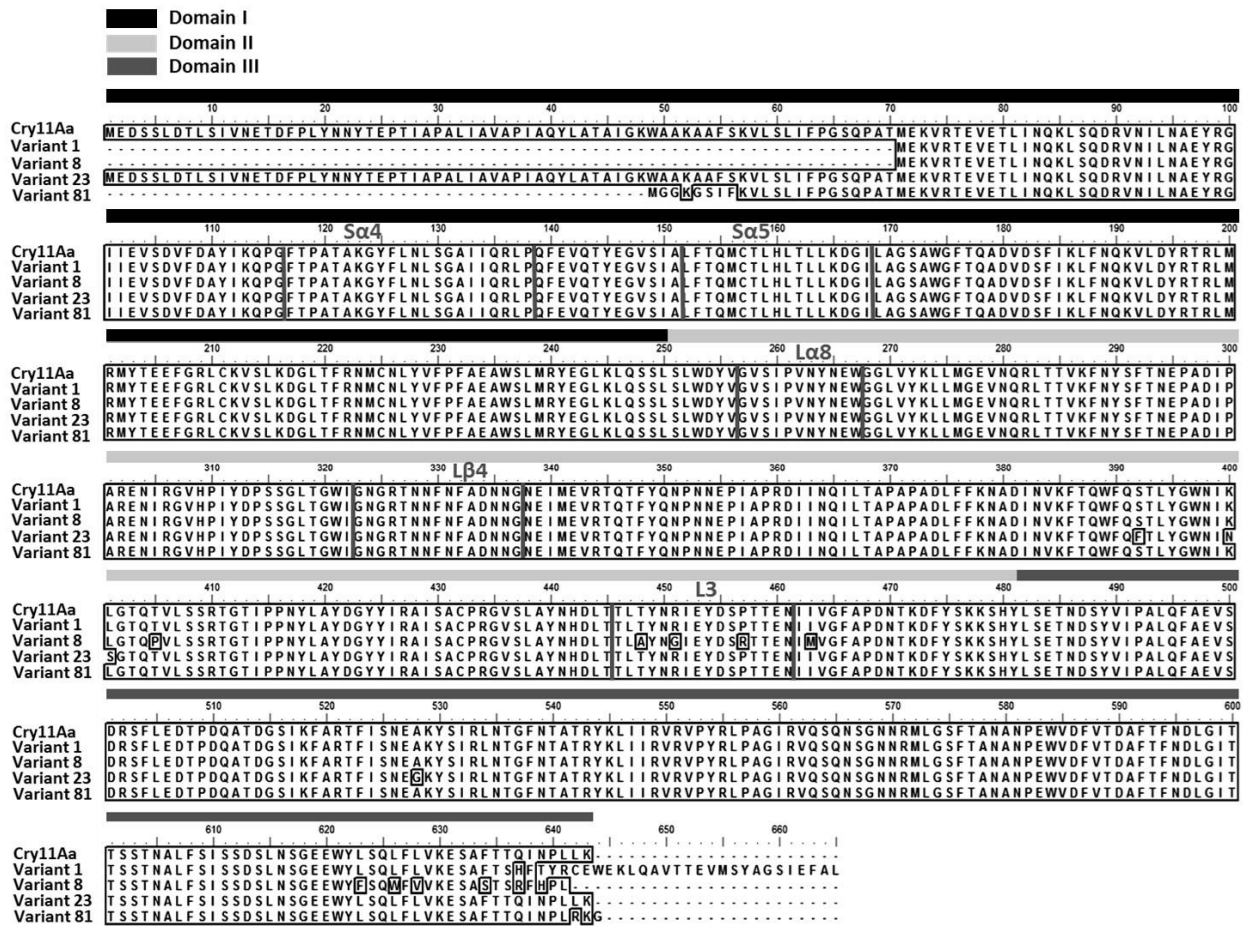
Supplementary Figure 1. Amplification, DNase I Digestion, Assembly and Reassembly of *cry11* Genes. **(A)** Image of 0.8% agarose gel electrophoresis of PCR products obtained with PCR4 primers for *cry11Aa*, *cry11Ba1* and *cry11Ba2* and pGE7 primers for *cry11Bb*. Lane 1 and 5: Molecular weight 1 kb (Fermentas), Lane 2: *cry11Aa*, Lane 3: *cry11Ba-2*, Lane 4: *cry11Ba-1*, Lane 6: *cry11Bb*. **(B)** DNA shuffling for *cry11* genes. Lanes 1, 10 and 12: Molecular weight 1 kb (Fermentas). Purified PCR products obtained with PCR4 primers for *cry11Aa*, *Ba1* and *Ba2* and pGE7 primers for *cry11Bb*, Lane 2: *cry11Aa*, Lane 3: *cry11Ba1*, Lane 4: *cry11Ba2*, Lane 5: *cry11Bb*. **(C)** Image of 2.5% agarose gel electrophoresis of the products of DNase I (0.0006 U) digestion. Lane 6: Molecular weight 25 bp (Bioline), Lane 7: digestion products after 7 min, Lane 8: digestion products after 8 min, Lane 9: digestion products after 9 min. **(D)** Image of 0.8% agarose gel electrophoresis. Lane 11: assembly of the DNase I-treated products from lanes 8 and 9 performed without primers. **(E)** Image of 0.8% agarose gel electrophoresis of the products of reassembly with primers PCR4 and PGE7. Lane 13: products of reassembly with primers PCR4F/R, Lane 14: products of reassembly with primers PGE7F/R, Lane 15: products of reassembly with primers PCR4F and PGE7R.

(A)

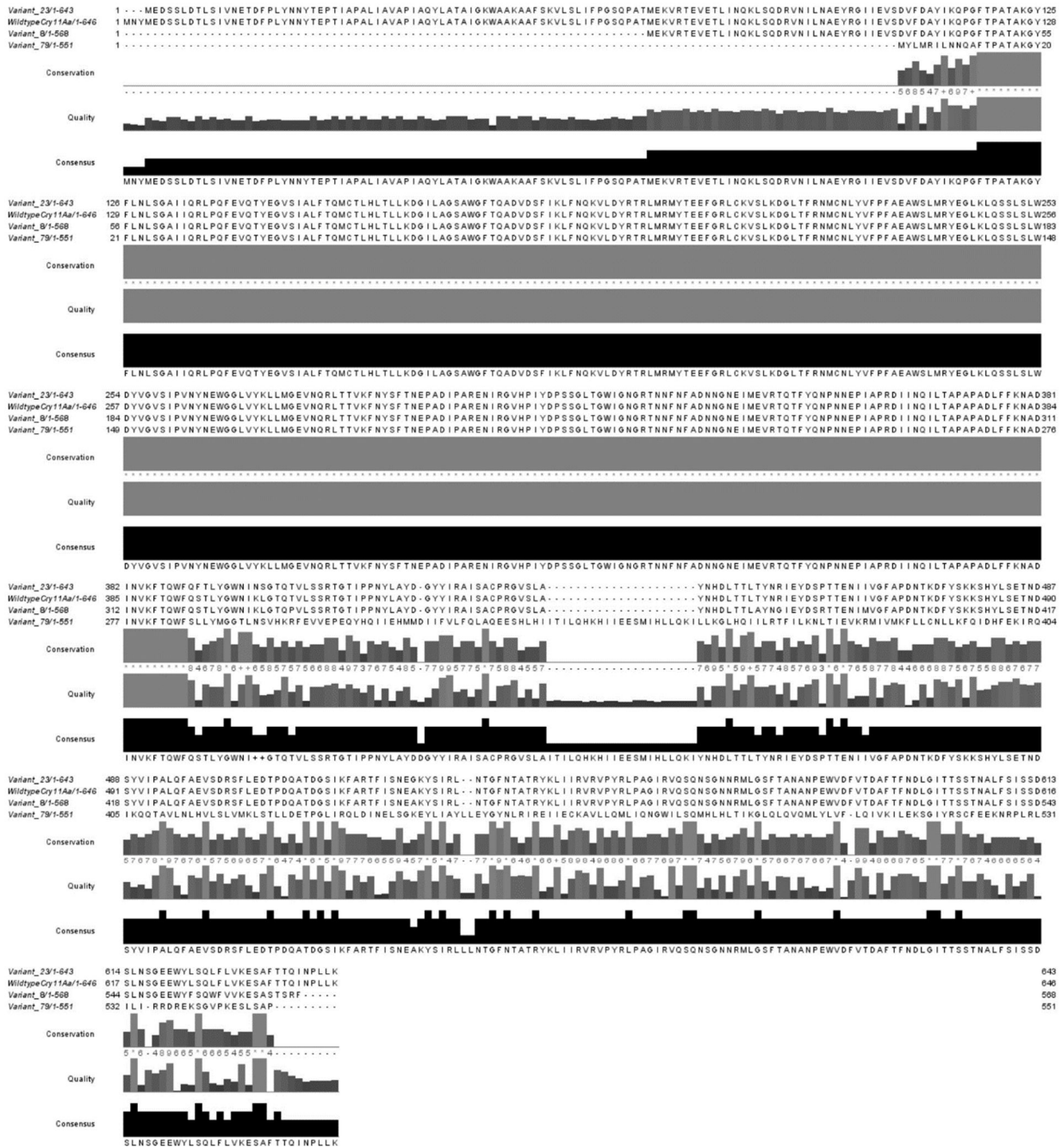




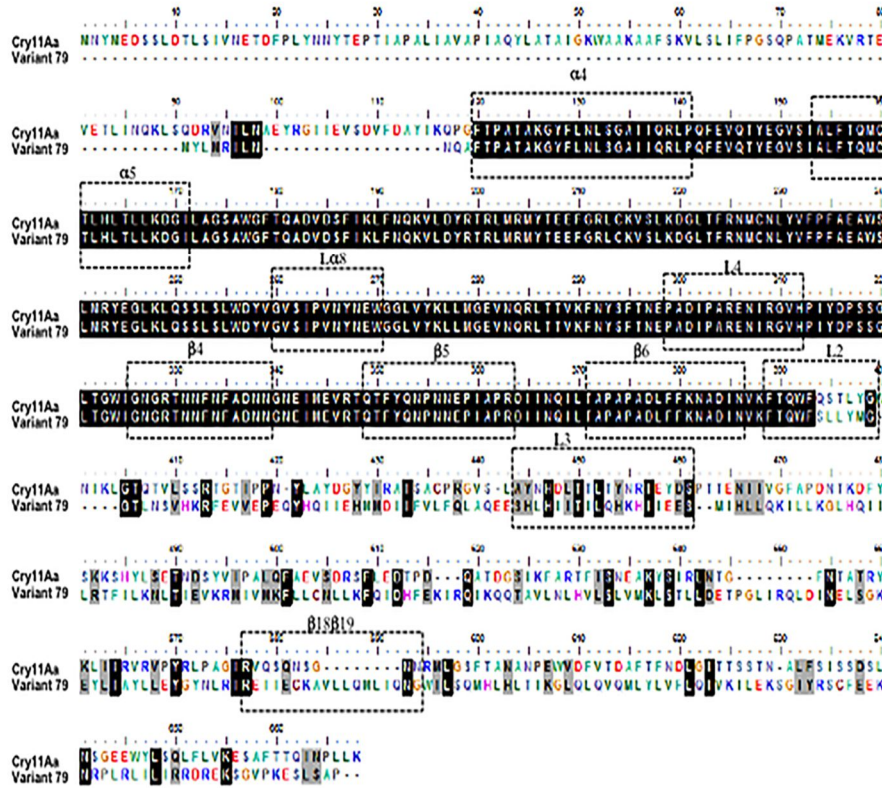
Supplementary Figure 2. Alignment of Deduced Amino Acid Sequences of Variants 1, 8, 23, 79 and 81. (A) Variants 1, 8, 23, and 81. The domains are defined above the amino acid sequence in horizontal gray bars. Helices $\alpha 4$ and $\alpha 5$ are denoted as $\alpha 4$ and $\alpha 5$, respectively. Loop $\alpha 8$, strand $\beta 4$ and loop 3 are denoted as $L\alpha 8$, $\beta 4$ and $L3$, respectively. Substitutions are indicated by closed boxes. **(B)** The conservation, quality and consensus sequence similarity of variants 8, 23, and 79. **(C)** Alignment of the deduced amino acid sequences of wild type Cry11Aa and variant 79. Helix regions are denoted as $\alpha 4$ and $\alpha 5$. Loop regions are denoted above the deduced amino acid sequence in dotted boxes as $L\alpha 8$, $L1$, $\beta 4$, $\beta 5$, $\beta 6$, $L2$, $L3$ and $\beta 18$ - $\beta 19$. Identical amino acids are shown in white color.



(A)

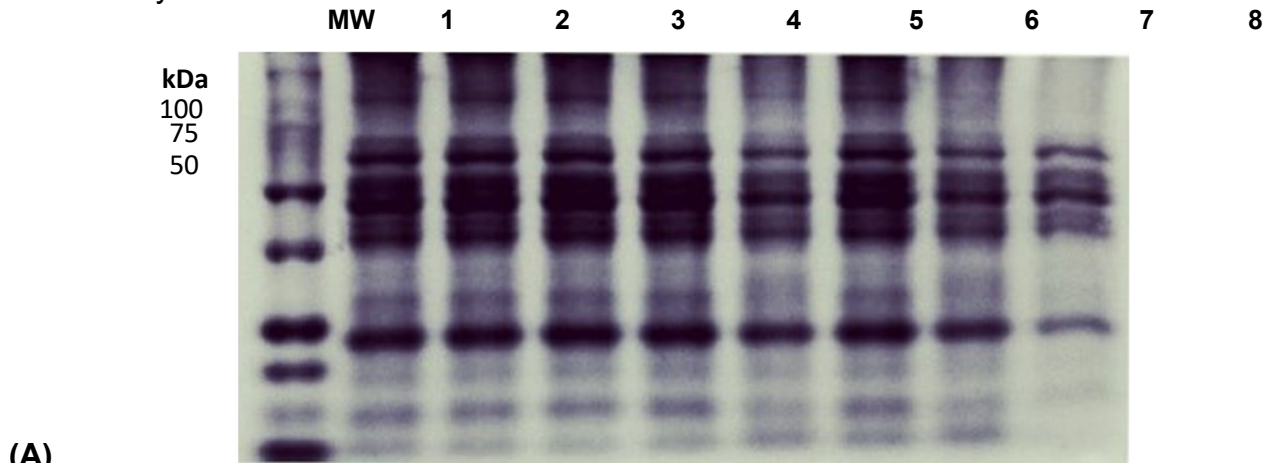


(B)

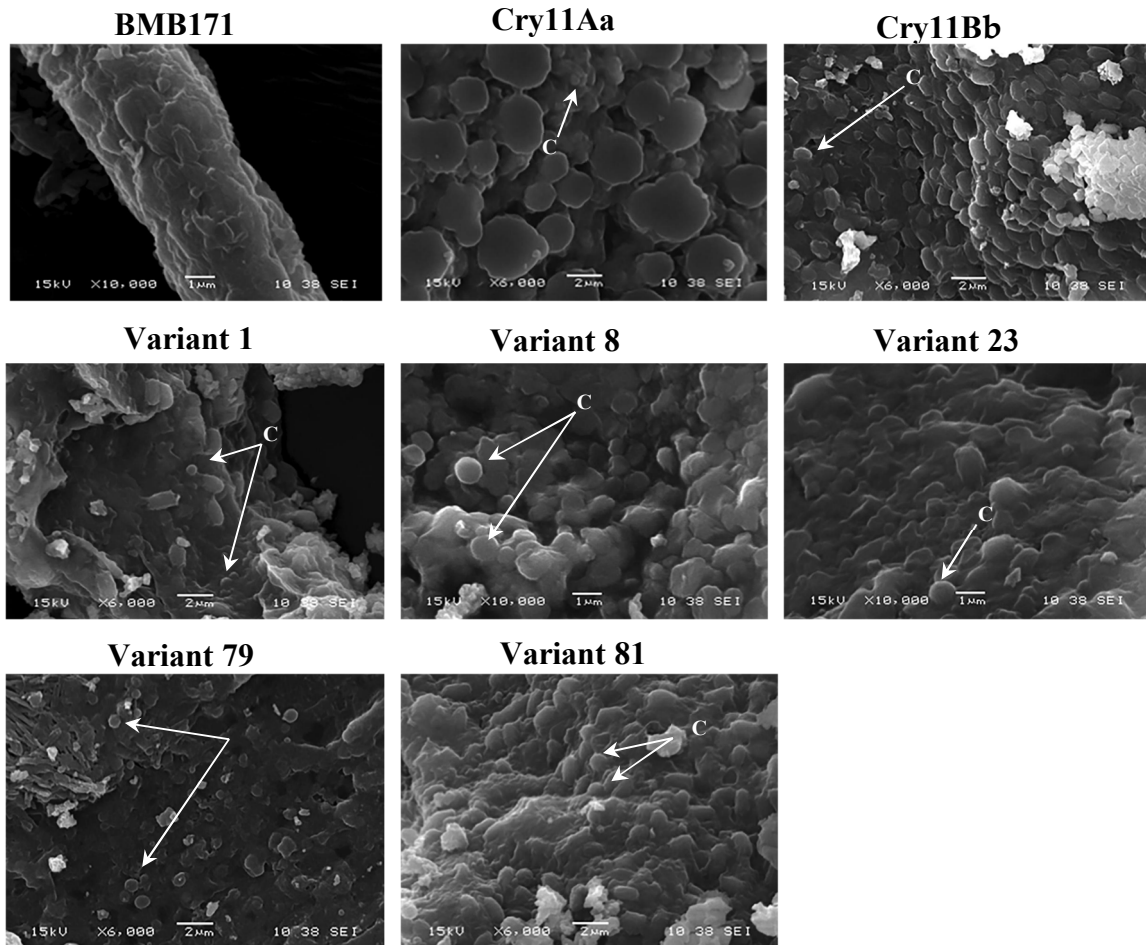


(C)

Supplementary Figure 3. Protein Composition of Crystals Produced by Variants 1, 8, 23, 79 and 81. (A) SDS-PAGE analysis. Lane 1. Kaleidoscope molecular weight standards (BioRad™); Lane 2: variant 1; Lane 3: variant 8; Lane 4; variant 23; Lane 5: variant 79; Lane 6: variant 81; Lane 7: Cry11Aa; Lane 8: BMB171. **(B) SEM analysis.** Photomicrographs of variants 1, 8, 23, 79 and 81. Controls are Cry11Aa, Cry11Bb and the acrysaliferous strain BMB171. Scale bars: 1 and 2 • m. White arrows and the letter C indicate crystals.

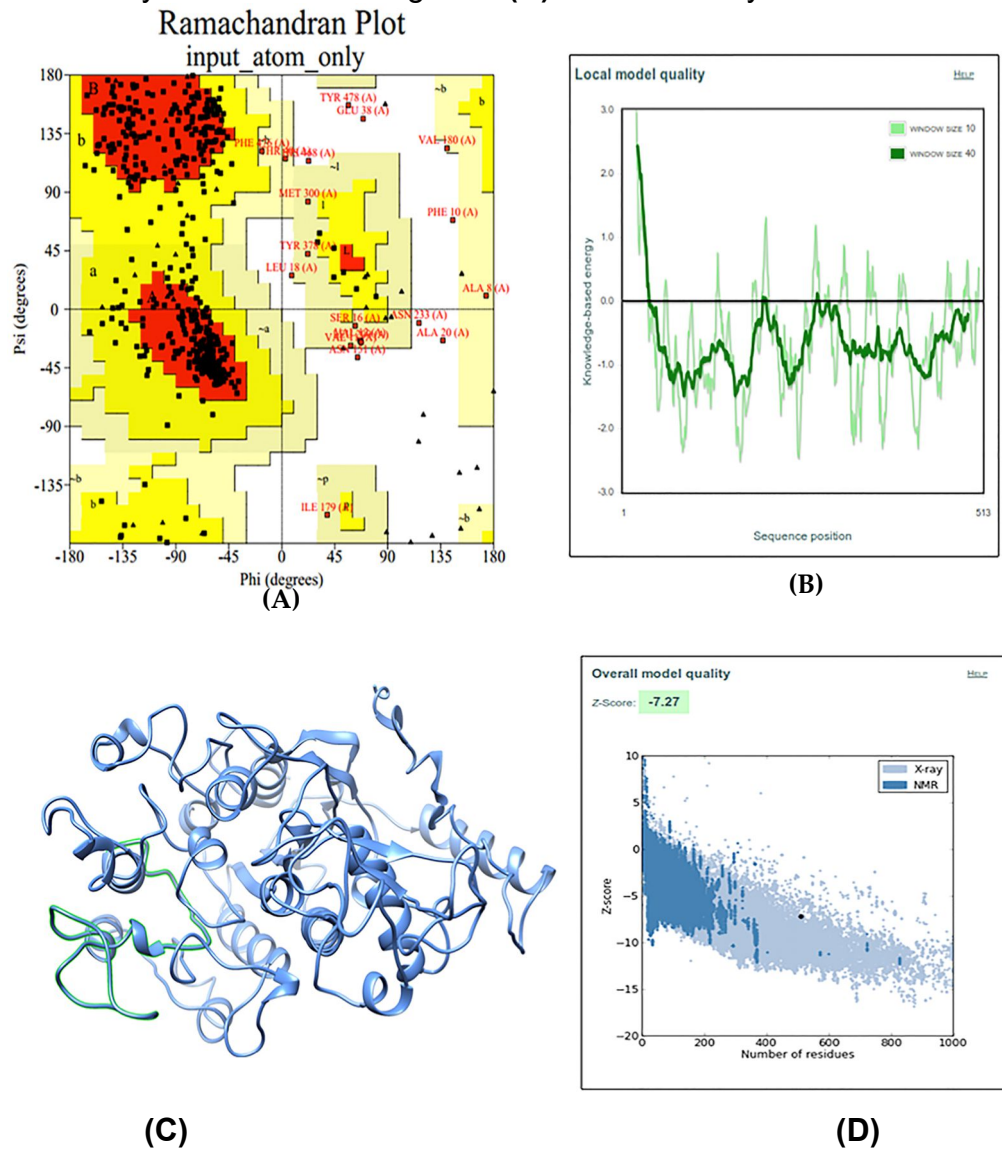


(A)

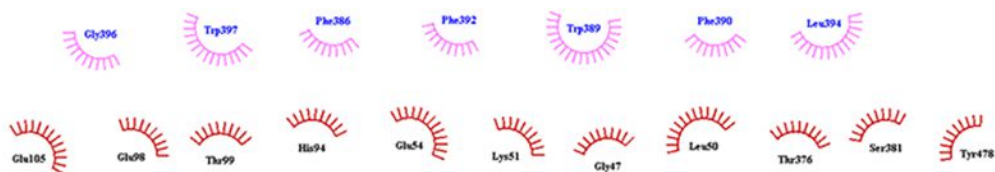


(B)

Supplementary Figure 4. Prediction of the 3D Structure of ALP1. (A) Ramachandran plot analysis generated using the program Procheck on the SwissModel Server. (B) Energy curve. (C) Predicted structure of ALP1. The flexible region that was selected for interaction with Cry11Aa is shown in green. (D) Z-score analysis.



Supplementary Figure 5. Molecular Docking of the Interactions of Domain II variant 23 with ALP1. Interactions formed by 12-amino acid peptides within domain II of Variant 23.



Supplementary Table 1. List of Strains, Constructs and Primers used to Perform DNA Shuffling

Strain	Construct name	Gene	Primers	bp
<i>E. coli</i>	pTOAa	<i>cry11Aa</i>	PCR4F: 5'-	2.516
DH5 α TOP10 [®]	pTOBa-1	<i>cry11Ba</i>	ATAACAATTTACACAGGA-3'	1.600
(Life Technologies)	pTOBa-2	<i>cry11Ba</i>	PCR4R: 5'-	780
	PTOBb	<i>cry11Bb</i>	TTGTAAAACGACGGCCAGTG-3'	3.700
<i>E. coli</i> JM109 [®]	pGEBb	<i>cry11Bb</i>	pGE7F: 5'-	3.500
(Promega)			GATGTGCTGCAAGGCGATT-3'	
			pGE7R: 5'- TTACGCCAAGCTATTTAGGTG-3'	

Supplementary Table 2. Scores for *Cry11Aa* and Variants Obtained from Analysis Servers.

Protein	Z-score	ERRAT	Verify3D
Cry11Aa	-6.49	51.33	71.05
Variant 8	-5.72	51.07	75.18
Variant 23	-6.71	59.49	80.56
Variant 79	-5.28	43.06	59.99